# A FULL-SCALE AND MODEL STUDY OF CONVECTIVE HEAT TRANSFER FROM ROOF MOUNTED FLAT-PLATE SOLAR COLLECTORS

## VOLUME TWO

## EXPERIMENTAL DETAILS, RESULTS AND CONCLUSIONS

A thesis submitted to the Faculty of Architectural Studies,
University of Sheffield, for the degree of Doctor of Philosophy

PETER S. CHARLESWORTH

Department of Building Science
University of Sheffield,
SHEFFIELD
S10 2TN

MARCH 1986.

TO MY MOTHER AND FATHER -

FOR THEIR CONTINUOUS SUPPORT

THROUGHOUT MY ACADEMIC CAREER

"The cooling of a hot body exposed to the air is effected partly by radiation, and partly by conduction from the surface of the body to the air in contact with it. The activity of surface conduction is greatly quickened by wind, which continually brings fresh portions of cold air into contact with the surface, in place of those which have been heated".

- Deschanel's Natural Philosophy

1888

## SUMMARY

This study is concerned with the convective heat transfer, due to the action of the wind, from the upper surface of roof mounted flat plate solar collectors. The ability to predict the quantity of heat transferred from a collector, in this manner, is necessary in order to facilitate the evaluation of the overall efficiency of a collector panel.

Previous methods of determining this convection coefficient have generally relied upon extrapolations of small scale wind tunnel results to full-scale values. The validity of these methods is questionable, and it was found that there was a lack of full-scale data relating to the convection coefficient from the upper surface of a flat-plate collector. It was also found that no systematic attempt to relate model results to full-scale values had been made.

Full-scale experiments have been performed to evaluate the convective heat transfer coefficient, h, from the upper surface of a roof mounted flat plate. The convection coefficient was found to be dependent upon the wind speed as measured above the roof ridge line, $V_{6R}$, and to some extent upon the direction of the prevailing wind, $\Theta$. Relationships between h and $V_{6R}$ are presented, as are relationships between h and $V_H$ (the wind speed measured at the mid-panel height) and h and $V_{10}$ (the meteorological 10m wind speed).

Small scale wind tunnel experiments were also performed. This was in order to assess the potential of using wind tunnel model results to predict accurately full-scale convective heat losses. These experiments showed some qualitative agreement with the full-scale tests. However, extrapolation of these model results to full-scale values rendered heat transfer coefficients in excess of those found in the full-scale work. Therefore the use of previously derived full-scale results from wind tunnel studies must be treated with caution. It is suggested that the full-scale results, presented here, represent a more satisfactory means of evaluating the convective heat transfer from the upper surface of roof mounted flat plate solar collectors.

## ACKNOWLEDGEMENTS

A thesis such as this could never be completed without the help and understanding of many people. I should like, first and foremost, to thank my supervisor Dr. Stephen Sharples for his invaluable help and advice during my time spent in the Department of Building Science.

The technical staff of the department suffered my, often capricious, requests for materials, models and site visits, etc. with humerous stoicism. I am therefore deeply indepted to Messrs. Roy Webster, Peter Williams, Lol Wildgoose and Roger Grace not only for their technical ability but also for making the department a pleasant place to spend one's time.

I also owe great thanks to Hazel Hall for turning my rather untidy original drafts of this thesis into a final form of excellent quality.

The SERC provided the funding for this research and I am grateful for its support.

Finally I should like to thank the Crewe crew for putting up with my ever changing moods especially in the writing up stage of the research.

# CONTENTS

## VOLUME ONE

## CHAPTER ONE

## INTRODUCTION

# CHAPTER TWO

# FUNDAMENTAL CONVECTIVE HEAT TRANSFER

# CHAPTER THREE

# REVIEW OF EXPERIMENTAL ANALYSIS OF FORCED CONVECTIVE HEAT TRANSFER

VOLUME TWO

# CHAPTER FOUR

# EXPERIMENTAL DETAILS OF THE FULL-SCALE MEASUREMENTS OF THE CONVECTIVE HEAT TRANSFER FROM A LARGE FLAT PLATE IN THE NATURAL ENVIRONMENT

# CHAPTER FIVE

# EXPERIMENTAL RESULTS OF THE FULL-SCALE MEASUREMENTS OF FORCED CONVECTIVE HEAT TRANSFER AT THE NORTON SITE

# CHAPTER SIX

# DETAILS OF THE WIND TUNNEL MODEL EXPERIMENTS

# CHAPTER SEVEN

## RESULTS OF WIND TUNNEL MODEL EXPERIMENTS

# CHAPTER EIGHT

# CONCLUSION

# CHAPTER FOUR

# EXPERIMENTAL DETAILS OF THE FULL SCALE MEASUREMENT OF THE CONVECTIVE HEAT TRANSFER FROM A LARGE FLAT PLATE IN THE NATURAL ENVIRONMENT

## Introduction

Previous chapters have reviewed theoretical and experimental convective heat transfer from flat plates and geometries more directly related to flat plate solar collectors. It was concluded that there was a lack of full scale convective heat transfer data for large flat plates in the outdoor environment. Therefore a series of experimental measurements of this type were undertaken.

Full scale measurements of convective heat transfer in the natural environment pose many problems which are not encountered in a controlled laboratory situation. This chapter discusses these problem areas, and describes the development of an experimental test apparatus and technique designed to overcome them.

## 4.1 The Choice, Location and Description of the Site Employed for the Full Scale Convective Heat Transfer Measurements

The first problem encountered in performing full-scale measurements was of locating a suitable site at which the experimental work could be carried out. This section discusses the methodology employed in the choice of such a site and describes the relevant characteristics of the site used for the full-scale measurements.

### 4.1.1 A discussion of the factors governing the choice of a site for the performance of the full-scale heat transfer measurements

In order to assess the suitability of any potential full-scale site, four criteria were to be applied. These critera, in order of importance, are presented below.

(i) Building Geometry

This study is primarily concerned with heat loss from flat plate solar collectors placed on the roofs of low rise dwellings. It is, therefore, desirable to obtain a site which offers a building of geometry and size compatible with those of standard housing stock.

(ii) Surrounding terrain

The terrain should be reasonably uniform in all directions around the site, with no large buildings nearby. If the terrain were not uniform then the wind velocity profile would become directional dependent, thus making the comparison of data obtained from different wind directions difficult. Large structures in close proximity to the test building would distort the local wind flow over the test site. This would make the results of any experiments less applicable to other, otherwise geometrically similar, situations.

(iii) Accessibility and occupancy

The site should be at such a distance from the University so as not to make the transportation of equipment and personnel too time consuming. The site building itself should be accessible at all times including nights and weekends. This

would facilitate the utilisation of continuous data collection over prolonged periods. Occupancy patterns within the building should be such that they would suffer minimum disruption by the installation and running of a full-scale test rig.

(iv) Structural considerations

Some minor structural alterations to the site building may be required in order to facilitate the installation of the test rig. Hence the building should be of such a shape and size that this installation could be carried out easily and safely, with a minimum amount of damage to the building concerned.

It can be imagined that the location of a site to fulfil all of the criteria would not be without difficulty. Specific conflicts can be found, even within the criteria themselves.

Sheffield is a big city and the probability of a site near to the University being free from the influence of large buildings is minimal. The ideal site to satisfy criterion (i) would be an actual low rise dwelling e.g. A semi detached house. This would cause problems with occupancy patterns, structural alterations and the safety of installation of equipment on the roof.

With these points in mind it was realised from the start that the location of an ideal site would prove difficult and that concessions in each of the above four categories might have to be made.

### 4.1.2 The location of a site suitable for the performance of the full-scale convective heat transfer measurements

As a first approach to the problem the University Estates and Buildings office was consulted. This was in order to ascertain whether the University owned any property which would

fulfil the requirements stated in Section 4.1.1. This approach was made because it was felt that if the site was University owned then the problems of accessibility and occupancy would be minimised.

Four sites were offered, three within the urban area of Sheffield, the fourth some three miles from the city centre.

Despite their closeness to the University the first three sites were rejected. Each for essentially similar reasons. They were all very large detached buildings with unusual roof shapes. This would pose problems with the installation of equipment on the roof and of local flow conditions around the structure. All three were occupied, two being used as offices by departments within the University. It was thought that this may have presented problems with accessibility and occupancy patterns. Finally, whilst the surrounding terrain of the urban sites was fairly uniform, they would not be entirely free from wind conditions influenced by the presence of large nearby structures of the type usually found in urban city areas.

The fourth site was examined and despite its distance from the University was accepted and finally used for the full-scale convective heat transfer measurements.

### 4.1.3 A description of the site used for the performance of the full-scale convective heat transfer measurements

The building used for the full-scale heat transfer measurements was a large double fronted garage, situated on the University sports playing fields at Norton, some 3 miles S-SE of

the University. It has dimensions, in plan, of 9.60 x 5.03m, with its long axis running roughly East-West. The garage is 4.59m high at the ridge with a roof pitch of 35° (see Figure 4.1).

It is a gable ended structure, thus replicating, despite its size, normal low-rise dwelling geometry. The Building Research Establishment, Garston, UK, use, for their full-scale low rise building wind loading research programme, a semi-detached house of plan dimensions 13.3 x 7.0m. This house can be fitted with roofs of various pitch; with the 35° pitch roof it has a ridge height of 7.3m. Thus the garage site at Norton has linear dimensions approximately 0.7 times those of the standard house used by the Building Research Establishment.

The terrain surrounding the building is reasonably uniform and flat. Four views, looking approximately North, South, East and West of the garage, are shown in Figures 4.2, 4.3, 4.4 and 4.5 respectively. From these views it can be seen that South of the building is a long stretch of open grass land with a fetch length approximately 250m. To the North there is some housing stock but the ground slopes away behind the row of buildings shown. There are no major obstructions and the roofs of the houses nearest the garage are level with its base. To the West there is a gravel car park 50m in length and then some houses. The Eastern quadrant is also fairly clear from obstructions save for a small garage situated 3m away from the test site building. This small garage is approximately 3m high.

As to accessibility and occupancy patterns, these again provided no real problems. The site could be reached, by van, from the University within 20 minutes and the Estates and Buildings Office furnished the author with keys for both the main gate to the playing field site and to the garage itself.

The building is only normally used for the storage and repair of the playing field groundsman's equipment. Hence there was no real disturbance of the occupants by the installation of the test-rig or the retrieval of data.

Minor structural alterations to the building could be carried out, with the approval and supervision of the University Estates and Buildings Office.

Thus, this site and building, whilst not ideal - the main discrepancy being in building size, was felt to satisfy adequately the four criteria stated in Section 4.1.1 for it to be used for the full-scale convective heat transfer measurements.

## 4.2 The Choice of the Method to be Employed to Evaluate the Convective Heat Transfer from a Large Flat Plate in the Natural Environment

From a consideration of the work reported in Chapter Three of this thesis it can be seen that four main methods have been employed for the determination of the convective heat transfer coefficient from a flat plate. These are:

(i) Steady state energy balance on a heated plate e.g. Parmelee and Huebscher [1947].

(ii) Single plate and heat meter e.g. Rowley [1932].

(iii) Dual plate and heat meters e.g. Ito et al [1972].

(iv) Mass transfer analogy e.g. Sparrow [1971].

The most predominant method for evaluating the heat transfer coefficient from a flat plate is that of applying an energy balance equation to a heated element. However, with the exception of Sturrock [1971] and Test [1981] measurements performed in the natural environment have utilised a two plate and heat meter system, as descibed in Section 3.7.

In order to assess the potential of the four systems shown above it is necessary to restate the objectives of this series of experiments. These are to evaluate, under a variety of wind speeds and directions, the average convective heat transfer coefficient from the upper surface of a flat plate solar collector in the natural environment.

In order to reduce the effects of surface length, temperature difference and surface roughness to a minimum, it was decided to evaluate the convective heat transfer coefficient from a smooth flat plate with dimensions similar to typical solar collectors, i.e. 1 x 2m. Also temperature differences between the plate and the ambient air of the order of 10-50 K were to be maintained. Once again these temperature differences are typical of actual flat plate collectors.

The governing factor in the choice of the system to be used for the measurements uses the large size of the plate.

The mass transfer method was eliminated immediately, not only for the difficulty in producing such a large flat surface of the required medium, but also because this method would require the installation, removal and weighing of the plate many times. This was thought to be impractical.

A heat meter system, especially a dual plate method seems, at first sight, to offer the optimum solution. By careful use, the two plate system elimates the need to measure the solar irradiance and long wave radiation incident on the plate (see Section 3.7).

However, in order to make accurate measurements of the heat transfer coefficient, using this system, it is required that the two adjacent plates be kept at slightly different uniform temperatures, approximately a 5K difference for the plate temperature ranges under consideration here. This is not a realistic representation of the temperature profile of the upper surface of a flat plate solar collector, and uniform temperatures over a plate this large would be difficult to maintain. Sharples [1981] describes the manufacture of a heat meter plate 0.25 x 0.25m in area and states that "the construction took several weeks as the process was slow and susceptible to breakages". If the overall convection coefficient of the plate was to be evaluated then this would require two heat meters some 6 times this area. These points, made above, led to a rejection of the use of a heat meter system for the situation under consideration here.

The use of the remaining method, i.e. an energy balance on an electrically heated plate, is not without its difficulties. Consider the steady-state energy balance equation for a plate electrically heated from behind, its upper surface exposed to the natural environment:

$$q_e + \alpha I + \epsilon R_L = \epsilon\sigma T_s^4 + q_{con} + h(T_s - T_A) \qquad (4.1)$$

where $q_e$ = electrical heat input $Wm^{-2}$

$\alpha$ = combined solar absorptance of plate for direct and diffuse short wave radiation

$I$ = total solar irradiance incident upon the plate $Wm^{-2}$

$\epsilon$ = long wave emittance of plate

$R_L$ = total long-wave irradiance incident upon the plate, $Wm^{-2}$

$\sigma$ = Stefan Boltzman constant = $5.6697 \times 10^{-8}$ $Wm^{-2}K^{-4}$

$T_s$ = plate surface temperature K

$q_{con}$ = heat losses via conduction $Wm^{-2}$

$h$ = convective heat transfer coefficient $Wm^{-2}K^{-1}$

$T_A$ = ambient temperature of surrounding air, K

Equation 4.1 can be re-arranged to give

$$h = \frac{q_e + \alpha I + \epsilon R_L - \epsilon\sigma T_s^4 - q_{con}}{(T_s - T_A)} \quad Wm^{-2}K^{-1} \qquad (4.2)$$

The main problem here is the variability of the incident solar irradiance I. The total solar irradiance incident on a surface consists of two parts, direct and diffuse. The direct solar radiation is the solar radiation flux, associated with the direct solar beam, from the direction of the sun's disk. Diffuse radiation reaches the surface from the rest of the whole sky hemisphere, from which it has been scattered in passing through the atmosphere.

Due to the variation of the earth's position relative to the sun and the daily rotation of the globe the value of I is highly variable, both annually and diurnally. The problem of the variabiity of solar irradiance is further exacerbated by cloud cover. A suitably placed large cumulus cloud may reflect the direct component of the solar irradiance thus increasing the intensity of the radiation incident on the earth's surface. As clouds are continually in motion, this increase in intensity will only usually persist, at a particular point on the globe, for a few minutes. Normally, the total solar radiation received on a surface, averaged over a period of time, will be less when there is cloud cover than when there is not.

Loudon [1965] in conjunction with Lumb [1964] proposed a simple multiplying factor to be applied to the total solar irradiance incident on a surface, for different cloud conditions. These range from 1.0 for a virtually clear sky through 0.7 for thin layers of medium cloud and 0.35 for thick layers of medium cloud to 0.17 for a very overcast sky. It must be noted that several categories of cloud cover may occur each day.

This variation of I may give rise to small but rapid changes in the temperature of a surface, especially one of low thermal capacitance such as a metal plate - which is likely to be used for heat transfer measurements.

One method by which this problem could be eradicated would be to follow the example of Ito et al [1972] who made measurements only at night. Sharples [1981] points out, however, that for large buildings the thermal regime existing around the building would be different during the day time than at night.

As solar collectors are designed specifically for operation during daylight hours and on average the mean wind speed is higher in the day than the night, (Lacy [1977]) it was felt that to make only night time measurements would be inadequate.

Because of these non-steady state conditions the only solution therefore available is to average data over a given period in order to minimise the effect of these time wise variations. Hence, with these possible limitations in mind, it was decided to utilise the method of applying an energy balance equation to an electrically heated flat plate.

## 4.3 A Description of the Electrically Heated Flat Plate used to Perform the Full-Scale Convective Heat Transfer Measurements

The plate was, essentially, a sandwich type construction held together by a wooden frame. An exploded view of the plate, showing its various components is given in Figure 4.6. Each constructional element is discussed in turn, below.

### 4.3.1 The exposed aluminium plate

Exposed to the environment was a 2mm thick aluminium plate of dimensions 0.92 x 1.83m. It can be seen from Figure 4.6 that the wooden weather sealing frame overhangs the plate by 10mm, thus giving it an exposed area of 0.89 x 1.81m. This was the plate area used in the caluclation of the heat transfer coefficient. Set into the plate, at centres of equal areas, were nine T-type (copper/copper nickel) thermocouples, each with a bead diameter of 0.5mm. They were positioned so as the centre

of the bead corresponded to the centre of the thickness of the plate. The thermocouples were held in position with epoxy resin, which was also used to smooth over the surface after the thermocouples were implanted.

The decision to embed the thermocouples in the plate itself and not stick them on the surface a method used by some experimenters e.g. Rowley [1930 (a)], was made after consideration of the following two points.

If the thermocouples were to be stuck to the surface of the plate they would be more exposed to natural weather conditions, such as rain, heavy winds or snow. This would render them more susceptible to breakage and hence replacement. Once the plate was installed on the building roof this replacement would be very tedious.

Rowley's main reason for fixing thermocouples to the surface and not to embed them within it was that a thermocouple thus placed would be measuring the body temperature of the material and not that of its surface. A consideration of Fourier's law of conduction, equation 2.2 shows

$$\Delta T = \frac{q\Delta x}{k} \quad , \quad K \tag{4.3}$$

where $\Delta T$ = The temperature difference across the plate K

$q$ = The heat flow W

$\Delta x$ = The plate thickness m

$k$ = Thermal conductivity $Wm^{-1}K^{-1}$

Thus if the temperature gradient $\Delta T$ within the plate is large then the above effect will be significant. In Rowley's case the ratio $\Delta x/k$ was of the order of 0.01; in this current series of experiments it is of the order of 0.00001. Thus the positioning of the thermocouples in the body of the material is justified as a power of one hundred thousand watts per square metre would be required to produce a temperature difference, across the plate surfaces of 1 K. As will be seen later the actual power levels used were of the order of a thousand times less than this value.

All the thermocouple leads were led out under the aluminium sheet and through a groove in the frame to a weather proofed connection box on the outside of the plate frame.

The exposed surface of the plate was sprayed several times - to give an even coating - with matt black paint. This paint had known values for its solar absorptance $\alpha_p$ and long wave emittance $\varepsilon_p$ of 0.97 and 0.90 respectively. These figures were supplied by Dr. Michael Hutchins of University College, Cardiff.

During the course of the full scale experiments the upper surface of the plate was frequently examined and if any flaking or blistering of the paint had occurred it was resprayed.

### 4.3.2 The heating element

Beneath the aluminium plate was the heating element. This element was constructed from a commercially available radiant ceiling heating system called "Flexel", it is manufactured by Thermaflex Limited, Scotland.

Flexel is a thin, flexible sheet of glass cloth which has been impregnated with a conducting P.T.F.E. dispersion. Copper strip electrodes are stitched along each of the long edges of the sheet, and electrical insulating film is laminated to each face. The total thickness of the heater is about 2mm.

A potential difference applied across the electrodes produces uniform resistive heating over the sheet. Temperatures of 393 K may be safely maintained, although the suggested normal operating temperature for domestic heating is 323 K. The area of sheet required was of non standard size and the author is grateful to Mr. R.M. Adams of Thermaflex for manufacturing a unit of the required dimensions. The power leads to the plate were led, via the connecting box on the side of the plate, into the building and to a specially designed power supply.

This supply consisted, of a solid state, phase controlled a.c. power regulator (this was supplied by Radio Spares Ltd., Serial number 308-584). A schematic circuit diagram of this device is shown in Figure 4.7. In this case the load resistance is provided by the Flexel sheet and the control resistance by 10 series connected 240 ohm standard resistors. Using this device it was possible to supply power to the plate at nine discrete levels.

It can be seen from equation 4.2 that the value of the electrical power input to the plate is required for the calculation of the convective heat transfer coefficient. The evaluation of the 9 power levels available to heat the plate was performed in a laboratory situation using an a.c. watt meter. The initial experiments consisted of the testing of the plate under still air conditions.

It can be seen from Figure 4.7 that if the control resistance is kept constant then the power supplied to the load will be dependent on the value of the load resistance $R_{load}$. No information on the value of the resistance of the Flexel sheet was available, however, the resistance of most conductors increase slightly with temperature.

The temperature of the aluminium plate, for a given nominal electrical power input, is likely to vary with time in the natural environment. This is due to the variability of the other energy inputs to the plate e.g. solar radiation and the forces acting to remove energy from its surface i.e. the wind. It was felt that these temperature changes, on the upper surface of the plate, may effect the temperature of the Flexel sheet and hence alter its resistance.

A second series of experiments were carried out using a large, variable speed fan to induce various temperature levels on the aluminium plate surface. Mean plate temperatures in the range 293-323 K were produced and it was found that the various power levels produced were constant within the accuracy of reading the watt meter. This indicates that either, the Flexel sheet has a low temperature coefficient of resistance or that its temperature is insensitive to the temperature of the aluminium plate. Either way, this implies that the power levels as presented in Table 4.1, in terms of $Wm^{-2}$ are adequate for the full range of environmental conditions encountered.

Table 4.1 Available Plate Power Levels Expressed in $Wm^{-2}$

| Power Level | Power Supplied to Plate $Wm^{-2}$ |
|---|---|
| 1 | 165 |
| 2 | 380 |
| 3 | 625 |
| 4 | 928 |
| 5 | 1225 |
| 6 | 1523 |
| 7 | 1785 |
| 8 | 2020 |
| 9 | 2220 |

4.3.3 The thermal insulation and plate frame

Despite the layer of bright aluminium foil placed behind the Flexel to reflect heat back in the direction of the exposed plate, back loss via conduction could not be eliminated completely.

To reduce this loss to a minimum two sheets, each 50mm thick, of expanded polystyrene foam were installed beneath the reflective aluminium foil. This foam (supplied by Sheffield Insulations Limited) has a stated maximum operating temperature of 353 K and a thermal conductivity of 0.037 $Wm^{-1}K^{-1}$.

In order to determine the heat lost by conduction, the temperature difference across the top sheet of foam was measured using five pairs of thermocouples. These thermocouples were of a similar type and installed in a similar manner to those described in Section 4.3.1. Four of the five pairs were positioned at the centre of equal quadrants of the foam surface, the remaining pair at the centre of the foam surface. Their leads were led away to the connecting box outside the plate.

The whole plate was held rigid and compressed very slightly, in order to afford good thermal contact between the various elements, by a 50mm wide softwood frame with a 10mm hardwood lip. The join between the aluminium plate and the overhanging lip was sealed using weather resistant silicon rubber. This was in order to prevent rain penetrating into the body of the plate. The area of the whole construction including the frame was 1.02 x 1.93m.

### 4.3.4 The connecting box

The connecting box on the side of the plate has already been mentioned. This box had dimensions of 10 x 10 x 350mm and was attached to one of the long edges of the plate frame, slightly off centre. Data signals were to be recorded at some distance away from the plate itself i.e. in the building. Connection of the cables leading into the building were made using the connecting box after the plate had been installed on the roof. This allowed the installation of the plate to be carried out free from the incumbrance of long lengths of trailing cables.

## 4.4 The Installation of the Heated Plate on the Test Building Roof

Two main methods of mounting the plate on the roof were discussed. The first involved removing tiles from the roof and bolting the plate to the roof joists. This method is usually employed for actual solar collectors (e.g. see Wozniak [1979]). After consultation with the University Estates and Buildings Office, this method was rejected. It was felt that this method would lead to too much structural damage of the building and, as the plate was to be removed after the experiments, that re-weather proofing the roof would be difficult.

The plate was eventually mounted on the south facing roof, with its long axis running parallel to the ridge line, by clamping it to a scaffolding frame. Figure 4.8 shows an overall view of the garage with the plate in position and Figure 4.9 illustrates the plate and its mountings on the roof. The plates left hand edge is 3.42m from the left hand gable end and its bottom edge is 0.82m, up the roof slope from the gutter line.

From Figure 4.9 it can be seen that the plate is clamped to two lengths of scaffolding on its long edges. This scaffolding is in turn clamped to two other lengths running up the roof pitch. Wooden beams were placed under this scaffolding spreading out the load of the plate across the roof span, thus preventing damage to the tiles.

Because the plate was not attached directly to the roof, it was necessary to counter balance its weight with two lengths of scaffolding running down the opposing roof pitch. These were clamped at the ridge line and can be just seen in Figure 4.9. Positioned in this manner the plate sat proud of the roof with a gap of some 200mm between its back and the tiles. This is not usually the case with actual collectors, so a valance made of 3mm ply-wood was attached to the edges of the plate. The distance between the top aluminium sheet and the roof tiles was 0.33m, thus giving the plate an aspect ratio of between 1:3 and 1:6 depending upon the direction of the wind.

With the plate in this position connections for the 19 thermocouples and the power leads to the "Flexel" sheet were made at the connecting box. The thermocouples were connected using standard miniature connectors, supplied by Comark Electronics Limited, to a multi-core thermocouple cable. This was fed into the building, by removing one of the ridge tiles, to a data logging system.

The "Flexel" power leads were led in a similar manner to the power supply and control unit as described in Section 4.3.2.

## 4.5 The Measurement of the Environmental Parameters Required to Evaluate the Convective Heat Transfer from the Full-Scale Heated Flat Plate

In order to evaluate the heat transfer coefficient from a flat plate in the natural environment using equation 4.2, it is necessary to measure the following environmental parameters: solar irradiance I, incident longwave radiation $R_L$ and the air

temperature $T_A$. As the heat transfer data is to be correlated against wind speed and wind direction these must also be measured. The measurement of each of these parameters is considered, in turn, in this section.

### 4.5.1 Solar radiation

Solar radiation, as described in Section 4.2, has wave lengths in the range 0.3 to 3.0 μm. An instrument for measuring the total hemispherical solar (beam + diffuse) radiation is known as a pyranometer. A full discussion on the types and operation of these instruments is given by Duffie and Beckman [1980].

The instrument used in this series of experiments was a Kipps pyranometer (see Figure 4.10). It utilises a thermopile detector to measure the temperature difference between the black detector surface and the white housing of the instrument. This temperature difference, and hence the output from the thermopile in millivolts, is proportional to the incident solar radiation. Two concentric, optically ground, glass hemispheres cover the detector surface. These protect the detector from the natural elements such as wind and rain; they also serve to prevent any incident long wave radiation reaching its surface. Glass can be considered opaque to radiation at wave lengths longer than 3 μm.

The intensity of solar radiation incident on an inclined surface is different to that on a horizontal surface. It is therefore necessary to place the pyranometer with its detector in the same plane as the heated plate. The instrument used, which was located on the roof of the building 0.3m from the top

left hand corner of the plate, (see Figure 4.9) was supplied with a horizontal positon calibration certificate. This calibration had been performed recently and stated that the instrument had a linear response of

$$I = 91.56\ e_p + 6.349 \quad Wm^{-2} \qquad (4.4)$$

where $e_p$ = the output from the thermopile, in millivolts

There is some evidence that the calibration of a pyranometer changes if the instrument is inclined to the horizontal. The reason for this appears to be changes in the natural convection patterns inside the glass dome, which changes the manner in which heat is transferred from the hot junctions of the thermopile to the cover and other parts of the instrument.

Norris [1974] measured the response of four pyranometers, when subjected to the radiation from an incandescent lamp source, at various inclinations. Although he found errors of up to 10% at large angles of inclination, the maximum error found at 35° - the pitch of the building roof was $\pm$ 2%. It was therefore felt that the use of equation 4.4 was justified.

### 4.5.2 Long wave radiation

All bodies at temperatures above absolute zero emit electromagnetic radiation. This is known as thermal radiation and its intensity is proportional to the fourth power of the absolute temperature of the body. The wavelengths of the emitted radiation is also dependent on the body temperature. Generally, the hotter the body the shorter the wavelengths

emitted. For example Duffie and Beckman [1980] show that the thermal radiation emitted from a source at a temperature of 400 K has wavelengths longer than 3 μm. Thermal radiation in the natural environment originates from sources at temperatures near the ambient temperature. Subsequently this radiation, which is emitted by the atmosphere, by buildings or by any other body at ordinary temperatures, has wavelengths greater than 3 μm. Hence it is known as long wave radiation.

Direct measurement of long wave radiation is difficult. One method which can be used is to measure the total radiation on a surface i.e. both long and short wavelengths, and subtract the amount of incident solar radiation from the value obtained. This method was employed in this series of experiments.

A Funk-type net radiometer, situated on a bracket at the West end of the roof and inclined at the correct angle (see Figure 4.11) was used to make these measurements. This instrument is similar in construction to the pyranometer described in Section 4.5.1. It is, however, different in two important aspects.

The single protective hemispherical bubble over the thermopile is made, in this case, of polythene and not glass. This material has the property of being transparent to both short and long wave radiation. Because the polythene is flexible it must be continually kept under pressure by dry air. This air was supplied via a length of tubing from a small pump situated inside the building. Before reaching the radiometer the air passed through an in line vessel containing dry silica gel; this gel was replaced at regular intevals with a fresh

supply. Due to its delicate nature the bubble was very susceptible to environmental deterioration and so this too was replaced at frequent intervals.

The second difference between this instrument and the pyranometer is that instead of the thermopile output being proportional to a temperature difference, it was proportional to the difference between the incoming radiation and the radiation received on its lower surface from a cavity. This cavity acted as a black body so:

$$R_L = \sigma T_c^4 + C_r e_r \quad Wm^{-2} \qquad (4.5)$$

where $R_L$ = the incident long wave radiation, $Wm^{-2}$

$\sigma$ = the Stefan Boltzman constant, $Wm^{-2}K^{-4}$

$T_c$ = the cavity temperature, K

$C_r$ = the radiometer calibration constant

$e_r$ = the thermopile output, millivolts

The radiometer cavity temperature was measured by a T-type thermocouple. If there is more incident long wave radiation than is being emitted by the cavity then the thermopile output will be +ve, if there is less it will be -ve.

A calibration constant of 33.6 $Wm^{-2}K^{-1}mV^{-1}$ was originally supplied by the manufacturers. This was some 20 years ago. With a view to the possible deterioration of the sensitivity of this instrument over this period it was recalibrated using the method recommended by Sharples [1981]. This calibration is described in the next section.

### 4.5.3 The calibration of the funk type net radiometer used in the full-scale convective heat transfer measurements

The radiometer was calibrated over the surface of a constantly stirred water bath, in a darkroom to prevent the incidence of any unaccountable short wave radiation. This highlights one possible failing of this calibration method, i.e. that the radiometer is calibrated only for long wave thermal radiation. It must be assumed therefore that the response of the thermopile is wavelength independent. A motor which drove the water bath stirer was shielded with aluminium foil for similar reasons to the above.

Surface tension held a T-type thermocouple within the first mm of the water; this facilitated the measurement of the water surface temperature $T_w$. The value of the total long wave emittance of the water is given by Holman [1981] as $\epsilon_w = 0.95 - 0.963$ for the temperature 273-373 K. A value of 0.95 was assumed for this calibration series.

The side of the thermopile opposite to the cavity was suspended centrally some 40mm above the surface of the water, level with the top of the sides of the bath. In plan the water bath had dimensions of 250 x 380mm; this gives the radiometer of a mean field of view of the water of approximately 84%. The remaining 16% of view "seen" by the radiometer consists of the glass sides of the water bath. Glass has an approximate emittance of $\epsilon_g = 0.94$ and the sides of the tank will be at a

temperature close to that of the water. Coupled with the fact the sides will emit radiation at large angles of incidence with respect to the thermopile, leads to the conclusion that the resultant errors produced by the restricted field-of-view will be somewhat less than the original figure of 16%.

In this situation, the heat flow $q_r$ across the thermopile and hence its output is given by:

$$q_r = C_r e_r = \sigma T_c^4 - \varepsilon_w \sigma T_w^4 \quad Wm^{-2} \tag{4.6}$$

Assuming $T_c$ to be constant throughout the calibration procedure the above can be rearranged to give

$$e_r = \frac{-1}{C_r} \varepsilon_w \sigma T_w^4 + \frac{\varepsilon_w \sigma T_c^4}{C_r} \quad mV \tag{4.7}$$

Therefore, plotting $e_r$ against $\varepsilon_w \sigma T_w^4$ should result in a straight line of gradient $-1/C_r$ and intercept $\sigma T_c^4/C_r$.

The water temperature was varied between 288 K and 296 K and throughout the calibration procedure $T_c = 294.1 \pm 0.5$ K. Twenty data points were taken and a linear regression of the radiometer output on $\varepsilon_w T_w^4$ was made i.e.

$$e_r = -0.024 \ \varepsilon_w \sigma T_w + 10.034, \quad mV \tag{4.8}$$

$$r = 0.984$$

where $r$ = the linear regression correlation coefficient

Comparing equations 4.7 and 4.8 gives $C_r = 41.8$ $Wm^{-2}$ $mV^{-1}$; this represents a decrease in sensitivity of the instrument, since the original calibration, of some 25%.

### 4.5.4 Air temperature

Air temperatures were measured using a shielded T-type thermocouple mounted on the arm of the radiometer (see Figure 4.11). This position was chosen because here it would be outside the influence of the temperature field created by the heated plate.

The shield allowed the free passage of air around the thermocouple whilst protecting it from (i) radiation by day from the sun, the ground and neighbouring objects (ii) loss of heat by radiation to the cold ground at night, and (iii) the detrimental effects of precipitation.

### 4.5.5 Wind speed and wind direction

Measurements of wind speed and wind direction were made with a 3-cup anemometer and a windvane supplied by Vector Instruments Ltd., Wales. They were mounted, together, on a bracket and mast which positioned them 1.5m above the ridge line of the building, at its most westerly point, thus giving them a distance above the ground of 6m. The mast arrangement is shown in Figure 4.11. Of course the anemometer and windvane could have been positioned at any height, within constructional possibility, above the roof. The choice of 1.5m was, in a way, arbitrary. However, a mast of this height provided a very stable structure, a much taller mast may have required guy ropes to ensure stability. Wind speed measurements at this position also show some compatibility with the only other known examination of the convective heat transfer from an inclined flat plate in the outdoor environment, i.e. those of Test [1981]. Test, as will be recalled from Section 3.4, evaluated the wind speed at a distance of about 1m above his test surface.

Cables from the two instruments led into the building through the hole made by removing one of the ridge tiles to a junction box and power supply unit. Connections from this box were made to the data logging system. The output from the anemometer was linear with wind speed, i.e.

$$V_{6R} = 4.83\ e_a \quad ms^{-1} \tag{4.9}$$

where $V_{6R}$ = the wind speed 6m above the ground over the roof, $ms^{-1}$

$e_a$ = the output from the anemometer, volts

The value 4.83 was derived from the calibration data supplied by the manufacturers and was stated to be accurate to 2% over wind speeds in the range 0-15 $ms^{-1}$; these are speeds likely to be encountered in the natural environment at this height.

One type of problem often encountered using this type of instrument occurs with the measurement of low wind speeds. At these speeds the wind may not be strong enough to overcome the inertia inherent in the anemometer. The lightweight construction and bearing mechanism of this instrument give it the low operating speed of 0.2 $ms^{-1}$. The only drawback with this design is that it is more susceptible to free stream turbulence and short duration gusts in the wind.

A similar minimum operating speed is quoted for the windvane, and its accuracy is stated as better than $\pm$ 2%. The output from the windvane is also in volts, and corresponds to a range of 600° with automatic switching at the range extremities. This means that the output can be either +ve or -ve. The instrument was so positioned as to give a reading directly proportional to the angle of incidence of the wind on the plate, $\Theta$. This angle is defined in Figure 4.12.

If the output $e_v$ from the windvane is +ve then

$$\Theta = 45 \quad e_v \qquad \text{degrees} \qquad (4.10)$$

and if it is -ve then

$$\Theta = 360 + 45 \quad e_v \qquad \text{degrees} \qquad (4.11)$$

If the wind incidence angle is greater than 180° then it is converted into its -ve counterpart by simply subtracting 360° from its value.

Wind speeds were also measured at various heights above the ground at a site on the playing field in front of the building. The reasons for making these measurements are given below.

The most widely available wind statistics in Britain are from Meteorological stations. These stations measure the wind speed at a standard height of 10m above the ground and away from any obstructions. It was therefore felt necessary to evaluate this wind speed and compare it to the wind speed measured over the roof in order to correlate the heat transfer measurements with this standard speed. This speed will be referred to as $V_{10}$.

The presence of the building may influence the flow characteristics of the wind around it. This may effect the wind speed $V_{6R}$ as compared to the wind speed at a similar height without any obstructions present $V_6$.

A recent model study by Kind [1983] produced correlations between the convective heat transfer coefficient and the free stream wind speed, as measured at the mid collector height, $V_H$. Several of the correlations discussed in Section 3.8 also require $V_H$ as an input to produce a design value of h for flat plate solar collectors. Therefore it was felt necessary to compare the free-stream wind speed at this height (in this case 3.6m) with the continuously measured roof wind speed $V_{6R}$.

These wind speed measurements were generally made at a position some 80m from the building using a cup anemometer with similar characteristics tq the one used to measure $V_{6R}$. Remote sensing of the output of this instrument in the building was considered impractical, as the long length of cable required would hinder the cutting of the playing field grass. Therefore its output was converted directly into wind speed values and recorded by a battery operated moving chart device placed at the foot of the anemometer mast. Both the anemometer and chart recorder were borrowed from the University's Geography Department for the duration of the experiment. No device was available to evaluate the wind direction at this position.

The mast was of a hydraulic type which could be pumped up to position the anemometer head at any height above the ground between 2 and 10m. Because the fields were in frequent use for the playing of sports, it was not possible to make continuous measurements of wind speed at this site during the heat transfer experiments. The mast and chart recorder as shown in Figure 4.13 are set up to measure the free-stream wind speed at mid-collector height.

## 4.6 The Method Employed for Recording the Data Obtained from the Full-Scale Convective Heat Transfer Measurements

All the signals from the instruments described in Section 4.5, except that from the free-stream anemometer, were carried along cables through the roof space of the building and connected to the input port of a Hewlett Packard 3497A data aquisition unit, as were the plate thermocouples. By

controlling this unit with a HP85 micro-computer, and associated software, it was possible to store these signals on miniature magnetic ribbon cassettes. The thermocouple outputs were recorded directly in degrees centigrade, the others as voltages. A full description of the logging system and its use is given the Hewlett-Packard Operators Handbook [1981].

Ideally, when measuring a number of parameters they should be recorded in time increments equivalent to the rate of variability of the fastest changing parameter. Here, this is the wind speed. This varies continuously about a mean value due to turbulence and gusts. However, due to the large number of inputs to the logger and the finite time required to store the data, it was not possible to record the whole data set at intervals of less than two minutes thirty seconds. The problems encountered when recording continuous variables at discreet intervals will be discussed in Section 5.1. Each block of recorded data will be subsequently referred to as a "scan".

## 4.7 The Experimental Procedure Employed in the Full-Scale Convective Heat Transfer Measurements

Before starting any experimental run the instrumentation and thermocouples were checked to ensure they were in working order. This was done by displaying their various outputs on the micro-computer screen. The pyranometer and radiometer covers were checked for deterioration and cleaned or replaced as necessary. If the silica gel, used for drying out the air supply to the radiometer, had turned pink it was replaced with a fresh supply. The windvane was provided with a remote calibration facility at a junction box in the building, this calibration was performed before the start of any run.

The plate was usually left between experimental runs with the heater element switched on, at one of the lower power levels given in Table 4.1. This was to ensure a shorter warm up period when the plate was switched to the required power level for the run, and to evaporate any moisture which had settled on the plate.

Power level 3 i.e. 625 $Wm^{-2}$ generally proved to be adequate for producing the required plate-air temperature, 10-50 K, under most conditions. However, other power levels were used at times in order to achieve a reasonable plate temperature under extreme conditions of air temperature and wind speed. Local 12 hour weather forecasts were consulted in order to ascertain, approximately, the meteorological conditions likely to be encountered during any experimental run. These forecasts were most useful in predicting the prevailing wind direction thus enabling an experimental run to be performed to examine a specific wind incidence angle.

The start of the run was marked by activating the data logger to take the first reading and the recording of the following information. Run number, tape number, date, time (GMT) and the heater power level.

Tape storage capacity limited the maximum length of each run to 26 h. Not all runs, however, were of this length. Runs of lengths as short as 8h were performed, usually to gather data under specific meteorological conditions, i.e. such as a particular wind direction, which persisted only for this duration.

At the end of the run the data tape was retrieved and returned to the University in order to be analysed. This analysis together with a discussion of the results obtained from the full-scale measurements will be described in Chapter Five.

## Conclusion

The setting up of an experimental rig to evaluate the convective heat transfer coefficient from a large flat plate, mounted on a building roof has been described. Problems encountered and justification of the methods used have been discussed.

It is readily understandable why experiments of this type are not often performed. They are difficult to make, laborious to maintain, time consuming to analyse and, because of their complexity, do not lend themselves to simple generalisations. However, these type of measurements are of vital importance in the quest to gain a deeper understanding of the convective behaviour of full scale heat transfer systems.

The forced convective heat transfer coefficient for the top surface of a solar collector is still evaluated using relationships derived from small scale wind tunnel studies, (see Section 3.8). These relationships show no dependence upon wind direction and show no dependence on plate size. One of the primary aims of this series of experiments is to justify or repudiate these assumptions. The results obtained from the full-scale measurements are presented in the next chapter.

Figure 4.1 Norton test site garage - before installation of experimental equipment

Figure 4.2 Terrain surrounding test site building - Northern aspect

Figure 4.3 Terrain surrounding test site building - Southern aspect

Figure 4.4 Terrain surrounding test site building - Eastern aspect

Figure 4.5 Terrain surrounding test site building - Western aspect

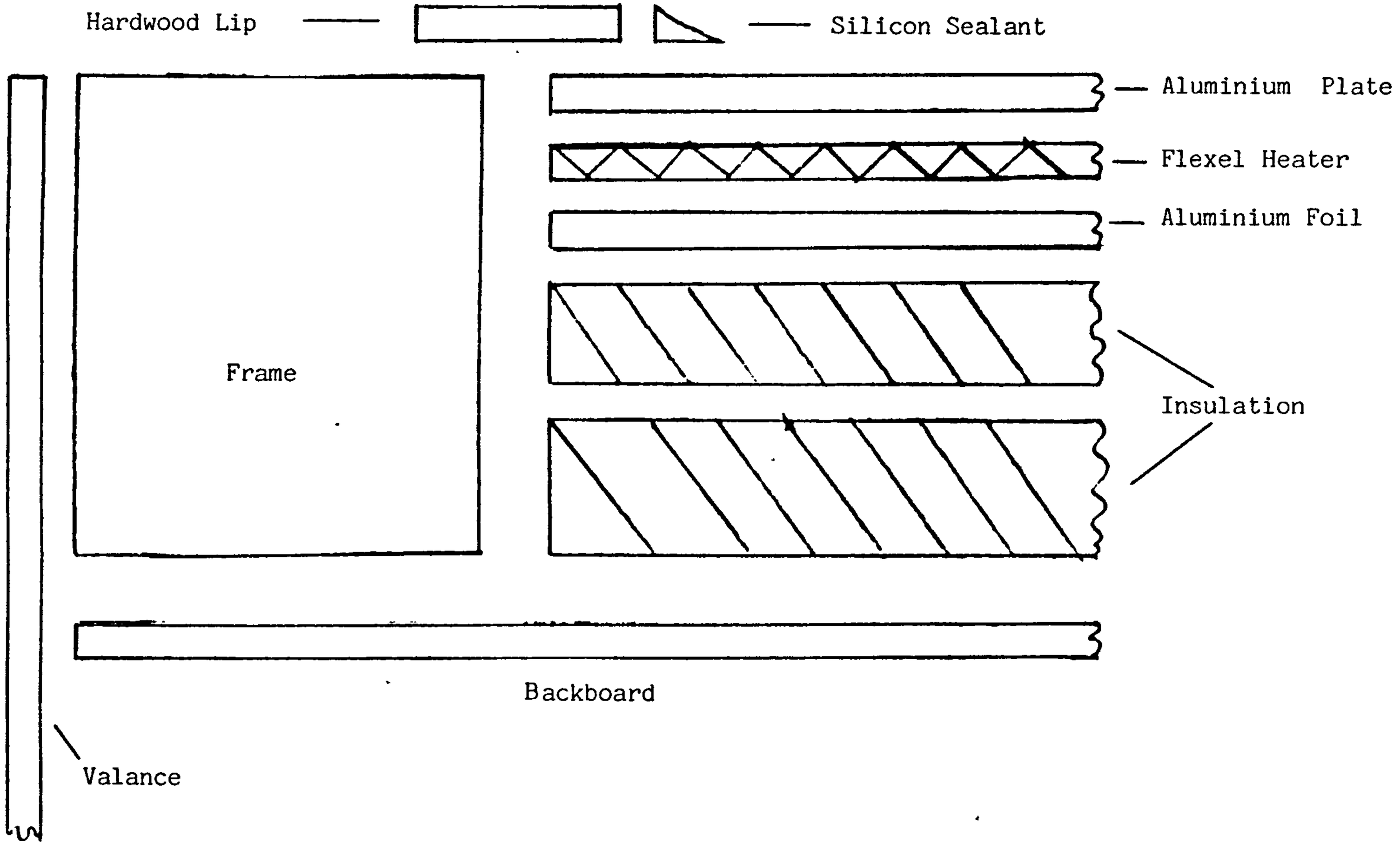


Figure 4.6 Exploded view of roof mounted heater plate

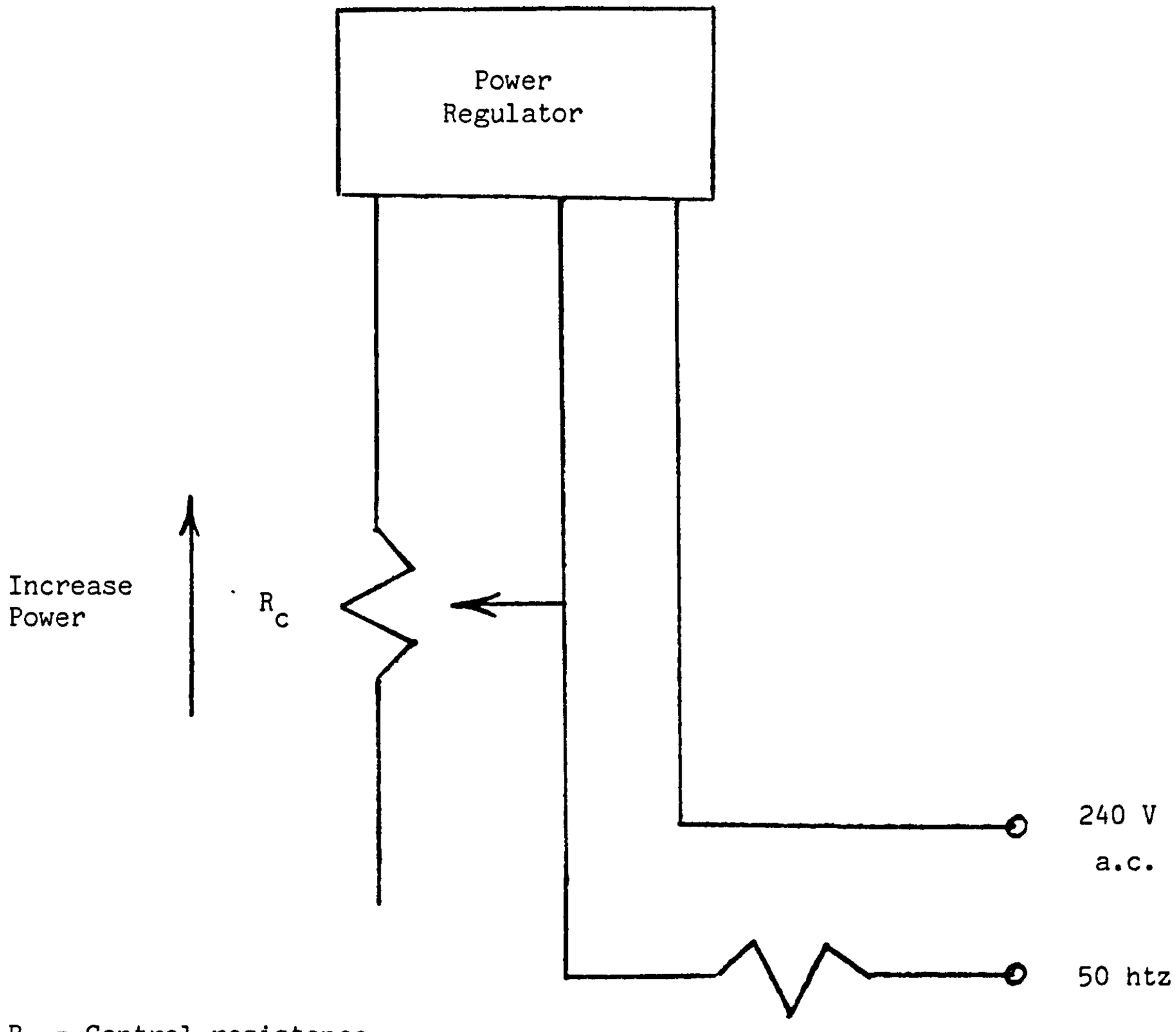


Figure 4.7 Schematic diagram of heater element power control circuit

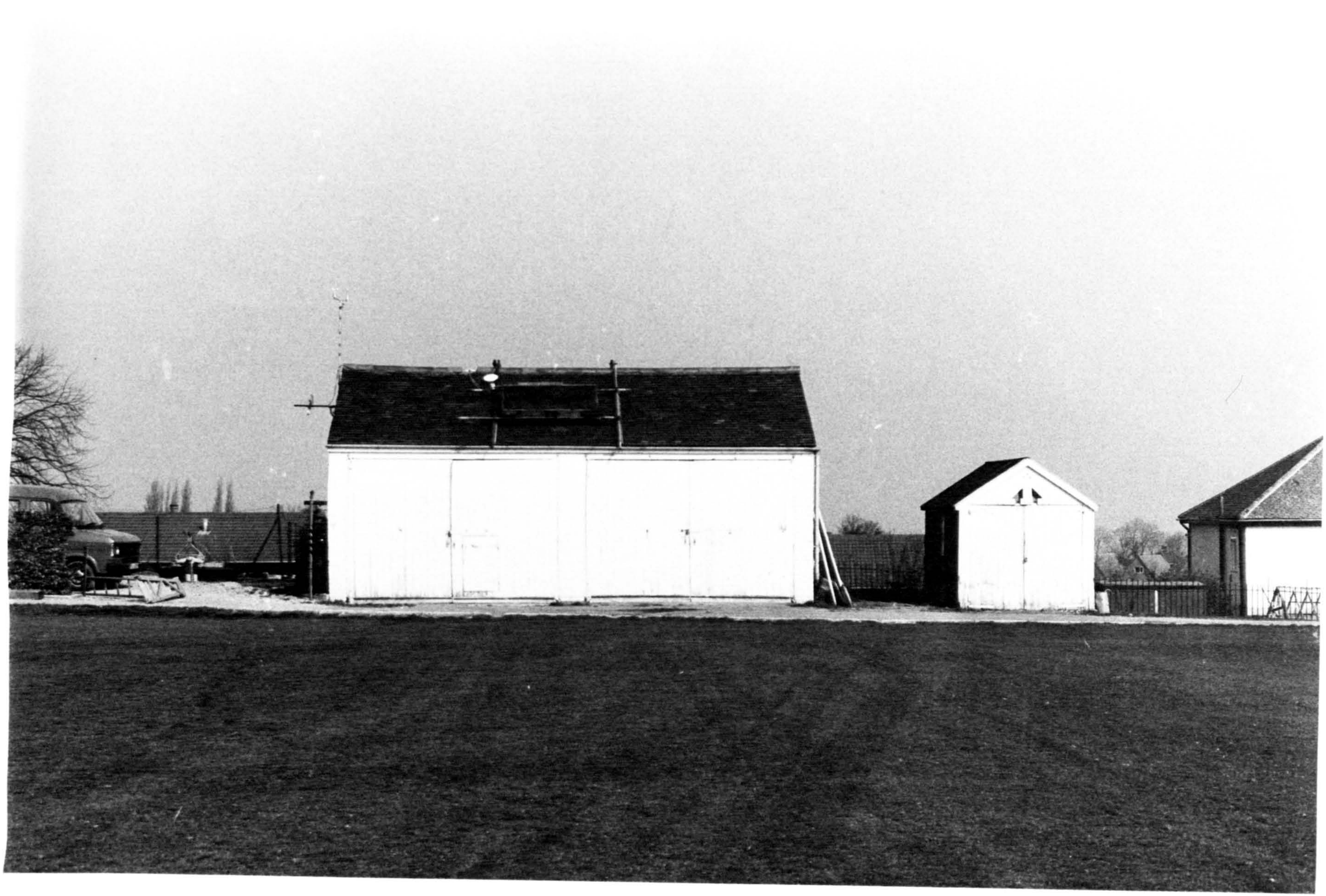

Figure 4.8 Overall view of heater plate and instrumentation mounted on the test building

Figure 4.9 Close up view of heater plate assembly mounted on the test building roof

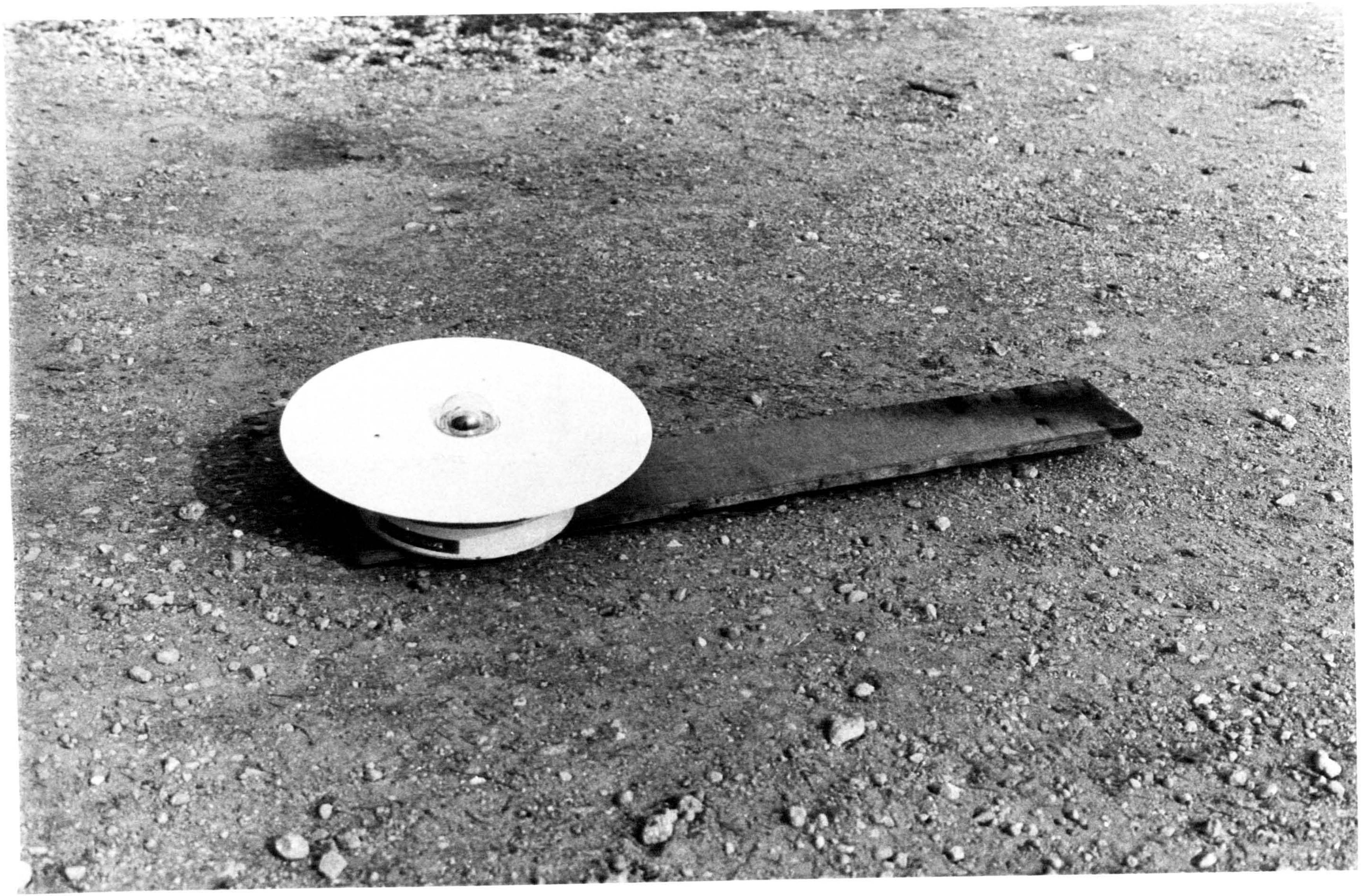

Figure 4.10 Kipps pyranometer used for measuring incoming short wave (solar) radiation

Figure 4.11 Gable end mounted anemometer, wind vane and net radiometer

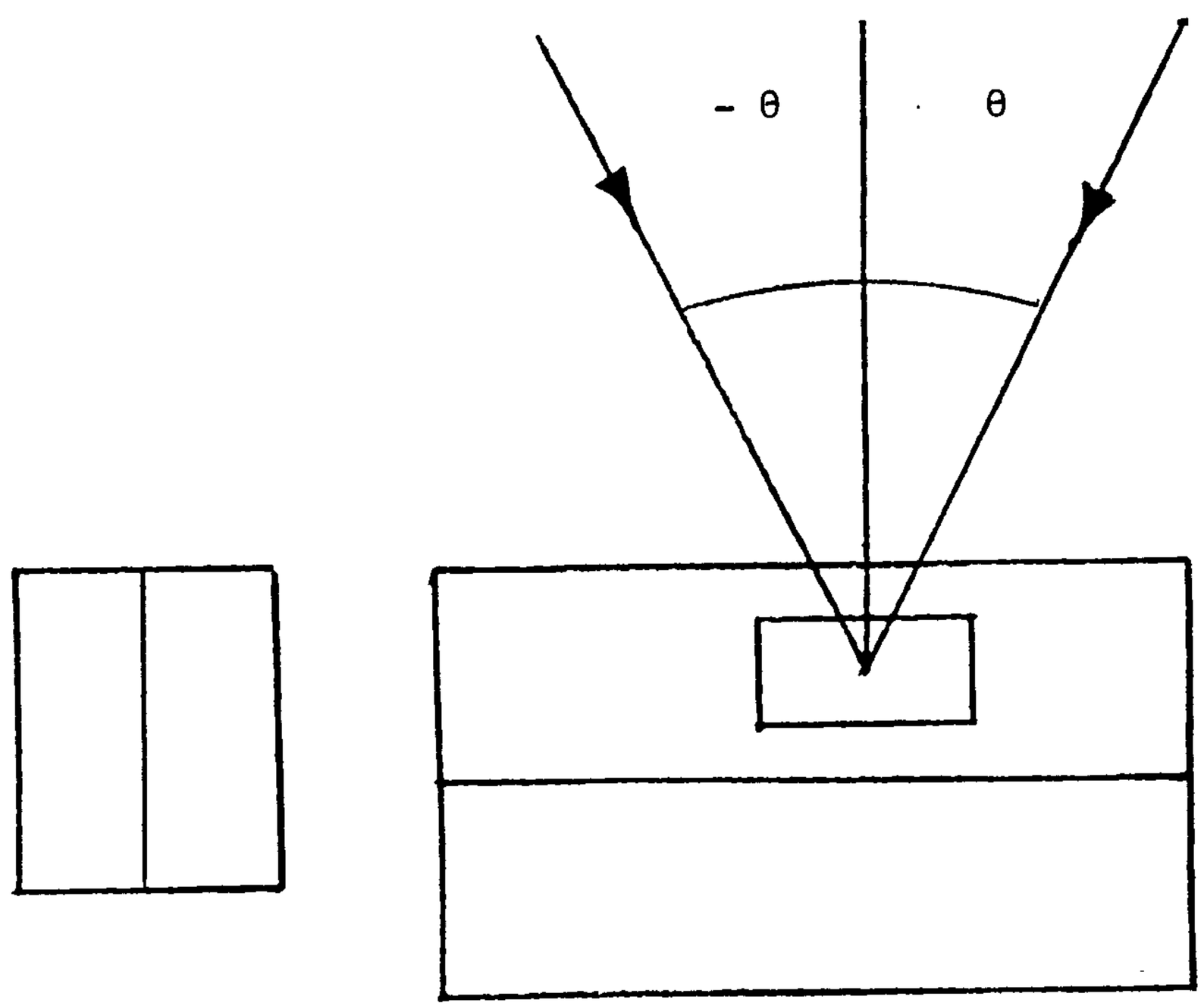


Figure 4.12 Nomenclature for defining wind incidence angle θ (Full scale and model studies)

Figure 4.13 Free stream wind speed anemometer

# CHAPTER FIVE

# EXPERIMENTAL RESULTS OF THE FULL-SCALE MEASUREMENTS OF FORCED CONVECTIVE HEAT TRANSFER AT THE NORTON SITE

## Introduction

The full-scale experimental measurements of the convective heat transfer coefficient, as described in the previous chapter, led to the gathering of large amounts of primary data. This data was reduced into a coherent set of results to obtain an understanding of the relationships existing within the observations. In this chapter it will be shown how the primary data was analysed and the results of this analysis will be presented in a readily understandable form. The problems encountered in performing the analysis will be discussed as will the errors associated with the full-scale measurements made in the outdoor environment.

## 5.1 The Analysis of the Data Obtained from the Full-Scale Convective Heat Transfer Experiments

### 5.1.1 The initial reduction of the primary data to mean hourly values

Between March 1984 and January 1985, 29 experimental runs of the type described in Section 4.7 were performed, with a total of 12,360 scans being made. This data was to be initially reduced to mean hourly values of wind speed and convective heat transfer coefficient. Each scan recorded the twenty-five signals from the plate and instrumentation, thus the hourly mean values were to be based on 600

pieces of information. The ideal method of handling such large amounts of data would have been to use a main-frame computer. Unfortunately, due to restraints on equipment, it was not possible to interface the microcomputer - on which the primary data was taken and stored - with the main frame computer available at the University of Sheffield. Therefore the data was analysed on the micro-computer itself using a specially written program. A listing of this program is shown in Appendix A, and a typical output from it is shown in Figure 5.1. As can be seen from Figure 5.1 the output gives the starting time of each set of 24 scans and mean hourly values of the convective and radiative heat transfer coefficients, along with the conduction losses through the back of the plate. Also included are mean hourly values of the environmental parameters (wind speed, wind direction - expressed as an angle of incidence to the plate, air temeprature, long wave and short wave radiation). Finally, the predominance of the wind direction is given as is the plate to air temperature difference.

Several points much be discussed in order to clarify the information presented by this output. These points will be examined, in turn, in the rest of this section.

### 5.1.2 Problems associated with the measurement of continuous variables at discrete intervals

Consider a parameter, y, which is varying continuously, and randomly, about a true mean value $\bar{y}$ for a given time period, t. The parameter is sampled instantaneously at discrete time intervals of $t_s$. If the first sample is taken at $t_o + t_s$, where $t_o$ is the start of the total time period, and the last at $t'$, (the end of the time period) then there will be a total of N samples taken where $N = t/t_s$. This situation is illustrated in Figure 5.2.

This shows a randomly variable step function being sampled 11 times over the period t. The aim of taking these samples is to evaluate the true mean, $\bar{y}$, of the data. The best estimate of the true mean is shown by Chatfield [1970], to be the mean of the samples taken, $\bar{y}'$, as opposed to the mode or median for example, where:

$$\bar{y}' = \frac{\sum_{i=1}^{N} y_i}{N} \qquad (5.1)$$

This estimate will have an error associated with it. The usual method of expressing this error is to give a confidence interval in which the true mean will lie. Cunningham [1981] states that this interval can be expressed as

$$\bar{y} = \bar{y}' \pm S_N \frac{\sigma_s}{\sqrt{N}} \qquad (5.2)$$

where $S_N$ = The Students t for N points, at the given confidence level

$\sigma_s$ = The Standard deviation of the sample

N = The Number of data points in the sample

The value of the multiplier $S_N$ depends on the level of confidence chosen and the number of data points, N. The distribution of $S_N$ was first obtained mathematically by Gosset [1908]. The standard deviation of the sample is given by:

$$\sigma_s = \sqrt{\frac{\sum_{i=1}^{N} (y_i - \bar{y}')^2}{(N - 1)}} \qquad (5.3)$$

As the value of $S_N$ for any given confidence level decreases with N, and the error given in equation 5.2 is proportional to $1/\sqrt{N}$, it is desirable to make N as large as possible in order to minimise the error on the measurements.

It has already been stated that the minimum available time between scans is 2 minutes 30 seconds. Therefore the only way to increase N is to maximise the averaging period. Meteorological wind speed records are most usually presented in the form of hourly averages, as is data for other environmental parameters. Therefore this period, i.e. one hour, was chosen for the averaging process. This gives a value to N of 24. Substituting in this value of N, and the value of $S_N$ for 24 data points at the 95% confidence level, into equation 5.2 gives:

$$\bar{y} = \bar{y}' \pm 0.422 \ \sigma_s \qquad (5.4)$$

An analysis of this type of applied to the wind speed data. This showed that the error on any hourly mean wind speed measurement was approximately $\pm$ 0.5 $ms^{-1}$ at the 95% confidence level. With a constant electrical heat input from behind, the temperature of the plate is not only dependent upon the wind speed but also the variability of the environmental energy inputs of short and long wave radiation. If these inputs fluctuate rapidly this may give rise to rapidly changing mean plate temperatures. The analysis described above was applied to the hourly evaluation of the mean plate temperature. The results of this analysis showed that the mean temperature of the plate can be defined to within $\pm$2K in the worst case.

The mean plate temperature for each individual scan is itself based on the arithmetic average of the readings from the 9 surface thermocouples. It was found that, for each individual scan, there was a temperature variation across the upper surface of the plate of approximately 5-10 K. Therefore the plate is not strictly isothermal.

The reason for this temperature difference across the plate can be explained in terms of the flow regimes which exist over the plate surface. The heated plate and building constitute a 3D bluff body placed in the highly turbulent 3D flow of the natural wind. Therefore the top surface of the plate will be subjected to highly complex flow regimes, such as separation bubbles, etc. Wind tunnel studies of bluff bodies placed in a 2D flow (see Section 3.4) have already shown that the local convective heat transfer from a surface will vary greatly, due to the presence of these various flow regimes.

Because the plate surface, at any instant, is subjected to a constant energy input over its surface, any variation of the local convective heat transfer coefficient will manifest itself as a temperature distribution across the plate surface, i.e. the lower the temperature at a given location, as measured by one of the plate thermocouples, the greater the convective heat transfer at that point. It was the intention of this series of experiments to investigate the average convective heat transfer coefficient over the plate hence no further study of these temperature variations was made.

One of the final products of the analysis is, of course, the convective heat transfer coefficient h. 95% confidence intervals of the order of $\pm$(0.50 - 4.07) $Wm^{-2}K^{-1}$ were found, with a general trend of an increase in absolute error with increasing h.

Whilst errors of these orders would be thought of as excessive in a controlled laboratory experiment they are considered to be acceptable in full-scale work, and the effect of the error on any one measurement is minimised by taking large amounts of data over a long period of time.

This type of error analysis adequately deals with the problems associated with wind speed and temperature, etc. The measurement of a mean hourly value of wind direction presents further difficulties.

### 5.1.3 Problems associated with the measurement of wind direction in the full-scale experiments

The wind direction varies about a mean value in a similar manner to the wind speed. Lacy [1977] shows that the wind direction oscillates about its mean value by approximately $\pm$ 15°. This, however, is not the main problem here. Consider the coordinate system shown in Figure 4.12. It can easily be imagined that a situation may arise where the wind will blow from a direction of +170° for half the number of scans recorded and from -170° for the other half, thus a simple arithmetic average of this data would lead to a value of 0° for the mean wind direction. This is, obviously, unacceptable. Surridge [1982] discusses this situation and states that it essentially breaks down to the problem of a circular parameter being recorded on a linear medium. He suggests that various techniques have been devised to over-come this, and that they usually rely on some "intelligence" in data recorder. With these two points in mind, the following procedure was employed to enable the wind direction data to be presented in a coherent manner.

The wind co-ordinate system was split into eight equal sectors, based around values of 0°, 45°, 90°, 135°, 180°, -135°, -90° and -45°. Thus the wind direction, $\Theta$, for a particular scan is classified as being in the 45° sector, for example, if it is in the range $22.5° < \Theta \leqslant 65.5°$ (other sectors been defined in a similar manner). The inclusion of the $\leqslant$ for the upper end of each range prevents the possibility of wind directions lying exactly at the interface of two sectors, being omitted from a classification.

Each of the measured wind directions, over a given hour are classified by the above method. The sector containing the most data points is presented as the wind direction in the output from the analysis. The predominance of the wind direction in this sector is also presented. This is defined as:

$$\text{Predominance, } P = \frac{N_\Theta}{24} \times 100 \quad ,\% \qquad (5.5)$$

where $N_\Theta$ = The number of scans over the hour giving a wind direction in the predominant sector.

Thus the predominance level is a measure of the stability of the wind direction over the hour.

5.1.4 Conduction losses

The conduction loss through the insulation behind the plate is given in watts and is evaluated from Fourier's Law, i.e.

$$q = -kA \frac{\Delta T}{\Delta x}$$

where q = Heat transfer rate, W

k = Thermal conductivity of insulation material, $Wm^{-1}K^{-1}$

$\Delta T$ = Temperature across insulation K

$\Delta x$ = Thickness of insulation, m

A = Area of insulation, $m^2$

Other conduction losses e.g. from the edge of the plate through the frame or down the thermocouple wires was considered to be negligible. For example, if the temperature difference between the edge of the plate and the outside of the frame was 30K there would be an energy loss in this direction is of the order of $10^{-4}$W, which is minimal as compared to the backloss from the plate through the insulation foam.

### 5.1.5 The radiative heat transfer coefficient

This study is primarily concerned with heat loss by the process of convection. It must be noted at this stage, that there will also be a net gain, or loss, of energy at the plate surface due to its radiant exchange with the environment.

Green [1979] states that the net radiative heat loss, per unit surface area, from the outer transparent cover of a solar collector, to the environment, is given by:

$$q_r = \varepsilon_c(\sigma T_c^4 - R_L) \qquad Wm^{-2} \qquad (5.6)$$

Where the subscripts r and c indicated radiation and cover values respectively.

Holman [1981] states that a radiation heat transfer coefficient, $h_r$ can be defined, in a similar manner to the convective heat transfer coefficient, as:

$$h_r = \frac{q_r}{(T_s - T_A)} \qquad Wm^{-2}K^{-1} \qquad (5.7)$$

Adapting equations 5.6 and 5.7 for the situation under consideration here and combining them, we have:

$$h_r = \frac{\varepsilon_p(\sigma T_s^{\,4} - R_L)}{(T_s - T_A)} \qquad Wm^{-2}K^{-1} \qquad (5.8)$$

With all the parameters on the right hand side being known or measured mean hourly values of the radiative heat transfer coefficient can be evaluated. These values are presented in the output as shown in Figure 5.1 under the heating Heat Transfer Coefficient - Radiative. Because of its secondary importance in this series of experiments, further examination of the radiative heat transfer coefficient will be deferred until after the discussion of the convective heat losses from the full-scale roof mounted plate.

## 5.2 Relationships between the Convective Heat Transfer Coefficient and the Wind Speed Measured over the Roof, $V_{6R}$

By consideration of the earlier experimental work reported in Chapter Three, it may be expected that the convection coefficient will be dependent upon the wind speed and the wind direction. Therefore, the mean hourly values, presented by the output, of initial interest are; the convective heat transfer coefficient h, the wind speed over the roof, $V_{6R}$, and the wind incidence angle, $\theta$. Each experimental run contained no more than a total of 26 hours of data, and there was never more than 15 sequential hours for which the wind direction was constant. Therefore, the data from all experimental runs was grouped together in terms of wind direction.

Figures 5.3 to 5.10 show plots of the heat transfer coefficient h against roof wind speed $V_{6R}$ for each of the eight defined wind direction sectors. The data is plotted irrespective of the predominance level of the wind direction, or of the value of any of the other measured parameters. From these figures it can be seen that the measured values of the convection coefficient lie approximately in the range $5 < h < 35\ Wm^{-2}K^{-1}$, the value of h tending to increase with wind speed.

To test if any distinct relationship existed between the two parameters a best straight line fit was applied to the data for each wind sector. These lines are also shown in Figure 5.4 to 5.11. The lines were determined using a least squares method on a microcomputer. Table 5.1 presents the regression lines obtained for each direction together with the number of data points N, the correlation coefficient, r, the significance level of this coefficient, p, (a significance level of 0.001 implies that this correlation has only a 0.1% probability of occuring by chance) and the wind speed range which the data encompasses.

Two points become immediately apparent upon examination of the data plots.

(a) Despite relatively high values of r, the scatter of the data is large

(b) The differences between the relationships obtained for each wind sector are small in comparison to this scatter.

TABLE 5.1 Linear regressions of h on $V_{6R}$ by wind direction

| Wind Angle θ | Number of Data Points | Regression Equation $h = Wm^{-2}K^{-1}$ | Correlation Coefficient r | Significance Level | Wind speed range $ms^{-1}$ |
|---|---|---|---|---|---|
| 0° | 65 | $h = 2.2\ V_{6R} + 8.3$ | 0.767 | $p < 0.001$ | $0.8 < V_{6R} < 6.7$ |
| 45° | 136 | $h = 2.6\ V_{6R} + 7.9$ | 0.675 | $p < 0.001$ | $0.6 < V_{6R} < 6.2$ |
| 90° | 42 | $h = 3.3\ V_{6R} + 6.5$ | 0.878 | $p < 0.001$ | $0.8 < V_{6R} < 6.2$ |
| 135° | 42 | $h = 2.2\ V_{6R} + 7.9$ | 0.716 | $p < 0.001$ | $0.8 < V_{6R} < 6.4$ |
| 180° | 36 | $h = 1.3\ V_{6R} + 8.3$ | 0.439 | $p < 0.001$ | $0.6 < V_{6R} < 4.9$ |
| -135° | 123 | $h = 2.3\ V_{6R} + 7.8$ | 0.618 | $p < 0.001$ | $0.3 < V_{6R} < 7.2$ |
| -90° | 39 | $h = 2.2\ V_{6R} + 11.9$ | 0.651 | $p < 0.001$ | $0.5 < V_{6R} < 6.7$ |
| -45° | 32 | $h = 3.9\ V_{6R} + 6.0$ | 0.834 | $p < 0.001$ | $0.5 < V_{6R} < 6.7$ |

The scatter is so large that it would be inadequate to describe the data sets merely by their regression lines and correlation coefficients. Brownlee [1953] states that confidence limits can be placed on regression lines. These limits are defined by lines drawn parallel to the regression line. The displacement of these lines, y, measured in units of y (h -$Wm^{-2}K^{-1}$, in this case) parallel to the y axis, is defined as:

$$\Delta Y = S_N \sqrt{1 - r^2} \sqrt{\frac{\sum (y - \bar{y})^2}{N - 2}} \qquad (5.9)$$

This analysis was performed for each data set taking a value for $S_N$ at the 95% confidence level. Table 5.2 presents the results of this analysis. From this it can be seen that in general there is slightly more scatter on the data for the -ve wind directions. This indicates that the presence of the small garage to the east of the measurement building could be having some effect on the wind flow, making it less easy to define a mean wind speed for these directions.

Table 5.2 shows that the 95% confidence limits are of the same order of magnitude as the measurements themselves. In experimental work errors are most often expresssed as a percentage of the actual measurement. Because the confidence limit lines are parallel to the regression line the error expressed as a percentage changes with the value of the roof wind speed $V_{6R}$. This percentage error is a maximum at the lower end of the wind speed range considered and is of the order of $\pm$ 50%. The percentage error decreases with increasing wind speed to a value of appromately $\pm$ 20% at the uppper end of the range i.e. 6-7 $ms^{-1}$.

These percentage errors are large enough to warrant an investigation into means by which they could be reduced.

### 5.2.1 Attempts to reduce the scatter on the correlations between h and $V_{6R}$

It was thought, initially, that there could be two possible reasons for the large amount of scatter in the data for each defined wind angle. Predominance levels as low as 33% were found for each wind direction; this would indicate that the wind, over the hour, was blowing at least equally from 3 of the defined sectors. If there is any significant dependence of the convective heat transfer coefficient, as correlated against wind speed with wind direction, then this effect would become more apparent the more well defined the wind direction. Figures 5.11 to 5.14 show plots of the convective heat transfer coefficient h against $V_{6R}$ for the 45° sector for predominance levels of P > 50, 60, 70 and 80 percent respectively. Table 5.3 is similar to Table 5.1, presenting values obtained from each of the plots described above, along with that obtained from the whole data set. From this it can be seen that the coefficients of the regression equation change only slightly with increasing prediminance levels. Whilst the correlation coefficient tends to increase slightly with predominance level, indicating less scatter on the data, its increase is not significant. This type of analysis was conducted on each data set, with similar results. It can be, therefore, concluded that the scatter of the data about the regression line is not a strong function of the predominance level of the wind direction.

Table 5.2 95% Confidence limits for the linear regressions of h on $V_{6R}$

| Wind Angle Θ | Displacement distance of 95% Confidence limit lines |
|---|---|
| 0° | ± 4.3 $Wm^{-2}K^{1}$ |
| 45° | ± 6.8 $Wm^{-2}K^{1}$ |
| 90° | ± 4.7 $Wm^{-2}K^{1}$ |
| 135° | ± 5.6 $Wm^{-2}K^{1}$ |
| 180° | ± 6.6 $Wm^{-2}K^{1}$ |
| -135° | ± 8.2 $Wm^{-2}K^{1}$ |
| -90° | ± 7.9 $Wm^{-2}K^{1}$ |
| -45° | ± 7.8 $Wm^{-2}K^{1}$ |

A second possible cause of the scatter was thought to be caused by the wide range of plate - air temperatures experienced during the series of experiments. Rowley [1930 (a)] indicates that the convective heat transfer coefficient increases slightly with this parameter. The following procedure was adopted to test whether this was the case in this series of experiments. The convective heat transfer data for each wind direction was further subdivided according to wind speed, i.e. all the data for a given wind speed range were grouped together. The ranges chosen were 0.0-1.0 $ms^{-1}$, 1.1-2.0 $ms^{-1}$,

TABLE 5.3 Linear regressions of h on $V_{6R}$ for the 45° section with various wind predominance levels

| Predominance Level P% | N | Regression Equation $h - Wm^{-2}K^{-1}$ | Correlation Coefficient | Significance Level | Wind speed range $ms^{-1}$ |
|---|---|---|---|---|---|
| All Data | 136 | $h = 2.6\ V_{6R} + 7.9$ | 0.675 | $p < 0.001$ | $0.6 < V_{6R} < 6.2$ |
| $p >= 50$ | 89 | $h = 2.7\ V_{6R} + 7.5$ | 0.723 | $p < 0.001$ | $0.6 < V_{6R} < 6.2$ |
| $p >= 50$ | 45 | $h = 2.7\ V_{6R} + 7.4$ | 0.720 | $p < 0.001$ | $0.7 < V_{6R} < 6.2$ |
| $p >= 70$ | 27 | $h = 2.6\ V_{6R} + 7.6$ | 0.770 | $p < 0.001$ | $1.3 < V_{6R} < 6.2$ |
| $p >= 80$ | 7 | $h = 2.3\ V_{6R} + 9.1$ | 0.746 | $p < 0.005$ | $1.7 < V_{6R} < 4.0$ |

etc. These ranges were chosen because, as shown earler in Section 5.1.2, the hourly mean wind speed could not be defined to better than $\pm$ 0.5 $ms^{-1}$. The convective heat transfer coefficient for data points in a given wind speed range was then plotted against the mean plate to air temperature difference for that hour.

The plots for 4 wind speed ranges for the 45° wind direction are shown in Figures 5.15 to 5.18. These are typical of the results of the whole data set. No regression analysis is presented because it is obvious that there is no significant relationship between the two variables. Therefore it can be concluded that the variation in the plate to air temperature does not account in any way for the large amount of scatter in the original data set. Because they make best possible use of the data, i.e. include the maximum range of wind speeds etc., the original regression equations, as presented in Table 5.1 are adequate.

### 5.2.2 Comparison of the current results with previously experimentally derived linear relationships

It was shown in Chapter Three that several workers had produced linear relationships between the convective heat transfer coefficient and wind speed. The experiments conducted on smooth plates in the parallel flow of wind tunnels could be summarised by equation 3.95, i.e.

$$h = 2.9\ V_\infty + 10.0 \qquad Wm^{-2}K^{-1} \qquad (5.10)$$

where $V_\infty$ = the free-stream wind speed of the wind tunnel, $ms^{-1}$

The work of Test et al [1981] is described in Section 3.4.3. He measured the convective heat transfer from an inclined 1.22 x 0.81m plate in the natural environment and correlated the results against the wind speed as measured approximately 1m above the heated plate, with the result:

$$h = 2.56V + 8.55 \qquad Wm^{-2}K^{-1} \qquad (5.11)$$

Kind et al [1983] presented linear relationships derived from extrapolations from his model work, which is described in Section 3.6.5. He states his results are applicable to a collector 2.4m long; for a wind angle of 90° Kind gives:

$$h = 2.2\ V_H + 4.0 \qquad Wm^{-2}K^{-1} \qquad (5.12)$$

and for a wind angle of 135°

$$h = 1.3\ V_H + 4.0 \qquad Wm^{-2}K^{-1} \qquad (5.13)$$

where $V_H$ = The wind speed measured at the mid collector height, $ms^{-1}$

Ito et al [1972] in his experimental work on forced convection from high rise building facades produced linear correlations between h and the wind speed measured by a mast mounted roof anemometer. He examined several locations on the building facade and the relationship for his 4th floor centre site is:

$$h = 2.0\ V_R + 3.5 \qquad Wm^{-2}K^{-1} \qquad (5.14)$$

where $V_R$ = The wind speed measured 8m above the building roof, $ms^{-1}$

For this position, which can be taken as representing an "average location" for the site Ito also obtained the following expression

$$h = 8.6\ V_s + 3.2 \qquad Wm^{-2}K^{-1} \qquad (5.15)$$

where $V_s$ = The wind speed as measured 0.3m from the building facade

From his full scale measurements Sturrock [1971] suggests that for an average location on a 26m high building

$$h = 6.0\ V_R + 5.7 \qquad Wm^{-2}K^{-1} \qquad (5.16)$$

Nicol [1977], from his work on convective heat loss from a window, gives:

$$h = 4.35\ V_R + 7.55 \qquad Wm^{-2}K^{-1} \qquad (5.17)$$

Sharples [1981] conducted convective heat transfer experiments at four locations on an 84m high tower block. His measurements at the centre of the fourteenth floor facade produced the following linear correlations, for windward data

$$h = 0.99\ V_s + 3.4 \qquad Wm^{-2}K^{-1} \qquad (5.18)$$

$$h = 1.1\ V_R + 0.9 \qquad Wm^{-2}K^{-1} \qquad (5.19)$$

$$h = 1.6\ V_{10} + 3.3 \qquad Wm^{-2}K^{-1} \qquad (5.20)$$

where $V_{10}$ = The wind speed as measured at a nearby meteorological station $ms^{-1}$

Direct comparison between the equations presented above and the results of the current work given in Table 5.1 would be unwise, since they encompass a wide variety of site geometries and wind speed measurement locations. However, two points are worthy of note.

(i) The equation due to Test et al [1981] is in good agreement with the current work as is the wind tunnel derived correlation.

(ii) Formulations involving the surface wind speed $V_S$ show poor agreement with the current work as do the results of Sturrock [1971].

Test et al [1981] results were based on experimental measurements conducted on a plate of similar geometry to that used in the current series and the wind speed was measured at a similar distance away from the plate. Sturrock's [1971] heating element was several orders of magnitude smaller than that used here. The other two correlations, due to Ito et al [1972] and Sharples [1981], which show disagreement with the current results, involve wind speeds measured at entirely different locations to that at the Norton site and were performed on buildings of dissimilar geometry.

This indicates that three basic factors govern the formulation of linear dimensional relationships between the convective heat transfer coefficient and wind speed, in full scale work:

(a) Plate size

(b) Plate and site geometry

(c) Location of wind speed measurement

These three factors must be taken into account when making comparisons between seemingly similar experiments. Also, if an experiment is being set up to evaluate h from a particular building geometry, care must be exercised to ensure that the experimental set up replicates factors (a) and (b), as given above, as closely as possible. For example, if the convective heat loss from a 1 x 2m window is to be evaluated using a heated plate method then the plate

should be of the same order of magnitude in size as the window and should replicate all the geometrical features of that window, e.g. recesses. This methodology has, of course, been followed in this current series of experiments for the simulated solar collector measurements.

It is of interest to note however, that the early wind tunnel work as represented by equation 5.10 also shows good agreement with the current series of experiments, despite the obvious physical differences between the two sets of experimental work. Therefore the use of relationships developed by this procedure, i.e. measurements in a wind tunnel, would not lead to large errors when applied to the situation under consideration here.

### 5.2.3 The fitting of power law relationships to the convective heat transfer data

It will be recalled from Chapter Two that the fundamentally derived dimensionless theoretical formulae for the convective heat transfer coefficient from a flat plate are power law relationshps. If these formula are applied to a plate with the characteristic dimension of the full-scale heated plate i.e. x = 1.193m then the following relationshps are found. For laminar flow:

$$h = 4.01\ V_\infty^{0.5} \qquad Wm^{-2}K^{-1} \qquad (5.21)$$

and for turbulent flow

$$h = 6.36\ V_\infty^{0.8} \qquad Wm^{-2}K^{-1} \qquad (5.22)$$

where $V_\infty$ = the true free-stream wind speed $ms^{-1}$

In order to make a more accurate comparison between the measured data and the theoretical relationships a power law curve fitting routine was applied to the data for each wind direction. The results of this analysis are presented in Table 5.4. A direct assessment of 95% confidence limit errors, as given for the linear relationships, was not possible with this type of curve fit. However, they will be of the same order of magnitude as those presented in Table 5.2.

Figure 5.19 presents the two theoretically derived relationships together with the experimentally evaluated curves for the 180° and -45° wind incidence angles. These two directions represent the two extremes of the observed curves. From this is can be seen that there is reasonable order of magnitude agreement between the theory and the experimentally derived curves. This is the best that could be expected from this type of comparison, due to the obvious geometrical dissimilarity between the full-scale experimental set up and the idealised case of a streamlined plate in a uniform flow which forms the basis of the theoretical predictions. It must be reiterated that the theoretical relationships are based on the true free-stream wind speed $V_\infty$. Whilst $V_{6R}$ is outside the influence of the boundary layer over the plate it is still within the shear flow region of the atmospheric boundary layer and may be influenced by local flow conditions induced by the building.

The only other worker who has produced power law relationships between h and wind speed from full-scale work is Sharples [1981]. For his 14th floor centre location he gives, for windward data:

$$h = 3.1\ V_s^{0.61} \qquad Wm^{-2}K^{-1} \qquad (5.23)$$

and

$$h = 1.8\ V_R^{0.80} \qquad Wm^{-2}K^{-1} \qquad (5.24)$$

TABLE 5.4 Power regressions of h on $V_{6R}$ by wind direction

| Wind Angle θ | Number of Data Points | Regression Equation $h = Wm^{-2}K^{-1}$ | Correlation Coefficient | Significance Level | Wind speed range $ms^{-1}$ |
|---|---|---|---|---|---|
| 0° | 65 | $h = 9.3\ V_{6R}^{0.44}$ | 0.821 | $p < 0.001$ | $0.8 < V_{6R} < 6.7$ |
| 45° | 136 | $h = 9.5\ V_{6R}^{0.46}$ | 0.747 | $p < 0.001$ | $0.6 < V_{6R} < 6.2$ |
| 90° | 42 | $h = 9.5\ V_{6R}^{0.48}$ | 0.804 | $p < 0.001$ | $0.8 < V_{6R} < 6.1$ |
| 135° | 42 | $h = 8.3\ V_{6R}^{0.51}$ | 0.751 | $p < 0.001$ | $0.8 < V_{6R} < 6.4$ |
| 180° | 36 | $h = 9.2\ V_{6R}^{0.25}$ | 0.559 | $p < 0.001$ | $0.6 < V_{6R} < 4.9$ |
| -135° | 123 | $h = 9.6\ V_{6R}^{0.41}$ | 0.754 | $p < 0.001$ | $0.3 < V_{6R} < 7.2$ |
| -90° | 39 | $h = 11.7\ V_{6R}^{0.41}$ | 0.777 | $p < 0.001$ | $0.5 < V_{6R} < 6.7$ |
| -45° | 32 | $h = 9.1\ V_{6R}^{0.57}$ | 0.600 | $p < 0.001$ | $0.5 < V_{6R} < 6.7$ |

This 14th floor location can be considered to be an "average site" for his building.

Figure 5.20 shows a comparison between Sharples' relationships and those derived here for the 180° and -45° wind directions. From this figure it can be seen that the present correlations give higher values of h for a given wind speed than for those of Sharples. Despite the fact that neither of Sharples' wind speed measurement locations corresponds exactly with the location used for the current series of experiments, Figure 5.20 indicates that there is a substantial difference between the convective heat transfer from a large building facade and a roof mounted flat plate solar collector.

The model work of Sparrow et al has been described and discussed in Section 3.3, with the conclusion that the convective heat transfer from flat plates, inclined or otherwise, could be given as

$$h = 5.1\ V^{0.5}\ x^{-0.5} \qquad Wm^{-2}K^{-1} \qquad (5.25)$$

Substitution of the characteristic length of the roof mounted heated plate i.e. x = 1.193m, into the above equation yields

$$h = 4.7\ V^{0.5} \qquad Wm^{-2}K^{-1} \qquad (5.26)$$

Sparrow also notes that for an inclined plate elevated above a host surface the convective heat transfer may experience upto a two fold enhancement (due to the formation of a rapidly recirculating flow induced by the elevation step) over that predicted by equation (5.26). If this enhancement is accounted for then equation 5.26 comes very much into line with the results presented in Table 5.4.

If the dimensionless relationship of Kind et al [1983] i.e.

$$Nu = 0.613\ Re^{0.54} \qquad (5.27)$$

is dimensionalised in terms of the characteristic plate length then

$$h = 5.83\ V_H^{0.54} \qquad (5.28)$$

Kinds' model collectors were not elevated above the roof surface and so are more compatible with Sparrow's unelevated plate experiments rather than the situation under consideration here. Figure 5.21 shows the results of Sparrow and Kind, together with the power fits for the 180° and -45° wind directions given in Table 5.4. This figure shows that some compatibility exists between previously performed model work and the full-scale measurements made here. It is of interest to note that the best agreement lies with the Sparrow [1981] elevated plate work. It will be recalled that Sparrow's [1981] experiments were performed on a surface raised above another non active plane surface and not placed on a model building of any kind. This indicates that replicating local geometrical features i.e. plate elevation, may be of as much importance in model convective heat transfer measurements as reproducing the overall building shape.

### 5.2.4 A comparison of the linear and power regression equations obtained from the full-scale measurements

From Tables 5.1 and 5.4 it can be seen that the correlation coefficient for the power law relationships are in general slightly higher than for those of the linear regressions, the only exceptions being for the 90° and -45° cases where the reverse is true. However the significance level of each pair of coefficients is not different except for the data for 180° where the power law relationship improves the significance level from $p < 0.01$ to $p < 0.001$.

In order to make a direct comparison of the two types of relationship the value of h, as predicted by the linear and power regression lines, was evaluated at three wind speeds for each wind direction. These values are presented in Table 5.5. It can be seen that apart from the values for $V_{6R}$ = 0 $ms^{-1}$ the derived convective heat transfer coefficients are very similar, with a maximum difference occurring at the larger wind speed value. The predicted values for this wind speed i.e. $V_{6R}$ = 6 $ms^{-1}$ are consistently lower for the power law than the linear regression fit. Table 5.5 also presents the percentage difference between the two derived values for the 6 $ms^{-1}$ wind speed.

The tabulated values show that the maximum difference between the two is 15.9%. This difference is not large when compared to the actual errors on the lines themselves as given in Table 5.2. At the lower end of the wind speed range i.e. $V_{6R}$ = 0 $ms^{-1}$ the difference is obviously much larger because the power law relationship takes no account of the effect of natural convection. Natural convection will take place under still conditions, and at the lower end of the measured wind speed ranges (as given in Table 5.1) then mixed natural and forced convection will take place.

As the intercept of the linear regression lines lie in the range 5.9 - 11.9 $Wm^{-2}K^{-1}$ natural convection plays a substantial role in the heat loss from the upper surface of the plate. For this reason, and the fact that the linear and power curve fits otherwise agree very well, it is recommended that the linear relationships given in Table 5.1 be used as opposed to the power fits shown in Table 5.4.

Table 5.5 Comparison of the value of h obtained from linear and power regression lines for 3 wind speeds by wind direction ($V_{6R}$ - $ms^{-1}$)

| Angle Θ | Fit Type | $Wm^{-2}K^{-1}$ $h(V_{6R} = 0)$ | $h(V_{6R} = 3)$ | $h(V_{6R} = 6)$ | % Difference $h(V_{6R} = 6)$ |
|---|---|---|---|---|---|
| 0° | Linear | 8.3 | 14.8 | 21.3 | 4.5% |
| | Power | 0.0 | 15.0 | 20.4 | |
| 45° | Linear | 7.7 | 15.7 | 23.5 | 7.9% |
| | Power | 0.0 | 15.8 | 21.7 | |
| 90° | Linear | 6.5 | 16.3 | 26.1 | 15.9% |
| | Power | 0.0 | 16.2 | 22.5 | |
| 135° | Linear | 7.9 | 14.6 | 21.2 | 2.0% |
| | Power | 0.0 | 14.6 | 20.8 | |
| 180° | Linear | 8.3 | 12.3 | 16.2 | 12.2% |
| | Power | 0.0 | 12.1 | 14.4 | |
| -135° | Linear | 7.8 | 14.5 | 21.3 | 6.3% |
| | Power | 0.0 | 15.1 | 20.1 | |
| -90° | Linear | 11.9 | 18.4 | 24.8 | 2.1% |
| | Power | 0.0 | 18.3 | 24.3 | |
| -45° | Linear | 5.9 | 17.5 | 29.1 | 14.8% |
| | Power | 0.0 | 17.1 | 25.3 | |

### 5.2.5 The natural convection coefficient of the heated flat plate

It was stated in Section 2.3, that for a large heated plate placed in the outdoor environment, the most probable mechanism of heat transfer from its surface would be forced, as opposed to natural, convection. This is due to the fact that absolutely calm conditions rarely exist in the outdoor environment. The current series of experiments has vindicated this, with minimum mean hourly values of $V_{6R}$ of about 0.5 $ms^{-1}$ being found.

It can be considered from the linear relationships presented in Table 5.1 that the best estimate of the natural convection coefficient of the heated plate available from the current series of experiments is the mean of the intercepts of each of the eight regression lines. The natural convection coefficient should be, theoretically, independent of wind direction. By applying an error analysis of the type discussed in Section 5.1.2 the natural convection coefficient of the plate can be defined as $8.1 \pm 4.2$ $Wm^{-2}K^{-1}$ to the 95% confidence level.

This value represents the minimum rate of convective heat transfer from the plate, and as can be seen from Table 5.5 represents a substantial fraction of the total convective heat loss as predicted by the presented regression equations. For example at $V_{6R} = 6$ $ms^{-1}$ the convective heat transfer coefficient is only approximately 2-3 times as large as its minimum, natural convection, value. This indicates that a more direct evaluation of the natural convection from a large inclined plate i.e. under still conditions,would be an area worthy of further research.

## 5.3 The Effect of Wind Direction on the Convective Heat Transfer Coefficient

### 5.3.1 A comparison between the regression lines obtained for each wind direction

Figure 5.22 presents the linear regression lines for each wind sector; the dotted segments represent extrapolation outside the range of wind speeds actually measured. From this figure and a consideration of the values presented in Table 5.5 it can be seen that the maximum difference between the regression lines occurs at the range extremities. Without taking into consideration the scatter of the points about each line, the value of h at $V_{6R} = 0$ (this is a representative value of the natural convection coefficient) is in the range $5.9 < h < 11.9$ $Wm^{-2}K^{-1}$. At a value of $V_{6R} = 6$ $ms^{-1}$ the values of h are in the range $16.2 < h < 29.1$ $Wm^{-2}K^{-1}$; if the 180° case is removed then the lower end of this range is raised to 21.0 $Wm^{-2}K^{-1}$. This 180° case is the only wind direction which appears, at first sight, to give a regression line which is significantly different to the rest of the directions considered. If the regression lines for each wind direction are not significantly different it may be the case that the data would be better utilised by plotting the heat transfer coefficient against wind speed irrespective of wind incidence angle.

One method by which two regression lines may be compared is given by Brownlee [1958]. If the two lines are given by

$$y_1 = a_1x + b_1 \tag{5.29}$$

and

$$y_2 = a_2x + b_2 \tag{5.30}$$

then the first step towards comparing the regression coefficients $a_1$ and $a_2$ i.e. the slopes of the lines is to obtain the weighted average residual variance $\sigma^2_w$ where

$$\sigma_w^2 = (n_1 \sigma_1^2 + n_2\sigma^2_2)/(n_1 + n_2) \qquad (5.31)$$

where $\sigma$ = the standard deviation of the data, measured in units of y parallel to the y-axis, given by equation 5.3.

n = the degrees of freedom, i.e. N-2 where N = the number of points in the data set.

The subscripts refer to each regression equation and the weighted average. The variance of $a_1$ is then:

$$\frac{\sigma_w^2}{\sum_1 (x-\bar{x})^2} \qquad (5.32)$$

A similar definition holds for the variance of $a_2$. The variance of their difference is then defined as

$$\sigma_{12} = \frac{\sigma_w^2}{\sum_1 (x-\bar{x})^2} + \frac{\sigma_w^2}{\sum_2 (x-\bar{x})^2} \qquad (5.33)$$

The students t value, $S_N$, is then calculated using

$$S_N = \frac{|a_1 - a_2|}{\sigma_{12}} \qquad (5.34)$$

Table 5.6 presents the value of $S_N$, obtained in the above manner, for each pair of regression lines. In this case a value of $S_N$ = 0 would correspond to a confidence level (that the slopes of the lines are different) of zero percent. If $S_N > 3.46$ then the

Table 5.6 Values of the students t, $S_N$, for each pair of linear regression lines

| Wind Angle | 0° | 45° | 90° | 135° | 180° | -135° | -90° |
|---|---|---|---|---|---|---|---|
| 45° | 1.06 | | | | | | |
| 90° | 3.02 | 1.46 | | | | | |
| 135° | 0.00 | 0.83 | 2.38 | | | | |
| 180° | 1.90 | 2.39 | 3.76 | 1.60 | | | |
| -135° | 0.18 | 0.94 | 1.96 | 0.94 | 1.56 | | |
| -90° | 0.00 | 1.01 | 2.15 | 0.00 | 1.30 | 0.26 | |
| -45° | 3.48 | 2.69 | 1.04 | 2.72 | 3.59 | 3.12 | 2.68 |

confidence level that the slopes are different is 100%. The values of $S_N$ lie in the range $0.00 < S_N < 3.59$, thus some pairs of lines have slopes which are significantly identical and other pairs are significantly different. The slopes of the 0°, -90° and 135° directions are identical. The greatest difference in slopes occurs between the -45° and 180° wind angles. In general the values of $S_N$ are greater than unity; this corresponds to a confidence level of 60% that the slope of the lines are different. Therefore it would not seem unreasonable to plot each set of wind direction data as a separate line. The obvious limitation to the analysis presented above is that it takes no account of the intercept of the line on the h axis. But as, theoretically, this intercept should be independent of wind direction, this discrepancy is not to be considered as too much of a limitation on the above analysis.

### 5.3.2 The relationship between the convective heat transfer coefficient and wind direction

Table 5.5 has already presented values of the convective heat transfer coefficient, as derived from the linear regression equations, for each wind direction as evaluated at 3 values of $V_{6R}$. The values of $V_{6R}$ chosen represent approximately the extremes and the mid point of the wind speed ranges encountered. It must be noted that, in all cases, the values for $V_{6R} = 0$ ms$^{-1}$ are extrapolations outside the ranges considered, by 0.3 - 0.8 ms$^{-1}$ depending on wind direction. The $V_{6R} = 6$ ms$^{-1}$ for the 180° wind direction is also an extrapolation

outside the range encountered by 1.1 $ms^{-1}$. Whilst a regression equation is only strictly valid over the range of the independent variable which occured in the data used, the extrapolation in this case is justifiable due to the basic linearity of the data and the fact that the extrapolation is only made to a maximum of 20% outside the range encountered. Figure 5.23 presents the values derived from Table 5.5, graphically.

Bearing in mind the points made in the earlier sections of this Chapter on the scatter of the data, two basic features emerge from Figure 5.23. Firstly, as stated earlier the natural convection coefficient, as defined by the intercept of the regression line with the y-axis, can be given by $h = 8.1 \pm 4.2\ Wm^{-2}K^{-1}$. Secondly, for wind speeds greater than zero, the convective heat transfer coefficient shows a slight but distinct dependence on the wind direction, this variation becoming more distinct the greater the wind speed. The convective heat transfer coefficient is at a minimum for a wind direction of 180°, i.e. when the collector surface is leeward, rises to a maximum when the wind is blowing approximately parallel to the long axis of the building, and again reaches a local minimum when the wind is blowing directly normal to the plate surface i.e. $\Theta = 0°$, the local minimum lying between the two extreme values.

The maximum difference between values of h for each wind direction - as predicted by the regression lines - occurs at the upper end of the wind speed range. At $V_{6R} = 6ms^{-1}$ $h(180°) = 16.2\ Wm^{-2}K^{-1}$ and $h(-45°) = 29.1\ Wm^{-2}K^{-1}$. These figures represent approximately $\pm$ 30% deviations from the mean value, therefore, especially at these higher wind speeds it would be unwise to predict h using relationships which showed no dependence upon wind direction.

Sparrow [1982] measured the convective heat transfer from an isolated model roof structure placed in a wind tunnel (see Section 3.3.4 for further details of this work). He concluded that the convective heat transfer coefficient was essentially similar for both windward and leeward wind flows, i.e. 0° and 180°, and that no sheltering effect was observed when the roof surface was leeward. The results of this current series of experiments are in direct conflict with those of Sparrow in that the 180° wind direction produces the lowest heat transfer coefficient.

This must not be taken as a complete repudiation of Sparrow's conclusions. It does, however, serve to illustrate the inadequacy of using wind tunnel model tests to predict full-scale convective heat transfer behaviour in the outdoor environment. Especially if the model and full scale buildings have dissimilar geometries or are subjected to different types of wind flows. For example, in Sparrow's work the model consisted of the roof pitch only and the heat transfer surface was flush with the roof. The test surface was also subjected to a uniform wind flow with a low turbulence level. The natural wind is a shear flow with high levels of free stream turbulence.

The dependence of h upon wind direction does, however, show reasonable agreement with the later model work of Kind [1983] as described in Section 3.6.5. Kind states that the convective heat transfer coefficients, for his model, were highest when the collector array was aligned with the wind direction i.e. $\pm$ 90° and lowest when the collector array is on the leeward side of the building i.e. $\theta$ = $\pm$ 135° and 180°.

A further detailed comparison of the work of Kind with that undertaken here is not advisable because, apart from the obvious differences between model and full-scale work, Kind modelled collectors which were flush with the roof and the convective heat transfer coefficients were measured at wind speeds evaluated at the mid collector height not at a height of 1.5m above the roof.

The reason for this variation of h with wind direction could be due to the fact that differing flow regimes or local wind velocities over the plate may be created by the wind blowing at various angles to the building. An examination of the flow regimes around and over the building was not possible in the full scale work.

## 5.4 Relationships Involving the 10m Meteorological Wind speed, $V_{10}$

### 5.4.1 The relationship between $V_{6R}$ and $V_{10}$

One of the major problems encountered in comparing convective heat transfer experiments is that of the varying positions at which wind speed measurements are taken. This has already been discussed, in Section 3.7, for the case of comparing various full scale measurements from high rise buildings.

The most widely available wind speed statistic in the UK is the meteorological 10m wind speed, $V_{10}$. Ideally continuous measurement of this wind speed should have been made concurrently with the convective heat transfer measurements. Because of the reasons stated in Sections 4.5.5 it was not possible to do so. However, it was possible to take enough measurements of the 10m wind speed, $V_{10}$, over open terrain, i.e. the playing field in front of the building, to make a reasonable comparison with the roof wind speed $V_{6R}$. By examining 67 simultaneously recorded mean hourly values of $V_{6R}$ and $V_{10}$ the following regression line was developed.

$$V_{6R} = 0.48\ V_{10} + 1.17 \quad ms^{-1} \quad (1.3 < V_{10} < 12.0) \qquad (5.35)$$

$$r = 0.938$$

The above equation represents data obtained from several wind directions, and the high value of r indicates that there is little dependence of the relationship on this parameter. Examination reveals that equation 5.35 predicts that $V_{6R}$ will have a value of 1.17 $ms^{-1}$ if $V_{10}$ = 0 $ms^{-1}$. This, at first, may seem unreasonable, for two sites so close together, for one to experience absolutely calm conditions and the other not. However, it must be remembered, that these absolute conditions occur very infrequently, and that the data on which equation 5.35 is based is heavily biased towards the upper end of the range of wind speeds considered. Sharples [1981] in making a similar comparison between the wind speed over a building roof, $V_R$, and the 10m wind speed found intercepts as large as 6.6 $ms^{-1}$.

For wind speeds of $V_{10} >$ 2.5 $ms^{-1}$. Equation 5.35 predicts the expected relationship between wind speeds measured at two heights i.e. the lower the measuring point the lower the measured value of the wind speed. However for $V_{10} <$ 2.5 $ms^{-1}$ the value of $V_{10}$, as predicted by equation 5.35 is less than $V_{10}$.

Under normal circumstances wind speed increases with height above the ground and the temperature of the air decreases. However, if a temperature inversion occurs, as often happens over open country on clear nights, the inversion layer will be calm or with only a gently drift of air. Under these conditions the variation of wind speed with height can be quite complex and may depend upon local topographical influences. This phenomena goes some way towards explaining the relationship between $V_{6R}$ and $V_{10}$ as predicted by equation 5.35.

### 5.4.2 The relationships between the convective heat transfer coefficient and $V_{10}$

Because concurrent measurements of the convective heat transfer coefficient and $V_{10}$ were not generally possible, the only method of obtaining an expression relating these two parameters is by direct substitution into the regression equations presented in Table 5.1. This has been done and the results are presented in Table 5.7. Figure 5.24 shows these relationships graphically. This replotting, in terms of the meteorological wind speed, has the effect of "flattening out" the relationships changing their slopes quite radically. By this direct substitution the intercepts are also increased. This highlights the fact that different, absolute, relationships between the convective heat transfer coefficient and the wind speed, may be obtained merely by measuring the wind speed at different heights or locations.

Due to its general availability it is recommended that any further full scale measurements of convective heat transfer in the natural environment should include, if possible, concurrent measurements of the 10m wind speed. This measurement should be made at a position close too, but free from the influence of, the site under test.

The only other work on convective heat transfer which has included measurements of the 10m wind speed $V_{10}$ is that by Sharples [1981]. This series of experiments has been described in Section 3.7. Figure 5.25 shows the h v $V_{10}$ relationships for two sites on the 18 storey tower block used by Sharples for his experiments, together with the relationships found in this series of experiments for $\Theta$ = 180° and -45°. Both pairs of lines represent the extremes of the regressions found in each case.

TABLE 5.7 Relationships, by wind angle, between the convective heat transfer coefficient, h, and the meteorological 10m wind speed, $V_{10}$

| Wind Angle | h, $Wm^{-2}K^{-1}$ | Wind Speed Range $ms^{-1}$ |
|---|---|---|
| 0° | $h = 1.1\ V_{10} + 10.8$ | $1.3 < V_{10} < 11.5$ |
| 45° | $h = 1.3\ V_{10} + 10.9$ | $1.3 < V_{10} < 10.5$ |
| 90° | $h = 1.6\ V_{10} + 10.3$ | $1.3 < V_{10} < 10.3$ |
| 135° | $h = 1.1\ V_{10} + 10.5$ | $1.3 < V_{10} < 10.9$ |
| 180° | $h = 0.6\ V_{10} + 9.9$ | $1.3 < V_{10} < 7.8$ |
| -135° | $h = 1.1\ V_{10} + 10.4$ | $1.3 < V_{10} < 12.6$ |
| -90° | $h = 1.9\ V_{10} + 10.5$ | $1.3 < V_{10} < 11.5$ |
| -45° | $h = 1.9\ V_{10} + 10.5$ | $1.3 < V_{10} < 11.5$ |

An in depth comparison between the two series of experiments would be unwise. Sharples' building was some 15 times the height of that currently under study, of a completely different geometry and the surfaces used for the heat transfer experiments were vertical. The wind speed measurements were made at a site some 400m distant from the building, which was not completely exposed. Finally the relationships presented in Table 5.7 were derived indirectly. However, it is interesting to note that the relationships show some agreement indicating that convection relationships developed at sites of differing geometries can be compared if sufficient attention is given to the location of the wind speed measuring position.

Green et al [1981] recommend that if the 10m wind speed is known then the equation due to Sparrow et al [1977] be used for the evaluation of h, which for this case is:

$$h = 5.1\ V_{10}^{0.5}\ \ Wm^{-2}K^{-1} \qquad (3.36)$$

A comparison of this equation and the 10m wind speed expressions obtained here for $\Theta = 180°$ and $\Theta = -45°$ is given in Figure 5.26.

From this it can be seen that Sparrows' equation underestimates h, the comparison being worse for the -45° direction than the 180°. An obvious fault of Sparrows' equation is his failure to take into account natural convection effects. Whilst Green states that Sparrows' equation is only strictly valid for wind speeds in the range 4.5 - 24.0 $ms^{-1}$, 10m wind speeds lower than 4.5 $ms^{-1}$ will often be encountered. Therefore if the 10m wind speed is known it is suggested that the relationships presented in Table 5.7 be used for the evaluation of h.

## 5.5 The Relationship between $V_{6R}$ and the Free Stream wind speed Measured at the Same Height above open Ground $V_6$

The results of most full-scale convective heat transfer experiments have been correlated in terms of a wind speed measured at a specific point above the test building, e.g. Ito et al [1972]. There have been suggestions by Evans [1980] that wind speeds above high rise buildings are effected by the building as much as 8m above it.

Whilst not, perhaps, of fundamental importance in these experiments it was felt it would be of some interest to compare the wind speed as measured over the roof to that measured at a similar height, above the ground, over open terrain, $V_6$.

By examining 70 mean hourly values of the two wind speeds it was possible to obtain the following relationship:

$$V_{6R} = 0.61\ V_6 + 0.50 \quad (2.0 < V_6 < 13.0)\ ms^{-1} \qquad (5.37)$$

$$r = 0.953$$

Again, as with the correlation with the 10m meteorological wind speed, no major directional effect was observed. Hence the wind speed as measured above the roof is generally much lower than that measured in the free stream. This gives a further indication that any convective heat transfer correlations involving a wind speed measured above a building structure will be unique to that site. The application of such results to other buildings, especially of different size or geometry, must be approached with caution.

This also lends further weight to the argument that in all forced convection experiments, full-scale, or model, h, be correlated against a standardised wind speed. As one of the main reasons for undertaking this type of experiment is often to produce results which can be applied to similar building geometries elsewhere i.e. without measurements of h being taken at that site, then a design wind speed must also be known. It is, therefore, reitterated, that future convective heat transfer measurement be correlated directly with the meteorological 10m wind speed which is the only wind speed statistic which is widely available.

## 5.6 Relationships Involving the Free-Stream Wind Speed as Measured at the Mid-Plate Height $V_H$

### 5.6.1 The relationship between $V_{6R}$ and $V_H$

One further wind speed measurement was felt to be of interest, that of the free-stream wind speed measured at mid-collector height $V_H$. This height is 3.6m in this series of experiments. The importance of this wind speed lies in the fact that the most recent model studies carried out in this area, i.e. those of Kind et al [1983] which are described in Section 3.6 correlated the heat transfer results with this wind speed. It is also recommended that this wind speed be used as the input to the current dimensional equations used to predict the wind loss from flat plate solar collectors, as discussed in Section 3.8.

Two points must be noted in the discussion of the $V_H$ data. Firstly, the measurement of $V_H$ was made at a different location to those of $V_6$ and $V_{10}$ i.e. at a distance some 150m away from the test building, as opposed to 80m for the other two free-stream wind speeds. This was for no specific technical reason, and was only due to the fact that the previously used area of the playing field was required by the groundsmen for preparation of the turf.

Secondly, the range of wind speeds covered by this series of experiments was much less than that for $V_6$ and $V_{10}$. Further measurements were not possible, i.e. to obtain a greater range of wind speeds, because at this time the chart recorder used for the measurement of $V_H$ was vandalised making it inoperable. These two points further illustrate the problems of making full-scale measurements in that the conditions under which the experiments are performed are often beyond the control of the experimenter.

$V_{6R}$ was found to be a linear function of $V_H$ i.e.

$$V_{6R} = 0.65\ V_H + 0.46 \quad (0.5 < V_H < 5.0)\ ms^{-1} \qquad (5.38)$$

$$r = 0.887$$

This relationship is similar to that shown earlier for $V_{6R}$ v $V_6$ i.e. equation 5.37. An analysis similar to that applied to the various regression lines of h v $V_{6R}$, i.e. to test if the slopes of the lines are different, was applied to the two regression equations. The result indicated that the slope of the lines were significantly different.

### 5.6.2 The relationships between the convective heat transfer coefficient and $V_H$

Once again, as with the 10m wind speed it was not possible to make continuous measurements of $V_H$ during the full-scale experiments. Hence the relationships between h and $V_H$ were derived in a similar manner to those involving $V_{10}$ i.e. by direct substitution of equation 5.38 into the regression equation presented in Table 5.1. The results of this substitution are given in Table 5.8. Figure 5.27 shows plots of the regression lines for 90° and 135° together with the lines developed by Kind et al [1983], for the same directions, and the line of Jurges [1924], quoted by Duffie and Beckman [1980] as being applicable if the wind speed at the midcollector height is known.

There is relatively good agrement between the three references despite the discrepancies of geometry, in the case of Jurges, and size in the case of Kind. It must be noted that Kind's work is only strictly valid for wind speeds in the range 4-24 $ms^{-1}$ and those presented by Table 5.8 in the range 0-5 $ms^{-1}$.

## 5.7 Relationships Involving the Radiative Heat Transfer Coefficient, $h_r$

In Section 5.15 it was shown that a radiative heat transfer coefficient, $h_r$, could be derived in a similar manner to the convective coefficient, i.e.

$$h_r = \frac{\epsilon_p (\sigma T_s^4 - R_L)}{(T_s - T_A)} \quad Wm^{-2}K^{-1} \qquad (5.39)$$

TABLE 5.8 Linear regressions of h on $V_H$ by wind direction

| Wind Angle θ | Relationship h, $Wm^{-2}K^{-1}$ | Wind speed range $ms^{-1}$ |
|---|---|---|
| 0° | $h = 1.4\ V_H + 9.3$ | $0 < V_H < 5.0$ |
| 45° | $h = 1.7\ V_H + 9.1$ | $0 < V_H < 5.0$ |
| 90° | $h = 1.1\ V_H + 8.0$ | $0 < V_H < 5.0$ |
| 135° | $h = 1.4\ V_H + 9.0$ | $0 < V_H < 5.0$ |
| 180° | $h = 0.9\ V_H + 9.4$ | $0 < V_H < 5.0$ |
| -135° | $h = 1.4\ V_H + 8.8$ | $0 < V_H < 5.0$ |
| -90° | $h = 1.4\ V_H + 12.9$ | $0 < V_H < 5.0$ |
| -45° | $h = 2.5\ V_H + 7.7$ | $0 < V_H < 5.0$ |

All the parameters on the right hand side of equation 5.39 were either known or evaluated during the full-scale experiments. Therefore, it was possible to present mean hourly values of the radiative heat transfer coefficient from the upper surface of the heated plate.

Equation 5.39 is an expression of the radiative energy balance on the surface, normalised in terms of the plate - air temperature difference. If the outgoing radiation from the surface $\epsilon_p \sigma T_s^4$ is greater than the incoming, $\epsilon_p R_L$, and $T_s > T_A$ then $h_r$ will be positive. However if $\epsilon_p \sigma T_s^4$ is less than $\epsilon_p R_L$ and $T_s > T_A$ then the radiative heat transfer coefficient will become negative. This would indicate that there is a radiative gain at the surface.

This series of experiments was designed specifically to examine a plate which was heated to a temperature above that of its surroundings so throughout the full-scale tests $T_s$ was greater than $T_A$. In all cases it was found that $h_r$ was positive, hence there was always a radiataive loss from the upper surface of the flat plate, i.e. $\epsilon_p \sigma T_s^4$ was always greater than $\epsilon_p R_L$.

One of the main reasons for undertaking these measurements of $h_r$ was to be able to compare the heat loss from the upper surface of the plate by the two transfer mechanisms i.e. convection and radiation. The parameters which effect the convection loss i.e. wind speed and wind direction have already been discussed. It is therefore necessary to gain on understanding of the parameters which effect the radiative heat loss from the plate. If $h_r$ can be paramaterised it may also be possible to obtain design values for the radiative heat transfer coefficient from a flat plate solar collector.

### 5.7.1 Parameterisation of the radiative heat transfer coefficient $h_r$

It can be seen from equation 5.39 that $h_r$ is dependent upon $\varepsilon_p$, $T_s$, $T_A$ and $R_L$. $\varepsilon_p$ is a constant and the other three parameters are measured during the experiment. It has been shown by previous workers that $R_L$ is a function of the ambient air temperature $T_A$. (A full discussion of the dependence of $R_L$ on $T_A$ can be found in the review paper by Cole [1976]). Atmospheric longwave radiation originates mainly from water vapour and carbon dioxide in the lowest few hundred metres of the atmosphere. Therefore clouds are powerful sources of atmospheric radiation and hence the value of $R_L$ will depend not only upon the ambient air temperature but also on the amount of cloud cover present over the measuring site.

Two equations are generally accepted the first, for clear skies - due to Swinbank [1963] gives:-

$$R_L = 5.31 \times 10^{-13} T_A^{\,6} \quad Wm^{-2} \tag{5.40}$$

The second, due to Angstrom [1915], is for totally overcast skies and states:

$$R_L = 0.96 \quad \sigma T_A^{\,4} \quad Wm^{-2}K^{-1} \tag{5.41}$$

Equations also exist for predicting the value of $R_L$ under partially overcast skies and these are also discussed by Cole [1976].

The equations presented above are for long wave radiation on an horizontal surface. Inclined surfaces, such as the roof mounted heated plate receive radiation not only from the atmosphere but from the ground and any surrounding buildings as well. Therefore, the simple dependence of $R_L$ on $T_A$ may not hold for the situation under consideration here.

In order to test this measured mean hourly values of $R_L$ were regressed against mean hourly values of $T_A$. As previously given relationships between $R_L$ and $T_A$ are of a power law form than this type of curve fit was applied to the current data with the result that.

$$R_L = 1.53 \times 10^{-16} T_A^{7.48} \quad Wm^{-2} \qquad (5.42)$$

$$r = 0.659$$

where $T_A$ = Air temperature, K.

The regression coefficient of equation 5.42 is significant at the $p < 0.001$ level.

In the light of the discussion presented above it can be expected that the radiative heat transfer coefficient $h_r$ will be a function of both the plate and the air temperature i.e. $h_r = f(T_s, T_A)$. From equations 5.39 and 5.42 it would be possible to derive a series of curves of $h_r$ v $T_s$ for constant air temperature and of $h_r$ v $T_A$ for constant plate temperature. This process would be tedious to perform and would go little way to deriving a simple method for deriving design values of $h_r$, as it would mean that both $T_A$ and $T_s$ would have to be known.

### 5.7.2 The dependence of $h_r$ upon the plate - air temperature difference

Initial examination of the data revealed that the radiative heat transfer coefficient lay in range $4.0\ Wm^{-2}K^{-1} < h_r < 12.0\ Wm^{-2}K^{-1}$, i.e. generally lower than the convection coefficient, and that the higher values of $h_r$ tended to occur at lower values of the plate - air temperature difference. Figure 5.28 shows a plot of $h_r$ v $\Delta T$ ($T_s$ - $T_A$). The values have been taken from the $\Theta = 45°$ data file. It was not expected that $h_r$ would be dependent in any way upon wind direction, and this direction was chosen merely because it contained a large number of scans.

From this Figure it can be seen that the information gained from the initial observation of the data is correct. However, it must be noted that for the lower values of $\Delta T$ there is a wide spread of values of $h_r$. The scatter in the data is reduced at higher values of $\Delta T$, but the number of data points for these higher temperature differences is less.

A simple power curve fitting routine was applied to the data with the result that:

$$h_r = 19.2\ \Delta T^{-0.32} \qquad (5.43)$$

$$r = 0.541$$

Whilst this regression coefficient appears low it is still significant to the $p < 0.001$ level.

This type of analysis was performed on the data contained in each wind direction file, the results are presented in Table 5.9.

Table 5.9 Power law relationships between $h_r$ and $\Delta T$, by wind angle

| Wind Angle $\theta$ | Power Law Relationship $\Delta T = (T_s - T_A)$, K $h_r$ - $Wm^{-2}K^{-1}$ | Correlation Coefficient |
|---|---|---|
| 0° | $h_r = 39.9\ \Delta T^{-0.59}$ | 0.657 |
| 45° | $h_r = 19.2\ \Delta T^{-0.32}$ | 0.541 |
| 90° | $h_r = 33.6\ \Delta T^{-0.50}$ | 0.781 |
| 135° | $h_r = 15.2\ \Delta T^{-0.29}$ | 0.392 |
| 180° | $h_r = 50.3\ \Delta T^{-0.66}$ | 0.503 |
| -135° | $h_r = 14.4\ \Delta T^{-0.29}$ | 0.409 |
| -90° | $h_r = 6.1\ \Delta T^{-0.05}$ | 0.123 |
| -45° | $h_r = 32.3\ \Delta T^{-0.53}$ | 0.718 |

### 5.7.3 Total heat loss from the upper surface of the heated flat plate

It has already been shown that the convective heat transfer coefficient is a function of the wind speed. For a given constant energy input to the plate, the plate temperature may be expected to be a function of the wind speed, i.e. the higher the wind velocity the lower the plate temperature. So as the value of $h_r$ tends to decrease with plate - air temperature then it may also be expected to increase with wind speed. If this is the case then the total heat loss from

the upper surface of the collector will increase with wind speed. Hence the wind speed could be used to predict the total heat loss from the upper surface of the plate. To test if this hypothesis is true the mean plate temperature difference $\Delta T$ was regressed against the roof wind speed $V_{6R}$. There was found to be no real dependence of $\Delta T$ upon $V_{6R}$. To further emphasise this point a least squares linear regression line was applied to the data from the 45°; wind sector with the results that.

$$T = -2.6\ V_{6R} + 31.6 \quad , K \qquad (5.44)$$

$$r = 0.292$$

The low value of r indicates that the application of this regression line would be inadvisable despite the fact that it shows the general trend predicted, i.e. $\Delta T$ decreases as $V_{6R}$ increases.

The total heat loss from the upper surface of the flat plate can be expressed as the sum of the two heat transfer coefficients, i.e. ($h + h_r = h_t$); h tends to increase with wind speed as should $h_r$. Figure 5.29 shows a plot of $h_t$ against the roof top wind speed $V_{6R}$ for the 45° wind incidence angle. Also shown in a linear least squares fit line which has the form.

$$h_t = 3.1\ V_{6R} + 13.6 \qquad Wm^{-2}K^{-1} \qquad (5.45)$$

$$r = 0.737$$

A similar analysis was applied to the data for the other wind directions and the results are presented in Table 5.10.

TABLE 5.10 Total heat loss from the top surface of the heated flat plate $h_t = (h + h_r)$ expressed as a function of wind speed

| Wind Angle | Number of Data Points | Linear Regression Equation $h_t$, $Wm^{-2}K^{-1}$ | Regression Coefficient | Significance Level p |
|---|---|---|---|---|
| 0° | 65 | $h_t = 3.1\ V_{6R} + 12.8$ | 0.692 | $p < 0.001$ |
| 45° | 136 | $h_t = 3.1\ V_{6R} + 13.6$ | 0.737 | $p < 0.001$ |
| 90° | 42 | $h_t = 3.3\ V_{6R} + 14.6$ | 0.739 | $p < 0.001$ |
| 135° | 42 | $h_t = 2.1\ V_{6R} + 14.7$ | 0.676 | $p < 0.001$ |
| 180° | 36 | $h_t = 1.7\ V_{6R} + 14.3$ | 0.500 | $p < 0.001$ |
| -135° | 123 | $h_t = 2.3\ V_{6R} + 13.7$ | 0.633 | $p < 0.001$ |
| -90° | 39 | $h_t = 2.1\ V_{6R} + 17.8$ | 0.634 | $p < 0.001$ |
| -45° | 32 | $h_t = 3.8\ V_{6R} + 12.2$ | 0.689 | $p < 0.001$ |

It can be seen from this table that the total heat loss form the upper surface of the plate can be adequately expressed as a linear function of the wind speed. As the slopes of the lines presented in Table 5.10 are generally the same or greater than those presented in Table 5.1 i.e. for the convection coefficient only, it can be said that the value of $h_r$ tends to increase with wind speed or is constant with that parameter.

Hence, at least for the present set of measurements, the wind speed can be used as the parameter to predict not only the convective heat loss from the upper surface of the plate but also the total heat loss (convection + radiation).

## Conclusion

The following points can be concluded from the full-scale measurements at the Norton Site.

(i) For the range of wind speeeds measured over the roof i.e. $0.3 < V_{6R} < 7.2\ ms^{-1}$ the convective heat transfer coefficient of the plate was found to be in the range $5 < h < 35\ Wm^{-2}K^{-1}$.

(ii) The dependence of h upon the wind speed, as measured over the roof $V_{6R}$ was found to be adequately expressed by linear relationships of the type.

$$h = a V_{6R} + b \qquad Wm^{-2}K^{-1}$$

where the constants a and b are dependent upon wind direction (see Table 5.1).

(iii) In general it was found that the greatest rates of heat transfer from the plate occurred when the wind was blowing parallel to the ridge line.

(iv) The lowest rates of heat transfer were found when the plate surface was leeward to the wind flow.

(v) The wind speed over the roof $V_{6R}$ was found to be a linear function of the free stream wind speed $V_6$ with $V_{6R}$ being generally less than $V_6$ i.e. the presence of the building distorts the wind flow around it enough to affect the wind speed upto at least 1.5m above the ridge line.

(vi) Linear relationships were found to exist between $V_{6R}$ and both $V_H$ and $V_{10}$ ($V_H$ being the wind speed at mid collector height and $V_{10}$ being the 10m meteorological wind speed).

(vii) Hence linear relationships between h and both $V_{10}$ and $V_H$ are also given (see Tables 5.7 and 5.8).

(viii) Radiative heat transfer coefficient values $h_r$ in the range $4 < h_r < 12\ Wm^{-2}K^{-1}$ were found during the experimental series.

(ix) The radiative heat transfer coefficient could be adequately parameterised in terms of the mean plate - air temperature difference, $\Delta T$, higher values of $h_r$ being found at lower values of $\Delta T$ (see Table 5.9).

(x) The mean plate - air temperature difference showed a slight dependence upon wind speed, it tending to decrease with this parameter.

(xi) The total heat transfer coefficient of the plate i.e. $h + h_r$ was also found to be adequately expressed as linear functions of wind speed (see Table 5.10).

**********

| TIME HOUR (GMT) | WIND SPEED (M/S) | PREDOM-INANCE % | INC. ANG. (DEG.) | AIR TEMP. (DEG.C) | LONG WAVE (W/M^2) | SHORT WAVE (W/M^2) |
|---|---|---|---|---|---|---|
| 0 | 3.8 | 83 | 45 | 5.6 | 304 | 0 |

| HEAT TRANSFER COEFFICIENTS (W / M^2 / DEG.C) | | PLATE-AIR TEMP.DIFF. (DEG.C) | CONDUCTION LOSSSES WATTS |
|---|---|---|---|
| CONVECTIVE | RADIATIVE | | |
| 19.3 | 7.2 | 14.4 | 9.3 |

**********

Figure 5.1 Typical output from initial analysis programme - See Appendix A

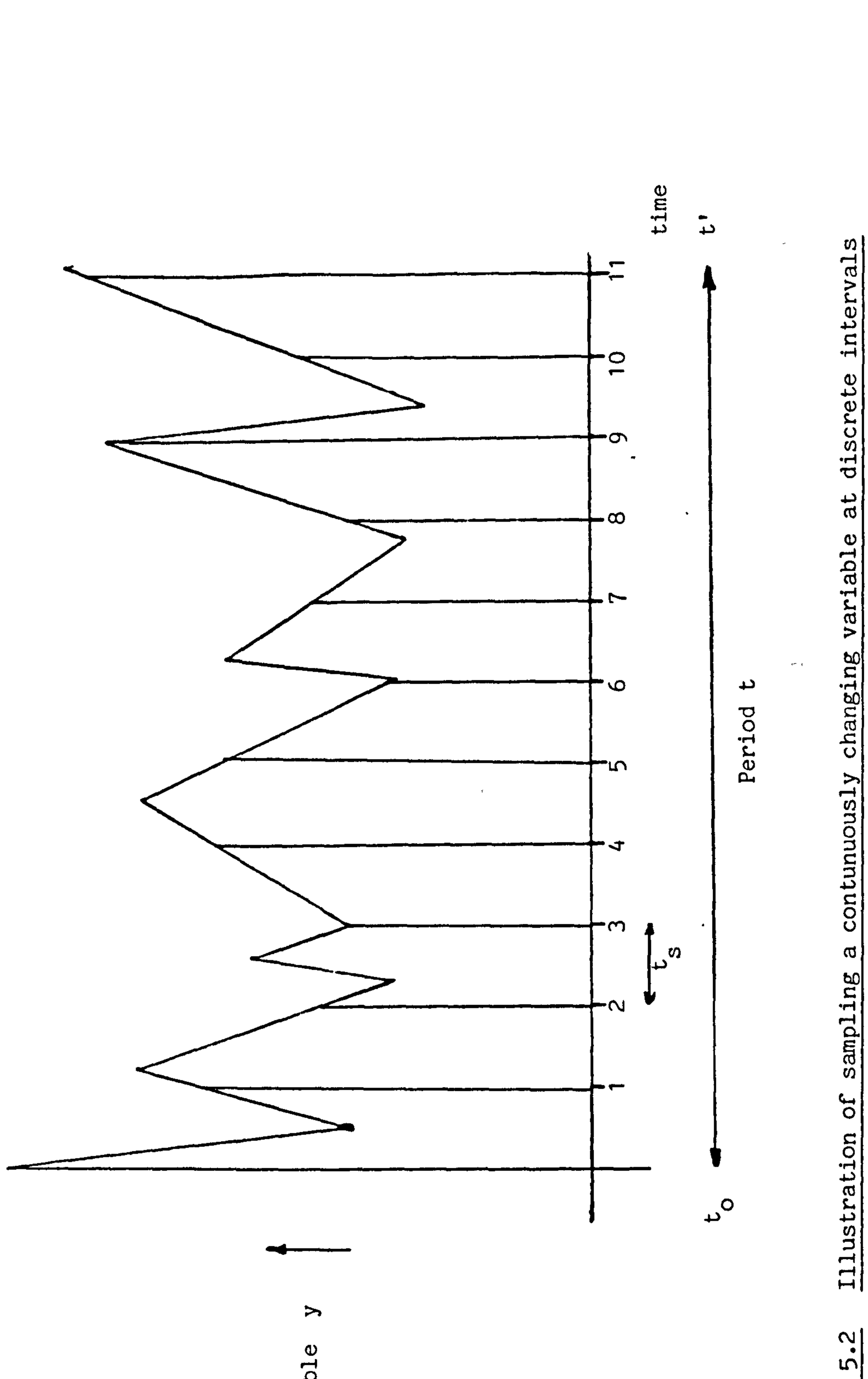


Illustration of sampling a continuously changing variable at discrete intervals

Figure 5.2

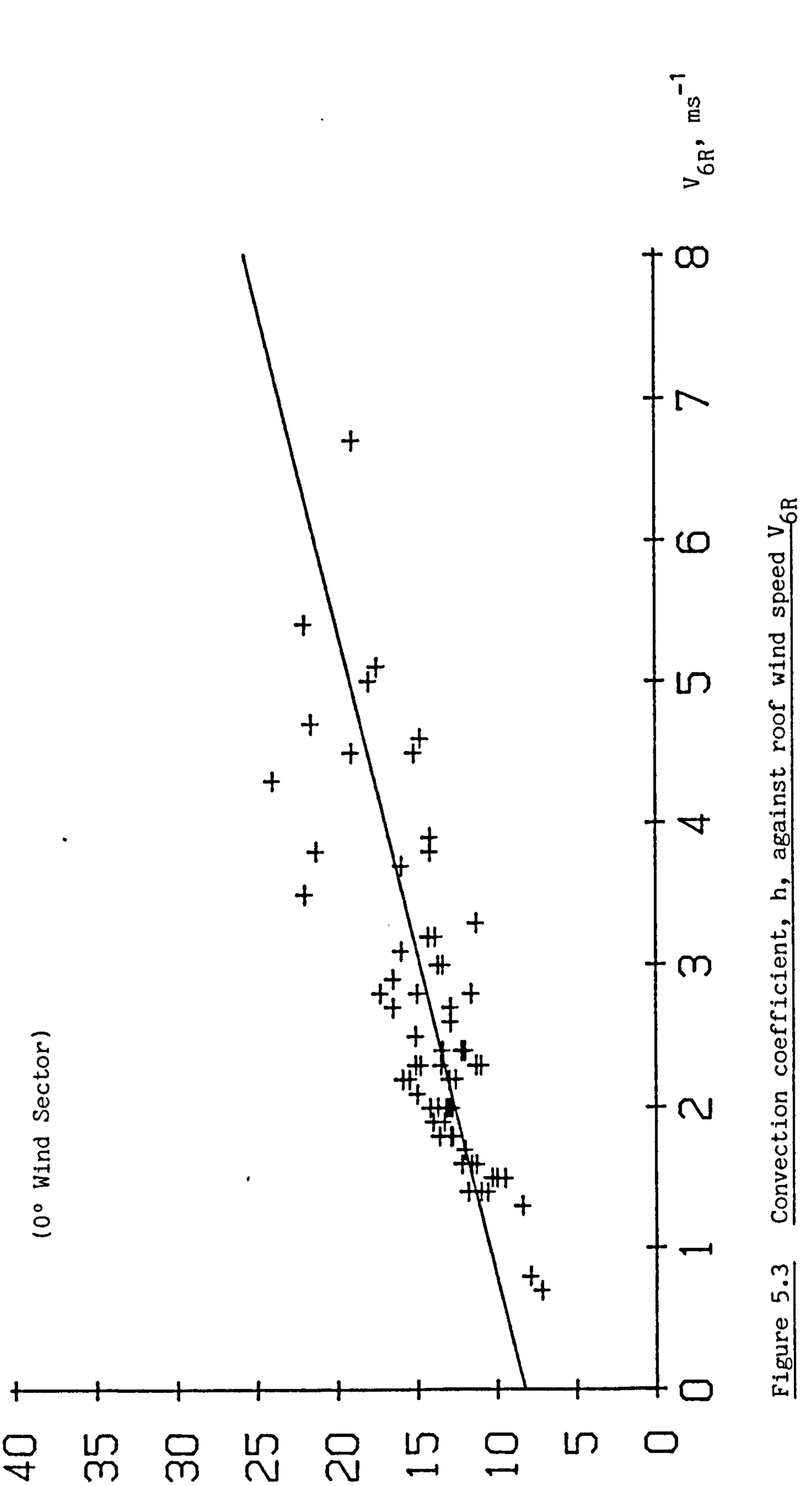


Figure 5.3 Convection coefficient, h, against roof wind speed $V_{6R}$

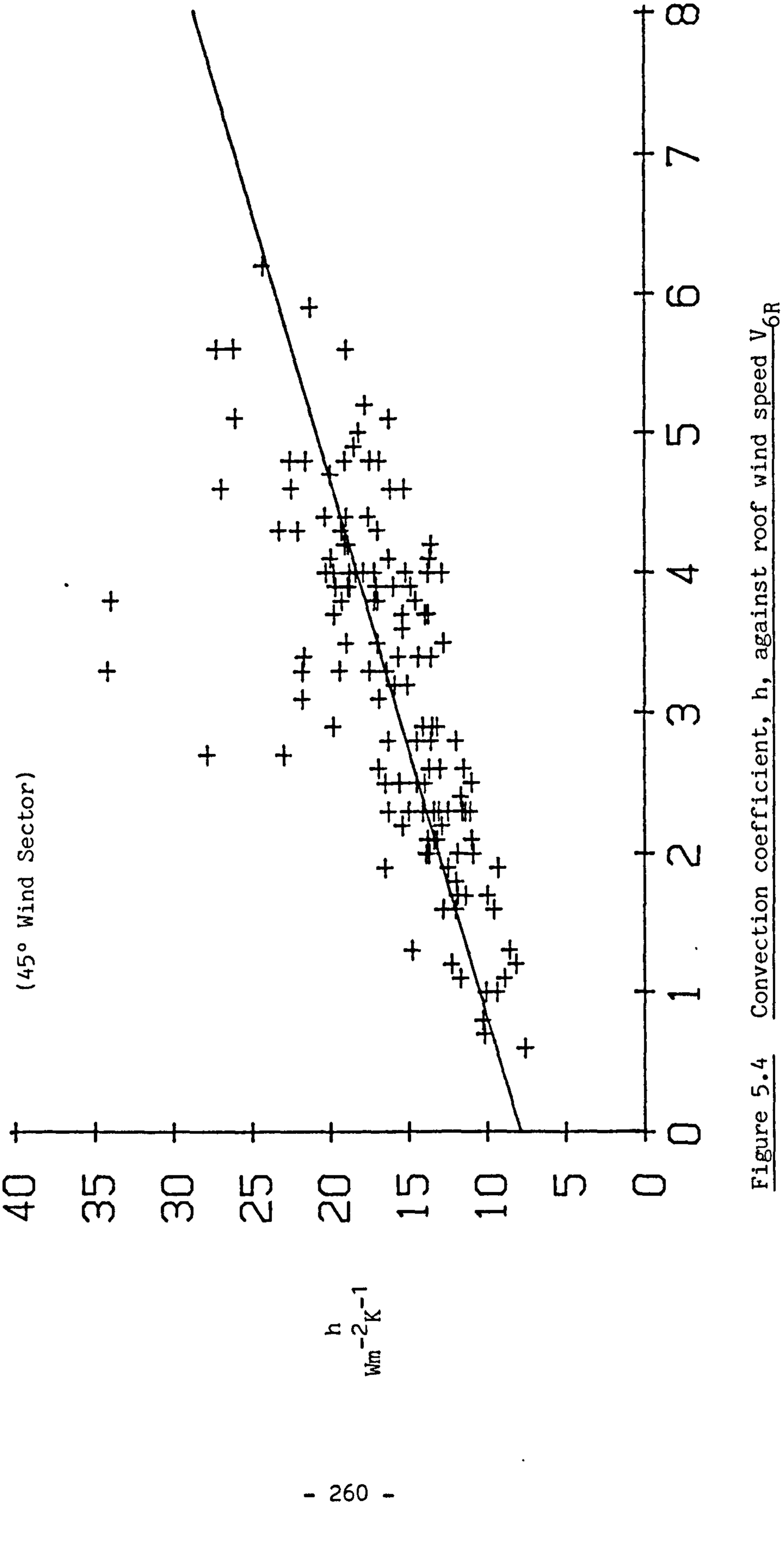


Figure 5.4 Convection coefficient, h, against roof wind speed $V_{6R}$

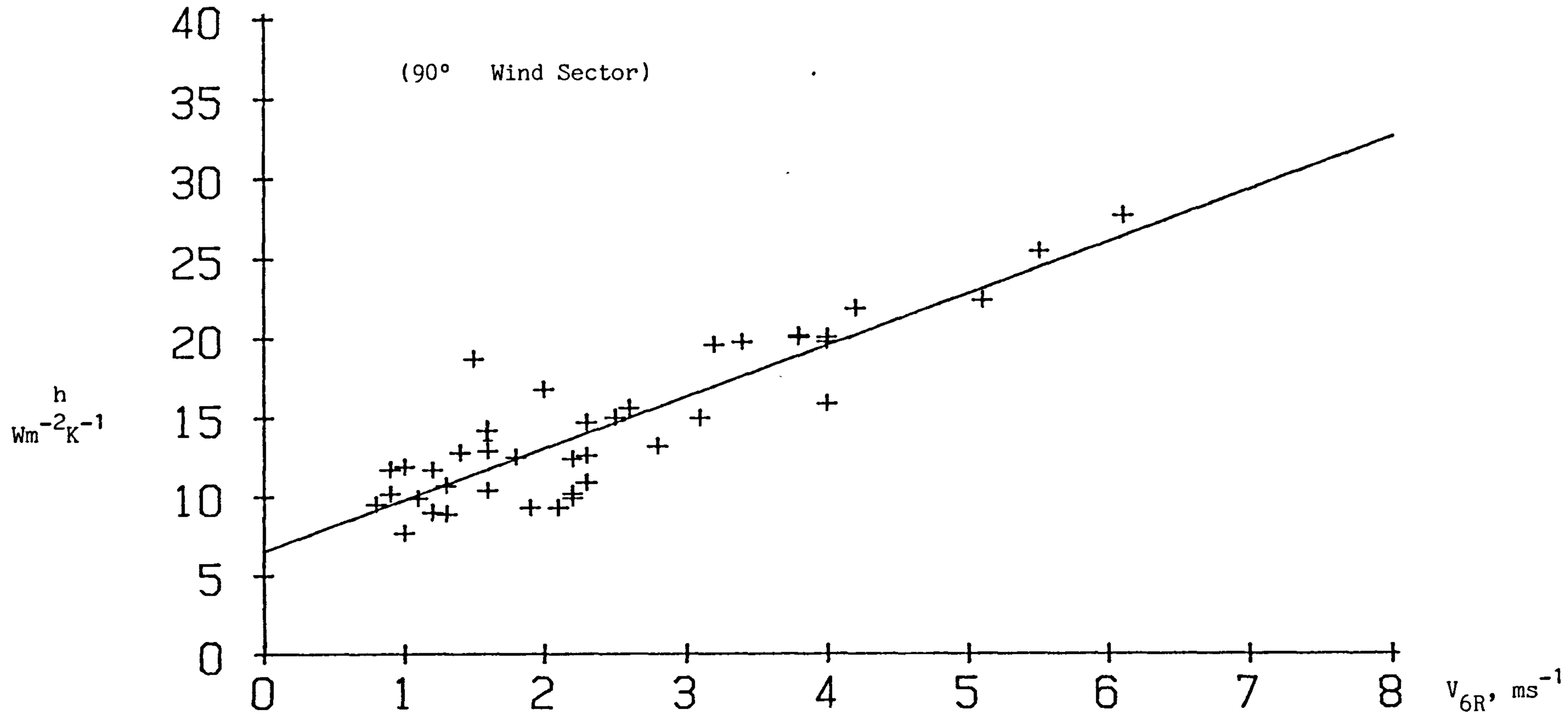


Figure 5.5 Convection coefficient, h, against roof wind speed $V_{6R}$

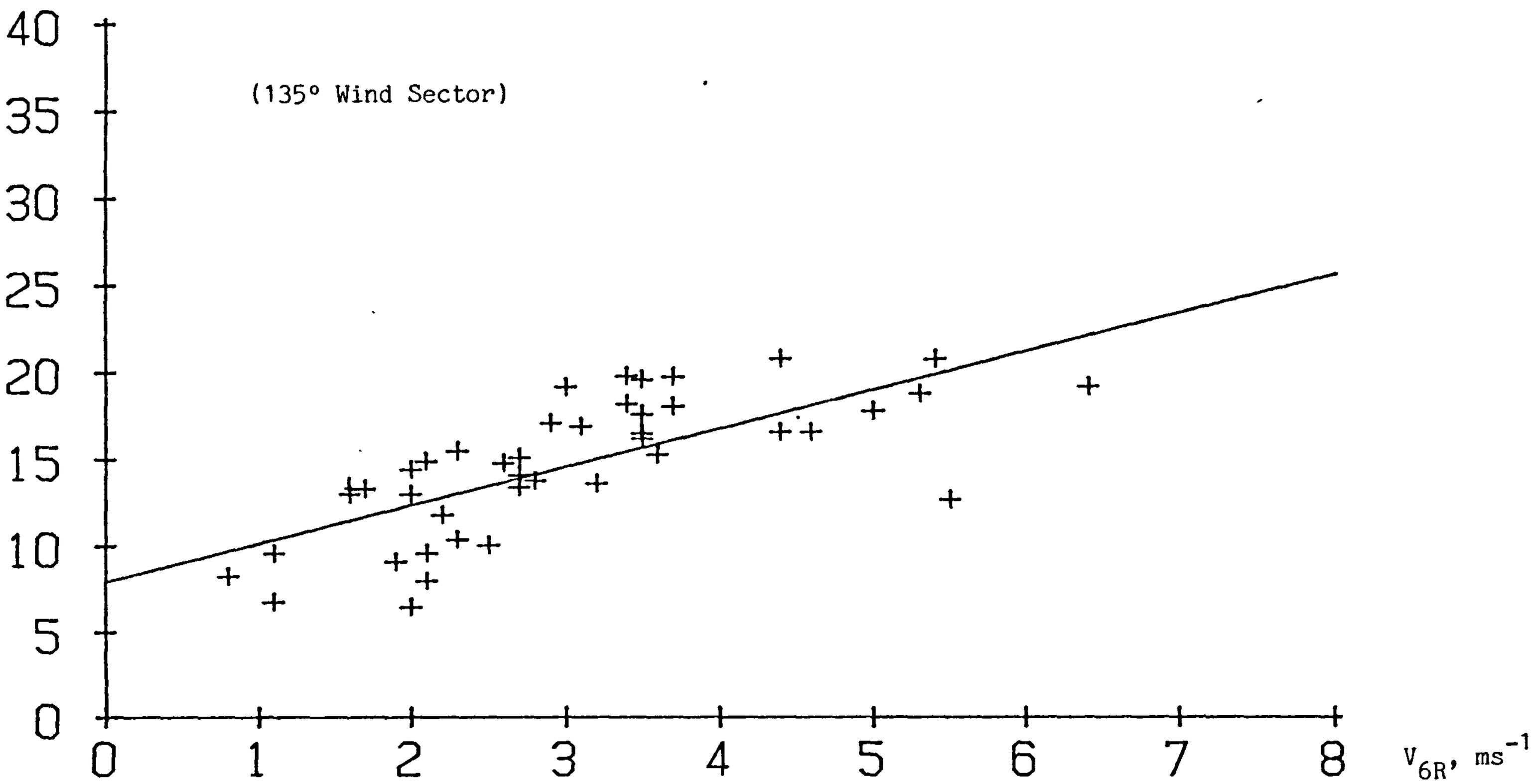


Figure 5.6 Convection coefficient, h, against roof wind speed $V_{6R}$

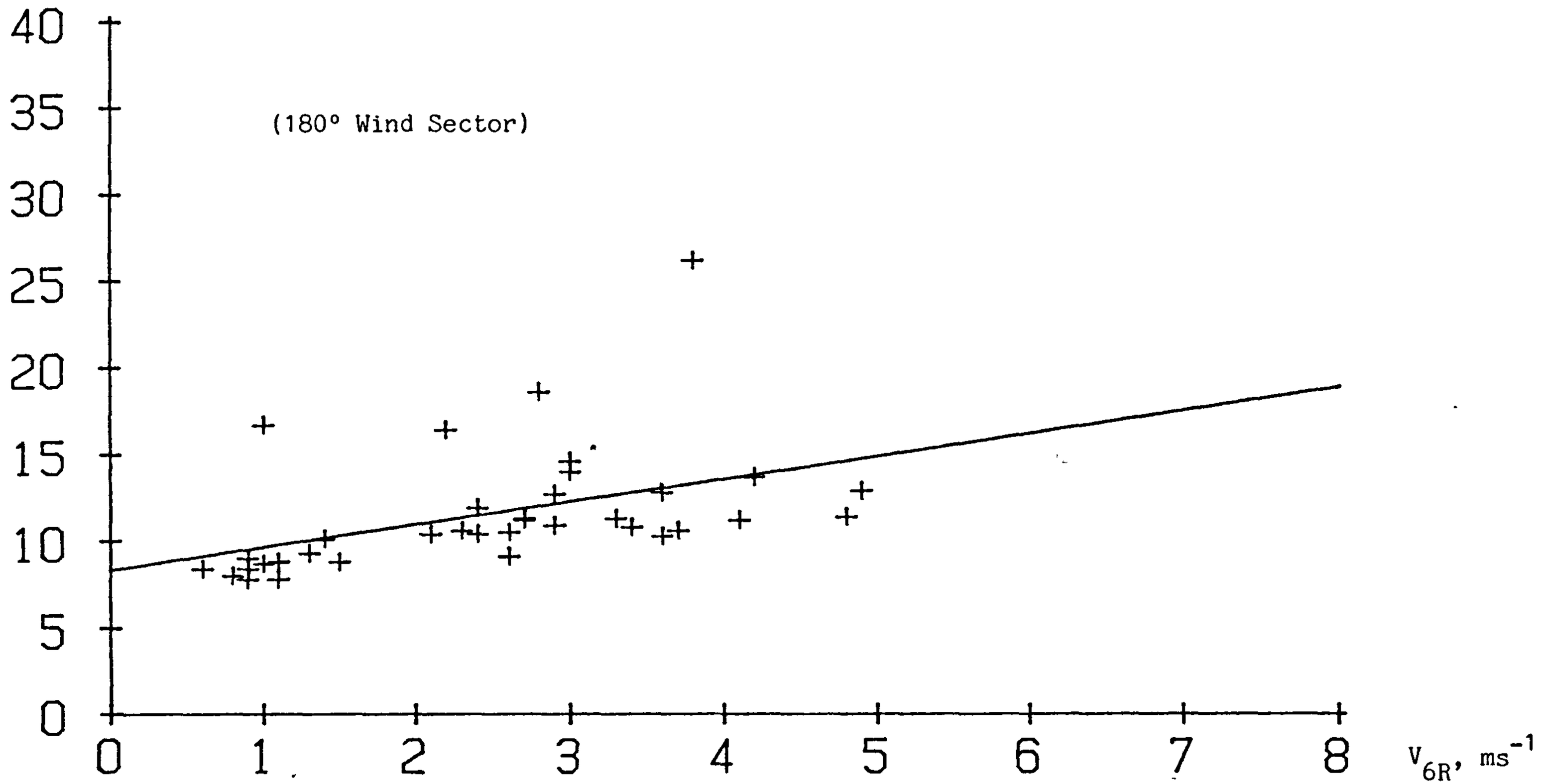


Figure 5.7 Convection coefficient, h, against roof wind speed $V_{6R}$

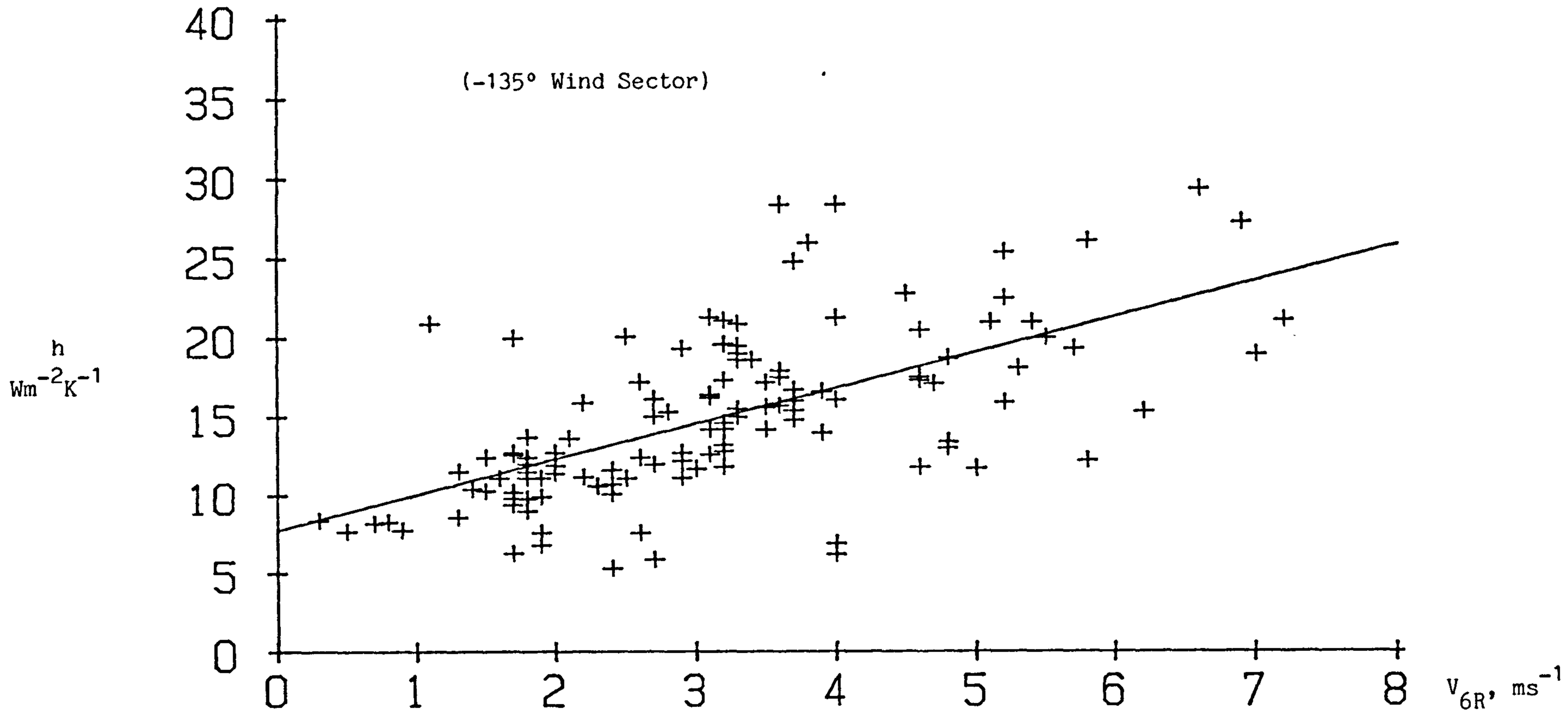


Figure 5.8 Convection coefficient, h, against roof wind speed $V_{6R}$

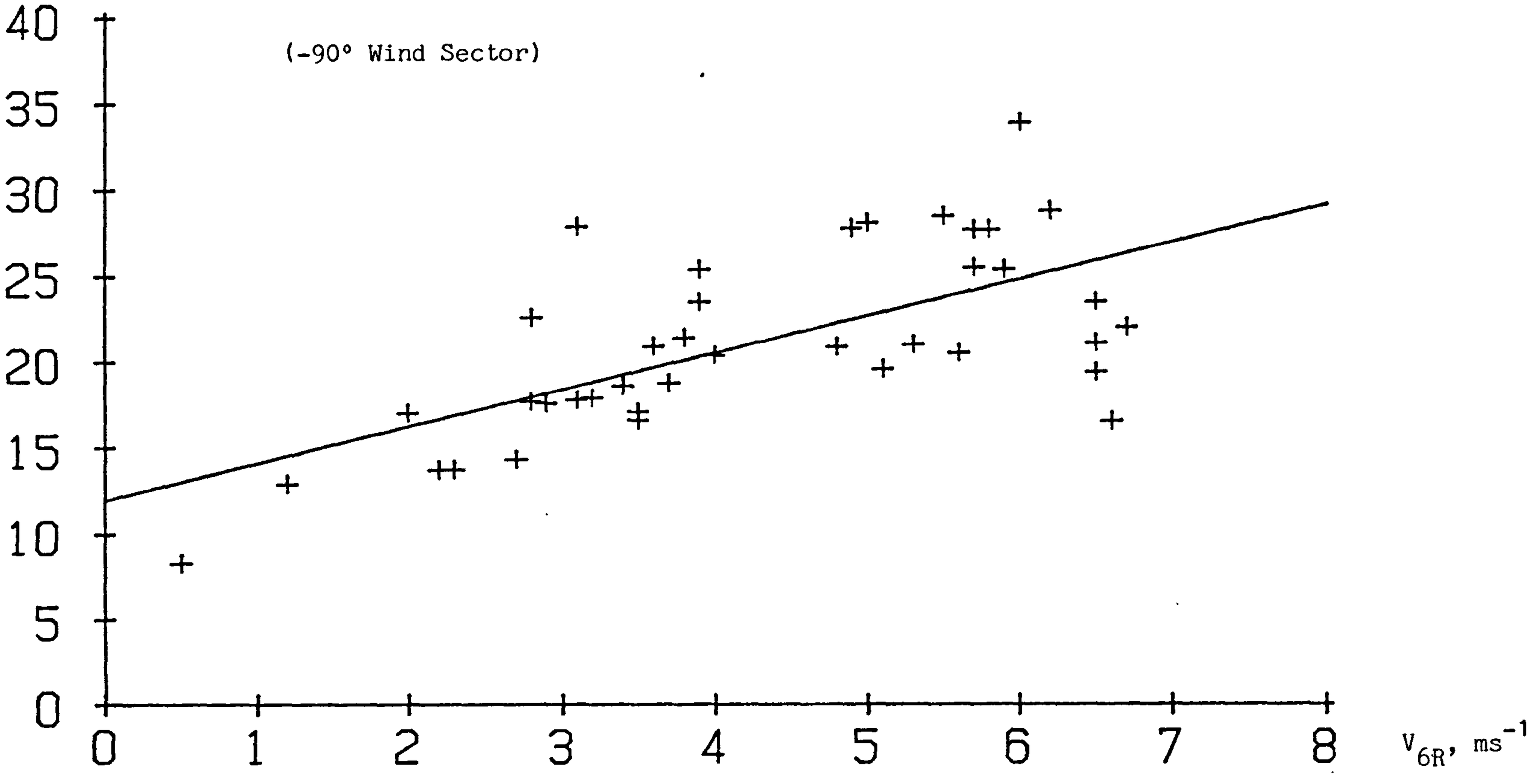


Figure 5.9 Convection coefficient, h, against roof wind speed $V_{6R}$

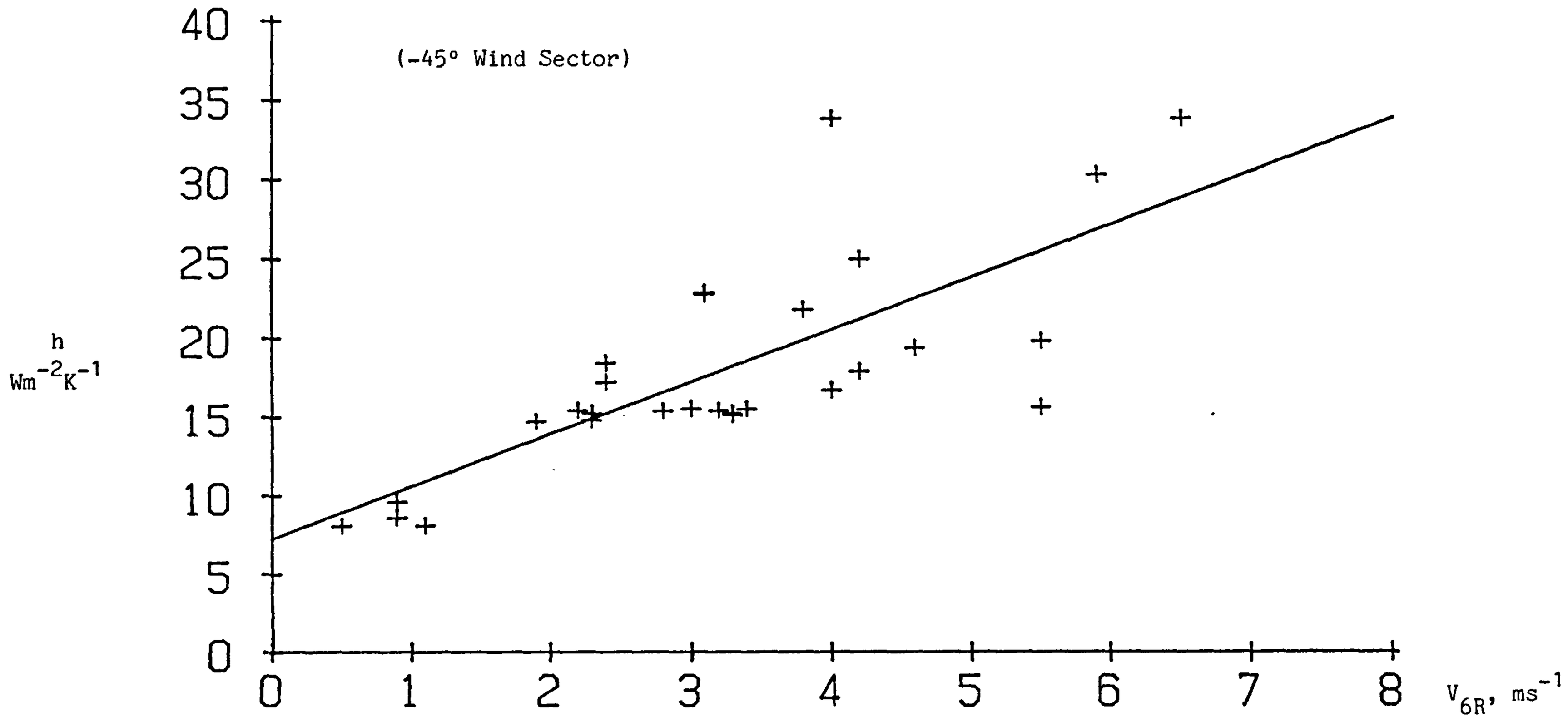


Figure 5.10 Convection coefficient, h, against roof wind speed $V_{6R}$

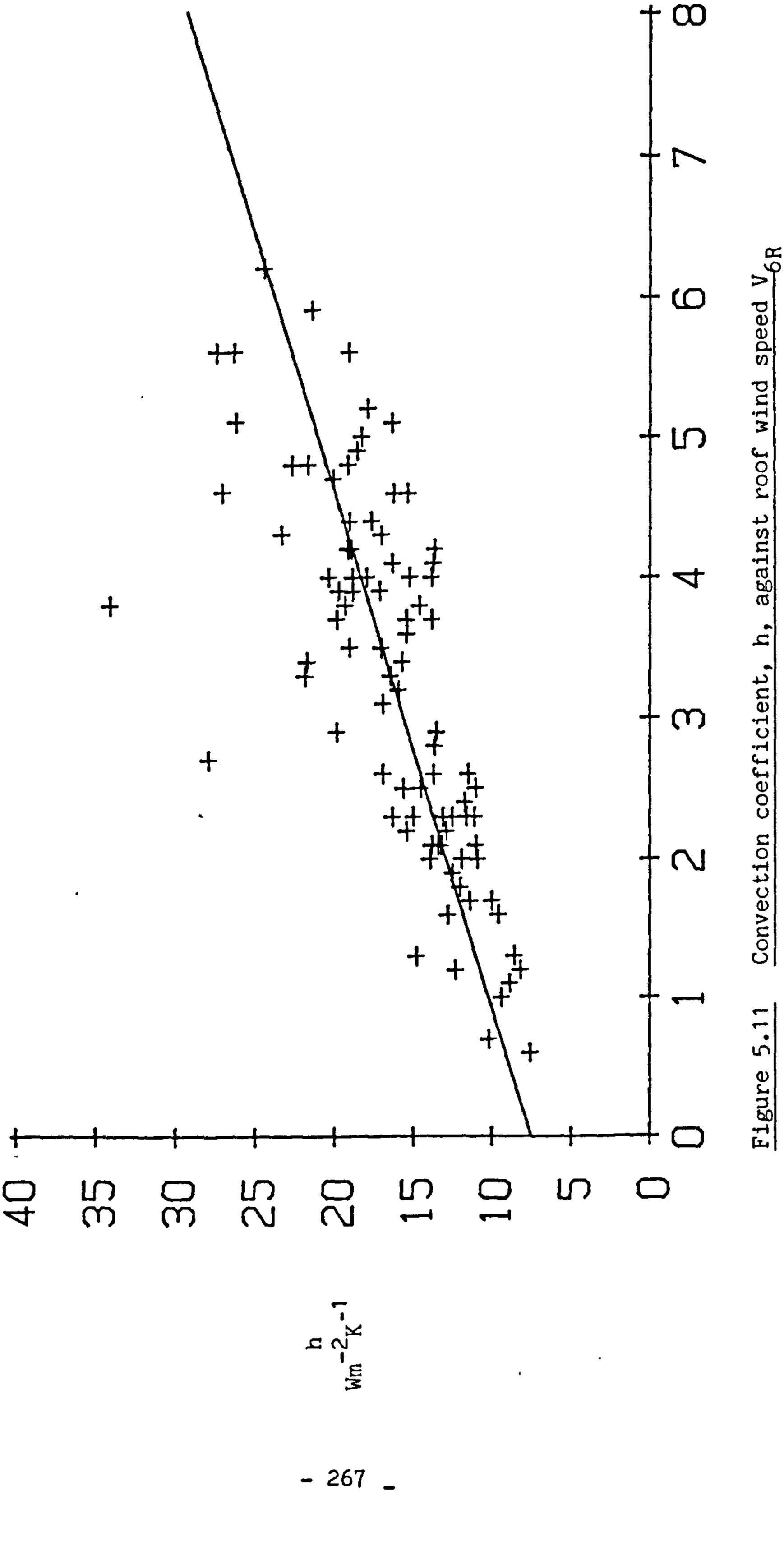


Figure 5.11 Convection coefficient, h, against roof wind speed $V_{6R}$
45° wind sector (Predominance, P > 50%)

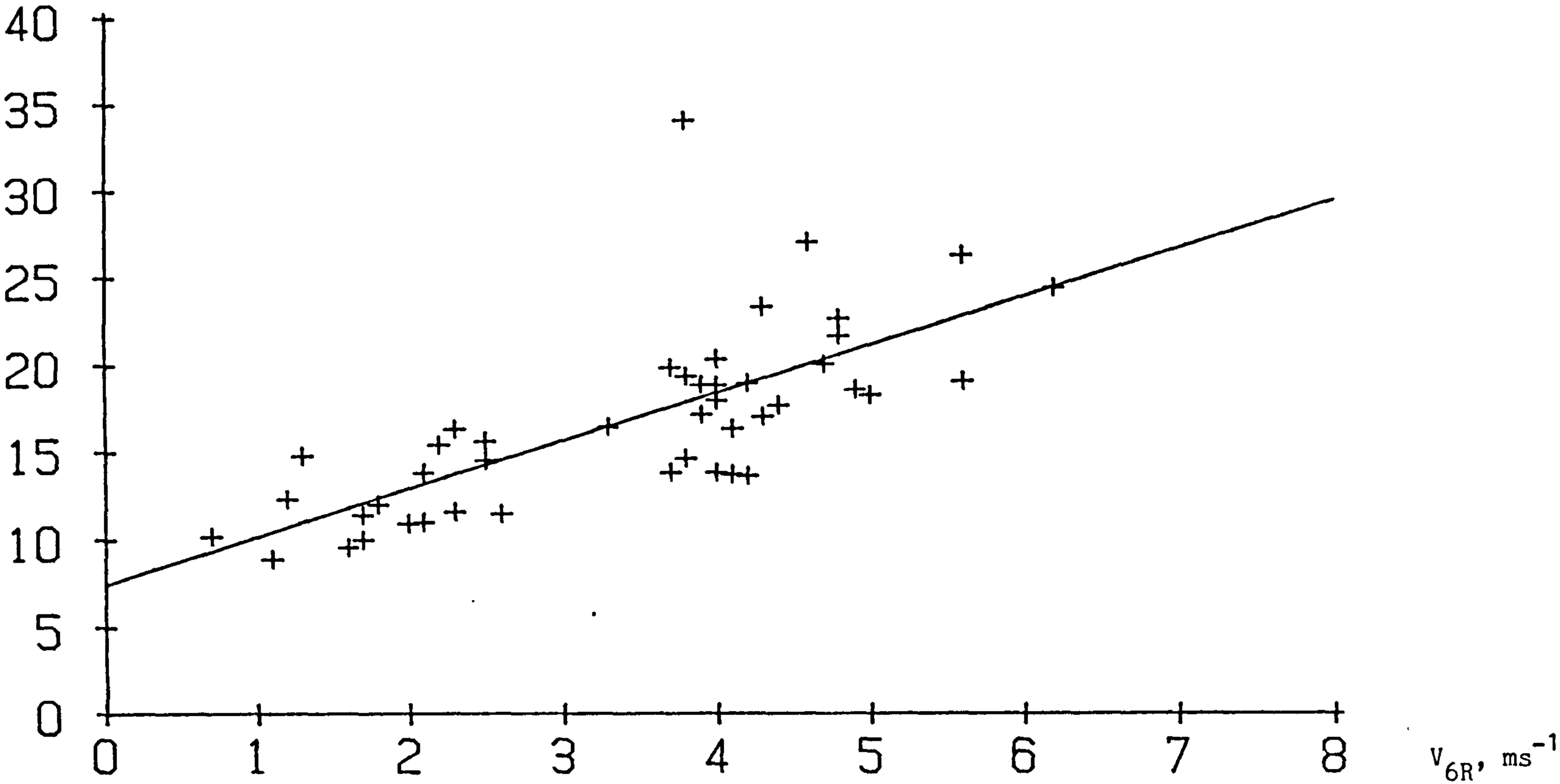


Figure 5.12 Convection coefficient, h, against roof wind speed $V_{6R}$
45° wind sector (Predominance, P > 60%)

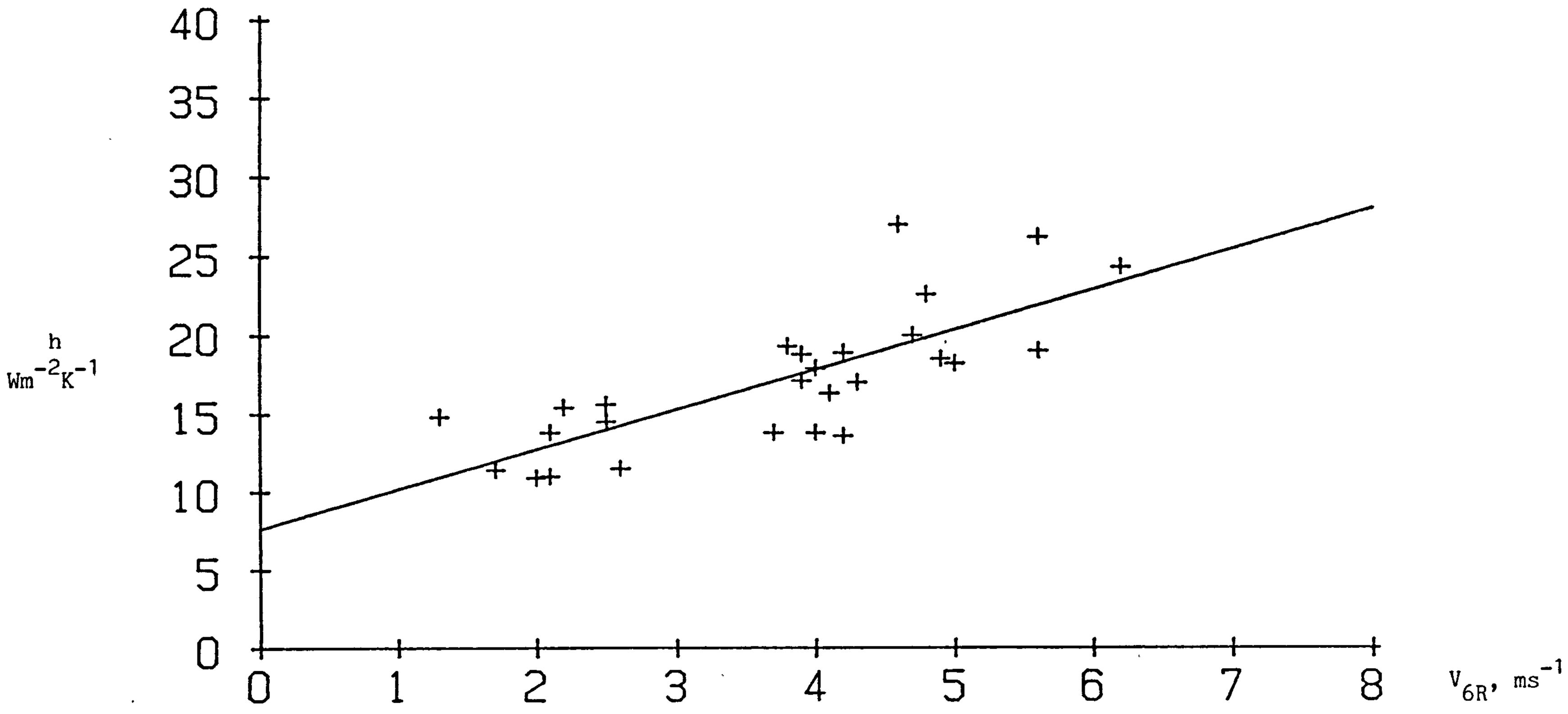


Figure 5.13 Convection coefficient, h, against roof wind speed $V_{6R}$ 45° wind sector (Predominance, P > 70%)

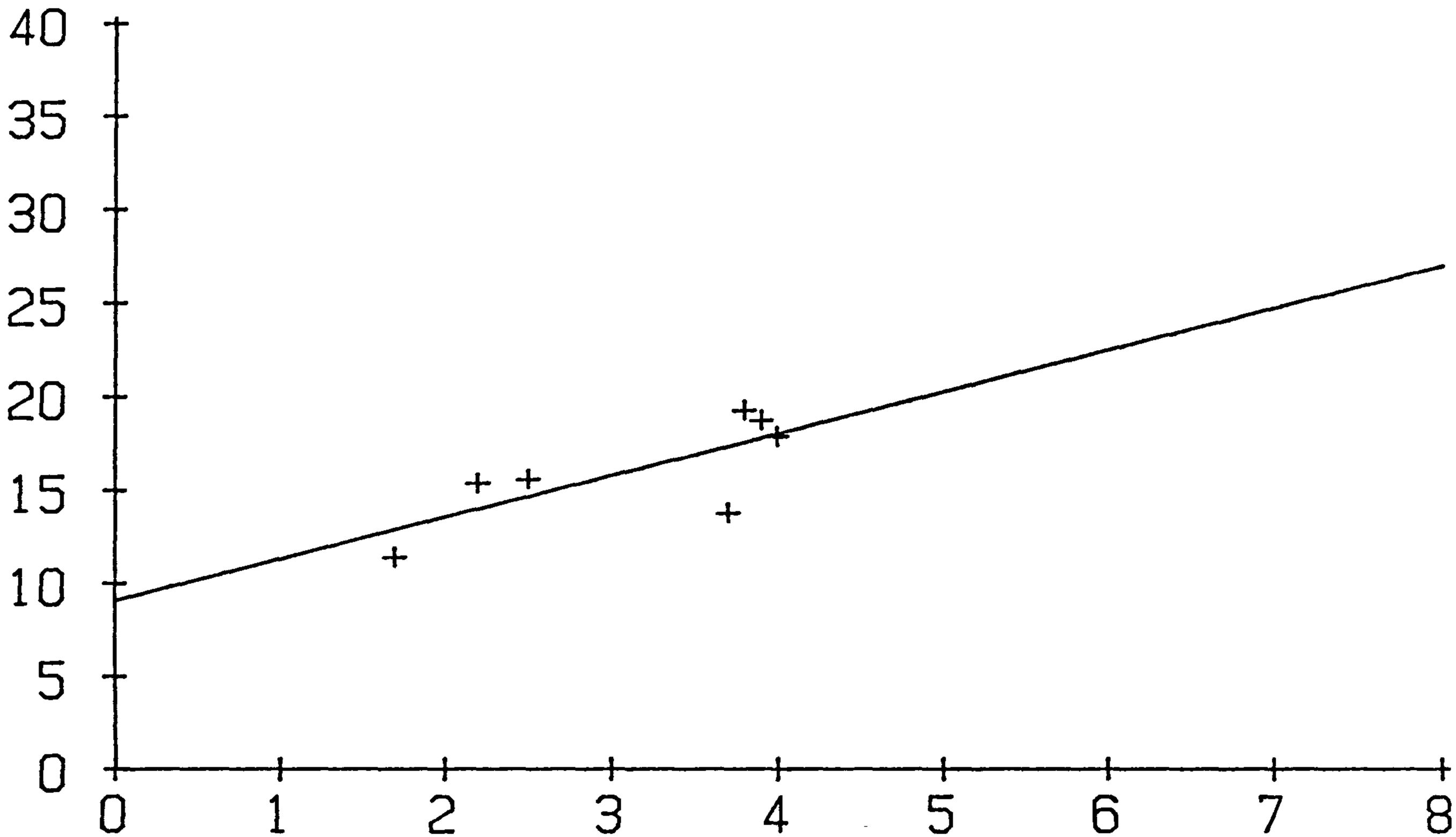


Figure 5.14 Convection coefficient, h, against roof wind speed $V_{6R}$
45° wind sector (Predominance, P > 80%)

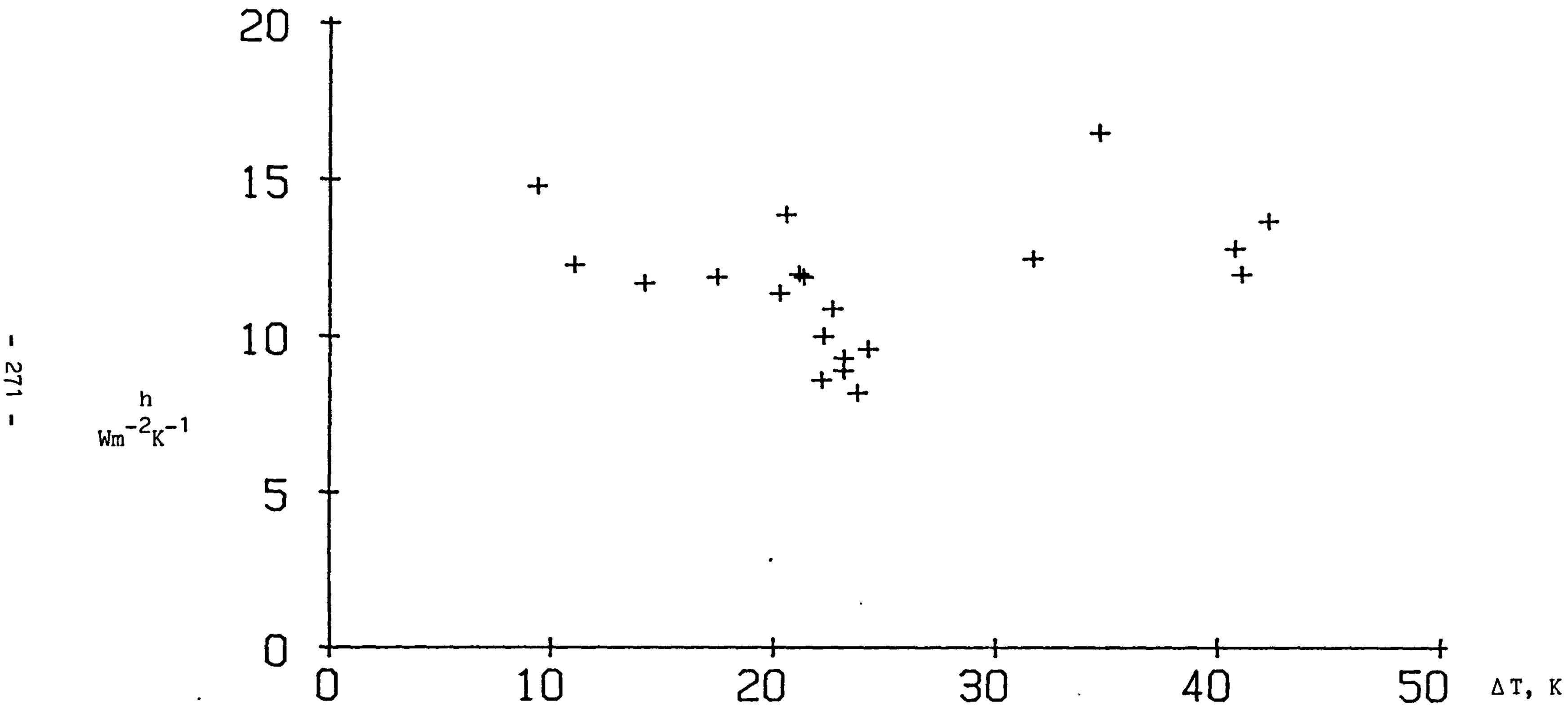


Figure 5.15 Convection coefficient, h, against plate-air temperature difference, $\Delta T$, 45° wind sector ($1.1 < V_{6R} < 2.0$ $ms^{-1}$)

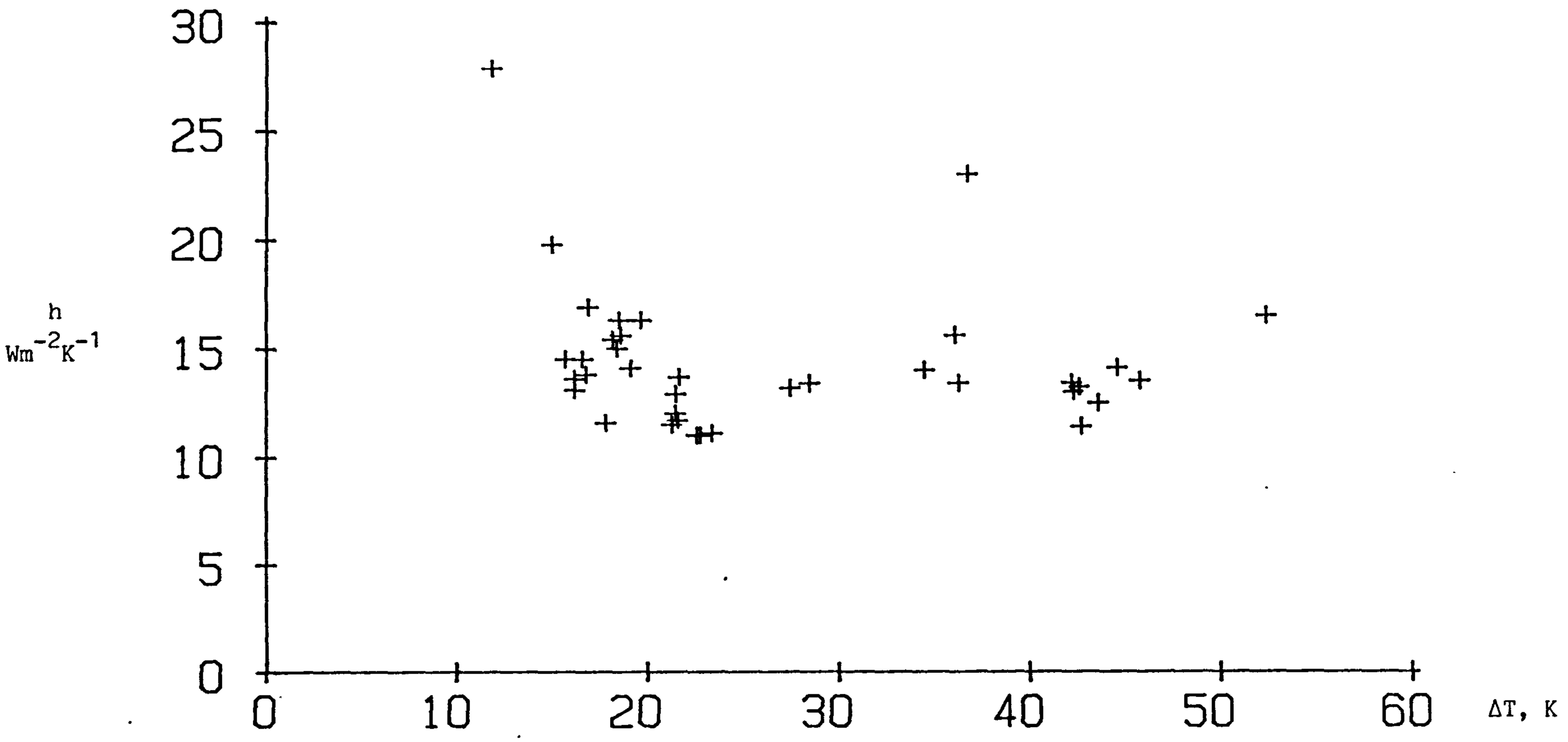


Figure 5.16 Convection coefficient, h, against plate-air temperature difference ΔT. 45° wind sector ($2.1 < V_{6R} < 3.0\ ms^{-1}$)

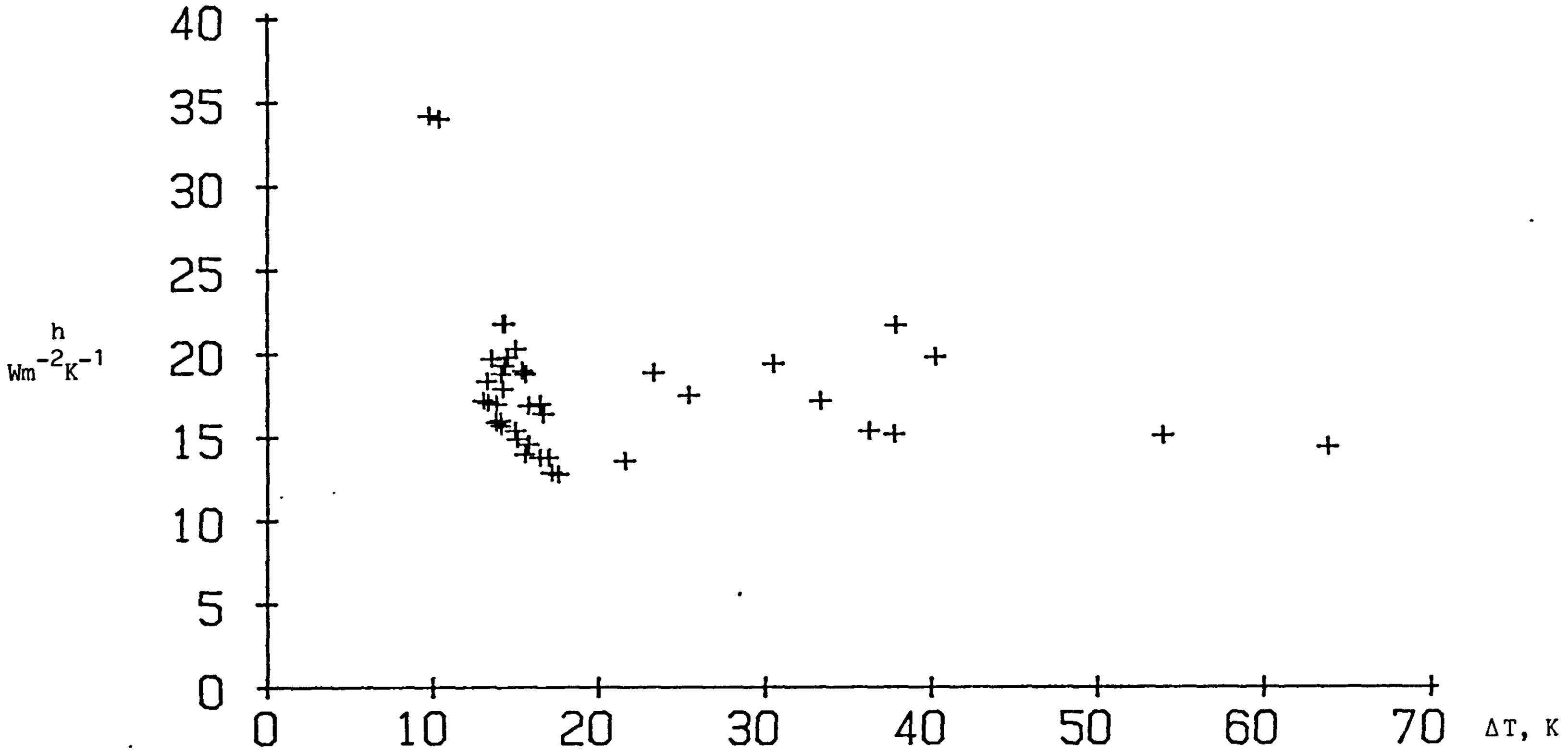


Figure 5.17 Convection coefficient, h, against plate-air temperature difference $\Delta T$.
45° wind sector ($3.1 < V_{6R} < 4.0\ ms^{-1}$)

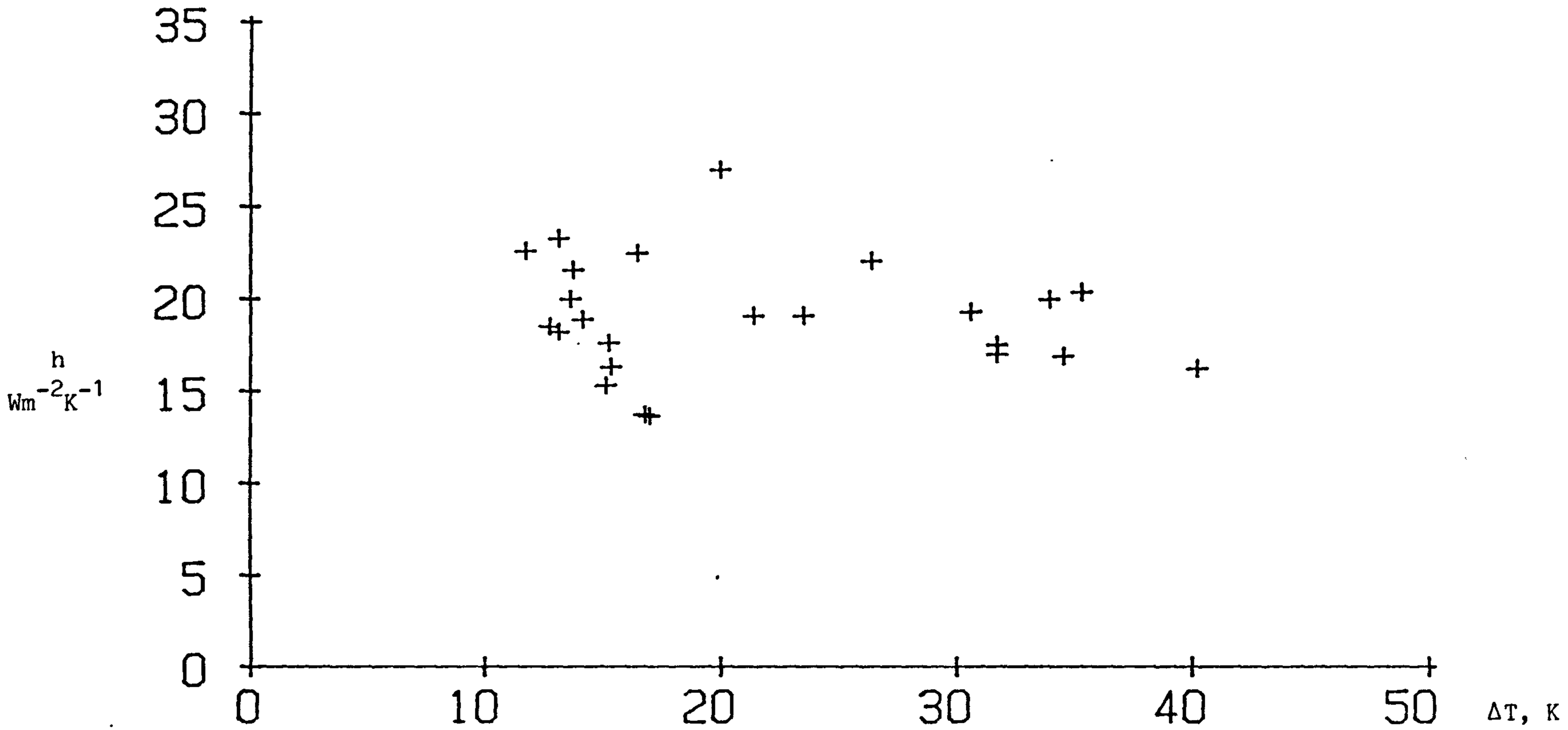


Figure 5.18 Convection coefficient, h, against plate-air temperature difference, ΔT. 45° wind sector ($4.1 < V_{6R} < 5.0\ ms^{-1}$)

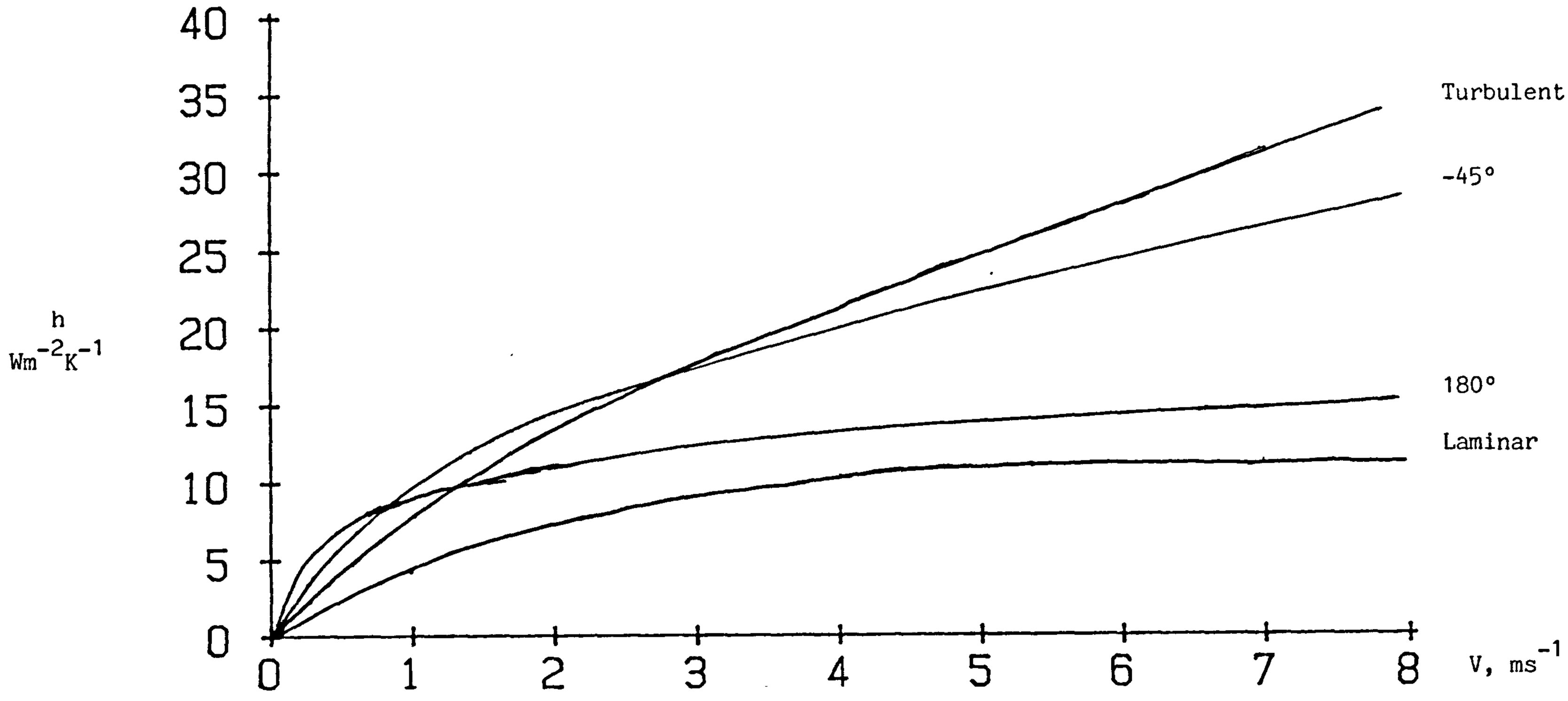


Figure 5.19 Comparison between laminar and turbulent theory with derived power law curves for the 180° and -45° wind sectors

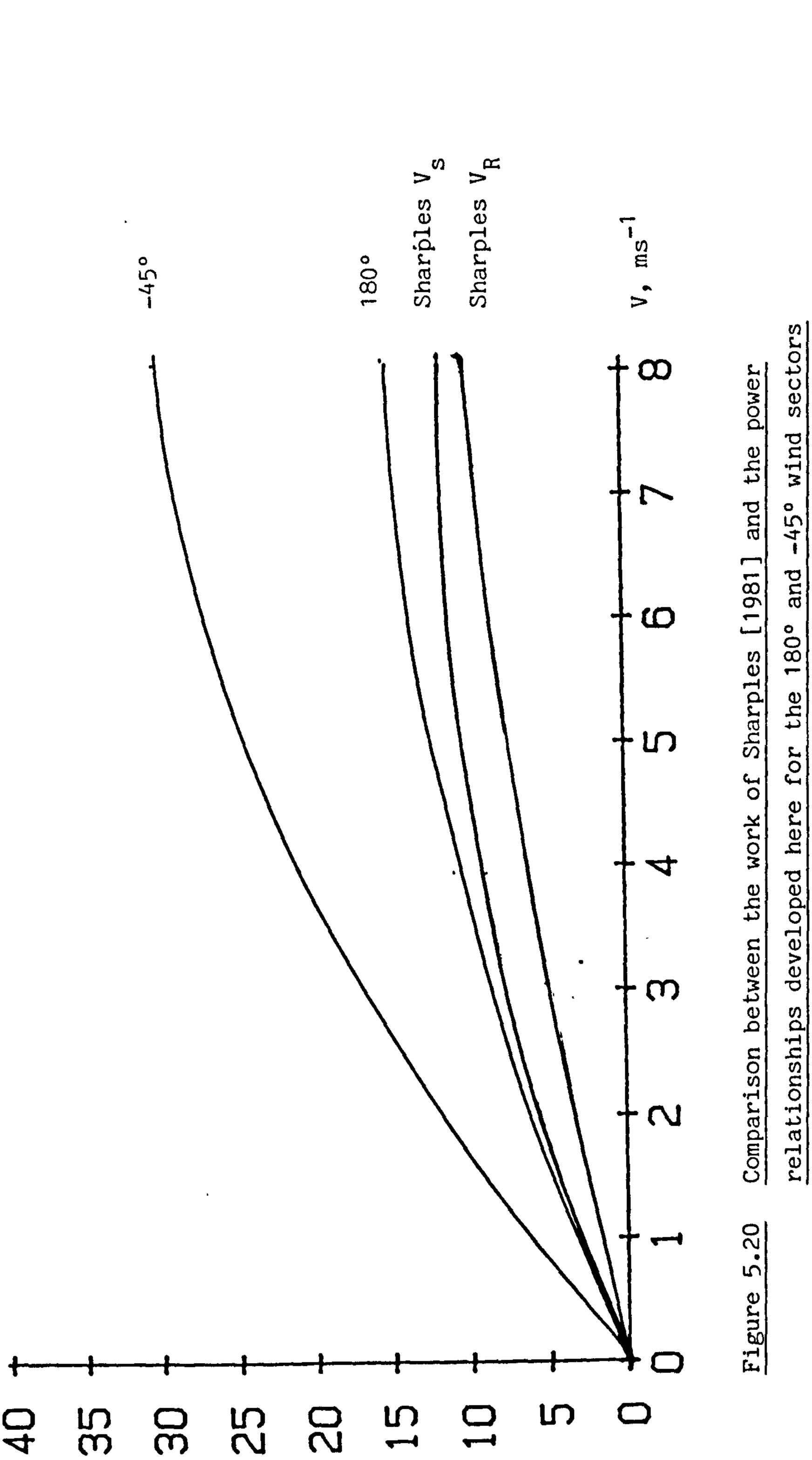


Figure 5.20 Comparison between the work of Sharples [1981] and the power relationships developed here for the 180° and -45° wind sectors

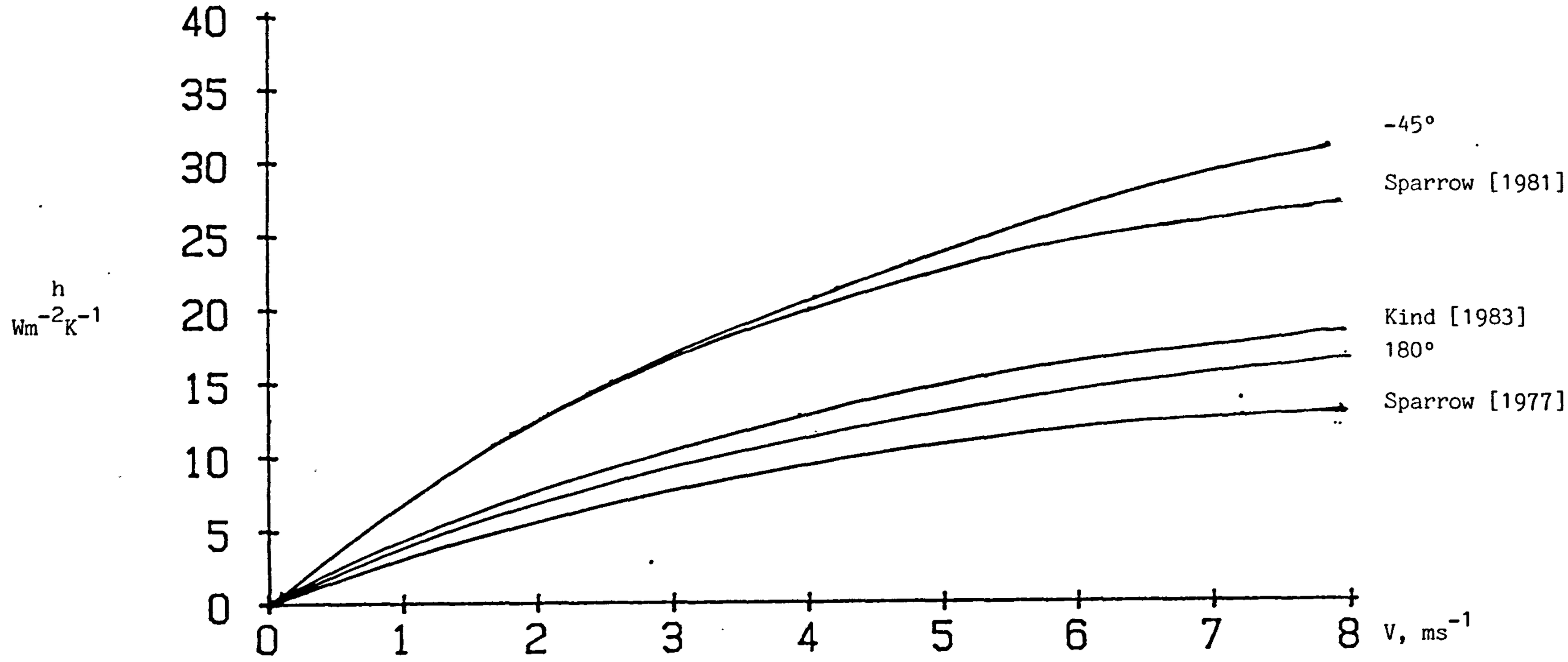


Figure 5.21 Comparison between the model work of Sparrow [1977, 1981] and Kind [1983] with the full scale 180° and -45° wind sector equations.

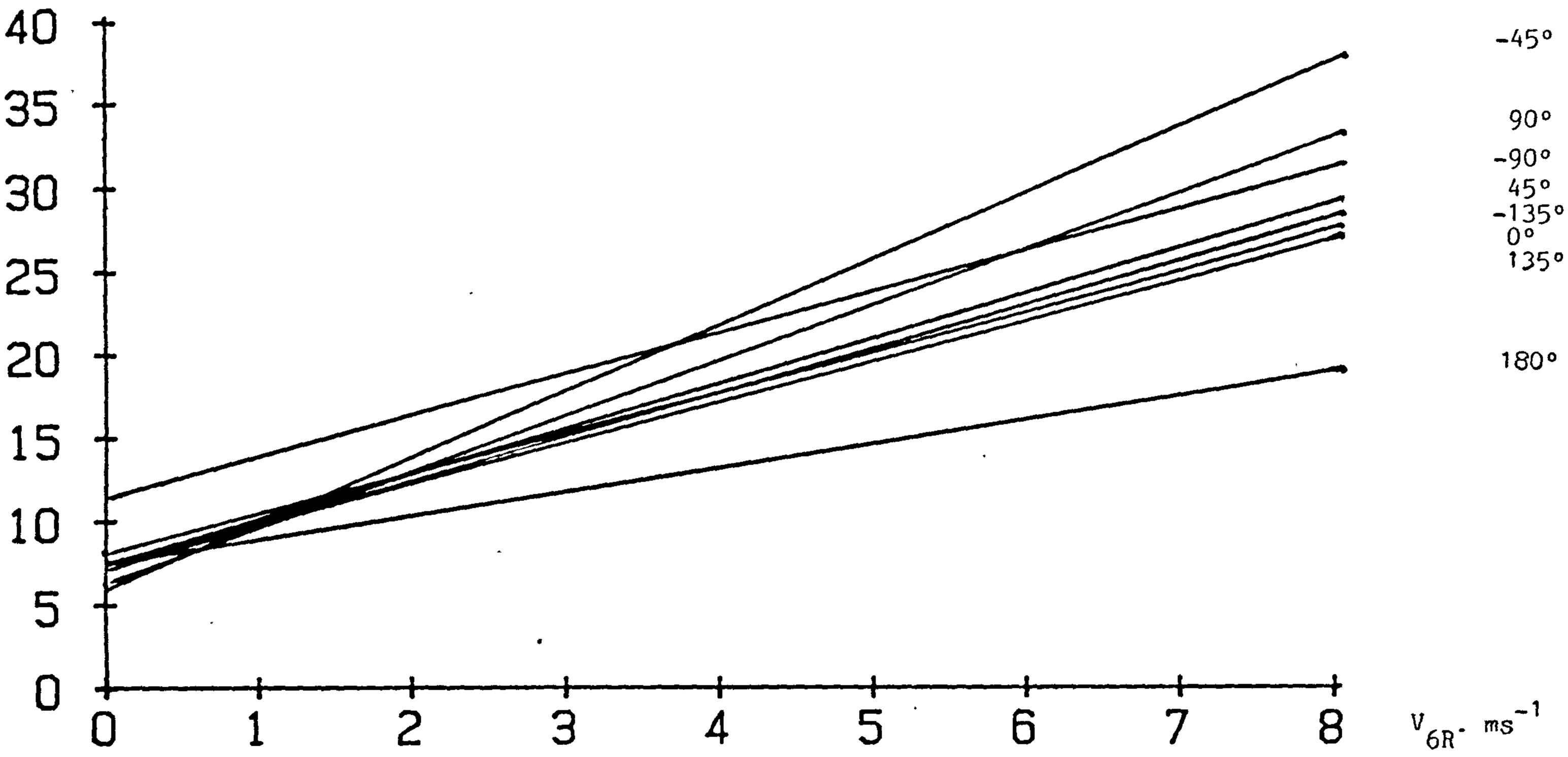


Figure 5.22 Convection coefficient, h, against roof wind speed, $V_{6R}$, for each wind incidence angle sector

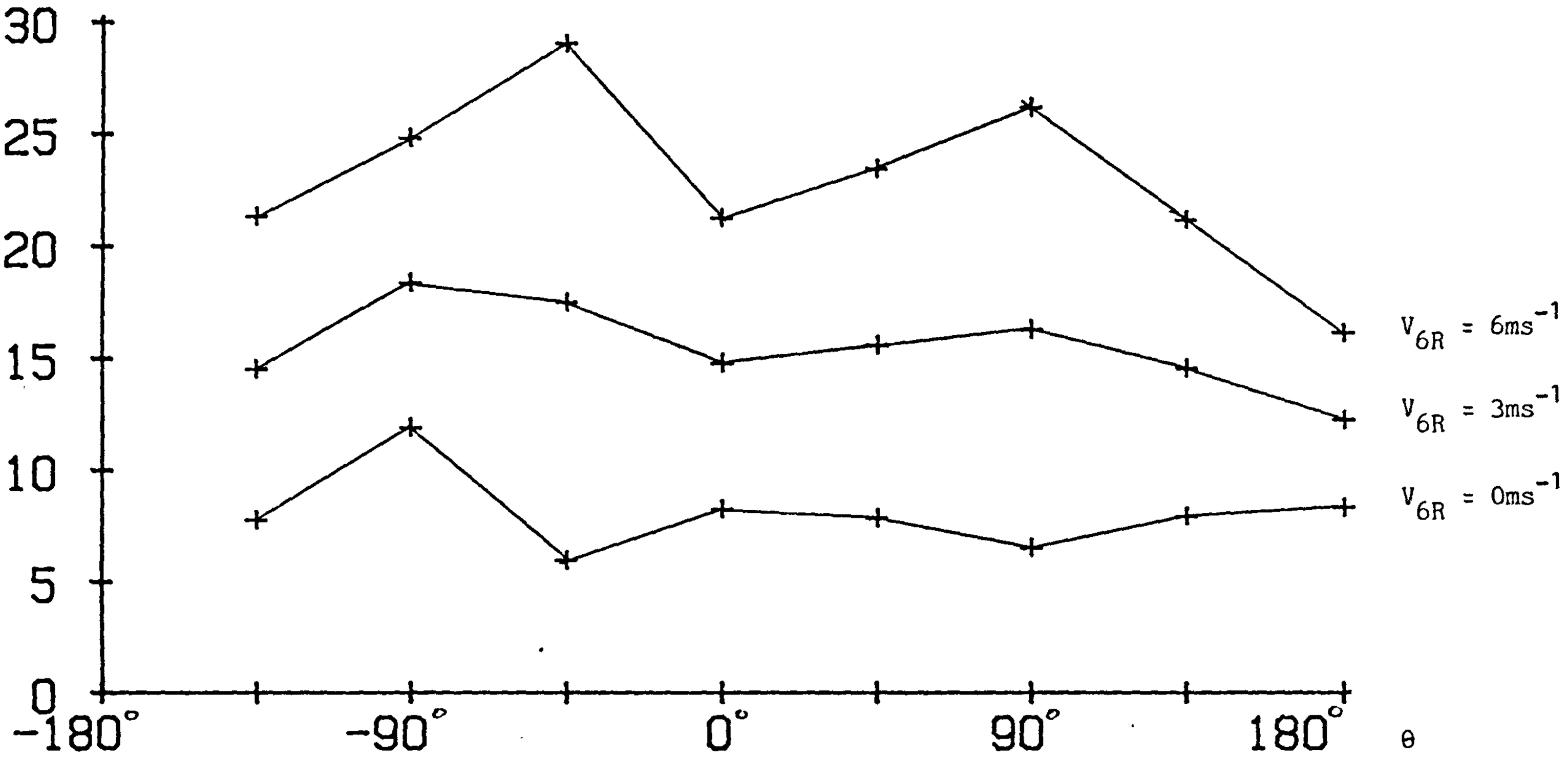


Figure 5.23 Convection ceoffient, h against wind incidence angle θ for three values of roof wind speed $V_{6R}$

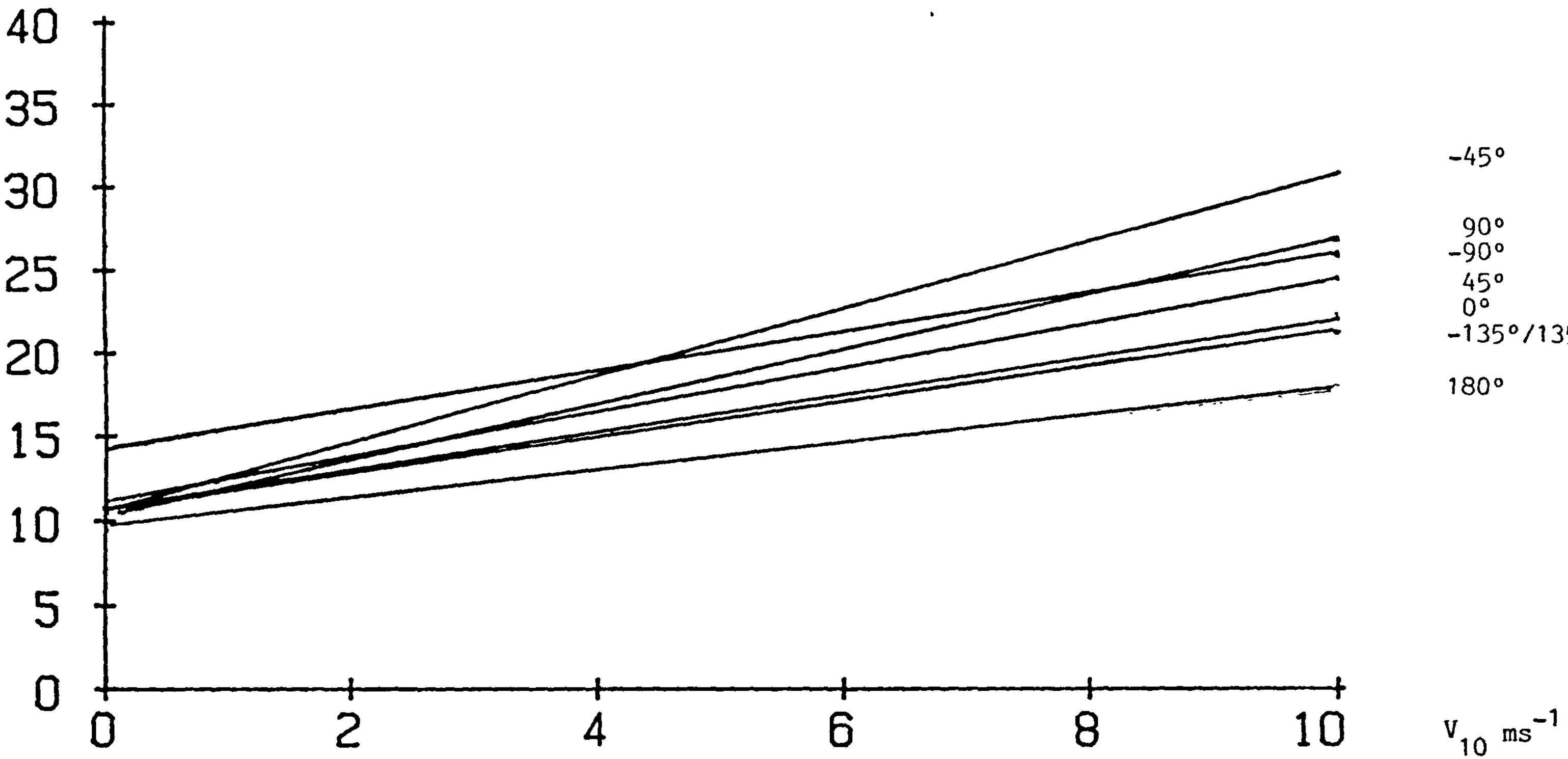


Figure 5.24 Convection coefficient, h, against meteorological 10m wind speed, $V_{10}$, for each wind incidence angle sector

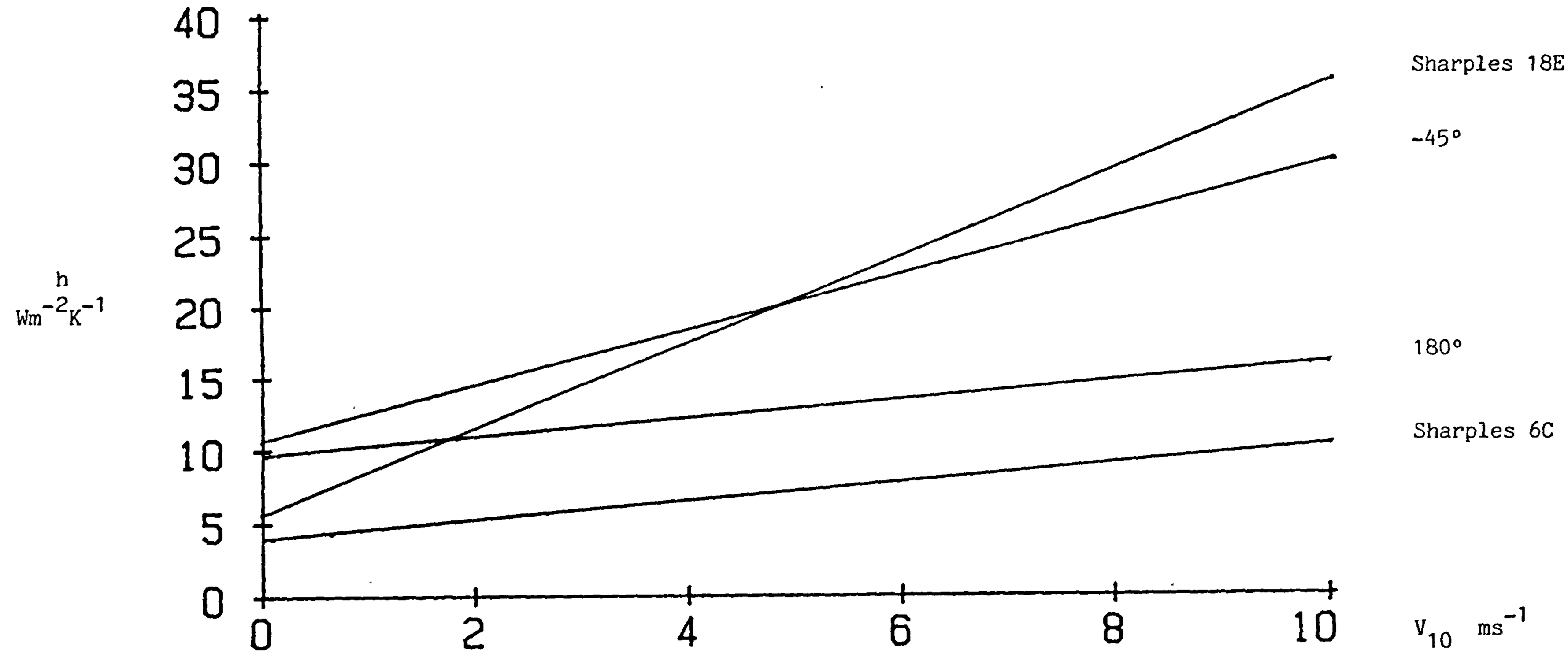


Figure 5.25 Comparison between Sharples [1984] $V_{10}$ relationships and those developed here for the 180° and -45° wind sectors

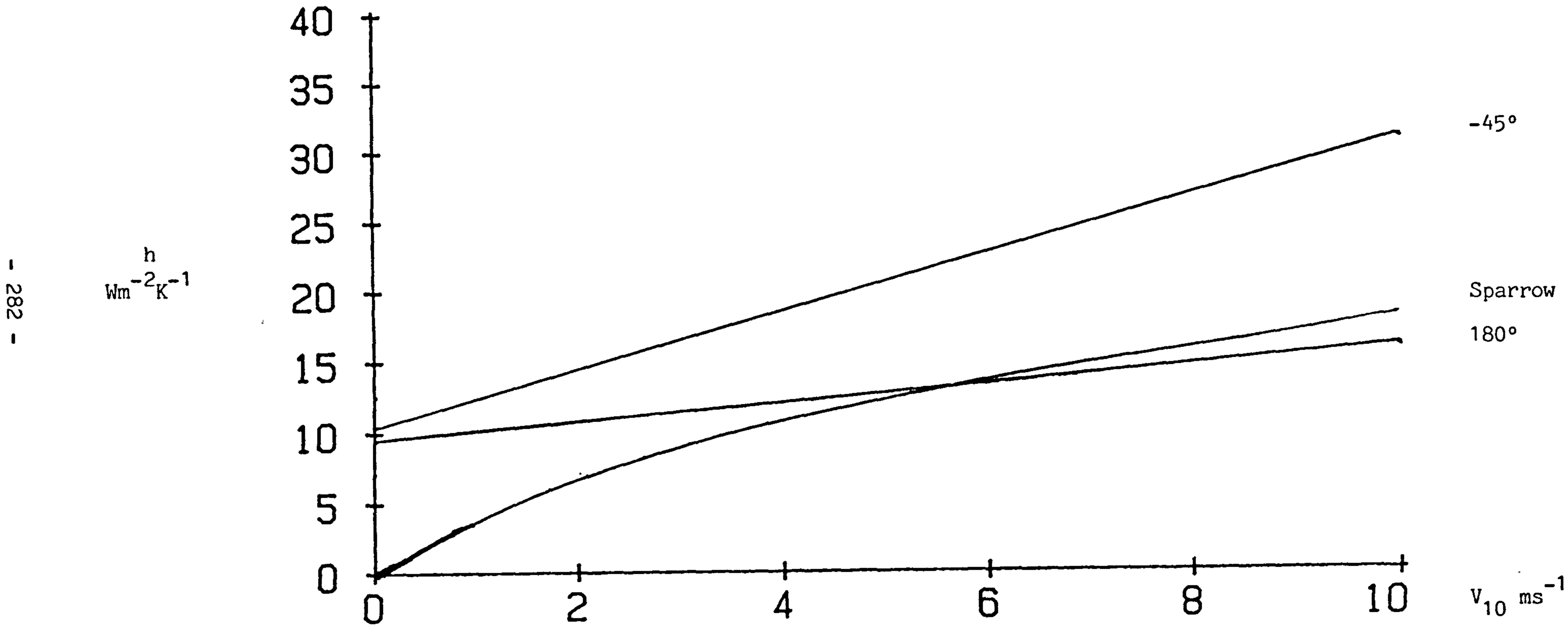


Figure 5.26 Comparison of the current work with Sparrows [1973] equation as recommended by Green [1981] for use with the 10m meteorological wind speed, $V_{10}$.

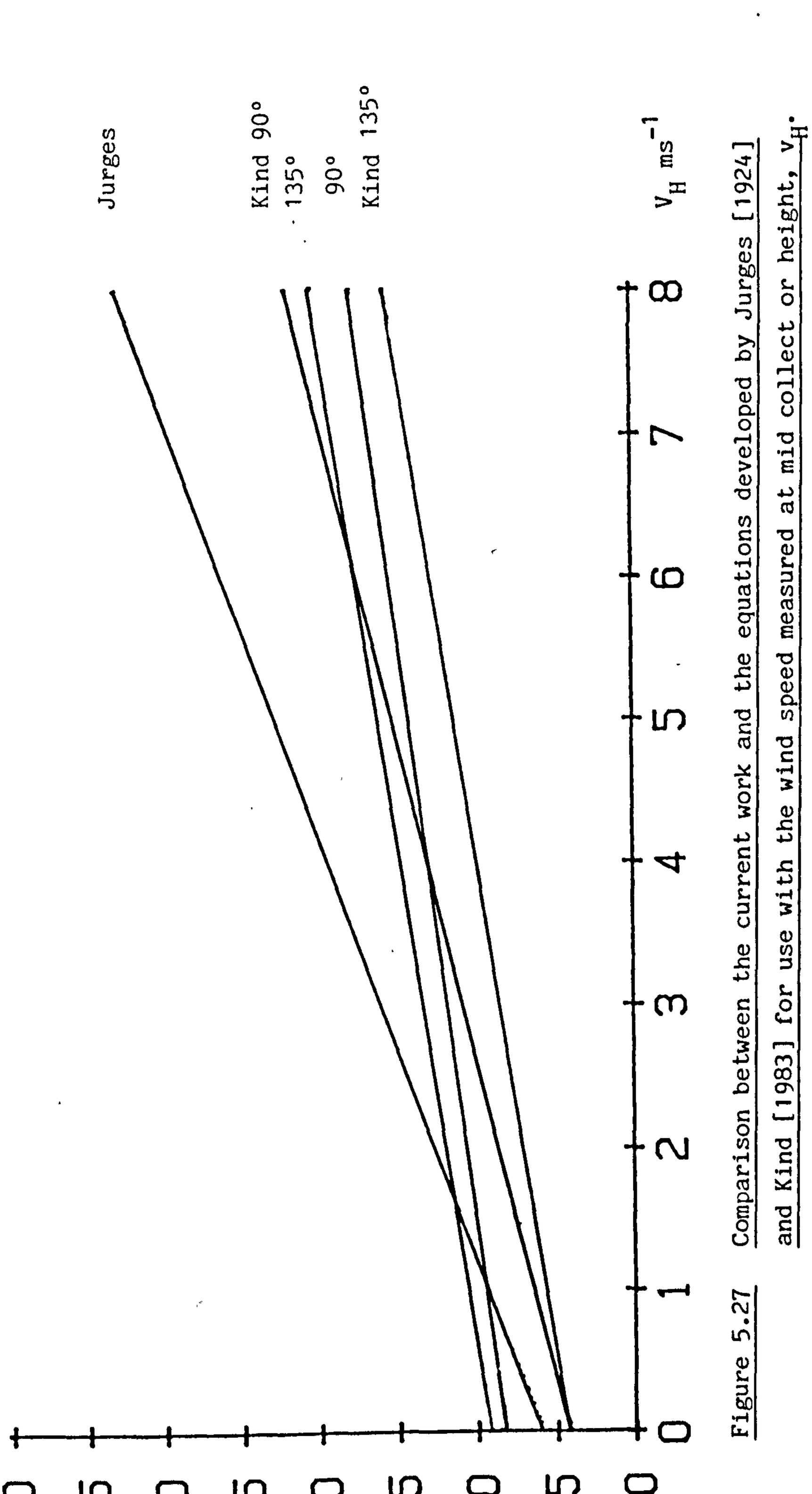


Figure 5.27 Comparison between the

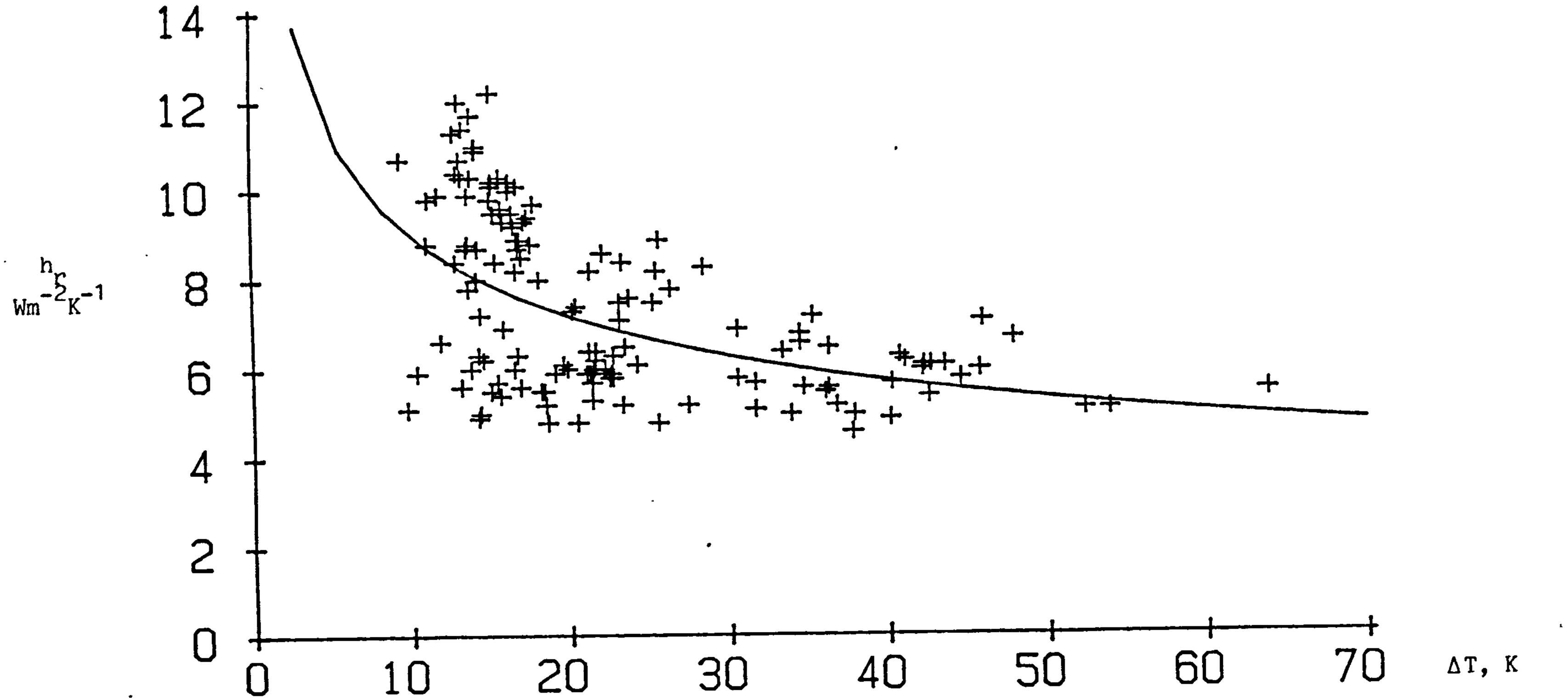


Figure 5.28 Radiative heat transfer coefficient, $h_r$, against plate-air temperature difference, $\Delta T$. (45° wind sector)

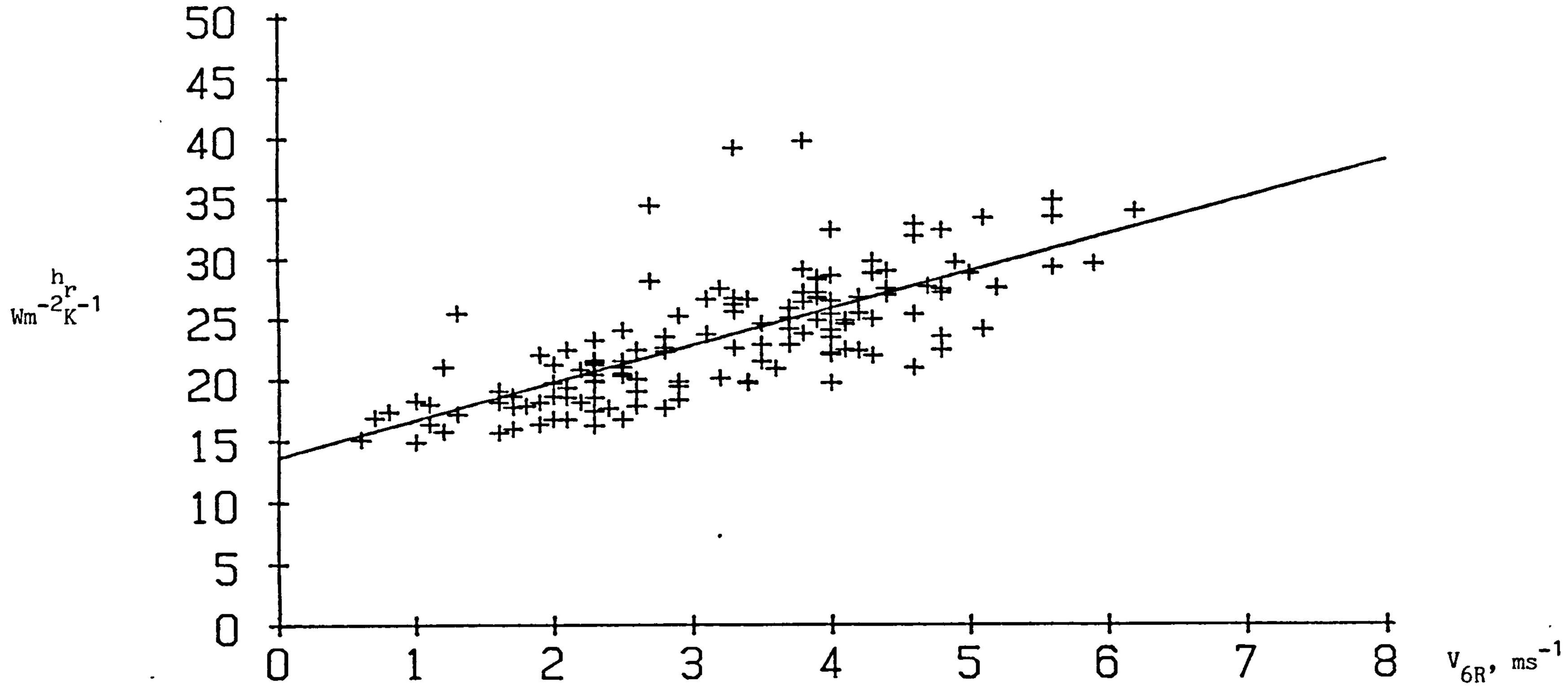


Figure 5.29 Total heat transfer coefficient, $h_t = h + h_r$, against roof wind speed, $V_{6R}$. (45° wind sector)

# CHAPTER SIX

# DETAILS OF THE WIND TUNNEL MODEL EXPERIMENTS

## Introduction

Chapters Four and Five described the experimental details and the results obtained from the full-scale convective heat transfer measurements. These experiments, whilst of fundamental importance, were difficult to perform, laborious to maintain and produced results which had large errors associated with them.

Wind tunnel experiments tend to be easier to perform, yield more accurate results and offer the advantage that the parameters involved e.g. wind speed, air temperature, etc. are more controllable than in full-scale work. Therefore such a series of wind tunnel model experiments was performed.

The objectives of the model studies were two fold, i.e.

(i) To compare the results obtained with those of the full-scale experiments in order to assess the potential of extrapolating wind tunnel model results to full-scale values.

(ii) To compare the results with previous wind tunnel experiments performed on model buildings of a similar geometry, e.g. Kind et al [1983] or Kelnhofer and Thomas [1976].

This chapter describes the essential features of the wind tunnel, models and instrumentation used for the performance of the wind tunnel model experiments.

## 6.1 A General Description of the Wind Tunnel used for the Model Convective Heat Transfer Experiments

The model convective heat transfer experiments were performed in the boundary layer wind tunnel at the University of Sheffield. An exterior view of the tunnel is shown in Figure 6.1. The tunnel has a cross-sectional working area of 1.2 x 1.2m and an overall length of 7.2m. The large working section design is based on a 1.2 x 1.2m module size, having a fixed roof and floor construction rigidly connected by steel frames. The side walls originally consisted of a series of 1.2 x 1.2m panels, six of which were made of 12.5mm thick, clear acrylic sheet, the other six being 25mm block board sheet painted matt black on the inside.

The convective heat transfer coefficient of the model plates was to be evaluated in an essentially similar manner to the method employed in the full-scale measurements, i.e. a steady state energy balance on a flat plate. Therefore, the radiative gain at the plate surface had to be known, or evaluated. In order to make this parameter more easily defineable the clear acrylic panels were covered, on the outside, with thick matt black card. Whilst this coating in no way alters the emissivity of the internal surface of the acrylic sheet, it does perform the function of making the radiative environment inside the tunnel less dependent on the radiation conditions outside in the rest of the laboratory. These external conditions may vary considerably, due to the fact that the laboratory is lit by artificial lighting, and natural daylight from windows and skylights. Also as the temperature of the laboratory changes throughout the day, the longwave radiation emitted by the walls and

ceiling of the room will change. A full description of the evaluation of the radiative gain at the plate surface will be given in Section 6.7. The roof of the wind tunnel was also painted matt black except for 3 small rectangular sections made of acrylic sheet. These, originally used to allow artificial light into the tunnel, were also covered with black card.

Recessed into the floor of the 5th modular section (5.4m downstream from the tunnel entrance) is a 1.1m diameter turntable, the upper surface of which is flush with the rest of the floor section. The models used for the convective heat transfer experiments were to be positioned at the centre of this turntable. The turntable, which was marked in 5°, intervals could be rotated and fixed at any position so the models could experience the effect of the wind blowing from any direction.

The wind flow was created by a constant speed fan, located upstream from the working section. This sucked air through the mouth of the tunnel and past the working sections, the air first passing through a fence - spire - roughness element configuration (described in the next section). With the fan running at its constant speed wind speeds in the range 3.1 - 25.0 $ms^{-1}$ could be obtained. This variation is obtained by feathering the blades of the fan to the required pitch by blowing compressed air across its face.

## 6.2 A Description of the Method used to Create a Simulated Atmospheric Boundary Layer in the Wind Tunnel

The simulation of the atmospheric boundary layer in wind tunnels has already been discussed briefly in Section 3.6.2, as have the characteristics of the natural wind (Section 3.6.1). In the wind tunnel

used for this current series of experiments the major characteristics of the boundary layer are simulated by the use of a fence-spire-roughness element configuration, as recommended by Counihan [1973].

A honeycomb, 150mm thick with a 15mm cell size, was positioned at the inlet flare of the tunnel. The layer filled the entrance to the tunnel and served to straighten out the incoming flow.

320mm downstream of the honeycomb was a castellated fence which spanned the width of the tunnel. The castellations were, alternately, 195 and 230mm high, with a gap and castellation width of 150mm.

Each gap in the fence was aligned with one of a set of spires which were positioned in a row across the tunnel 200mm downstream of the fence. The spires were triangular, with base dimensions of 200 x 200 x 65mm and each tapered to an apex at a height of 900mm.

Roughness elements immediately followed the spires. Each element was cut from foam rubber and measured 75 x 75 x 37.5mm high. The elements are arranged in a staggered array, each separated by 150mm in the longitudinal direction and 75mm in the lateral direction. Each row of elements spanning the tunnel width contained 8 units and there were 16 rows of elements between the spires and the section containing the turntable. This arrangement gives a total fetch length of roughness elements of 3.78m.

The use of this threefold arrangement, as opposed to one which just uses rougness elements placed on the tunnel floor, means that the relatively short length of the tunnel is adequate to produce a boundary layer of reasonable thickness. This is because the fence provides an initial depth to the layer and the thus retarded flow then

mixes into the developing layer via the turbulence induced by the spires. Under ideal conditions the fence- spire combination should produce a flow at the first row of roughness elements identical to that which would have been developed had the elements extended over a longer fetch length.

## 6.3 The Characteristics of the Simulated Atmospheric Boundary Layer Created by the Wind Tunnel

The physical characteristics of the boundary layer produced by the method described in the previous section have been investigated by Lee [1977]. Since this report was published the introduction of a more powerful fan system has rendered the wind tunnel capable of maintaining velocities much greater than Lee's quoted maximum of 9.8 $ms^{-1}$. The relevant characteristics of the boundary layer may be expected to be slightly dependent on velocity. Lee measured these characteristics when the tunnel was running at its previous maximum speed (9.8 $ms^{-1}$). As this speed lies approximately in the middle of the range currently available (3.1 - 25.0 $ms^{-1}$), the findings of Lee's report can still be considered valid for this current series of experiments. This assumption is given further credence by the work of Evans and Lee [1983]. They examined the velocity profile of the boundary layer when the tunnel was running near its new maximum speed. The shapes of the two measured profiles were essentially identical.

### 6.3.1 The velocity profile of the simulated atmospheric boundary layer

The velocity profile is the most obvious characteristic of a boundary layer. An example of this profile, as measured over the centre of the turntable, is shown in Figure 6.2. The maximum velocity (in this case 9.8 $ms^{-1}$) was obtained at a height of 800mm above the

centre of the turntable, is shown in Figure 6.2. The maximum velocity (in this case 9.8 $ms^{-1}$) was obtained at a height of 800*mm* above the centre of the turntable. This velocity is maintained to a height of approximately 1100*mm*, and is known as the gradient wind speed $V_G$. Above this height the boundary layer produced by the smooth roof exerts a retarding effect on the profile. It must be noted that the side walls will also produce boundary layers adjacent to their surfaces. Lee [1977] states that these layers are 125mm thick at the turntable centre position. This means that almost the entire turntable is subjected to uniform lateral flow conditions.

It has been shown in Section 3.6 that a boundary layer velocity profile of this type can be described mathematically by two basic forms of equation. One, a power law, is best suited to a description of the entire profile. The other, of logarithmic form, better describes the velocity profile near the ground i.e.

$$\frac{V_1}{V_2} = \left(\frac{Z_1}{Z_2}\right)^{\alpha} \qquad (6.1)$$

and

$$\frac{V_1}{V_{*2}} = \frac{1}{k} \ln\left(\frac{Z_1}{Z_o}\right) \qquad (6.2)$$

where $V_1$ and $V_2$ are the velocities at heights $Z_1$ and $Z_2$ above the tunnel floor, $V_*$ is the friction velocity, $Z_o$ is the roughness length and $\alpha$ and k are constants. The important parameters in these equations are the value of the exponent, $\alpha$, in the power law equation and the roughness length, $Z_o$, in the logarithmic equation. Lee gives the following values to these two parameters $\alpha = 0.29$ and $Z_o$ = 3.0mm. Comparison of this value of $\alpha$ with those shown in Table 3.3 indicate that it lies at the upper end of the rural range and at the lower end of the urban terrain range.

Lee also quotes the friction velocity to be $V_* = 0.065\ V_G$ i.e. in the case of the profile shown in Figure 6.2 $V_* = 0.637$. This value is in good agreement with that found by Flay [1982] for a site with similar surrounding terrain to the Norton site used for the full-scale measurements.

### 6.3.2 The turbulence characteristics of the simulated atmospheric boundary layer

The other main factors which are of importance when simulating the natural wind in wind tunnels are the turbulence characteristics of the boundary layer (e.g. see Cermak [1975]). It will be recalled from Section 3.5 that turbulence can be considered as three coplanar velocity fluctuations U', V' and W' superimposed upon the mean velocity of the flow V.

The distributions of all three components of the turbulence intensity (See Section 3.5 for a definition of these parameters) based on both local and gradient velocity are presented by Lee. In the lower region of the layer, where models are likely to be placed, the turbulence intensities for all three components, i.e. longitudinal, vertical and lateral lie in the range 15-40%. This is in general agreement with the values found for the natural wind, as reported earlier in Section 3.6. In their non-dimensionalised form the turbulence intensity ratios are

$$\frac{U^*}{V_*} = 2.58,\ \frac{V^*}{V_*} = 1.84,\ \frac{W^*}{V_*} = 1.23$$

where $U^* = \sqrt{\overline{U'^2}}$, etc.

This is again in good agreement with the ratios given by Counihan [1975] and Flay [1982] as reported in Section 3.6.1 Turbulence is further characterised by its longitudinal scale length $LU_x$. This length was measured at 3 heights, Z, above the tunnel floor and was found to increase with increasing height, as in the natural environment. Its value ranged from $LU_x$ = 0.255m at Z = 100mm to $LU_x$ = 0.314m at Z = 400mm.

The final quantity of interest in defining the characteristics of the natural wind is the Reynolds stresses. Lee shows that in the first 200mm above the tunnel floor these lie in the range

$$0.003 < \frac{\overline{U'V'}}{V_G^2} < 0.0045$$

A similar range given by Counihan [1975], covering both rural and urban terrains near the ground is 0.002 - 0.0045. Thus the values of $\alpha$, turbulence intensity and Reynolds stresses all agree reasonably well with the measured data from the natural environment over rough rural and urban terrain. The obvious mis-match lies in the values of $Z_o$ and $LU_x$. It is these parameters which govern the scaling factors to be used when producing models to be used in the wind tunnel.

## 6.4 The Development of a Linear Scaling Factor to be used for the Model Convective Heat Transfer Experiments

### 6.4.1 The basic modelling philosophy employed for wind tunnel convective heat transfer experiments

For the evaluation of convective heat transfer from bluff bodies, the modelling guidelines are simple, i.e. that the shapes should be geometrically similar. This is because for a bluff body it is its shape alone which governs the flow characteristics around it, e.g. the flow will always separate at a sharp edge. The only possible

complication to this may arise from the fact that for flow over a plate the transition point from laminar to turbulent flow may alter with free-stream turbulence. As the free-stream turbulence in both the natural environment and the wind tunnel are of the same order this effect is minimised.

Therefore, all that is necessary in this case is to make a model of the building under consideration with sufficient of its surroundings to constitute a realistic description of the site. It was felt that in this case this could be achieved by producing a model of the test building itself and of the small adjacent garage. Both Iqubal and Khatry [1976] and Kind et al [1983] followed this philosophy, in that they each measured the convective heat transfer from model buildings in isolation. It must be remembered, however, that Kelnhofer and Thomas [1976] examined the sheltering potential of nearby buildings in their model work, and found that some effect was noticeable. (See Section 3.6.4 for details).

### 6.4.2 A discussion of the factors which effect the development of a linear scaling factor between the wind tunnel models and the full-scale test building

There are several factors which must be taken into account when deciding upon the linear scale to which the models will be constructed. The models must be made to a scale compatible with the wind tunnel size and with the scaling factor used to describe the simulated natural wind. They must also be of such a size which makes the performance of the convective heat transfer measurements as easy and as accurate as possible.

It was noted in Section 6.3.2 that the two lengths $Z_o$ and $LU_x$ are generally used for the development of a linear scaling factor between the natural wind and its tunnel simulated counterpart. A further problem arises here due to the fact that neither of these parameters were actually measured in the full-scale work. No. measurements relating to the turbulence length $LU_x$, at the Norton site, are available at all and it would be unwise to try and develop an expression for $Z_o$ based on the measurements of the wind speed at various heights as described in Sections 5.4, 5.5 and 5.6. This is because the wind speed measurements were made non-concurrently with each other and cover a height range of only 3.7 - 10m above the ground.

By examination of the terrain surrounding the site and consultation of the terrain categories of Counihan [1975] shown in Table 3.3 it was decided to classify the site in the "rough" category. This encompasses rural to suburban sites and includes wooded areas. This classification at first sight, may seem a little puzzling. The most obvious feature of the terrain around the building is the long stretch of flat grassland in front of it. Classification by this terrain type would put the site into the moderately rough category, i.e. short grass, crops, etc.

However, if the wind blows over two adjacent terrain types, for example the wind blowing over a city near the coast and on to the sea, then some distance must be travelled before the wind reaches equilibrium again, i.e. attains the characteristic profile of the terrain over which it is blowing. The change from one profile to the other will be gradual and will start with the layers nearest the

ground, becoming increasingly deep with fetch length. A fetch length of 1 km is generally required for the new profile to develop fully, (British Standards Institute - Code of Practice [1972]). For layers near the ground this distance will be shorter and will depend upon the type of terrain surrounding the building. The code of practice gives values of fetch length required for fully developed flow. These are repeated here in Table 6.1.

Table 6.1 Fully Developed Flow Fetch Lengths for Various Ground Coverages

| Ground Coverage | Fetch Length |
|---|---|
| $\leqslant$ 10% | 500m |
| $\leqslant$ 15% | 250m |
| $\leqslant$ 30% | 100m |

The code does not make it clear exactly how these ground coverage percentages relate to each terrain category. However, in general the ground coverage will increase with increasing index of terrain category (see Table 3.3). The playing field in front of the test building offers the maximum change in terrain type, from that generally present in the locality, i.e. rural/suburban. The field has a ground coverage of zero and a fetch length of 250m, a distance well below that requried for a local profile of the atmospheric boundary layer to be created. It was for these reasons that the site

was placed in category 3 of Table 3.3 as this category best described the general terrain within 1km radius about the test site i.e. it is on the outskirts of a large city with well wooded parklands and forest areas in the vicinity

6.4.3 The development of a linear scaling factor based on wind flow considerations only

The value of $Z_o$ for roughness category 3 lies in the range 1.0 - 1.5m. Counihan [1975] shows that the value of $LU_x$ at the meteorological wind speed height of 10m lies typically in the range 60-70m for terrain types with $Z_o$ in the range 1-2m.

It is known that the value of $Z_o$ for the wind tunnel is 3mm. Direct comparison of this value with the mid value of the full scale range gives a scaling factor of (adopting equation 3.67 due to Jensen [1958]) 1.25/.003 = 417. The scaling factor based on the turbulence length scales is less easy to determine because their values change with height an iterative process must be performed in order to evaluate the scale factor.

This procedure has been described in detail by Cook[1978]. It was performed by Lee [1977] using his measured wind tunnel data and the empirical equation for the longitudinal integral scale of turbulence in the natural wind as developed by the Engineering Science Data Unit, i.e.

$$LU_x = \frac{25\ (Z)^{0.35}}{Z_o^{0.063}} \qquad (6.3)$$

Using this method Lee obtained scaling factors of 320, 370 and 415 - depending upon the height used in the first iteration. He therefore concluded that a scaling factor of 350 was adequately

represented by the tunnel characteristics. It would, therefore, seem that the ideal scale to employ, with regard to the flow characteristics of the wind, would be somewhere in the region of 1:375.

### 6.4.4 A discussion of the reasons for rejecting the scale factor as developed from wind flow considerations only

If a model of the test building was built to the scale developed in Section 6.4.4 it would have plan dimensions of 25.6 x 14.9mm and a height of 12.2mm. The convective heat transfer surface would have the approximate dimensions 5.3 x 2.6mm. Aside from the practical difficulties which would be encountered in producing a heater plate this small (the smallest heater unit encountered in the survey of previous work performed in Chapter Three, was that due to Kelnhofer and Thomas [1976] and it measured 12.7mm in diameter) the range of Reynolds numbers available would be greatly reduced from those of the full-scale work.

The literature survey also showed that only one piece of comparable work had been previously performed, involving a model with a heated section placed upon it. This was the work of Kind et al [1983] described in Section 3.6.5. Kind used a stated model scale of 1:32, and his building has plan dimensions of 356 x 270mm. His heated surface consisted of 6, 76 x 38mm, plates. This size of building and plate would cause minimal constructional difficulties and lead to the availability of a larger Reynolds number range. This size keeps the blockage, by the model, of the air flow in the tunnel to an acceptable level, which for this tunnel is approximately 3-5% (Lee and Evans [1984]).

### 6.4.5 The development of the linear scaling factors finally used for the wind tunnel model studies

Lee and Evans [1984] also used the boundary layer wind tunnel, described in Section 6.1, for their measurements of wind flow patterns across building roofs. They modelled the BRE standard semidetached house - described in Section 4.1.3 using a scale of 1:50. They state that there is little to be lost by a slight relaxation of the scaling laws, as developed in Section 6.4.3. The reason for this is that it is not known with any precision which of the flow parameters are primarily responsible for governing the shapes of flow patterns around bluff bodies.

This point is discussed further by Lee [1982], who postulates that the mechanics of the flow separation process may be dominantly dependent only upon the higher frequency part of the turbulence spectrum of the incident flow, i.e. not upon the large scale eddys of which $LU_x$ is a describing parameter. It has been shown that the convective heat transfer to a flow with high free-stream turbulence levels is independent of $LU_x$.i.e. Kestin [1961].

It is therefore concluded by Lee and Evans [1984] that, providing the scaling factors of the model and flow are of the same order and the relative mean velocity and turbulence distributions are correct, then the scaling laws as developed earlier can be relaxed with the confidence that any results obtained will still be reasonably accurate.

With all the above points in mind it was decided to conduct two series of model experiments using the linear scales of 1:32 and 1:64. The 1:32 scale was chosen because of its comparability with the work of Kind et al [1983]; the 1:64 because it would afford an opportunity to observe any scale effects as the model tended towards the scaling factor as derived from wind flow considerations, whilst still being of such a size that the convective heat transfer measurements could be performed accurately. Both scales, of course, are reasonably in line with that used by Lee and Evans [1984] for their wind flow pattern experiments in the same wind tunnel.

This means that the value of $Z_o$ i.e. 3mm represents full-scale values of 96 and 192mm for the 1:32 and 1:64 scale cases respectively. These full-scale values of $Z_o$ lie in the moderately rough terrain category which represents short grass and crops, etc. A height of 10m is represented by scale heights of 312.50mm and 156.25mm. The measured values of $LU_x$ in the wind tunnel lie in the range 0.255 - 0.314m over this scale height range. Taking an average value of 0.285m and multiplying by the two scaling factors gives values of $LU_x$ = 9.1m and 18.2m. These values are some 3 to 6 times less than values measured at a similar height in the outdoor environment. The scale mismatch of $Z_o$ and $LU_x$ must be noted when comparing this series of experiments with model studies by other workers or with the full-scale tests conducted earlier.

## 6.5 A Description of the Model Buildings used for the Wind Tunnel Convective Heat Transfer Experiments

As stated in Section 6.4.1 the test building was to be modelled in isolation except for the inclusion of the small garage immediately next to it. In each case i.e. 1:32 and 1:64 scales, the model test building was fabricated from sections of 6mm thick aluminium sheet and the small garage milled from a solid block of hard wood. Both buildings were modelled as plane sided structures. Minor architectural details such as eaves, gutters, the slightly rounded ridge line and window recesses were not modelled. This approximation to the actual building structure was felt justified in the light of the work of Sparrow [1982] and Kind et al [1983], both of whom concluded that for their model studies the effect of one of these features, i.e. eaves, on the convective heat transfer coefficient was minimal. Figures 6.3 and 6.4 show the dimensions of the model buildings for the 1:32 and 1:64 scales respectively. The maximum blockage offered to the flow is by the 1:32 scale model when the wind in blowing directly normal to the roof surface. This represents a blockage ratio of 3.4%. The ratio of model height to boundary layer is 1:6 for the 1:32 scale and 1:12 for the 1:64 scale. This blockage percentage and the height ratios are considered acceptable in normal tunnel modelling practice.

The walls, gable ends and roof sections of the test building were all manufactured from the 6mm thick aluminium sheet and were joined together using counter sunk allen-screws. A base plate was

also included in the construction which gave the building stability and allowed it to be secured firmly to the wind tunnel's wooden turntable at the required position. Both the base plate and the turntable had circular slots cut into them. This was to allow the passage of any instrumentation leads from the model to outside the wind tunnel.

A rectangular slot was cut in one roof section of each test building model; this was to accommodate the heated plates, which will be described in Sections 6.6.2 and 6.6.3. The dimensions of these slots were 58.8 x 33.4mm, for the 1:32 scale model and 17 x 34mm from the 1:64 scale case.

In one of the gable ends of each model was drilled a 1mm diameter hole; this was to allow a T-type thermocouple to be led through the model building and positioned 10mm above the ridge line. The thermocouple was held in place by a small piece of adhesive tape and facilitated the measurement of the air temperature in the wind tunnel.

On the opposite gable end two small brackets were located; these were to enable the shaft of a hot wire anemometer probe to be positioned at a scale height of 1.5m above the ridge line in a similar position to the cup anemometer in the full-scale measurements. The scale heights for the 1:32 and 1:64 scale models are 47mm and 23.5mm respectively. This probe and its calibration will be described in Sections 6.8.2 and 6.8.3.

The milled hardwood blocks which represented the scale models of the small garage were fitted with recessed brackets which enabled them to be secured firmly to the tunnel turntable with wood screws.

## 6.6 The Heated Plates used in the Model Convective Heat Transfer Studies

### 6.6.1 The choice of the heating element to be used for the model convective heat transfer studies

The heated plate used for the full scale convective heat transfer experiments had overall dimensions of 1.93 x 1.01m with an active heated surface of 1.81 x 0.89m i.e. the characteristic length of the heated surface was 1.193m - as defined in Section 2.2. Table 6.2 presents the ideal dimensions, and characteristic lengths required for the active surface of the heated plate for each model.

Table 6.2 Ideal Dimensions and Characteristic Lengths Required for the Active Surface of the Heated Plate for each Model Scale

| Scale | Dimensions mm | Characteristic Length mm |
|---|---|---|
| 1:32 | 56.6 x 28.3 | 37.7 |
| 1:64 | 27.8 x 13.9 | 18.5 |

It would also be desirable for the width of any framing of the plate to have scale linear dimensions also. For the 1:32 scale this width would be approximately 2mm and for the 1:64 scale 1mm. Any material used for the framing should have some thermal insulation properties in order to minimise the heat loss from the edge of the plate.

There were two basic options in the choice of element to be used for the heated plate. To either obtain a commercially produced unit of the required dimensions or, if none were available, to manufacture a plate of the required size from electrically conducting material.

Kelnhofer and Thomas [1976] in their model work had used strain gauges as heating elements. They states that the construction of heater units using these gauges required considerable care - presumably due to their delicate nature. A search through the literature of the manufacturers of strain gauges revealed that no units of the required dimensions were available.

Another possible source of a commercially available heating unit was thought to be platinum resistance thermometers. Burns [1976] in his measurement of the convective heat losses from a glass panelled room, placed on the top of a 4 storey building in Glasgow, used platinum resistance thermometers as his heating device. These units are far more durable than strain gauges. They consisted of a platinum element attached to an alumina sustrate and protected by a thin plastic film.

Matthey, the manufacturer of the "Thermafilm" resistance thermometers used by Burns [1976] was consulted and it was found that the units were available in two basic sizes i.e. 25.4 x 25.4mm and 5.0 x 32.0mm. Used individually neither of these units would satisfy the dimension criteria of the ideal heater size required. However, it is possible to connect these units, electrically, in series. If two of the larger units were connected in this manner this would lead to a heating element with dimensions of 50.8 x 25.4mm. This would have a characteristic dimension of 33.8mm, which is only some 10% less than that required for 1:32 scale heated plate. This was felt adequate and this system of heater units was used for the 1:32 scale heated plate.

For the 1:64 scale series the smaller units were considered. It was found that 3 of the smaller units connected in series would give a plate with an active surface with dimensions of 32.0 x 15.0mm and a characteristic length of 20.4mm. As this length is only some 10% greater than the ideal case presented in Table 6 it was felt that this combination could be used for the 1:64 scale plates.

### 6.6.2 The construction details of the 1:32 scale model heated plate

The construction of this model heated plate was very similar to that used in the full scale. It was a sandwich construction consisting of a metal plate, heating elements and insulation foam - held together and compressed by a rigid frame (see Figure 6.5).

The 50.8 x 25.4mm upper plate was made from 2mm thick copper sheet and instrumented with 3 T-type thermocouple of a similar nature to those used in the full scale work. These thermocouples were mortised into 1mm deep grooves cut in the exposed surface of the plate, their heads being at the positions shown in Figure 6.5. This figure also shows the 3mm balsa wood frame which surrounded the copper plate and the 1mm wide perspex frame which held the construction together. The leads from the 3 surface thermocouples were fed between the edge of the heated plate and the balsa wood frame. Both the upper surface of the copper plate and the balsa wood frame were sprayed matt black with the same type of paint used in the full-scale experiments.

Across the balsa wood frame at the position shown in Figure 6.5, i.e. at the mid point of one of the short sides of the plate, a further pair of thermocouples were placed. Readings from these instruments, along with a knowledge of the thermal conductivity of the balsa wood frame, would enable the heat loss through the frame to be evaluated.

Beneath the copper plate was, of course, the two, series coupled, resistance thermometers. These heaters, when connected to a d.c. power supply, would provide resistive heating to the copper plate from beneath. The copper plate would help even out the temperature distribution of the surface. The heaters, together, had exactly the same area as the copper plate, and each was 1mm thick. By making the balsa wood frame 3mm deep the back surface of the heater units were flush with the bottom edge of the balsa frame.

To the back of the heating elements was attached a T-type "Comark" self adhesive patch thermocouple measuring 25 x 10mm. The thermocouple was sandwiched between the element and the top of the layer of insulation foam. This foam completely filled the back of the plate and balsa wood frame area and extended below it to a depth of 50mm. Attached to the back of the foam was another patch type thermocouple. Readings form these two patch thermocouples and a knowledge of the thermal conductivity of the foam enabled the back loss from the heaters, by conduction, to be evaluated. The manufacturers of the foam - DOW Chemical Co. Ltd., supplied the figure of 0.033 $Wm^{-1}K^{-1}$ for this parameter.

All the leads from the previously mentioned thermocouples were led through a tight fitting slot cut in the foam, as were the power leads to the heating elements. The thermocouple leads were all 300mm long and terminated at standard miniature thermocouple connectors. The power leads were terminated at the male half of a 2mm diameter jack plug.

16mm below the top edge of the plate surface perspex lugs were cemented to the long edges of the perspex frame. When the plate was located, from behind, in the slot cut in the roof section, these lugs enabled it to be secured firmly in position with its top surface the required scale distance above the roof slope i.e. 10mm. The perspex frame was cemented together using plastic cement and given further strength by the addition of aluminium corner brackets below the locating lugs.

### 6.6.3 The constructional details of the 1:64 scale model heated plate

The constructional details of the 1:64 scale model heater plate are essentially similar to that used in the 1:32 scale tests. Some differences, however, are apparent; these are discussed below.

Because of its smaller area only 2 surface thermocouples, not 3, were used. These were positioned with their heads on the centre line between the two long edges of the plate and 8mm from each of the short edges. No balsa wood fram was included in the construction, the plate being directly attached to the perspex frame. The edge loss from the plate was estimated using the mean temperature of the plate surface and the temperature given a thermocouple morticed flush with the outside of the perspex frame and a knowledge of the thermal conductivity of the perspex. A balsa wood frame was not included in this 1:64 scale construction because the characteristic length of the model already exceeded the ideal length required.

The final differences between the 1:64 scale plate and that described earlier are that the insulation backing foam only extended 35mm below the heater units and the locating lugs enabled the plate surface to be positioned 5mm above the roof. This is, of course, the correct height for the 1:64 scale

### 6.6.4 The theoretical basis for the evaluation of the convective heat transfer coefficient from the model heated plates

The theoretical basis for the calculation of the convective heat transfer coefficient in these model studies was essentially similar to the procedure used in the full-scale work i.e. a steady state energy balance on the upper surface of the flat plate. However several fundamental differences are apparent.

There was no need to take account of the short wave gain at the plate surface as non was present in the wind tunnel. Due to its increased thickness to area ratio edge losses were felt to be important and these were evaluated in the manner described in Sections 6.6.2 and 6.6.3. The heat loss down the surface thermocouple and power leads was also evaluate using Fourier's conduction law. It was assumed that their "hot ends" were at the temperature of the plate and that the connecting blocks were thermally massive enough to act as an isothermal junction at room/tunnel temperature.

The convective heat transfer coefficient can then be evaluated from:

$$h = \frac{IE/A + \varepsilon R_L - q_{con} - \varepsilon\sigma T_p^4}{T_s - T_t} \qquad (6.4)$$

where I = The current to the plate, amps

E = The potential across the plate, volts

A = The area of the plate, $m^2$

$R_L$ = The incident radiation upon the plate, $Wm^{-2}$

$q_{con}$ = The total conduction losses from the plate i.e through the frame, back insulation and down the thermocouple and power leads, $Wm^{-2}$

$\varepsilon$ = The emissivity of the surface = 0.9

$\sigma$ = Stefan's constant = $5.669 \times 10^{-8}$ $Wm^{-2}K^{-4}$

$T_p$ = The surface temperature of the plate, taken as the the average of the 3/2 surface thermocouple readings, K

$T_t$ = The air temperature of the tunnel as measured by the gable end mounted thermocouple, K.

The values of I, E, $T_s$ and $T_A$ were all to be recorded during the experiment and hence all the terms on the right hand side of equation 6.4, with the exception of $R_L$, could be evaluated directly. Continuous recording of this parameter was not possible, as the only instruments available for its measurement e.g. a net radiometer was of a similar order of magnitude in size as the model buildings themselves. If this device was placed in the wind tunnel close to the model buildings it would induce unrealistic flow conditions over them. Therefore a separate series of experiments was undertaken to determine the radiative gain at the plate surface.

## 6.7 The Evaluation of the Radiative Gain at the Model Plate Surface

In order to obtain a steady state energy balance on the plate surface, it was necessary to assess the radiative environment of the wind tunnel. This was done by using a net radiometer similar to that used in the full scale experiments - described in Section 4.5.2. It was assumed that no short wave radiation was present in the tunnel and hence the radiation levels recorded by this device consisted of long wave radiation only.

The radiometer was placed on a bracket over the centre of the tunnel turntable at a height of 75mm and on angle of 35° to the horizontal. This height represents the mid point between the heights of the two model collector panels and the inclination is of course the same as the roof pitch.

By rotating the turntable it was found that the radiation level, $R_L$ was insensitive to the direction in which the radiometer was pointing. This is because of the reasonable uniformity of the emissivities of the surfaces "seen" by the thermopile. The other parameter on which the radiation level will depend is the temperatures of these surfaces, which in turn will depend on the tunnel air temperature. Using the laboratory's heating system and running the wind tunnel fan at various speeds it was possible to create tunnel air temperatures, $T_t$, in the range 290-297 K.

Over this range a linear relationship between the two parameters was developed, i.e.

$$R_L = 4.87\ T_t - 1011.84 \qquad Wm^{-2} \qquad (6.5)$$

Figure 6.6 shows a plot of this line over the given temperature range along with the lines developed from Stefan's law for black body radiation, with $\epsilon = 1$ and $\epsilon = 0.98$, also based on the tunnel air temperature. The three lines are very similar over the measured range. Equation 6.5 was used in the evaluation of the radiative input to the plate, $T_t$ being measured by the gable end mounted thermocouple.

## 6.8 Other Instrumentation used in the Model Convective Heat Transfer Study

As stated in the introduction to this Chapter, there are two main objectives to this series of model experiments. Firstly, to compare the results of this work with similar studies also performed in wind tunnels, and secondly to try and relate the results the model experiments to those obtained from the full scale test site at Norton.

In all cases the convective heat transfer coefficient will be, primarily, correlated with wind speed. Most previous experiments which have been performed in wind tunnels have related the convective heat transfer coefficient with the maximum free stream wind speed in the tunnel. In this case it is the wind speed at the top of the boundary layer, $V_G$. By measuring this wind speed it is also possible, from equation 6.1, to obtain the unobstructed wind velocity at any height above the tunnel floor.

It has already been shown in the full-scale work that the wind speed as measured over the roof, $V_{6R}$, is not the same as the wind speed measured, at a similar height over open ground, $V_6$. $V_{6R}$ was the only wind speed which was measured continuously during full scale convective heat transfer measurements. It was, therefore, felt necessary to evaluate this wind speed in the wind tunnel. The rest of this section describes the instrumentation used for the evaluation of, $V_G$, and the scale values of $V_{6R}$.

### 6.8.1 A description of the instrumentation used for the measurement of the gradient wind speed of the simulated atmospheric boundary layer

The gradient wind speed, $V_G$, i.e. that which exists at the top of the simulated boundary layer, was to be determined using a standard combined pitot-static tube and inclined water manometer arrangement. By inserting it through the tunnel ceiling the pitotstatic tube could be positioned so as to be able to measure the wind velocity in the constant speed region of the boundary layer. The actual distance above the tunnel floor of the tube head was 850mm. Several standard texts e.g. Ower and Pankhurst [1977] deal with the operation of this type of arrangement and it will be dealt with here only briefly.

The differential pressure, $\Delta p$, between the active and static head readings is proportional to the square of the flow velocity. By measuring $\Delta p$ with a water manometer the velocity can be expressed in terms of the water column height $C_h$ in mm $H_2O$ as:

$$V = K\sqrt{C_h} \quad ms^{-1} \tag{6.5}$$

Where K is a constant dependent upon air temperature and pressure. Ower and Pankhurst [1977] give the following expression for K:

$$K = 20.56\sqrt{\frac{T_a}{b}} \tag{6.6}$$

where $T_a$ = Air temperature K

$b$ = Barometric pressure mm Hg

A further approximation can be made if the measurements are performed in air near normal temperatures and pressures. This approximation was used for the calculation of the air velocity in this series of experiments and gives:

$$V = 4.0 \sqrt{C_h} \quad ms^{-1} \tag{6.7}$$

The value of $C_h$ was recorded manually during the experiments.

### 6.8.2 A description of the instrument used to measure the scale roof wind speed, $V_{6R}$

The measurement of the scale roof wind velocity, $V_{6R}$, was performed using a constant temperature hot wire anemometer. This probe consisted of a heated element surrounded by a 13mm diameter guard ring. The guard ring served the purpose of directing the flow over the heated element, and it was attached to the probe shaft, which was 6mm in diameter and 220mm long. The leads to the heating element were led through this shaft and were terminated at a standard electrical connecting block.

Once the probe was located on the gable end of the model building using the brackets described in Section 6.5 it was connected, via the connecting block, to its electrical control system. This system, by utilising a feedback bridge circuit, maintains the heated element at a constant temperature of 493 K.

As the velocity of the air past the sensor increases, the sensor will cool due to convection with a resulting decrease in its resistance. This will cause the voltage to decrease, changing the input to a differential amplifier. Hence there will be an increase in

the output of the amplifier so the current through the sensor is increased. The gain of the amplifier is sufficient to keep its two inputs balanced. Any change in the sensor resistance is immediately corrected by an increase or decrease in current through the sensor.

The output of the system is the voltage output of the amplifier which in turn is the voltage required to drive the necessary current through the sensor. Since the feedback keeps the resistances in the bridge circuit constant, the voltage across the bridge is directly proportional to the current through the sensor. Therefore, the square of the voltage output is directly proportional to the instantaneous heat transfer between the sensor and the air. The heat transfer is related to the velocity of the air flow over the sensor. Hence the voltage output from the circuit increases with air velocity.

The non-linearity of the velocity meter can be approximately described by the semi-empirical equation given originally by King [1914] and later modified by Bradshaw [1971] i.e.

$$h = A + B\,V^{0.45} \qquad (6.8)$$

where h = The heat loss from the sensor

and V = The flow velocity past the sensor

A and B are constants dependent upon the fluid properties and its temperature. Because of this non-linearity and the fact that the performance of an hot wire anemometer may alter throughout its life, it was necessary to calibrate this instrument before use.

### 6.8.3 The calibration of the hot wire anemometer used to measure the scale roof wind speed, $V_{6R}$

The probe was calibrated in a small wind tunnel of 150 x 150mm cross-section against a standard pitot-static tube and inclined manometer arrangement. (This can be seen in the foreground of Figure 6.1.) Before being calibrated the probe sensor was cleaned by dipping it in a solution of Isopropyl alcohol. The output from the probe is slightly dependent upon the ambient air temperature, so the calibrations were carried out at a temperature close to that attained by the air in the wind tunnel under normal operating conditions, i.e. about 298 K. Maximum accuracy was achieved by re-calibrating the probe several times during the course of the wind tunnel model experiments.

The probe was calibrated for wind speeds in the range 0-25 $ms^{-1}$; the upper end of this range is slightly higher than the maximum speed available in the wind tunnel at the top of its boundary layer. A typical calibration curve is shown in Figure 6.7.

## 6.9 Experimental Procedure used for the Model Convective Heat Transfer Experiments

The model buildings were located on the turntable and securely fastened with screws, the heater plate and hot wire probe were positioned and all the relevant connections were made to the data logging device. This device was the same as that used in the full scale work. Figures 6.8 and 6.9 show the two scale models positioned in the wind tunnel. All the thermocouple signals were to be recorded

by the logging system, as were the voltage input to the heated plates and the output from the hot wire anemometer. The reading from the inclined manometer and the current passing through the plates were recorded manually by hand. The plate current was needed to compute the electrical power supplied to the plate by the d.c. power source, which was connected to the heating elements via the 2mm jack plug.

The mainstream of experimental runs were to involve the measurement of the convective heat transfer coefficient from the model plate at a given wind velocity, $V_G$, and for each of the wind direction 0°, $\pm$ 45°, $\pm$ 90°, $\pm$ 135° and 180°. These directions correspond to the centre point of each wind sector used in the full scale measurements. Additional experimental runs were made to examine more closely the effect of wind direction. This was done by rotating the tuntable in 10° or 15° increments and evaluating the convective heat transfer from the plate for each angle of incidence. The natural convective heat transfer coefficient was to be evaluated under still conditions i.e. with the wind tunnel fan switched off.

Because of the undertaking of such a variety of measurements it is impossible to define a unique experimental procedure for the experimental series. However each run was commenced in asimilar fashion.

When the models were in position and the removable side door of the turntable was closed, the power supply to the plate and the wind tunnel fan were activated. The blades of the fan were then feathered to the required angle to create the wind speed chosen for the test. For experiments involving the determination of the natural convection coefficient the wind tunnel fan was not activated.

A "warm-up" period of approximately 1-1½ hours was then allowed. This enabled minor adjustments to the wind speed and plate temperature to be made. During this period it was also found that the temperature of the air in the tunnel rose to around 298 K or above. This is due mainly to the heat created by the wind tunnel fans motor.

The plate power and temperatures were recorded and the turntable rotated to its next angle. It was necessary then to allow some time for the plate to once again reach steady state conditions. Preliminary tests had shown that for a value of $V_G$ = 11.0 $ms^{-1}$ the plate required approximately 15 mins. to reach steady state conditions at a temperature of 20 K above the air temperature. This was starting with the plate in equilibrium with its surroundings. If the plate was already at some temperature above that of the air and the angle of incidence of the wind was altered, it was found that the plate reached steady state conditions at its new temperature in about 7 mins. Therefore, in this type of test a time of 13 mins was allowed before the parameters were recorded at the new wind angle.

It was found that the time required for the plate to reach steady state conditions was inversely proportional to the wind speed in the tunnel, the worst case being that for natural convection i.e. still air. For these experiments it was found that time to equilibrium were of the order 30-40 mins and allowances were made for this in the recording of the data. Conditions were assumed to be "steady-state" if the temperature difference between the plate surface and the air did not vary by more than $\pm$ 0.1 K, over a 5 min. period.

## Conclusion

This chapter has discussed the experimental methods and problems encountered in the measurement of the convective heat transfer from a model replica of the full-scale site placed in an atmospheric boundary layer wind tunnel. In the next chapter the results of this series of experiments will be presented and discussed.

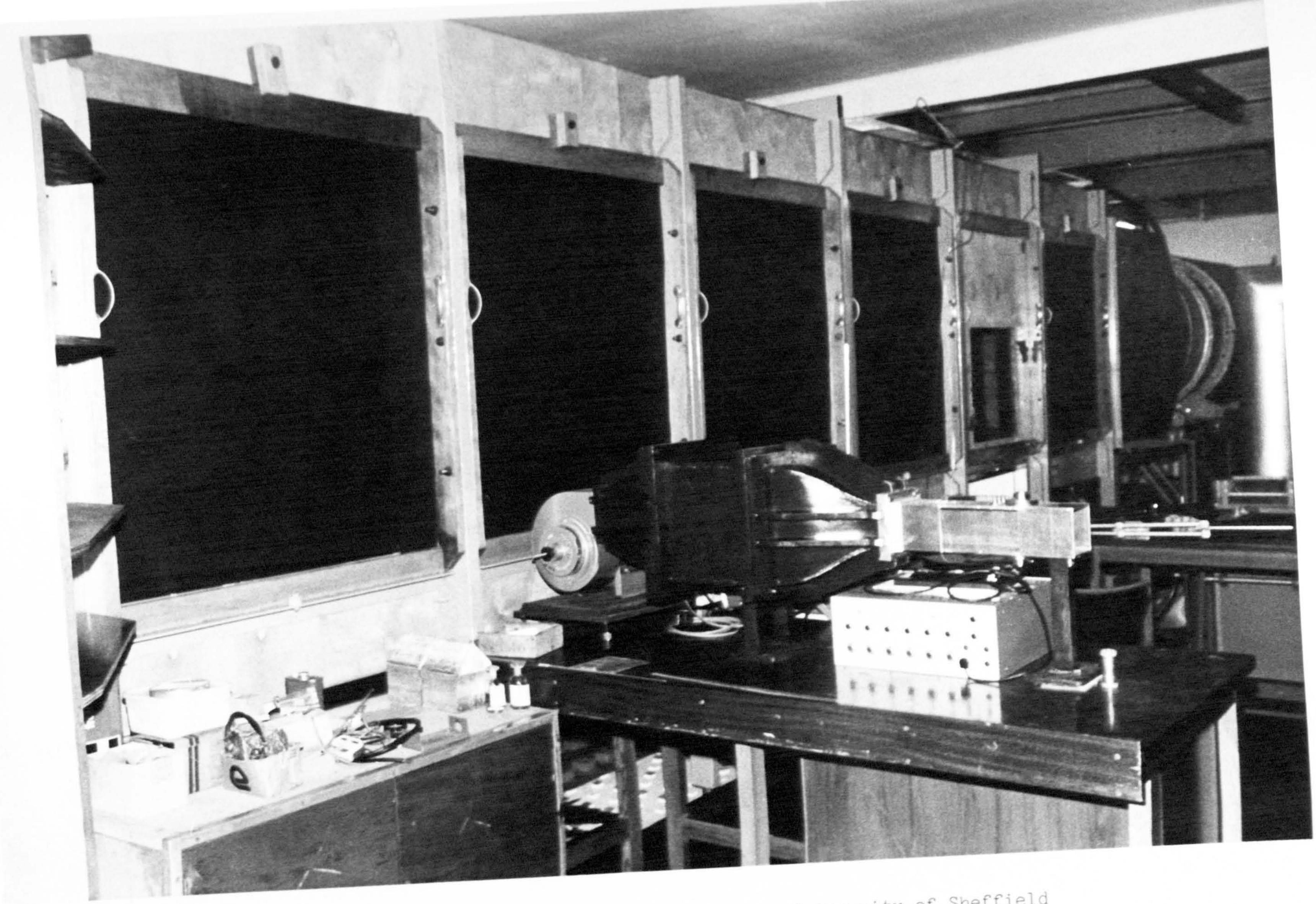

Figure 6.1 Exterior view of 1.2 x 1.2m boundary layer wind tunnel - University of Sheffield

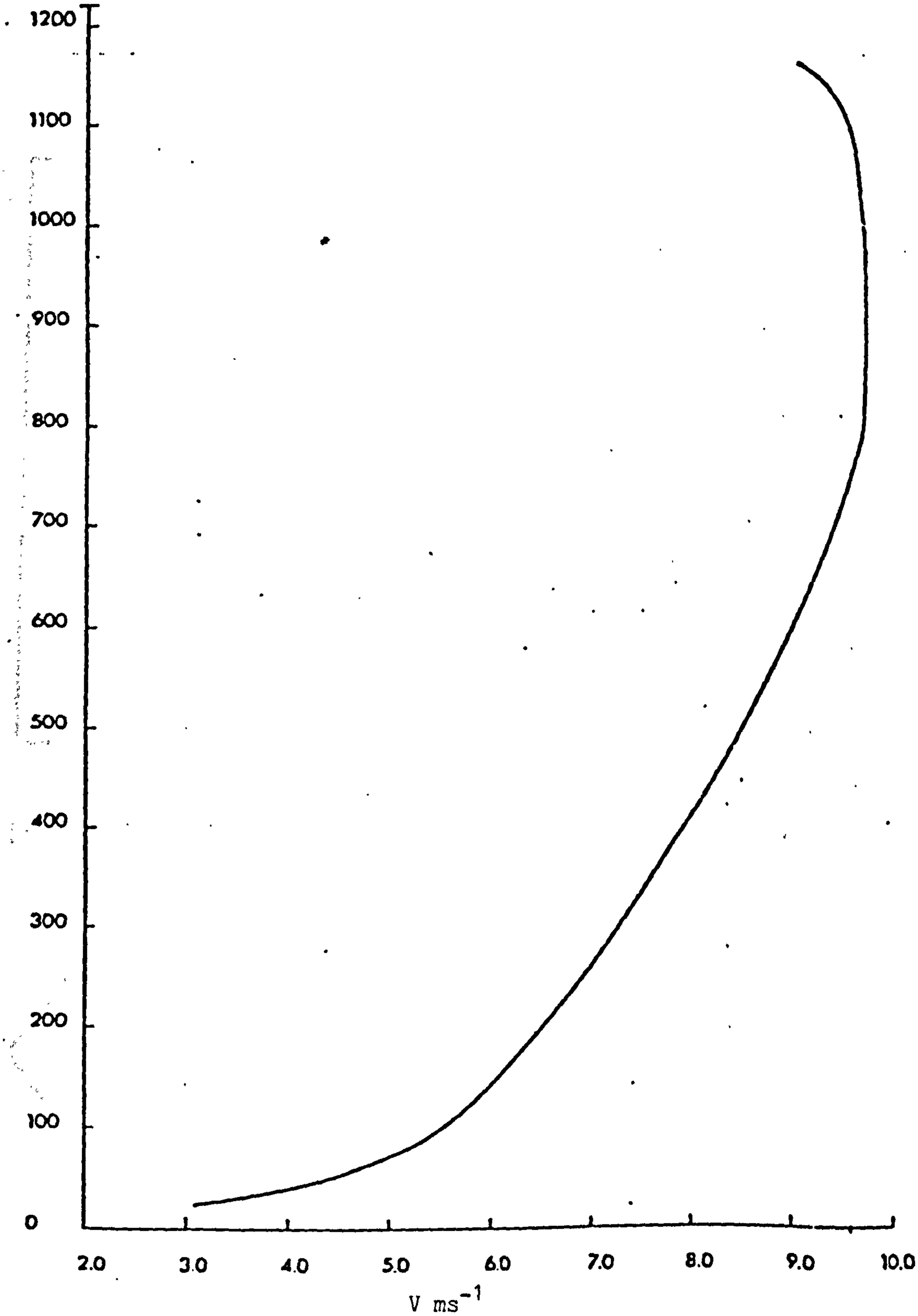


Figure 6.2 Velocity profile over centre of turntable

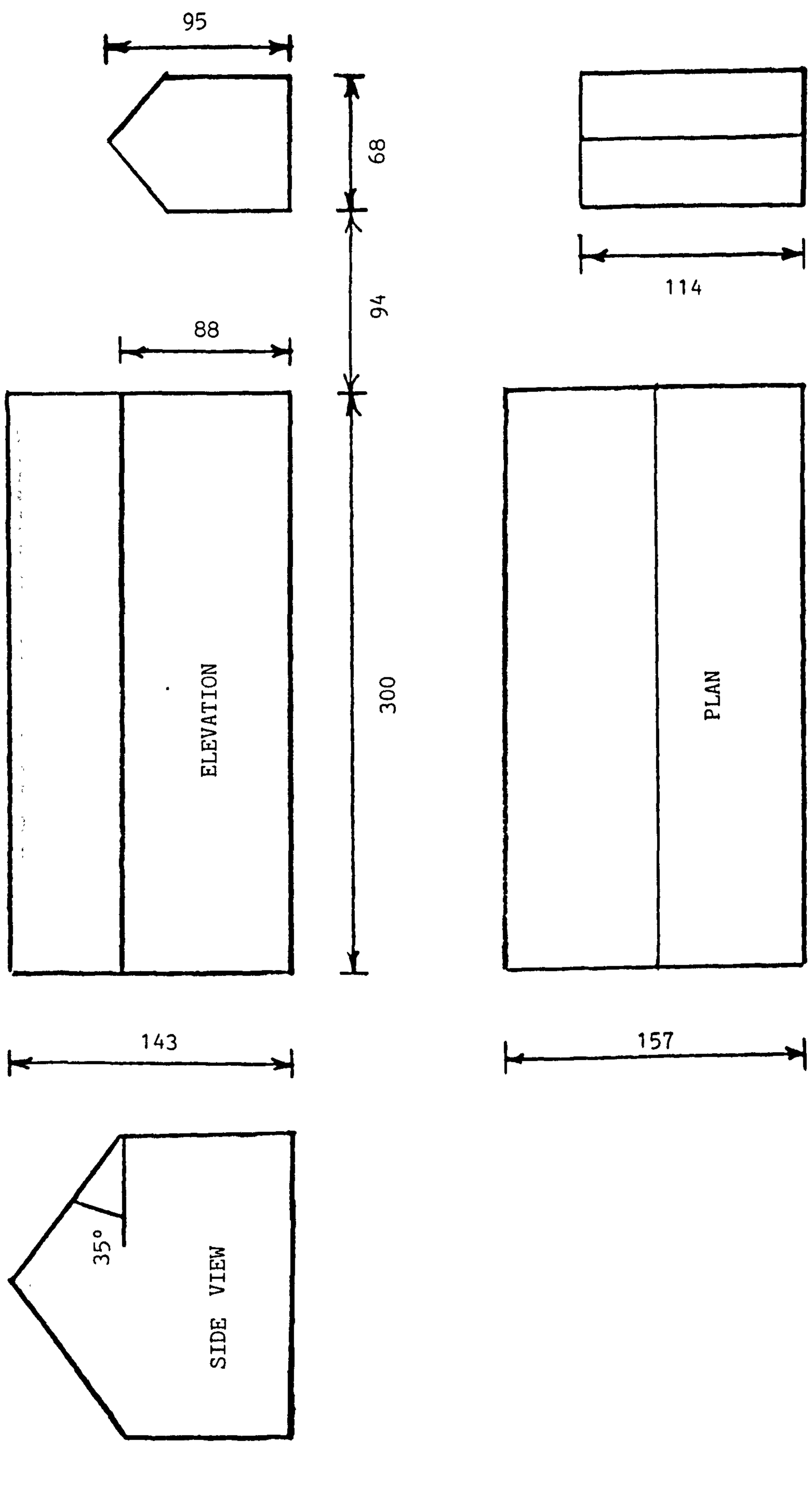


1:32 Scale model dimensions, all dimensions in mm

Figure 6.3

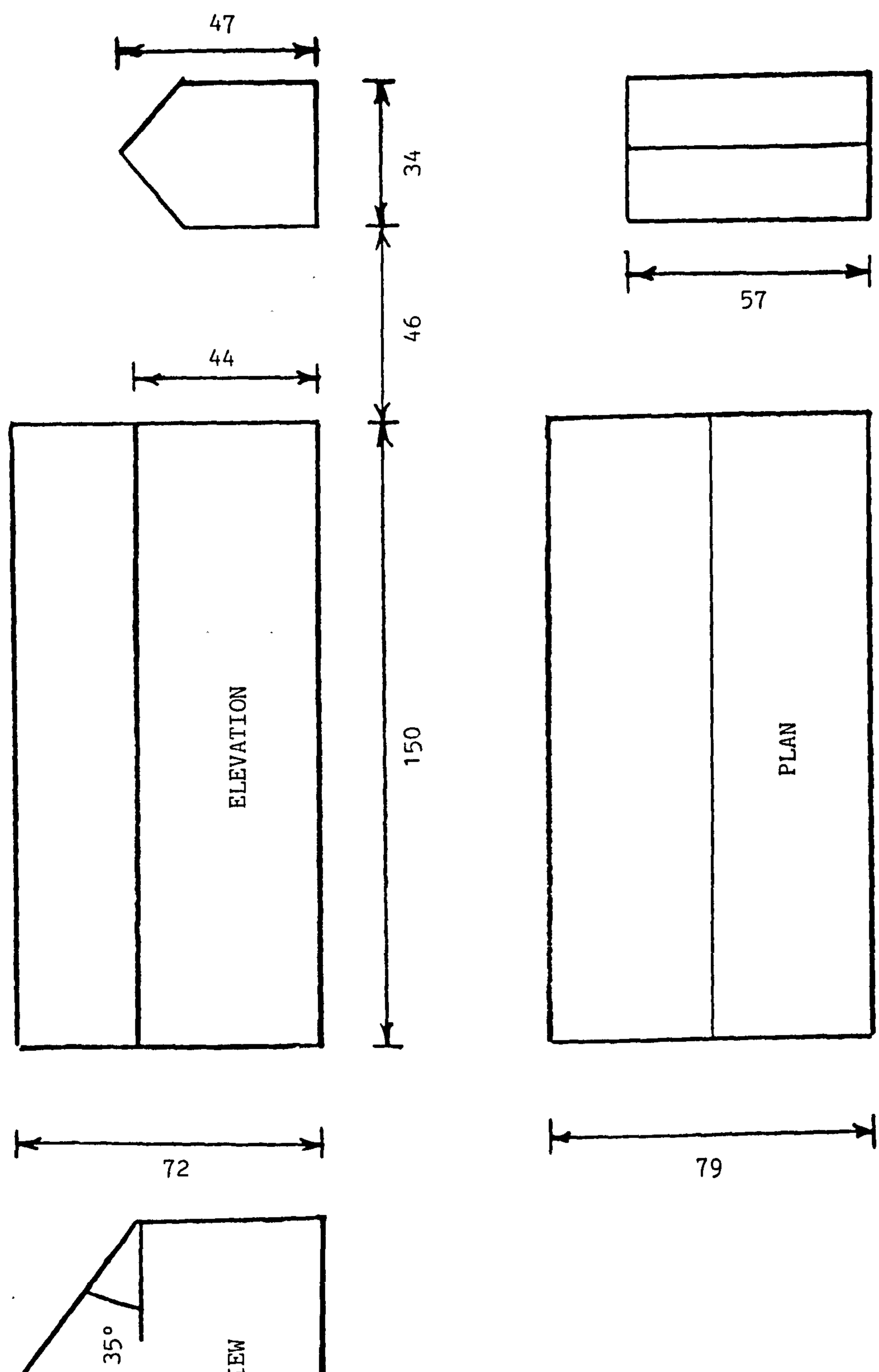


Figure 6.4 1:64 Scale model dimensions, all dimensions in mm

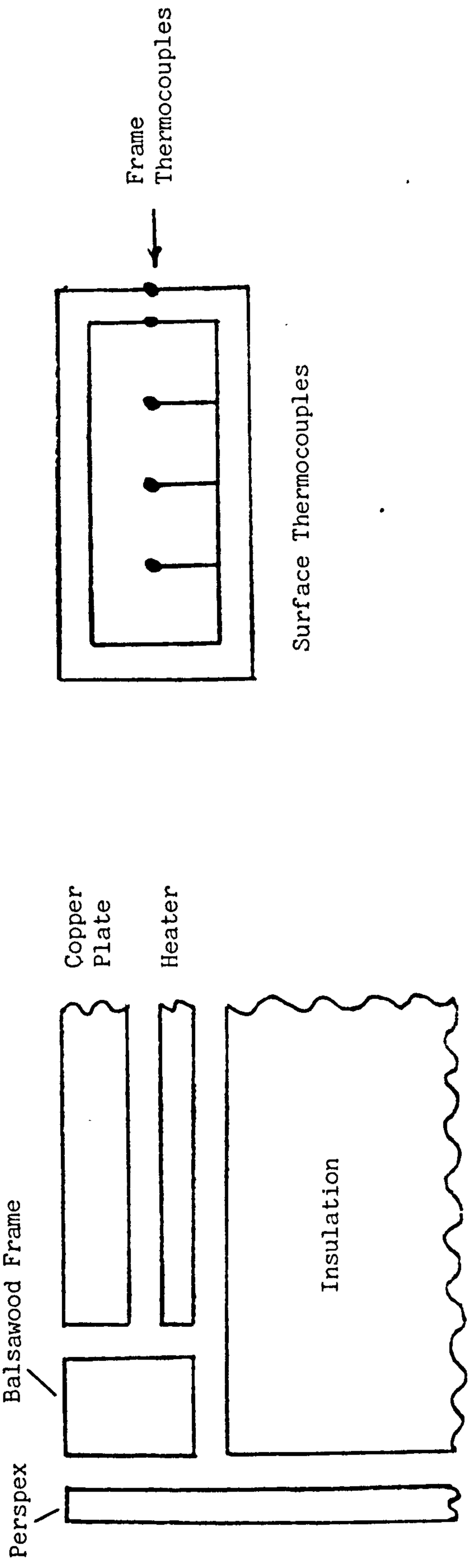


Exploded view of 1:32 scale model heater plate. Surface and frame thermocouple positions also shown

Figure 6.5

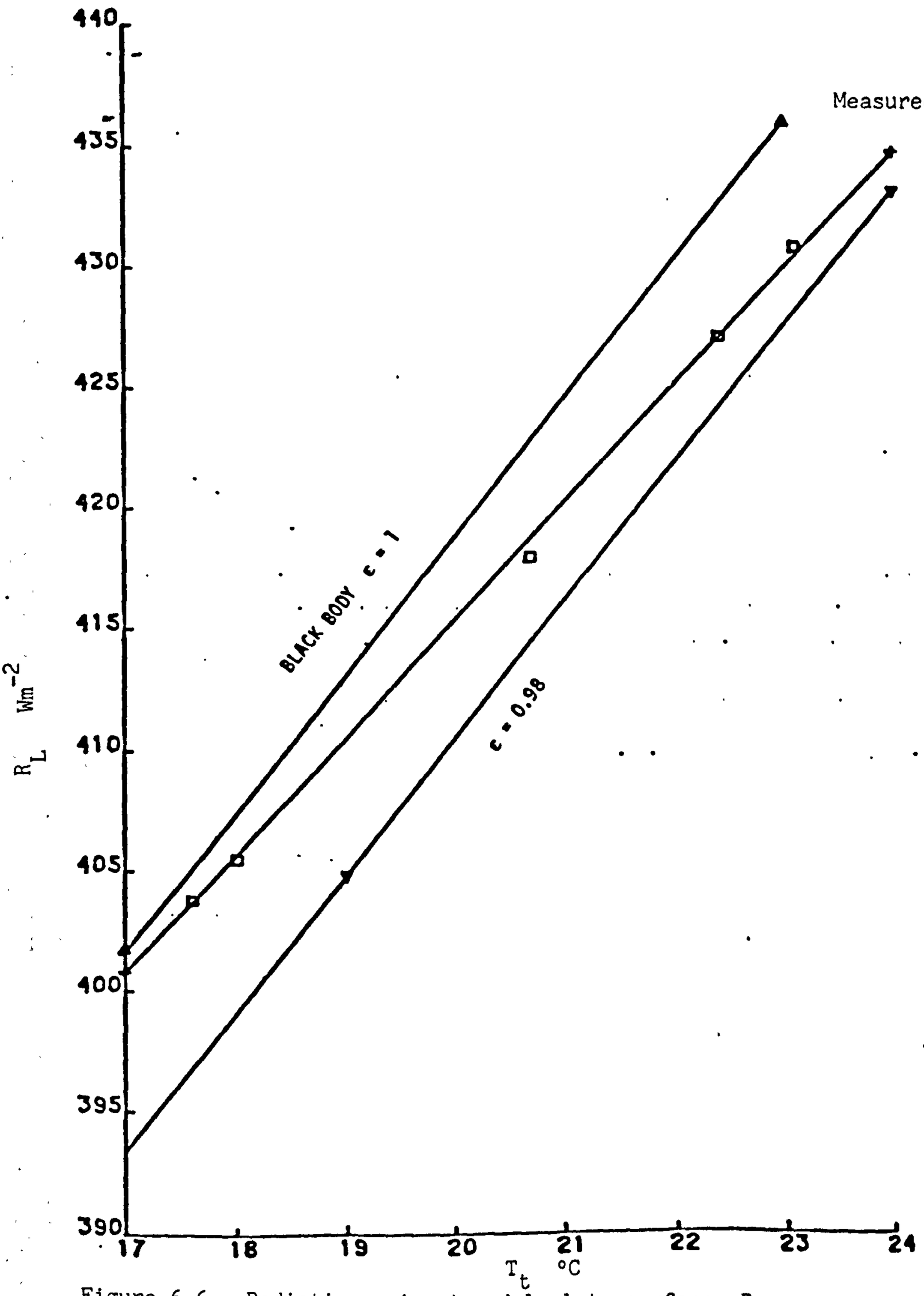


Figure 6.6 Radiative gain at model plate surface, $R_L$, against tunnel temperature $T_t$

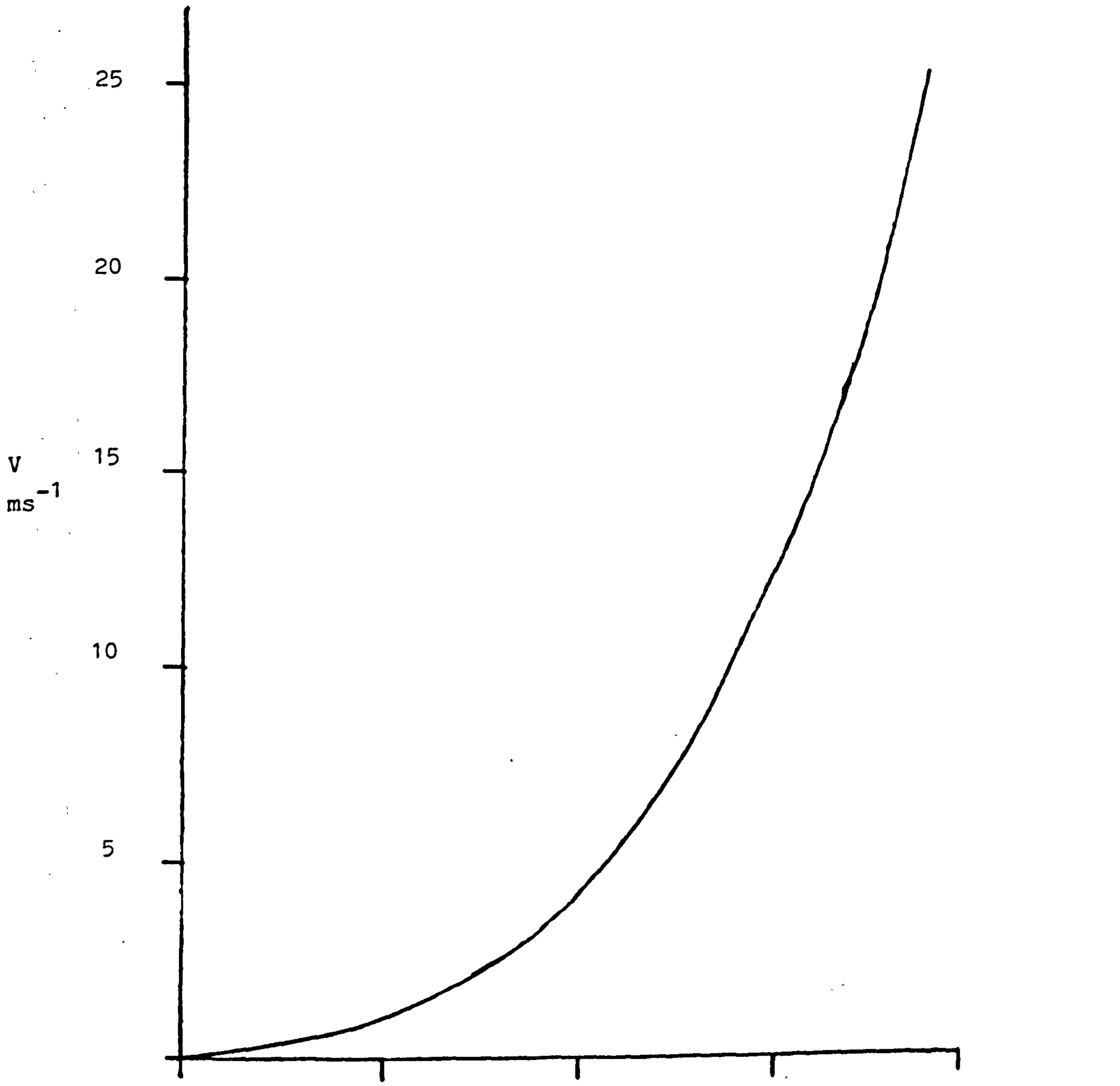


Figure 6.7 Probe output $e_p$ against wind speed V, for P.S.I. probe used in wind tunnel tests (typical calibration curve)

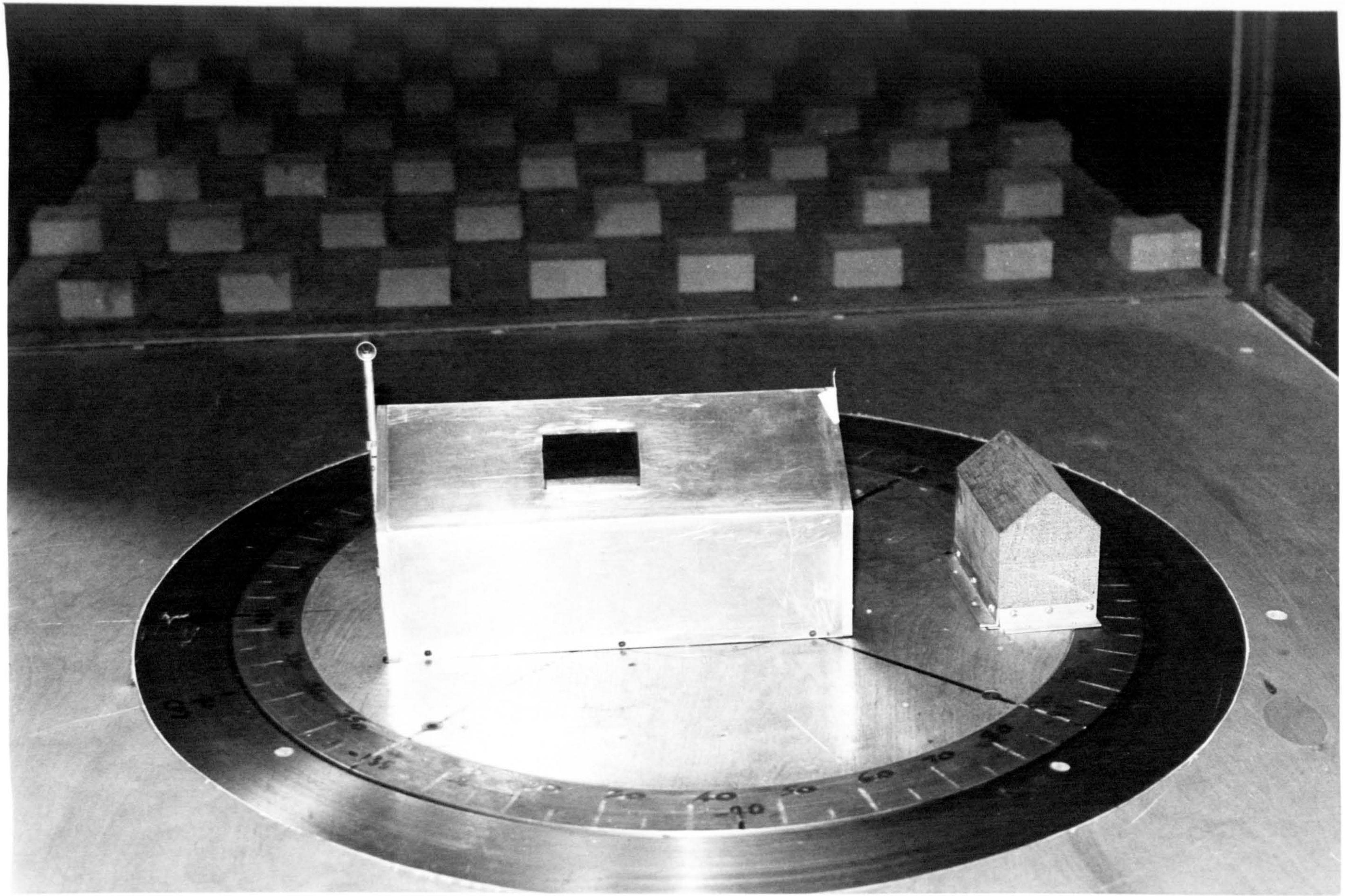

Figure 6.8 1:32 Scale model in position in wind tunnel

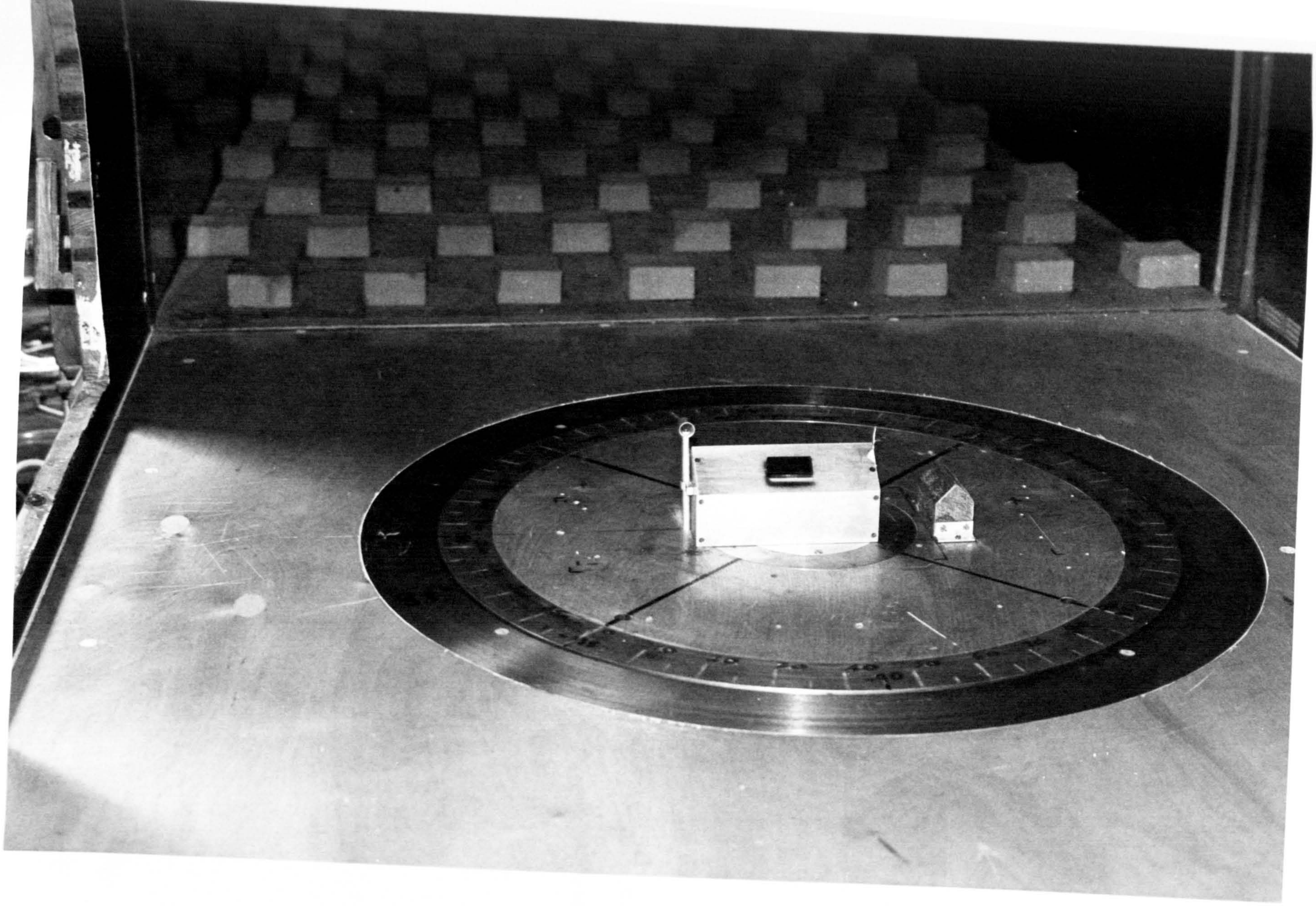

Figure 6.9 1:64 Scale model in position in wind tunnel

# CHAPTER SEVEN

# RESULTS OF WIND TUNNEL MODEL EXPERIMENTS

## Introduction

This chapter presents and discusses the results obtained from the wind tunnel series of experiments, as described in Chapter Six. The feasibility of using the wind tunnel results to predict full scale convective behaviour will be examined. Finally the current series of wind tunnel experimental results will be compared to those previously performed in this area.

## 7.1 Fundamental Results Obtained from the Wind Tunnel Experiments

The two scale models were tested separately. Initially the 1:32 scale model was examined, with a secondary series of experimental runs being performed with the 1:64 scale model.

Each scale model, used in the wind tunnel experiments, represented a heated plate of fixed size and geometry, placed in a wind flow with constant turbulance characteristics. Under these conditions, previous work has indicated that the convective heat transfer coefficient, of the plate, may be expected to be dependent upon the following parameters:

(a) Plate - air temperature difference

(b) Wind speed

(c) Wind direction

Unlike the full-scale experiments, in the wind tunnel tests each of these parameters could be systematically varied by the operator. The data was initially analysed in terms of the parameters. Two microcomputer programs (one for each scale) were written and used for this analysis. These programs extracted the relevant data from the magnetic tape, on which it was stored by the data logging device during the experimental runs. By using equation 6.4 the convective heat transfer coefficient was evaluated, i.e.

$$h = \frac{IE/A + \varepsilon R_L - q_{con} - \varepsilon \sigma T_p^4}{(T_p - T_t)} \quad Wm^{-2}K^{-1} \qquad (7.1)$$

where I = Current through the heater elements, A

E = Potential across the heater elements, V

A = Area of heater plate, $m^2$

$R_L$ = Incident longwave radiation on the plate , $Wm^{-2}$

$q_{con}$ = Total conduction losses from the plate (expressed in terms of the total plate area) , $Wm^{-2}$

$\varepsilon$ = Emissivity of the upper surface of the flat plate = 0.9

$\sigma$ = Stefan's constant = $5.669 \times 10^{-8}$ $Wm^{-2}K^{-4}$

$T_p$ = Mean plate surface temperature, K

$T_t$ = Mean ambient air temperature in wind tunnel, K

The conduction losses, $q_{con}$, were evaluated from the recorded plate temperatures and a knowledge of the thermal conductivities of the balsa frame, back insulation and power leads. $R_L$ was evaluated using the calibration equation discussed in Section 6.7

Two wind speeds were evaluated during the experimental runs; the wind speed over the roof $V_{6R}$ and the gradient wind speed of the tunnel $V_G$. One of the fundamental reasons for undertaking the wind tunnel series of measurements was to test the compatibility of the small scale results with the full-scale work described earler. The only wind speed evaluated continuously during the full scale tests was that measured over the roof, i.e. $V_{6R}$, therefore this wind speed was of primary interest during the analysis of the wind tunnel data.

This wind speed was evaluated from the output of the hot wire anemometer as described in Section 6.8.2. A simple subtraction of the air temperature from the mean plate temperature provided the mean plate-air temperature difference, $\Delta T$. The wind incidence angle, $\theta$, (in accordance with the nomenclature shown in Figure 4.12) was recorded manually in each case. The rest of this section examines the dependence of h upon each of these three parameters in turn.

### 7.1.1 Dependence of the convective heat transfer coefficient, h, upon the mean air-plate temperature difference, $\Delta T$

In the natural convection regime, i.e. $V_{6R} = 0\ ms^{-1}$, it would be expected that the convection coefficient, h, would show some dependence upon the mean plate-air temperature difference (see Section 2.3)

There is also some evidence (Rowley [1930] - see Section 3.1.3) that h may be dependent upon $\Delta T$ in the forced regime. Rowley's experiments were based on a heated plate some 0.3m square. More recent work by Kind et al [1983] on smaller plates (76mm x 38mm) mounted on model building roofs, produced no evidence that h was dependent upon $\Delta T$ in the forced regime.

By varying the power supplied to the plate heater elements, it was possible to achieve mean plate - air temperature differences over a range of approximately 2-45 K.

Figure 7.1 shows a plot of h v $\Delta$T, for the two scale models used, under natural convection conditions i.e. $V_{6R} = 0\ ms^{-1}$. Two points are immediately apparent form Figure 7.1. Firstly, that for both scales h tends to increase with increasing temperature difference. Secondly, the natural convection coefficient of the 1:64 scale plate is some 20-40% greater than the 1:32 scale value, for any given temperature difference (i.e. the smaller plate gives higher values of h).

This study is primarily concerned with flat plate solar collectors, which are located in the outdoor environment. The upper surface of the collector will rarely experience absolutely still wind conditions. Therefore, any in depth analysis of the natural convection data is unnecessary.

However, it should be noted that the simplified natural convection equation for an horizontal heated square plate in air, Holman [1981], is:

$$h = 1.32 \left[\frac{\Delta T}{x}\right]^{0.25} \quad Wm^{-2}K^{-1} \qquad (7.2)$$

where $\Delta T$ = mean plate - air temperature difference, K

x = characteristic dimension, m

Equation 7.2 predicts that h will increase with increasing $\Delta T$ and also increase with decreasing size. Therefore, the current results show at least qualitative agreement with equation 7.2.

For all cases where $V_{6R} > 0$ ms$^{-1}$ no systematic variation of h with $\Delta T$ was observed. This is illustrated in Figure 7.2 which shows a plot of h v $\Delta T$ for each of the two scale models under non-zero wind velocity conditions (for the 1:32 scale case $V_{6R}$ = 2.6 ms$^{-1}$ and for the 1:64 scale case $V_{6R}$ = 1.4 ms$^{-1}$.) This is in good agreement with the work of Kind et al [1983]. He performed experiments using small heated plates mounted on a model building roof. Kind states, that for experimental conditions which were identical except for the power supplied to the heater plates (and therefore the plate temperature) derived values of h agreed to within $\pm$ 2%.

For a given wind speed the deviation of h about its mean value, for all of the temperature differences examined in this current series of experiments, was approximately $\pm$ 2%.

Because h was found to be essentially independent of $\Delta T$ in the forced regime, it was not necessary to control strictly the plate - air temperature difference during the forced convection experiments. It was, however, kept within the range encountered during the full-scale convection experiments i.e. 10-60 K and most often maintained in the range 20-30 K.

### 7.1.2 The dependence of the convective heat transfer coefficient on the wind speed measured over the roof $V_{6R}$

The mainstream of experimental runs consisted of maintaining a constant air speed in the tunnel and evaluating the convective heat transfer coefficient at each of the following wind incidence angles 0°, $\pm$ 45°, $\pm$ 90°, $\pm$ 135° and 180°, these angles being the midsector wind angles from the full-scale experiments.

By performing several such runs it was possible to obtain plots of h v $V_{6R}$ for each of the wind incidence angles given above. Gradient wind velocities in the range $3.1 < V_G < 23.5$ $ms^{-1}$ were available. This gave roof wind speed velocities in the ranges $2.6 < V_{6R} < 19.4$ $ms^{-1}$ (for the 1:32 scale modes) and $1.4 < V_{6R} < 9.5$ $ms^{-1}$ (for the 1:64 scale model).

Figures 7.3 - 7.5 show plots of the convective heat transfer coefficient against roof wind speed for three wind angles (0°, 90° and 180°) for the 1:32 scale model. Figures 7.6 - 7.8 show similar plots for the 1:64 scale model.

The line drawn through the data points (which include a value for the natural convection coefficient at $V_{6R} = 0$ $ms^{-1}$) is a least squares linear regression line. This type of analysis was applied to the data for all the wind angles examined. Tables 7.1 and 7.2 show the results of the regression analysis for the 1:32 and 1:64 scales respectively. As can be seen from these tables the regression coefficients of the lines are very close to unity indicating that the lines are excellent fits to the data points. Therefore the linear relationships between h and $V_{6R}$ adequately describe the dependence of the convection coefficient upon the wind speed as measured over the roof. It will be recalled, however, that the fundamental theoretical relationships between the forced convection coefficient and wind speed are power law relationships (see Chapter Two). Also several experimenters have found power law relationships between h and wind speed in wind tunnel studies e.g. Sparrow [1977] and Iqubal and Khatry

TABLE 7.1 Linear relationships between h on $V_{6R}$ for the mid-sector wind incidence angles (1:32 scale)

| Wind Angle θ | Number of Data Points | Linear Relationship | Regression Coefficient r | Significance Level p | Wind speed range $ms^{-1}$ |
|---|---|---|---|---|---|
| 0° | 12 | $h = 14.6\ V_{6R} + 18.3$ | 0.998 | $p < 0.001$ | $0 < V_{6R} < 19.9$ |
| 45° | 8 | $h = 15.3\ V_{6R} + 16.1$ | 0.998 | $p < 0.001$ | $0 < V_{6R} < 19.9$ |
| 90° | 9 | $h = 15.3\ V_{6R} + 14.6$ | 0.997 | $p < 0.001$ | $0 < V_{6R} < 19.9$ |
| 135° | 8 | $h = 14.0\ V_{6R} + 13.2$ | 0.995 | $p < 0.001$ | $0 < V_{6R} < 19.9$ |
| 180° | 9 | $h = 13.3\ V_{6R} + 11.5$ | 0.997 | $p < 0.001$ | $0 < V_{6R} < 19.9$ |
| -135° | 8 | $h = 15.3\ V_{6R} + 12.5$ | 0.997 | $p < 0.001$ | $0 < V_{6R} < 19.9$ |
| -90° | 9 | $h = 15.0\ V_{6R} + 15.3$ | 0.998 | $p < 0.001$ | $0 < V_{6R} < 19.9$ |
| -45° | 8 | $h = 15.1\ V_{6R} + 16.6$ | 0.997 | $p < 0.001$ | $0 < V_{6R} < 19.9$ |

TABLE 7.2 Linear relationships between h on $V_{6R}$ for the mid-sector wind incidence angles (1:64 scale)

| Wind Angle θ | Number of Data Points | Linear Relationship | Regression Coefficient r | Significance Level p | Wind speed range $ms^{-1}$ |
|---|---|---|---|---|---|
| 0° | 5 | $h = 26.6\ V_{6R} + 30.3$ | 0.996 | $p < 0.001$ | $0 < V_{6R} < 9.5$ |
| 45° | 5 | $h = 24.2\ V_{6R} + 28.8$ | 0.997 | $p < 0.001$ | $0 < V_{6R} < 9.5$ |
| 90° | 5 | $h = 22.7\ V_{6R} + 28.0$ | 0.997 | $p < 0.001$ | $0 < V_{6R} < 9.5$ |
| 135° | 5 | $h = 19.1\ V_{6R} + 26.9$ | 0.997 | $p < 0.001$ | $0 < V_{6R} < 9.5$ |
| 180° | 5 | $h = 18.1\ V_{6R} + 24.5$ | 0.999 | $p < 0.001$ | $0 < V_{6R} < 9.5$ |
| -135° | 5 | $h = 20.9\ V_{6R} + 26.2$ | 0.998 | $p < 0.001$ | $0 < V_{6R} < 9.5$ |
| -90° | 5 | $h = 22.7\ V_{6R} + 26.2$ | 0.998 | $p < 0.001$ | $0 < V_{6R} < 9.5$ |
| -45° | 5 | $h = 23.9\ V_{6R} + 29.5$ | 0.998 | $p < 0.001$ | $0 < V_{6R} < 9.5$ |

Table 7.3 Power law relationships from the 1:32 scale wind tunnel model experiments

| Wind Angle $\theta$ | Power Law Relationship | Regression Coefficient r | Significance Level p |
|---|---|---|---|
| 0° | $h = 22.7\ V_{6R}^{0.85}$ | 0.996 | $p < 0.001$ |
| 45° | $h = 22.2\ V_{6R}^{0.87}$ | 0.998 | $p < 0.001$ |
| 90° | $h = 22.6\ V_{6R}^{0.88}$ | 0.974 | $p < 0.001$ |
| 135° | $h = 20.1\ V_{6R}^{0.89}$ | 0.993 | $p < 0.001$ |
| 180° | $h = 17.9\ V_{6R}^{0.94}$ | 0.996 | $p < 0.001$ |
| -135° | $h = 20.1\ V_{6R}^{0.91}$ | 0.984 | $p < 0.001$ |
| -90° | $h = 23.0\ V_{6R}^{0.89}$ | 0.972 | $p < 0.001$ |
| -45° | $h = 22.2\ V_{6R}^{0.87}$ | 0.985 | $p < 0.001$ |

Table 7.4 Power law relationships from the 1:64 scale wind tunnel model experiments

| Wind Angle θ | Power Law Relationship | Regression Coefficient r | Significance Level p |
|---|---|---|---|
| 0° | $h = 56.7\ V_{6R}^{0.65}$ | 0.984 | $p < 0.001$ |
| 45° | $h = 57.5\ V_{6R}^{0.65}$ | 0.973 | $p < 0.001$ |
| 90° | $h = 46.5\ V_{6R}^{0.65}$ | 0.961 | $p < 0.001$ |
| 135° | $h = 47.8\ V_{6R}^{0.64}$ | 0.985 | $p < 0.001$ |
| 180° | $h = 40.9\ V_{6R}^{0.65}$ | 0.974 | $p < 0.001$ |
| -135° | $h = 45.8\ V_{6R}^{0.67}$ | 0.932 | $p < 0.001$ |
| -90° | $h = 48.7\ V_{6R}^{0.68}$ | 0.975 | $p < 0.001$ |
| -45° | $h = 54.8\ V_{6R}^{0.66}$ | 0.984 | $p < 0.001$ |

[1977]. It was decided to apply this type of relationship to the current data. The least squares power fit analysis included all the data points used in the linear analysis, except the value for the natural convection coefficient, as the power law relationships are only strictly valid in the forced convection regime.

The results of this analysis are presented in Tables 7.3 and 7.4 for the 1:32 and 1:64 scales respectively. These power law relationships also have regression coefficients close to unity, indicating that they too are excellent fits to the data, with the obvious exception that they do not take into account natural convection effects.

The fundamental theoretical relationships between h and wind speed are derived, in their dimensionless form, in Chapter Two. These are for laminar flow.

$$Nu = 0.664\ Re^{0.5}\ Pr^{0.33} \qquad (7.3)$$

and for turbulent flow

$$Nu = 0.036\ Re^{0.8}\ Pr^{0.33} \qquad (7.4)$$

Table 7.5 illustrates the dimensional form of these equations for the two scale models used. Representative values of the properties of air were taken from tables in Holman [1981] and the characteristic length of the plates were employed.

Table 7.5 Dimensional form of fundamental forced convection equations for the two scale models used

| Model Scale | Laminar | Turbulent |
|---|---|---|
| 1:32 | $h = 21.3\ V^{0.5}$ | $h = 11.6\ V^{0.8}$ |
| 1:64 | $h = 27.4 V^{0.5}$ | $h = 12.8\ V^{0.8}$ |

Figure 7.9 shows the two fundamental equations for the 1:32 scale case together with the experimentally derived curve for $\Theta = 0°$. Figure 7.10 shows a similar comparison for the 1:64 scale model study. These two figures illustrate the fact that the theoretical equations which are based on a plate with a streamlined leading edge placed in a uniform parallel flow are inadequate for predicting the convective behaviour of a three dimensional inclined plate placed on a bluff body in a wind flow with a power law velocity profile, especially when the wind speed is measured close to the test building.

### 7.1.3 The dependence of the convective heat transfer coefficient upon the wind incidence angle, $\Theta$

In the full scale work it will be recalled, from Section 5.3, that the following method was used to examine the effect of the wind incidence angle on the convective heat transfer coefficient from the plate. Given values of $V_{6R}$ were substituted into the regression equations determined for each wind sector and the derived values of h were used to obtain a plot of h against $\Theta$.

This method could also have been employed in the analysis of the wind tunnel data. However, because the wind tunnel facilitates the control of the relevant parameters it was possible to examine the effect of wind incidence angle on h in more detail and with greater accuracy.

The following method was employed. With the tunnel air speed set at a constant value for the whole run, the convective heat transfer coefficient was evaluated through a full rotation of the turntable, 0-360° at 15° intervals. The turntable was then rotated back through 360° and the convection coefficient again evaluated at 15° intervals. The mean value of the convection coefficient $\bar{h}$ for the whole run was evaluated.

This interval, i.e. 15°, was chosen because it would include the midsector wind angles from the full-scale study i.e. 0°, ± 45°, ± 90°, ± 135° and 180°. Then the average of the two readings for each wind direction was evaluated (these never showed a difference of more than ± 0.2 $Wm^{-2}K^{-1}$).

For each wind direction the convection coefficient could then be expressed as a percentage of the mean value (i.e. $h/\bar{h}$ x 100%).

Figures 7.11 and 7.12 show plots of $h/\bar{h}$ x 100% against $\Theta$ for the 1:32 and 1:64 scale models respectively. Examination of these two figures yields the following information.

(i) For the 1:32 scale model the maximum deviations of h from $\bar{h}$ are +10% and -13%.

(ii) For the 1:64 scale model the maximum deviations of h from $\bar{h}$ are +12% and -17%.

(iii) The maximum heat transfer (in both scale cases) tends to occur when the wind incidence angle is in the range $-120° < \Theta < 120°$ i.e. windward. The minimum heat transfer occurs when $\Theta$ is outside the above range, i.e. leeward.

(iv) The shape of graphs for each scale are similar but not identical; this indicates that there may be some scale dependence of the effect of $\Theta$ on h.

(v) Both figures are generally symmetrical about $\Theta = 0°$ indicating that the presence of the small garage to the side of the test building has little influence on the convective heat transfer coefficient from the plate.

(vi) Both graphs exhibit local maxima at ± 120°; these are more pronounced in the 1:32 scale case and for this scale are the actual maxima in the heat transfer coefficient.

A further discussion on the effect of $\Theta$, upon h will be given in Section 7.3.3.

## 7.2 Comparison of the Wind Tunnel Model Study with the Full-Scale Site Measurements

One of the fundamental reasons for undertaking the wind tunnel study was to examine the potential of using the results obtained from small scale model experiments to predict accurately the convective behaviour of full-scale heat transfer systems. In order to assess this potential it is necessary to compare the results obtained from the two series of experiments.

### 7.2.1 General comparison between the full-scale and model study results

Both the full-scale work and the wind tunnel model study showed that the convective heat transfer coefficient h showed no dependence on the plate - air temperature difference in the forced regime. See Figures 5.15 to 5.18 and 7.2. Whilst the model study showed that the natural convection coefficient was dependent upon both scale and temperature difference, it was not possible to examine the natural convection coefficient in the full-scale work, as absolutely still conditions were not experienced during the trials. However it will be recalled from Chapter Five that the best estimate of the natural convection coefficient in the full-scale work was 8.1 $Wm^{-2}K^{-1}$. This value is again lower than the two scale model values, giving further indication that the natural convection coefficient in this series of experiments follows the expected pattern i.e. decreases with increasing absolute size of the heated surface.

The convection coefficient in the full-scale and wind tunnel studies were found to be dependent upon the wind incidence angle $\theta$; this will be examined in further detail in Section 7.2.2. In both the full-scale and wind tunnel studies the transfer coefficient was found to be linearly dependent upon the wind speed as measured over the roof. This will be examined further in Section 7.2.3.

### 7.2.2 A comparison between the full-scale and wind tunnel results with regards to the dependence of the convection coefficient upon the wind incidence angle, $\theta$

In order to compare the effect of $\theta$ upon h for the two series of experiments the following procedures was adopted. For the full-scale case, the value of the convection coefficient h (at $V_{6R} = 6\ ms^{-1}$) was obtained, for each wind sector, from the regression lines presented in Table 5.1. This was then normalised in terms of the mean coefficient $\overline{h}$ (i.e. the mean value of the coefficients found from each regression line) and expressed as a percentage i.e. $h/\overline{h} \times 100\%$.

In the model cases the percentage values, already presented in Figures 7.11 and 7.12 were averaged about each midsector wind angle. For example, the 0° midsector value is the average of the -15°, 0° and +15° values of $h/\overline{h} \times 100\%$. This was done in order to achieve a better comparison with the full-scale work, as the regression lines in this case were based on all the data which fell into a particular wind angle sector.

Figure 7.13 shows a plot of $h/\overline{h} \times 100\%$ against $\theta$ for each of the scale models and the full-scale test site. The individual data points are linked for clarity and it must be realised that the value of $h/\overline{h} \times 100\%$ for angles without data points may not lie on these lines. This fact is obvious for the model study work, see Figures 7.9 and 7.10.

Examination of Figure 7.13 reveals several points of interest.

(i) The variation of $h/\overline{h} \times 100\%$ is much greater for the full-scale test site than for either of the two scale models, it being approximately $\pm$ 30%.

(ii) There is some basic agreement between the three plots in that they all show minima rates of heat transfer when the plate surface is at 180° to the wind flow i.e. leeward.

(iii) The full-scale results and the 1:32 scale model series both show local minima of convection coefficient at $\Theta = 0°$. This local minimum does not appear in the 1:64 scale series results.

In the light of the points noted above, it can be concluded that the wind tunnel results could be used to predict general trends in the variation of h with $\Theta$ for the full-scale site. (The 1:32 scale series being in better agreement than the 1:64 scale results). However, the use of either wind tunnel scale results to predict the variation of h with $\Theta$ in any quantitative manner is not justified.

### 7.2.3 A comparison between the full scale and the wind tunnel results with regards to the dependence of the convection coefficient upon the wind speed as measured over the roof $V_{6R}$

In both the wind tunnel model studies and the full-scale work convective heat transfer coefficient was found to be adequately expressed as a linear function of the wind speed as measured over the roof (for each wind angle or sector examined).

For example, for the $\Theta = 0°$ wind direction the following relationships were derived.

$$\text{Full-scale} \quad h = 2.2\, V_{6R} + 8.3 \quad Wm^{-2}K^{-1} \tag{7.5}$$

$$\text{1:32 scale} \quad h = 14.6\, V_{6R} + 18.3 \quad Wm^{-2}K^{-1} \tag{7.6}$$

$$\text{1:64 scale} \quad h = 26.6\, V_{6R} + 30.3 \quad Wm^{-2}K^{-1} \tag{7.7}$$

It is, therefore, obvious that direct use of the dimensional model equations would lead to a gross overestimation of the convective heat transfer coefficient for the full-scale case. The $\Theta = 0°$ case is cited as an example but it can be seen from Tables 5.1, 7.1 and 7.2 that the above statement would be true for all wind incidence angles.

This mismatch of dimensional equations is, of course, to be expected as the convection coefficient is also dependent on the actual dimensions of the heated plate under consideration (see Section 3.1 for a discussion of the work of Parmellee and Huebscher [1946] on this point). The usual method of comparing heat transfer experiments performed on systems which are of different size, but otherwise geometrically similar, is by dimensional analysis.

Two parameters are of importance for this type of analysis. The Nusselt number Nu and the Reynolds number Re. These are defined as:

$$Nu = \frac{hx}{k} \quad , \qquad Re = \frac{V_\infty x}{\nu}$$

where $h$ = The convective heat transfer coefficient $Wm^{-2}K^{-1}$

$x$ = The characteristic dimension of the plate, (in this case 4 x Area/Perimeter length), m

$V_\infty$ = The free-stream air velocity $ms^{-1}$

$k$ = The thermal conductivity of the air $Wm^{-1}K^{-1}$

$\nu$ = Kinematic viscosity of the air $m^2s^{-1}$

A problem arises in applying this type of analysis to the current data. The only wind velocity measured continuously during the full-scale and wind tunnel model work was $V_{6R}$. Whilst this measured wind speed is outside the local boundary layer of the flat plate it is still within the atmospheric boundary layer of the earth (or wind tunnel) and therfore cannot strictly be interpreted as a free-stream wind velocity, $V_\infty$.

Therefore, the Reynolds number in this case must be redefined as

$$Re = \frac{V_{6R}\, x}{\nu}$$

with the original Nusselt number definition being valid.

In order to obtain dimensional relationships between h and $V_{6R}$ for the full-scale work and from the wind tunnel results consider the following general case.

$$h = A_t\, V_{6R} + B_t \qquad Wm^{-2}K^{-1} \qquad (7.8)$$

where $A_t$ and $B_t$ are constants.

Now

$$h = \frac{Nu\, k_t}{x_t}, \quad V_{6R} = \frac{Re\, \nu_t}{x_t}$$

where the subscript t refers to the model values of k, $\nu$ and x.

Therefore,

$$\frac{Nu\, k_t}{x_t} = A_t \frac{Re\, \nu_t}{x_t} + B_t \qquad (7.9)$$

$\therefore$

$$Nu = \frac{A_t\, \nu_t}{k_t} Re + \frac{B_t\, x_t}{k_t} \qquad (7.10)$$

Now for the full scale case (subscript f relates to full-scale values).

$$Nu = \frac{h\, x_f}{k_f}, \qquad Re = \frac{V_{6R}\, x_f}{\nu_f}$$

Substitution into equation 7.9 gives.

$$\frac{h\, x_f}{k_f} = \frac{A_t\, \nu_t}{k_t} \frac{V_{6R}\, x_f}{\nu_f} + \frac{B_t\, x_t}{k_t} \qquad (7.11)$$

Rearranging for h

$$h = A_t \frac{k_f}{k_t} \frac{\nu_f}{\nu_t} V_{6R} + B \frac{k_f}{k_t} \frac{x_t}{x_f} \qquad Wm^{-2}K^{-1} \qquad (7.12)$$

Both series of experiments were conducted in air under essentially the same conditions of temperature and pressure. Hence, approximately, $k_t = k_f$ and $\nu_t = \nu_f$.

Hence equation 7.12 can be simplified to (for the full-scale).

$$h = A_t V_{6R} + B_t \frac{x_t}{x_f} \qquad Wm^{-2}K^{-1} \qquad (7.13)$$

Therefore, the dimensional equations for the full-scale are identical to those presented for the two wind tunnel model studies except for the wind speed independent constant which must be multiplied by the ratio $x_t/x_f$. This ratio is 0.028 for the 1:32 scale work and 0.017 for the 1:64 scale series.

The linear regression lines for the full-scale work based on the wind tunnel model experiments are presented in Tables 7.6 and 7.7 (for the 1:32 scale and 1:64 scale extrapolations respectively).

Figure 7.14 shows a comparison between the regression lines derived from the two model studies and the actual regression line from the full-scale measurements for the $\Theta = 0°$ wind angle.

This figure illustrates that both 1:32 and 1:64 scale extrapolations grossly over-estimate the forced convection coefficient as found in the full-scale work whilst at the same time underestimating the natural convection coefficient, as defined as the intercept of the lines at $V_{6R} = 0\ ms^{-1}$. Hence the linear relationships as derived from the wind tunnel model scales are inadequate for predicting full-scale convective behaviour.

TABLE 7.6 Extrapolation of 1:32 scale series linear regression lines to full scale values

| Wind Angle Θ | Linear Extrapolation | |
|---|---|---|
| 0° | $h = 14.6\ V_{6R} + 0.5$ | $Wm^2K^{-1}$ |
| 45° | $h = 15.3\ V_{6R} + 0.5$ | $Wm^2K^{-1}$ |
| 90° | $h = 15.3\ V_{6R} + 0.4$ | $Wm^2K^{-1}$ |
| 135° | $h = 14.0\ V_{6R} + 0.4$ | $Wm^2K^{-1}$ |
| 180° | $h = 13.3\ V_{6R} + 0.3$ | $Wm^2K^{-1}$ |
| -135° | $h = 15.3\ V_{6R} + 0.3$ | $Wm^2K^{-1}$ |
| -90° | $h = 15.0\ V_{6R} + 0.4$ | $Wm^2K^{-1}$ |
| -45° | $h = 15.1\ V_{6R} + 0.5$ | $Wm^2K^{-1}$ |

TABLE 7.7 Extrapolation of 1:64 scale series linear regression lines to full scale values

| Wind Angle $\Theta$ | Linear Extrapolation | |
|---|---|---|
| 0° | $h = 26.6\ V_{6R} + 0.6$ | $Wm^2K^{-1}$ |
| 45° | $h = 24.2\ V_{6R} + 0.6$ | $Wm^2K^{-1}$ |
| 90° | $h = 22.7\ V_{6R} + 0.5$ | $Wm^2K^{-1}$ |
| 135° | $h = 19.7\ V_{6R} + 0.5$ | $Wm^2K^{-1}$ |
| 180° | $h = 18.1\ V_{6R} + 0.5$ | $Wm^2K^{-1}$ |
| -135° | $h = 20.9\ V_{6R} + 0.5$ | $Wm^2K^{-1}$ |
| -90° | $h = 22.7\ V_{6R} + 0.5$ | $Wm^2K^{-1}$ |
| -45° | $h = 23.1\ V_{6R} + 0.5$ | $Wm^2K^{-1}$ |

It will be recalled from Section 7.1.2 that power law relationships were also derived from the wind tunnel data (see Tables 7.3 and 7.4). These may also be extrapolated up to full-scale values, using dimensionless parameters. Once again considering the general case.

$$h = A_t V_{6R}^{B_t} \quad Wm^{-2}K^{-1} \tag{7.14}$$

Therefore

$$\frac{Nu\ k_t}{x_t} = A_t \left(\frac{\upsilon_t}{x_f}\right)^{B_t} Re^{B_t} \tag{7.15}$$

Rearranging

$$Nu = A_t \frac{x_t}{k_t} \left(\frac{\upsilon_t}{x_t}\right)^{B_t} Re^{B_t} \tag{7.16}$$

Taking full-scale values for Nu and Re

$$\frac{h\ x_f}{k_f} = A_t \frac{x_t}{k_t} \left(\frac{\upsilon_t}{x_t}\right)^{B_t} \left(\frac{x_f}{\upsilon_f}\right)^{B_t} V_{6R}^{B_t} \tag{7.17}$$

Hence

$$h = A_t \frac{k_f}{k_t} \frac{x_t}{x_f} \left(\frac{\upsilon_t}{\upsilon_f}\right)^{B_t} \left(\frac{x_f}{x_t}\right)^{B_t} V_{6R}^{B_t}, \quad Wm^{-2}K^{-1} \tag{7.18}$$

Assuming as a first approximation $k_t = k_f$ and $\upsilon_t = \upsilon_f$ gives:

$$h = A_t \frac{x_t}{x_f} \left(\frac{x_f}{x_t}\right)^{B_t} V_{6R}^{B_t}, \quad Wm^{-2}K^{-1} \tag{7.19}$$

The ratio $x_t/x_f$ is 0.028 for the 1:32 scale case and 0.017 for the 1:64 scale case. Therfore, the ratio $x_f/x_t$ is 35.7 for the 1:32 scale case and 58.8 for the 1:64 scale case. Hence full-scale power law relationships can be derived from the wind tunnel relationships presented in Tables 7.3 and 7.4. The power law extrapolations to full-scale values are presented in Tables 7.8 and 7.9 for the 1:32 scale and 1:64 scale cases respectively.

TABLE 7.8 Power law extrapolations to the full-scale from the 1:32 scale series results

| Wind Angle $\hat{\theta}$ | Power Law Relationship |
|---|---|
| 0° | $h = 13.3\ V_{6R}^{0.85}$ $Wm^{-2}K^{-1}$ |
| 45° | $h = 13.9\ V_{6R}^{0.87}$ $Wm^{-2}K^{-1}$ |
| 90° | $h = 14.7\ V_{6R}^{0.88}$ $Wm^{-2}K^{-1}$ |
| 135° | $h = 13.5\ V_{6R}^{0.89}$ $Wm^{-2}K^{-1}$ |
| 180° | $h = 14.4\ V_{6R}^{0.94}$ $Wm^{-2}K^{-1}$ |
| -135° | $h = 14.5\ V_{6R}^{0.91}$ $Wm^{-2}K^{-1}$ |
| -90° | $h = 13.5\ V_{6R}^{0.89}$ $Wm^{-2}K^{-1}$ |
| -45° | $h = 13.9\ V_{6R}^{0.87}$ $Wm^{-2}K^{-1}$ |

TABLE 7.9 Power law extrapolations to the full-scale from the 1:64 scale series results

| Wind Angle $\Theta$ | Power Law Relationship |
|---|---|
| 0° | $h = 13.6\ V_{6R}^{0.65}$ $Wm^{-2}K^{-1}$ |
| 45° | $h = 13.8\ V_{6R}^{0.65}$ $Wm^{-2}K^{-1}$ |
| 90° | $h = 11.1\ V_{6R}^{0.65}$ $Wm^{-2}K^{-1}$ |
| 135° | $h = 11.0\ V_{6R}^{0.64}$ $Wm^{-2}K^{-1}$ |
| 180° | $h = 9.8\ V_{6R}^{0.65}$ $Wm^{-2}K^{-1}$ |
| -135° | $h = 11.9\ V_{6R}^{0.67}$ $Wm^{-2}K^{-1}$ |
| -90° | $h = 13.2\ V_{6R}^{0.68}$ $Wm^{-2}K^{-1}$ |
| -45° | $h = 13.7\ V_{6R}^{0.66}$ $Wm^{-2}K^{-1}$ |

Figure 7.15 shows a comparison between the two-scale extrapolations and the power law relationship derived from the full-scale measurements for the $\Theta = 0°$ wind angle. Once again the extrapolations grossly over-estimate the convection coefficient (i.e. as with the linear extrapolation).

It can, therefore, be stated that it is not possible to extrapolate the wind tunnel model results to the full-scale with any accuracy. A discussion of the possible reasons for the failure of the wind tunnel results to predict accurately full-scale convective behaviour will be given in Section 8.1.

## 7.3 Comparison of Current Study with Previous Wind Tunnel Experiments

Many workers have performed experiments on convective heat transfer from flat surfaces in wind tunnels (see Chapter Three). However, for this comparison only those experiments performed using active surfaces of a similar size to those used in these model studies will be considered.

### 7.3.1 Comparison with previous work performed on small flat plates and three dimensional bluff bodies

Sparrow's mass transfer work on small flat plates gave a global correlation of

$$h = 18.6\ V^{0.5} \quad Wm^{-2}K^{-1} \qquad (7.20)$$

where V = The wind speed in the centre of the tunnel, $ms^{-2}$

Sparrow [1981] does, however, show that the heat transfer may be enhanced over this value when the active surface is elevated above a host surface which is inactive in the heat transfer process. This will be discussed later in this section.

Iqubal and Khatry [1977] examined the overall convection coefficient of a heated copper model of a greenhouse, placed in a boundary layer wind tunnel, with the conclusion that

$$h = 17.9\ V_G^{0.576} \quad Wm^{-2}K^{-1} \tag{7.21}$$

where $V_G$ = Gradient wind speed of the boundary layer, $ms^{-2}$

Kelnhofer and Thomas' [1976] more sophisticated experiments on a cubical model gave similar results, i.e.

$$h = 17.98\ V_G^{0.5} \quad Wm^{-2}K^{-1} \tag{7.22}$$

The most recent study in this area was due to Kind [1983]. Using a model of a detached dwelling with heated plates mounted flush with one roof pitch, he obtained the following general correlation for h, i.e.

$$h = 23.9\ V_H^{0.54} \quad Wm^{-2}K^{-1} \tag{7.23}$$

where $V_H$ = the wind tunnel free stream air speed at the height of the centre of the heated plates, $ms^{-1}$

Because Kind also gives information concerning the shape of the simulated atmospheric boundary layer of the tunnel (rural terrain) it is possible to derive a further relationship, i.e.

$$h = 19.9\ V_G^{0.54} \quad Wm^{-2}K^{-1} \tag{7.24}$$

where once again $V_G$ is the gradient wind speed of the tunnel.

Therefore, if Sparrow's measured wind velocity can also be taken as a free stream velocity there is good agreement between the above four mentioned pieces of work. Also, in order to make a comparison between the current series of results and those mentioned above, it is necessary to reanalyse the data in terms of the gradient wind speed $V_G$. Because the above four relationships between h and $V_G$ are power law relationships this type of curve fit was applied to the current data. Tables 7.10 and 7.11 present power law relationships between h and $V_G$ for the 1:32 scale and 1:64 scale results respectively.

TABLE 7.10 Power law relationships between h and $V_G$ for the 1:32 scale series results

| Wind Angle Θ | Power Law Relationship | |
|---|---|---|
| 0° | $h = 19.4\ V_G^{0.85}$ | $Wm^{-2}K^{-1}$ |
| 45° | $h = 18.9\ V_G^{0.87}$ | $Wm^{-2}K^{-1}$ |
| 90° | $h = 19.2\ V_G^{0.88}$ | $Wm^{-2}K^{-1}$ |
| 135° | $h = 17.1\ V_G^{0.89}$ | $Wm^{-2}K^{-1}$ |
| 180° | $h = 15.0\ V_G^{0.94}$ | $Wm^{-2}K^{-1}$ |
| -135° | $h = 16.7\ V_G^{0.91}$ | $Wm^{-2}K^{-1}$ |
| -90° | $h = 19.5\ V_G^{0.89}$ | $Wm^{-2}K^{-1}$ |
| -45° | $h = 18.8\ V_G^{0.87}$ | $Wm^{-2}K^{-1}$ |

TABLE 7.11 Power law relationships between h and $V_G$ for the 1:64 scale series results

| Wind Angle $\theta$ | Power Law Relationship |
|---|---|
| 0° | $h = 33.7\ V_G^{0.65}$ $Wm^{-2}K^{-1}$ |
| 45° | $h = 34.2\ V_G^{0.65}$ $Wm^{-2}K^{-1}$ |
| 90° | $h = 27.7\ V_G^{0.65}$ $Wm^{-2}K^{-1}$ |
| 135° | $h = 28.17V_G^{0.64}$ $Wm^{-2}K^{-1}$ |
| 180° | $h = 24.03V_G^{0.65}$ $Wm^{-2}K^{-1}$ |
| -135° | $h = 26.7\ V_G^{0.67}$ $Wm^{-2}K^{-1}$ |
| -90° | $h = 28.9\ V_G^{0.68}$ $Wm^{-2}K^{-1}$ |
| -45° | $h = 32.4\ V_G^{0.66}$ $Wm^{-2}K^{-1}$ |

For the sake of completeness linear relationships between h and $V_G$ are also shown in Tables 7.12 and 7.13 (for the 1:32 and 1:64 scales respectively.

A representative equation for the previously performed work is taken as:

$$h = 18.6\ V_G^{0.53} \quad Wm^{-2}K^{-1} \tag{7.25}$$

Figure 7.16 shows a comparison of this equation with those for $\Theta$=:0°as developed from the 1:32 and 1:64 scale series of experiments.

It can be seen from this figure that the current relationships give much larger values of h for corresponding values of $V_G$ than the previously derived experimental equations.

This mismatch is to be expected due to the differing geometries and definitions of used in the various tests. For example Sparrow's plate was isolated with a streamlined leading edge and Iqubal and Khatry's convection coefficient was the average over the whole building surface. One piece of work (already discussed in Section 3.3) has shown that local variations in surface geometry may have significant affects upon the convective heat transfer from it. This is the work of Sparrow [1981].

### 7.3.2 Comparison with previously performed work on active surfaces elevated above host inactive planes

Sparrow performed experiments upon small plates elevated above a host surface (see Section 3.3 for a detailed discussion of this work). He varied the three parameters of H - Step height, L - stream-wise length of active surface and W - width of forward thrusting skirt (see Figure 3.9).

TABLE 7.12 Linear relationships between h on $V_G$ for the mid-sector wind angles (1:32 scale)

| Wind Angle $\theta$ | Number of Points N | Linear Relationship $h - Wm^{-2}K^{-1}$ | Regression Coefficient r | Significance Level p |
|---|---|---|---|---|
| 0° | 12 | $h = 12.2\ V_G + 18.3$ | 0.998 | $p < 0.001$ |
| 45° | 8 | $h = 12.7\ V_G + 16.1$ | 0.998 | $p < 0.001$ |
| 90° | 9 | $h = 12.7\ V_G + 14.6$ | 0.998 | $p < 0.001$ |
| 135° | 8 | $h = 1170\ V_G + 13.2$ | 0.997 | $p < 0.001$ |
| 180° | 9 | $h = 11.1\ V_G + 11.5$ | 0.995 | $p < 0.001$ |
| -135° | 8 | $h = 11.7\ V_G + 12.5$ | 0.997 | $p < 0.001$ |
| -90° | 9 | $h = 12.5\ V_G + 15.3$ | 0.997 | $p < 0.001$ |
| -45° | 8 | $h = 12.6\ V_G + 16.6$ | 0.998 | $p < 0.001$ |

TABLE 7.13 Linear relationships between h on $V_G$ for the mid-sector wind angles (1:64 scale)

| Wind Angle θ | Number of Points | Linear Relationship h $Wm^{-2}K^{-1}$ | Regression Coefficient r | Significance Level p |
|---|---|---|---|---|
| 0° | 5 | $h = 11.2\ V_G + 30.3$ | 0.996 | $p < 0.001$ |
| 45° | 5 | $h = 11.0\ V_G + 28.8$ | 0.997 | $p < 0.001$ |
| 90° | 5 | $h = 10.3\ V_G + 28.0$ | 0.997 | $p < 0.001$ |
| 135° | 5 | $h = 8.8\ V_G + 26.9$ | 0.997 | $p < 0.001$ |
| 180° | 5 | $h = 8.2\ V_G + 24.5$ | 0.998 | $p < 0.001$ |
| -135° | 5 | $h = 9.5\ V_G + 26.2$ | 0.998 | $p < 0.001$ |
| -90° | 5 | $h = 10.3\ V_G + 26.2$ | 0.9978 | $p < 0.001$ |
| -45° | 5 | $h = 10.9\ V_G + 29.5$ | 0.998 | $p < 0.001$ |

His general conclusion was that the convection coefficient was enhanced over the value found for a similar (but unelevated) sized plate. The enhancement increased with increasing ratio of H/L and also increased with increasing ratio of W/L. The enhancement was greatest for lower angles of attack (i.e. the angle the surface made with the horizontal, ) but increasing ratios of W/L gave rise to enhancement at increasing angles of attack. For example with H/1 = 1/15 = 0.07 and W/L = 1/25 = 0.4 an enhancement of $h/h^* = 1.7$ was observed at $\Theta = 35°$, $h^*$ being the heat transfer from a similar unelevated surface.

In the current series of experiments a similar situation to Sparrow's work exists i.e. the heated plate is elevated above an inactive host surface (the roof), the main difference being that the inactive surface is itself an integral part of a 3D bluff body.

Considering the wind blowing directly onto the plate i.e. $\Theta = 0°$ then

H = the height of the plate above the roof

L = the short axis of the plate

W = the projection of the roof between the lower edge of the late and the gutter line

$\Theta$ = the roof pitch, i.e. 35°

In both the model and the full-scale work the relevant ratios are the same i.e.

H/L = 0.33

W/L = 0.82

These ratios are both greater than the maximum ratios tested by Sparrow (H/L = 0.2, W/L = 0.4). Therefore, greater enhancement of the convection coefficient is to be expected than discovered by Sparrow. This enhancement has, of course, been observed (see Figure 7.16). Sparrow also states that the enhancement is also Reynold's number (wind velocity) dependent and so therefore any relationship between h and wind speed may be expected to deviate away from the simple power law relationship given earlier. The exponent will be expected to alter as the flow over the plate will no longer be laminar.

If, however, it is assumed that the enhancement is independent of the Reynold's number then the enhancement can be described by a simple multiplying factor on the original flat plate global equation, i.e.

$$h = A\ 18.6\ V^{0.5} \quad Wm^{-2}K^{-1} \tag{7.26}$$

The exponent will be expected to alter as the flow over the plate will no longer be laminar.

This relationship is also illustrated in Figure 7.16 with A = 2.0. It can be seen that this equation is more in line with those developed from the current work.

It would, therefore, seem that the current work agrees with that of Sparrow in that the convective heat transfer from a surface will be greatly enhanced if it is placed above a host inactive plane and also inclined to the horizontal.

### 7.3.3 Comparison with wind velocity measurements made over model building roofs

One other piece of model work has significance in relation to the current series of measurements, this being an investigation by Lee and Evans [1984] into the wind flow patterns over building roofs. Their study was designed to evaluate wind speeds in close proximity to the roofs of low-rise dwellings.

Using the University of Sheffield's boundary layer wind tunnel (the same as used for this series of experiments) they performed experiments on a 1:50 scale model of the Building Research Establishments standard semi-detached house shape (see Eaton and Mayne [1974] for further details of this structure). The actual house measured 13.3 x 7.0m in plan with a wall height of 5.3m to the eaves, the ridge height varying with roof angle.

Therefore, the plan dimensions of the model house were 266 x 140mm with a wall height of 106mm. This makes it comparable in size to the 1:32 scale model of the Norton site test building (300 x 157mm in plan, 88mm wall height).

Using hot wire anemometers, wind speeds parallel to the roof surface were measured. Six equally spaced positions across the roof span were simultaneously examined and the measured wind speed was the average wind speed in the first 6mm above the roof surface (300mm full-scale).

Measurements were made over a clear roof and above small panels standing proud of the roof surface (designed to represent retrofit solar collectors). Lee and Evans state that no panel proximity effects were found. Therefore, the clear roof measurements were adequate for both cases.

Many tests were performed examining various roof pitches, roof attachments i.e. chimneys and eaves and end attachments to the building structure. (A full account of all tests is given by Evans and Lee [1983]).

However, many basic features were common to all tests and of course only certain tests have relevance to the current series of wind tunnel experiments. Lee and Evans present their results in terms of the wind speed function $V_{COLL}/V_H$ where $V_{COLL}$ is the wind speed measured over the roof or model solar panel and $V_H$ is the undisturbed approach wind speed at the roof ridge line.

Figure 7.17 presents Lee and Evans' results for flow over a plain duo-pitch house with a 22.5° roof pitch. The Norton test site has this geometry and this set of results (state Lee and Evans) illustrates many of the features for flow over windward and leeward roof slopes found elsewhere in their data set.

Two points must be noted on examination of these results. Firstly, that only wind angles between 0°-180° were examined. This is because the building was modelled in isolation and presumably the -ve wind angles would produce a mirror image, about $\Theta = 0°$, of the data presented. Secondly the wind angle in this series of experiments is defined with an inverse sign convention to the current series.

Figure 7.17 illustrates the ratio of $V_{COLL}/V_H$ for each of the 6 positions examined over the range of wind angles. The aim of this section is to make a comparison between these wind speed ratios and the variation of convection coefficient with wind incidence angle (see Figures 7.11 and 7.12). Because of the position of the heated plate on the roof positions 3 and 4 in Lee and Evans' notation are most pertinent to this comparison.

The shape of the $V_{COLL}/V_H$ curves are similar for both positions but the features are more pronounced in the position 4 case. This shows that the ratio $V_{COLL}/V_H$ starts off slightly below unity at $\Theta$ = 0°, rises to a maximum slightly above unity at $\Theta$ = 60°, reaches a minimum of about 0.7 at $\Theta$ = 90°, again rises to a maximum of approximately 1.1 at $\Theta$ = 120° and then dips down to its absolute minimum value of about 0.4 at 180°.

Considering Figure 7.11 (the variation of $h/\bar{h}$ x 100% with for the 1:32 scale model) it can be seen that the shape of this curve illustrates similar features. The minimum heat transfer occurs in the region of 180° with local minima at $\Theta$ = 0° and $\pm$ 100°. Maximum heat transfer occurs at $\Theta = \pm$ 120° with local maxima at $\Theta = \pm$ 60°. Therefore, in this case, the variation of convection coefficient is closely related to the ratio of $V_{COLL}/V_H$ as measured by Lee and Evans over the roof pitch of a model building of similar size and geometry. It will be recalled that there was also some agreement between this model work and the full-scale dependence of h upon (see Section 7.2.2).

Now consider the 1:64 scale model case (see Figure 7.12). This model building has linear dimensions of approximately 0.5 of the model building examined by Lee and Evans. Once again a certain amount of agreement is shown i.e. minimum heat transfer occurs in the region of $\Theta$ = 180° and their are local maxima at $\Theta = \pm$ 120°. There is, however, conflict in this case is that the maximum heat transfer occurs in the region of $\Theta$ = 0°.

This disagreement can be partly attributed to the difference in absolute size of the models. The 1:32 scale model giving good agreement was of a similar size to the Lee, Evans building. Lee and Evans did not attempt to examine any scale effects upon $V_{COLL}/V_H$ and this is, perhaps, an area for further work as would be a study of similar parameters in a full-scale experimental set up.

Because of the slight dissimilarities of building geometry it is difficult to make a qualitative comparison between Lee and Evans' work and the current series. However, it can be broadly concluded that the forced convection coefficient is a function of the wind speed as measured over the first 6mm of the roof surface (300mm in the full-scale).

## Conclusion

With reference to wind tunnel model results reported in this chapter the following concluding points can be made:

(I) The natural convection coefficient, i.e. at $V_{6R} = 0\ ms^{-1}$ was found to increase with the plate - air temperature difference, the increase being more pronounced in the 1:64 scale model case.

(II) For identical temperature differences the natural convection coefficient for the 1:64 scale model (i.e. the smaller plate) was found to be larger than for the 1:32 scale model.

(III) The forced convection coefficient, i.e. $V_{6R} > 0\ ms^{-1}$ was found to be independent of the plate - air temperature difference. This is an agreement with the work of Kind [1983].

(IV) Linear and power relationships were found to exist between h and $V_{6R}$ (see Tables 7.1, 7.2, 7.3 and 7.4). The linear relationships take into account natural convection effects whilst the power relationships do not.

(V) The convection coefficient in both model cases was found to be much greater than that predicted by the fundamental theoretically derived relationships based on flat plates placed in a uniform parallel flow.

(VI) The convection coefficient was found to be slightly dependent upon the wind incidence angle $\Theta$ in both model cases. This dependence was not the same for both scale models and differences of the order of $\pm$ 15% about the mean value were observed.

(VII) With regards to the dependence of h upon $\Theta$ the wind tunnel model results exhibited some of the general features found in the full-scale work, especially in the 1:32 scale case. However, even in this case no real quantitative agreement was observed.

(VIII) Attempts to extrapolate the wind tunnel model data to fullscale values were made, using both linear and power law relationships. However, it was found that these extrapolations overestimated the convection coefficient, as found from the full-scale measurements, often by as much as an order of magnitude.

(IX) The current series of results tended to give higher values of h than those found in previous work although reasonable agreement was found with Sparrow's [1981] work on active surfaces elevated above passive host planes.

(X) A comparison was made between the current heat transfer results and the measurement of wind speeds across model building roofs performed by Lee and Evans [1984]. It was found, especially for the 1:32 scale series model, that wind angles which produced high values of h also tended to give high values of the wind speed over the roof surface. Low values of h corresponded to low wind speeds.

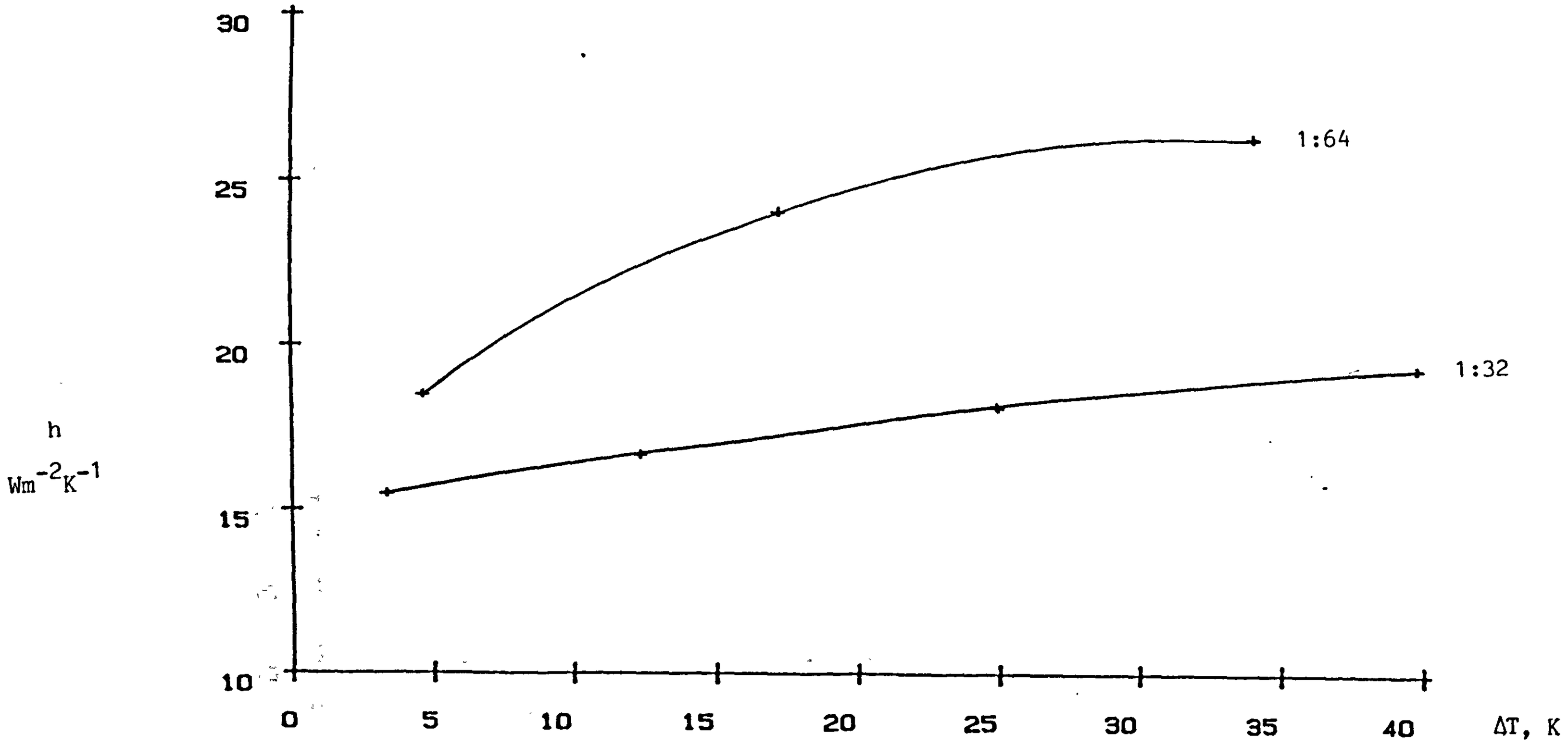


Figure 7.1 Natural convection coefficient h against temperature difference ΔT

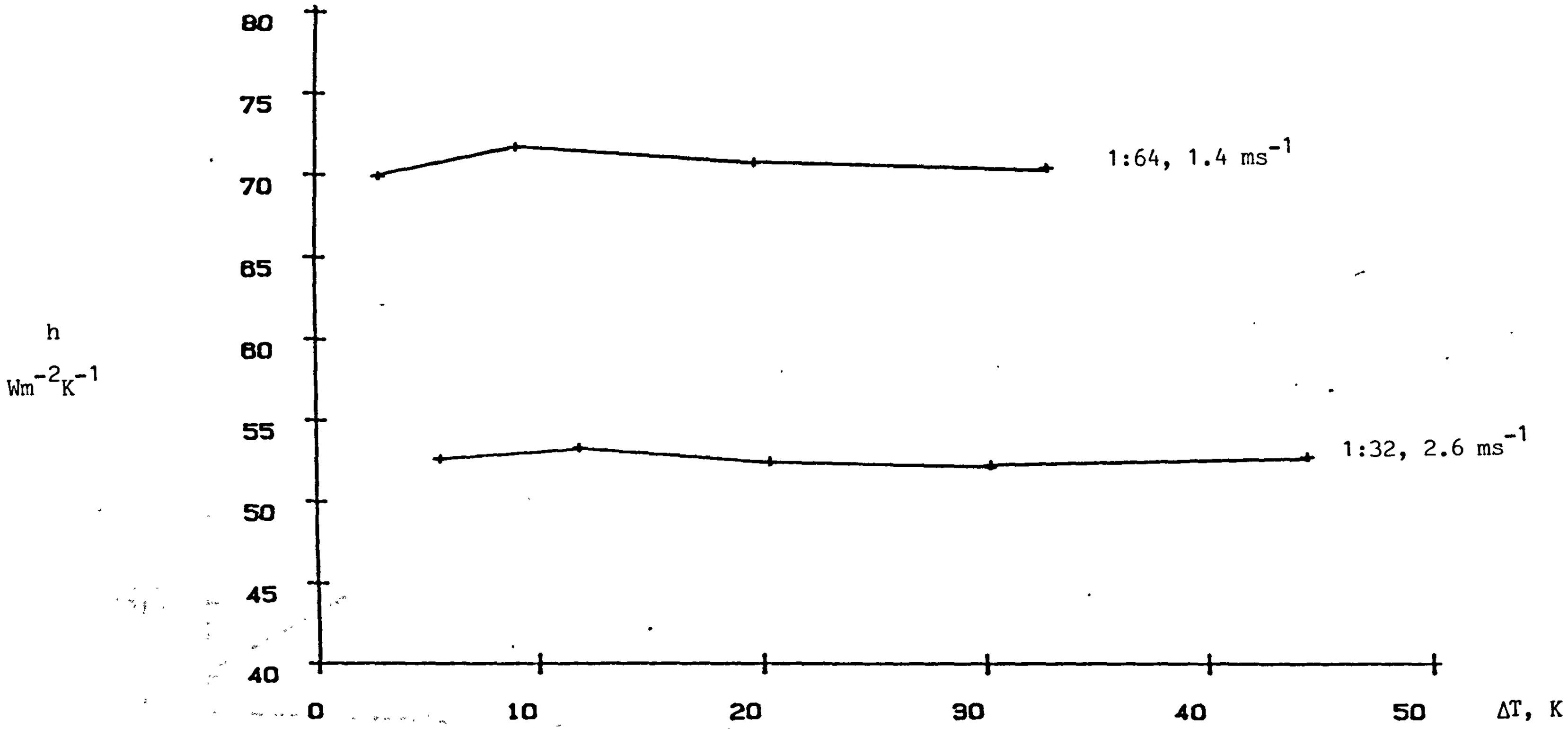


Figure 7.2 Convection coefficient, h, against temperature difference ΔT

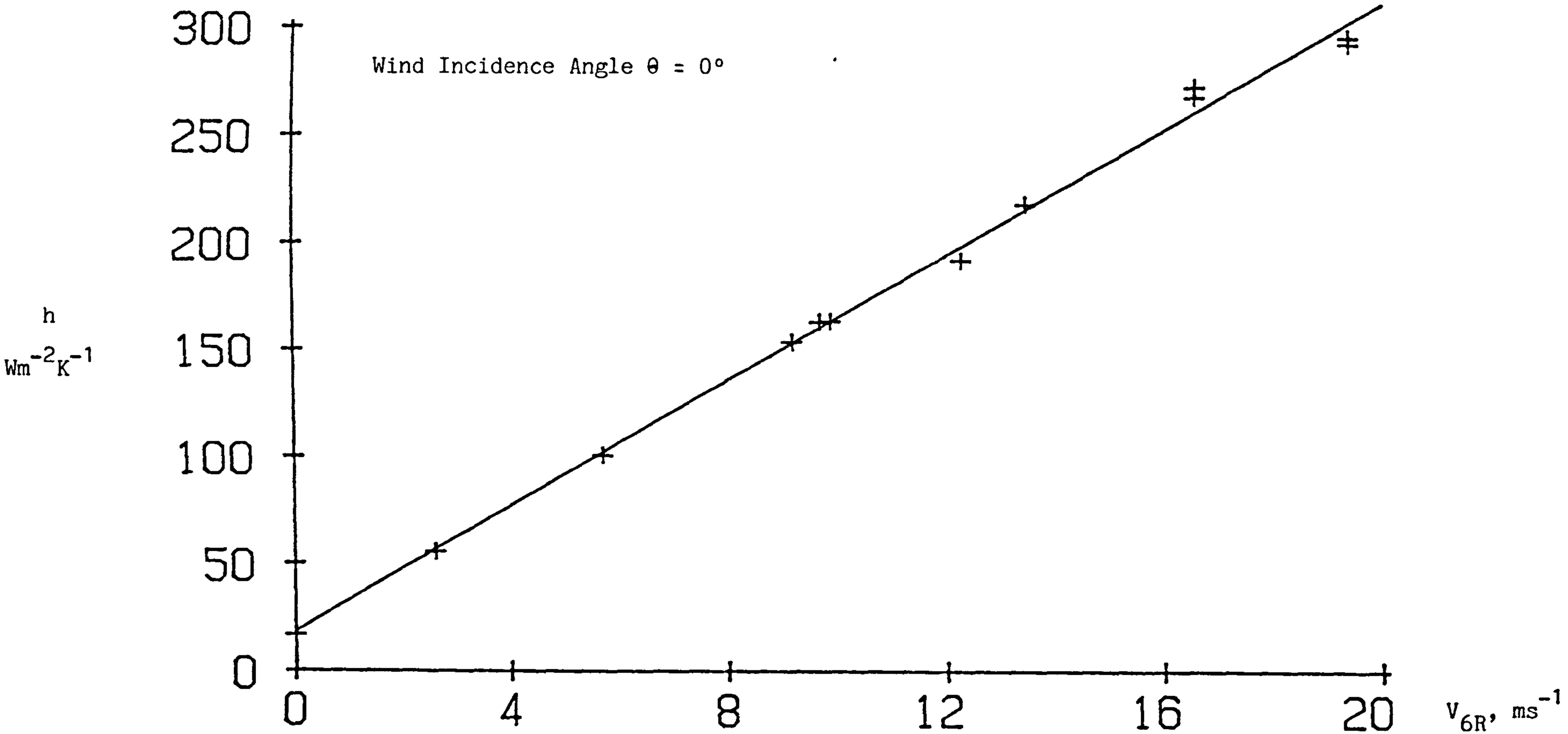


Figure 7.3 Convection coefficient h, against roof wind speed $v_{6R}$ (1:32 scale)

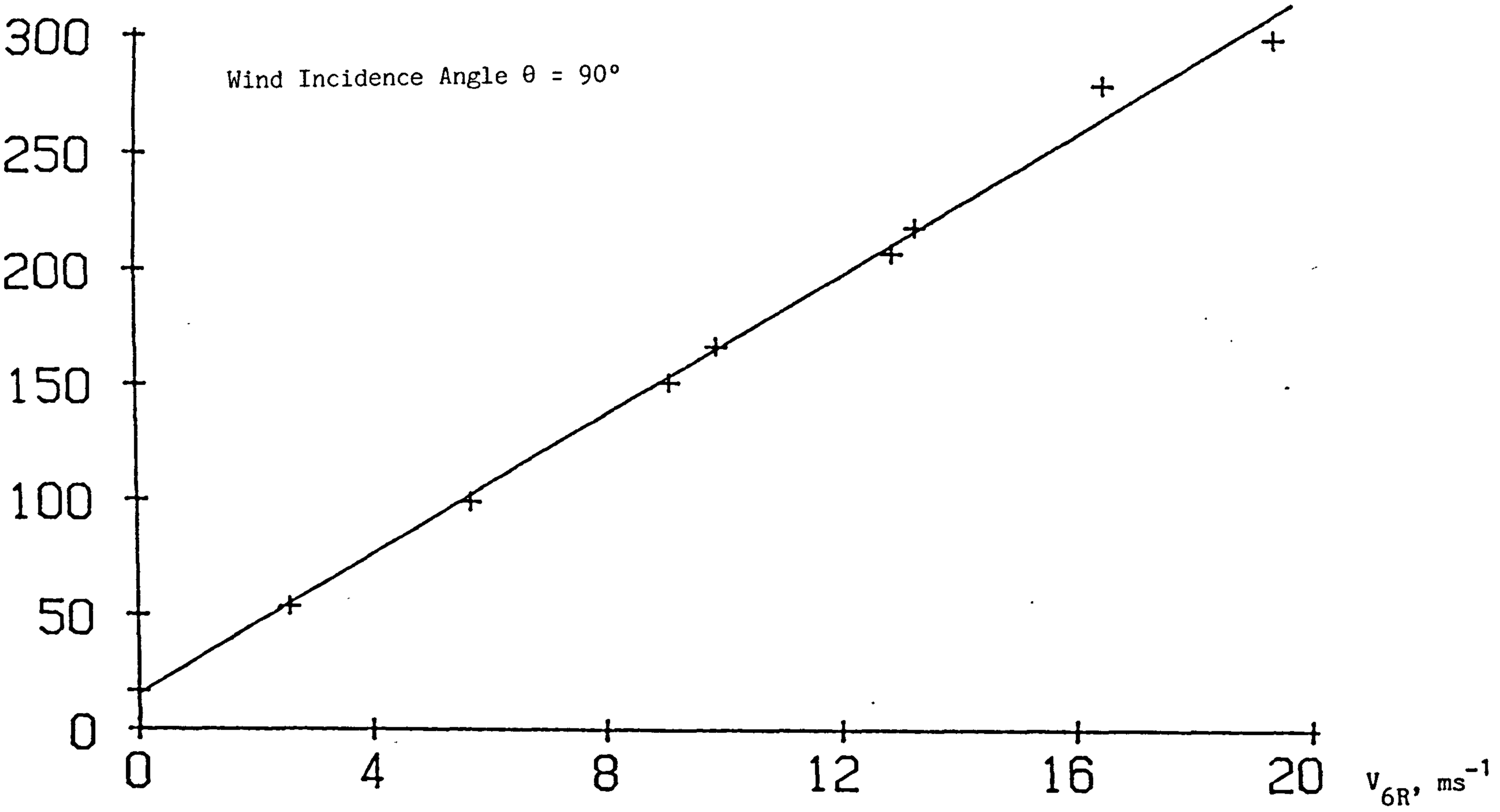


Figure 7.4 Convection coefficient, h, against roof wind speed $V_{6R}$ (1:32 scale)

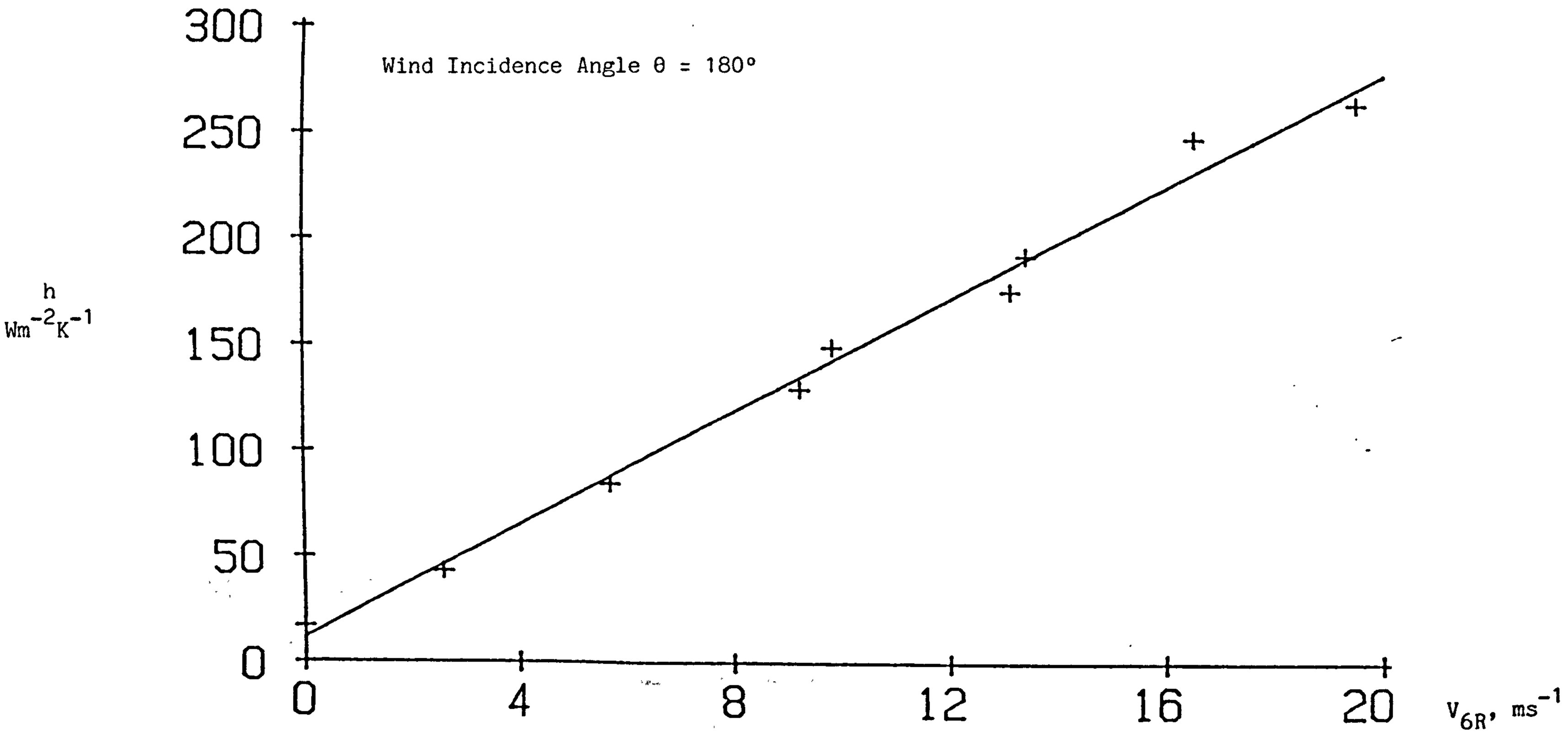


Figure 7.5 Convection coefficient, h, against roof wind speed, $V_{6R}$, (1:32 scale)

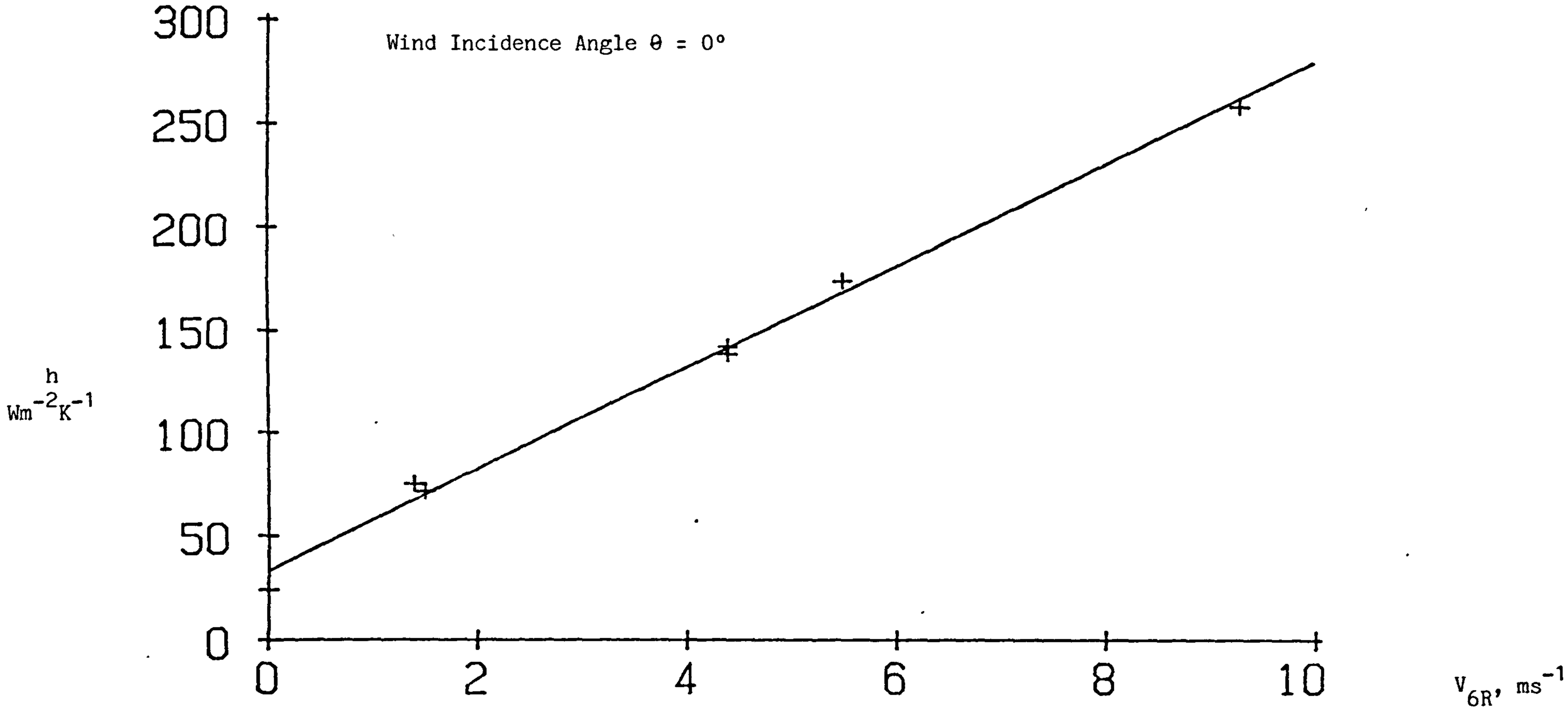


Figure 7.6 Convection coefficient, h, against roof wind speed, $V_{6R}$ (1:64 scale)

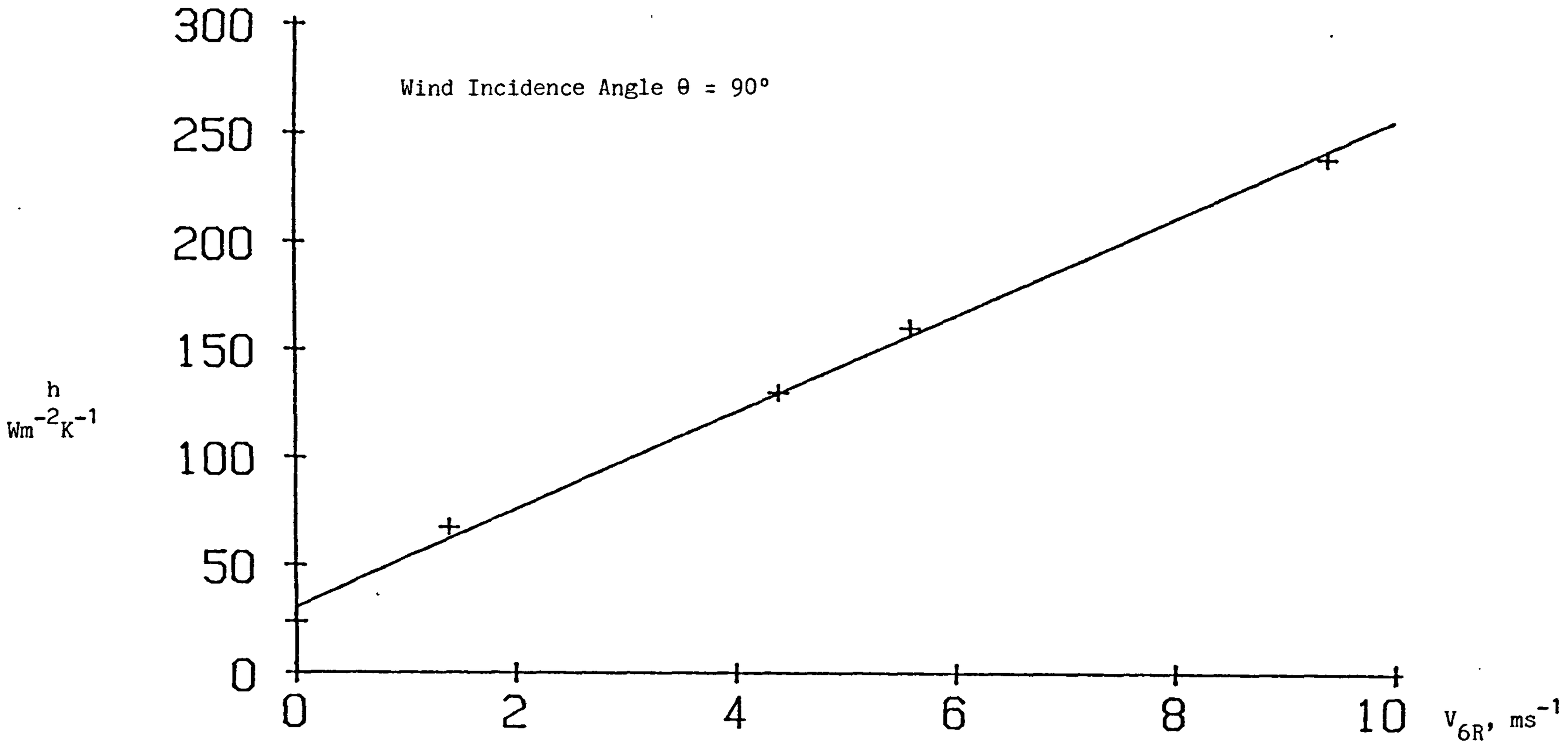


Figure 7.7 Convection coefficient, h, against roof wind speed, $V_{6R}$, (1:64 scale)

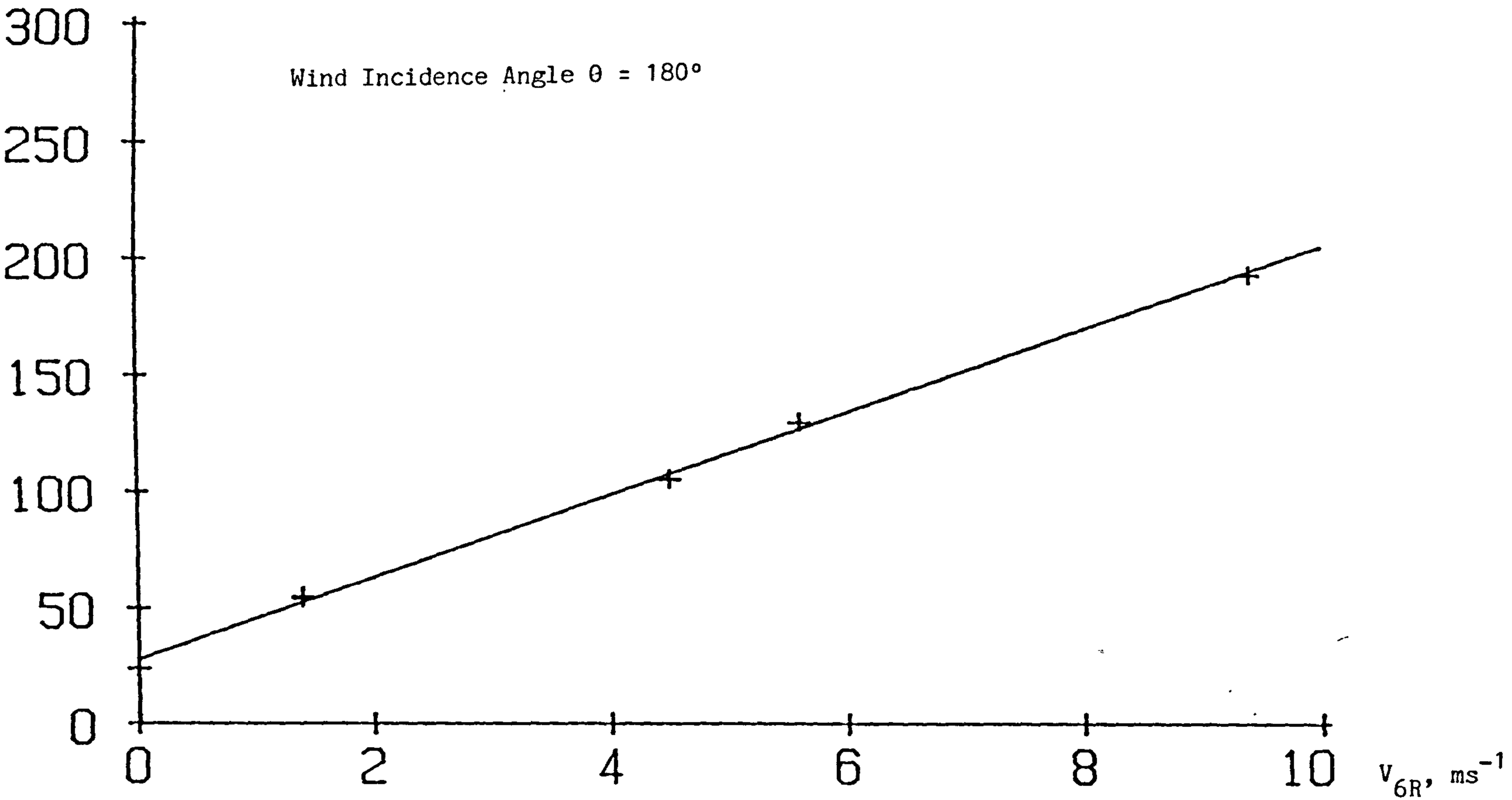


Figure 7.8 Convection coefficient, h, against roof wind speed $V_{6R}$ (1:64 scale)

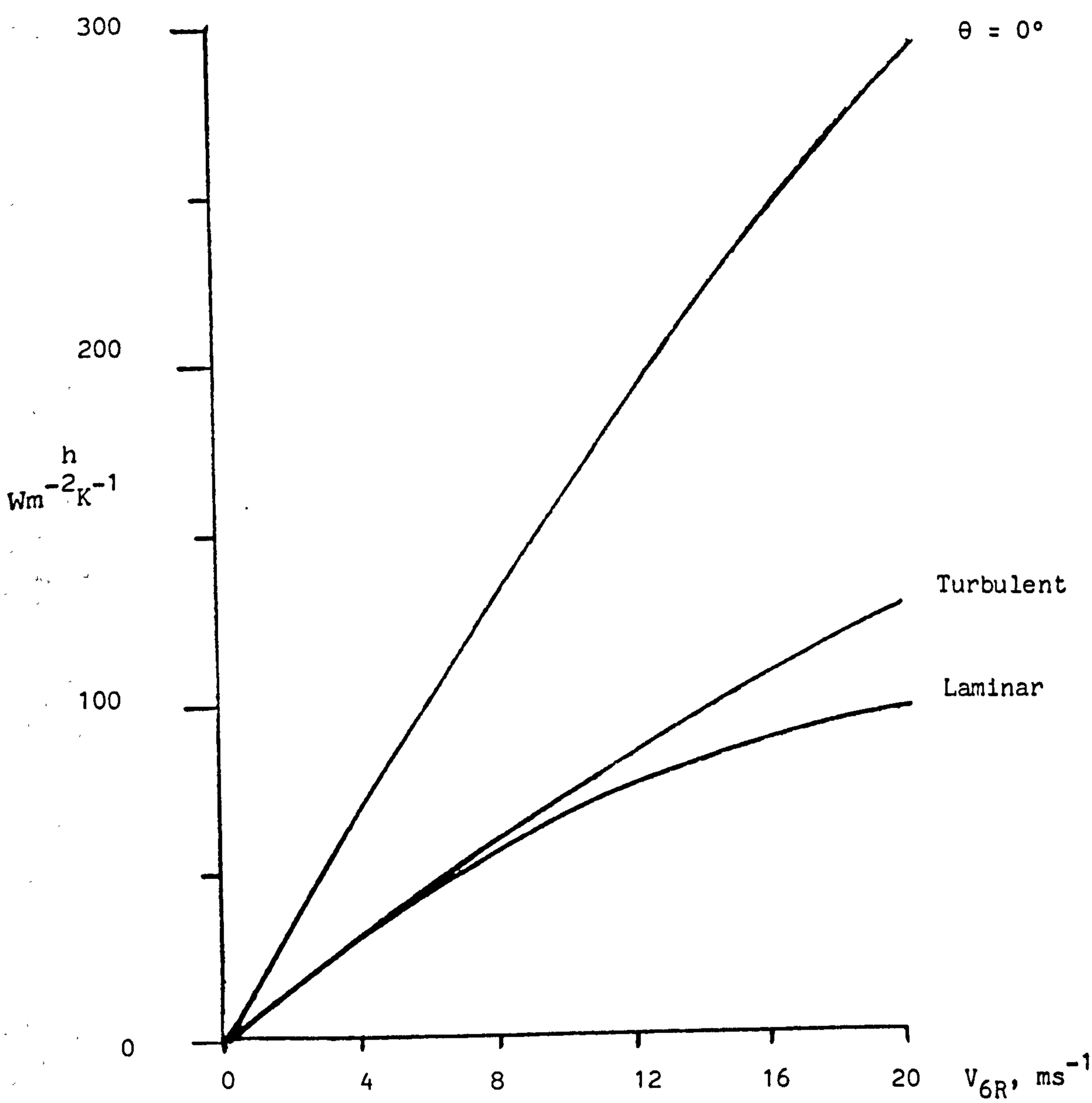


Figure 7.9 Comparison of laminar and turbulent flat plate theory with θ = 0° power law results (1:32 scale model series)

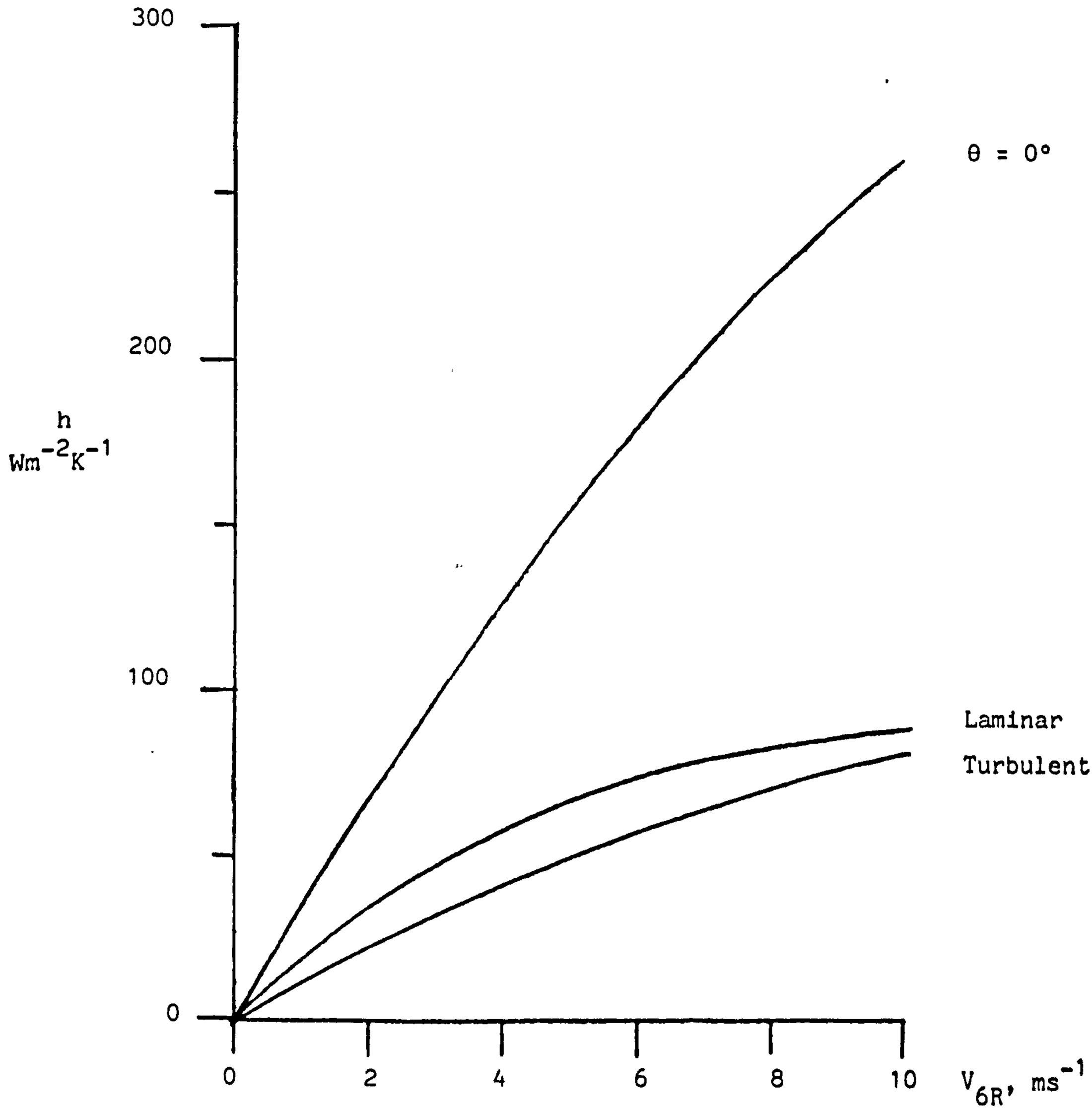


Figure 7.10 Comparison of laminar and turbulent flat plate theory with θ = 0° power law results (1:64 scale model series)

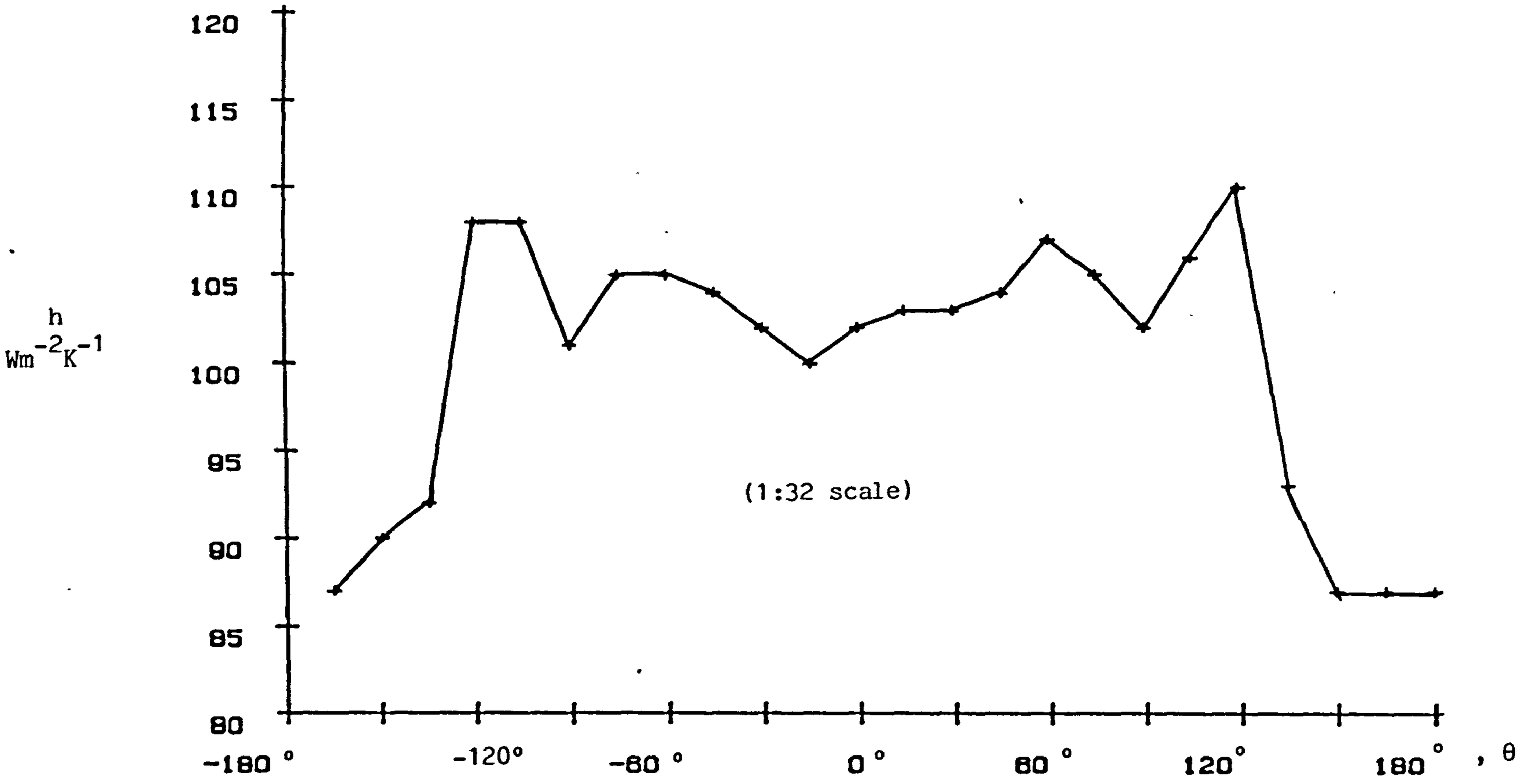


Figure 7.11 Convection coefficient, h, against wind incidence angle , θ.

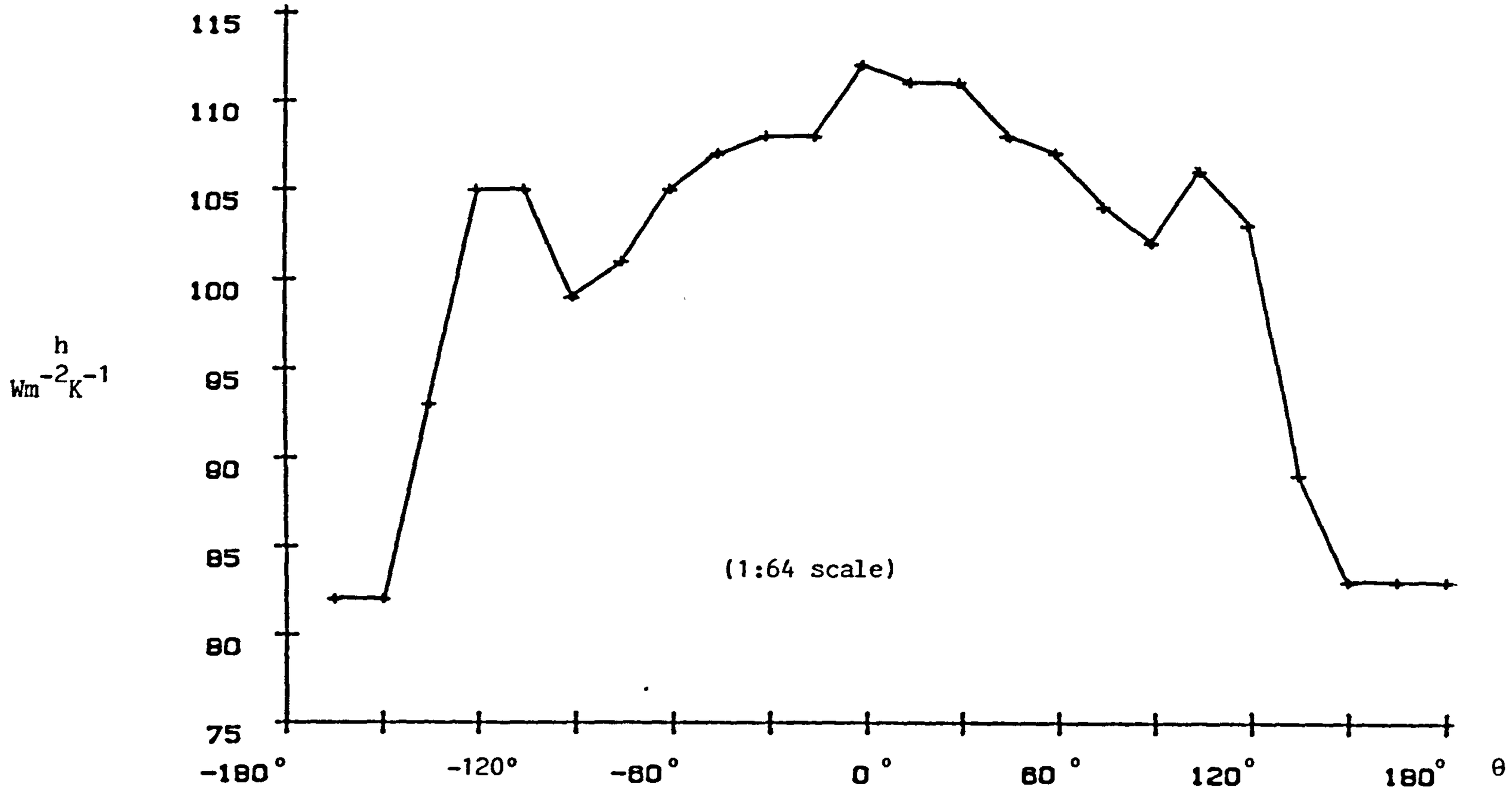


Figure 7.12 Convection coefficient, h, against wind incidence angle θ

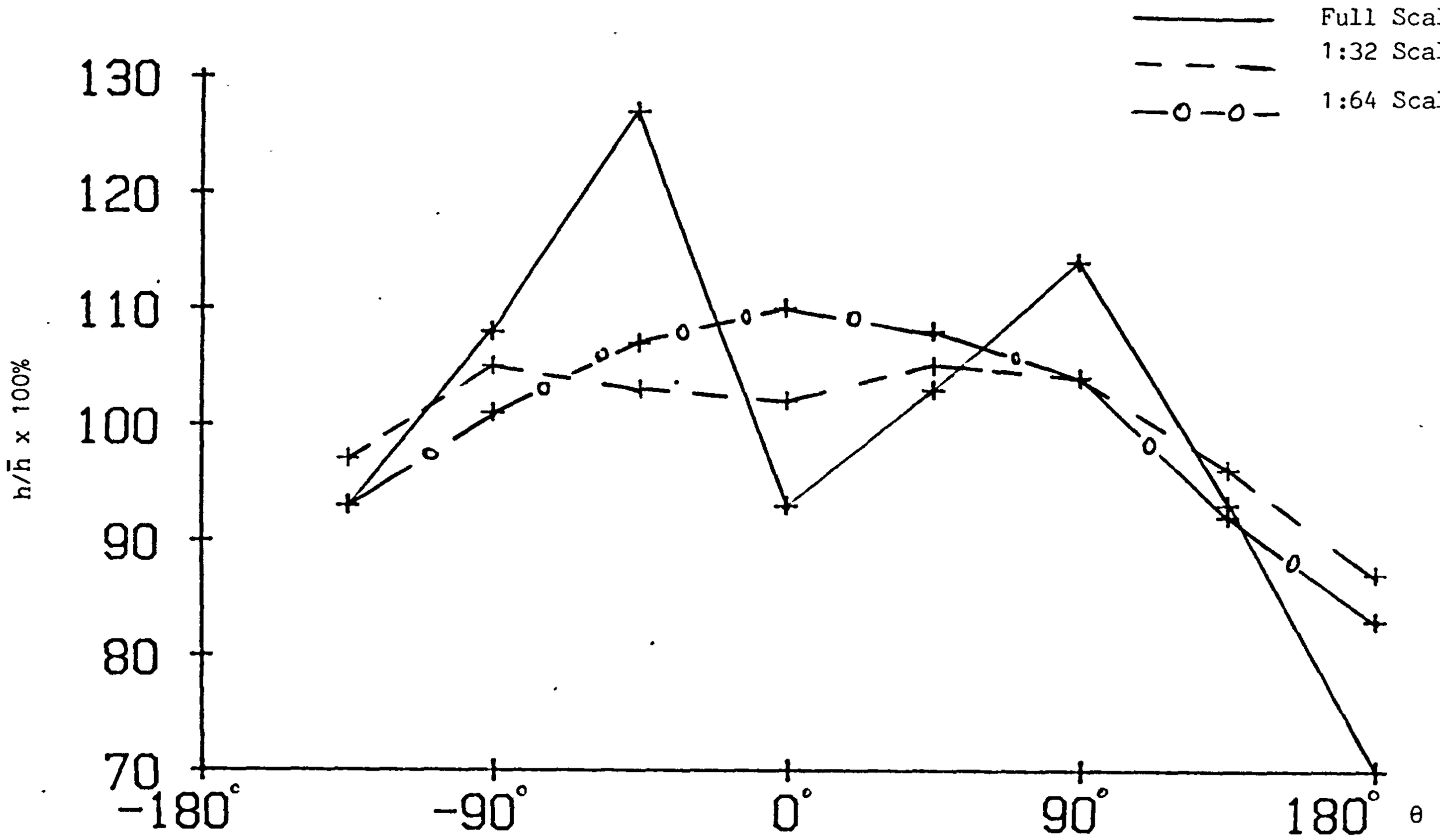


Figure 7.13 Normalised convection coefficient against wind incidence angle, θ

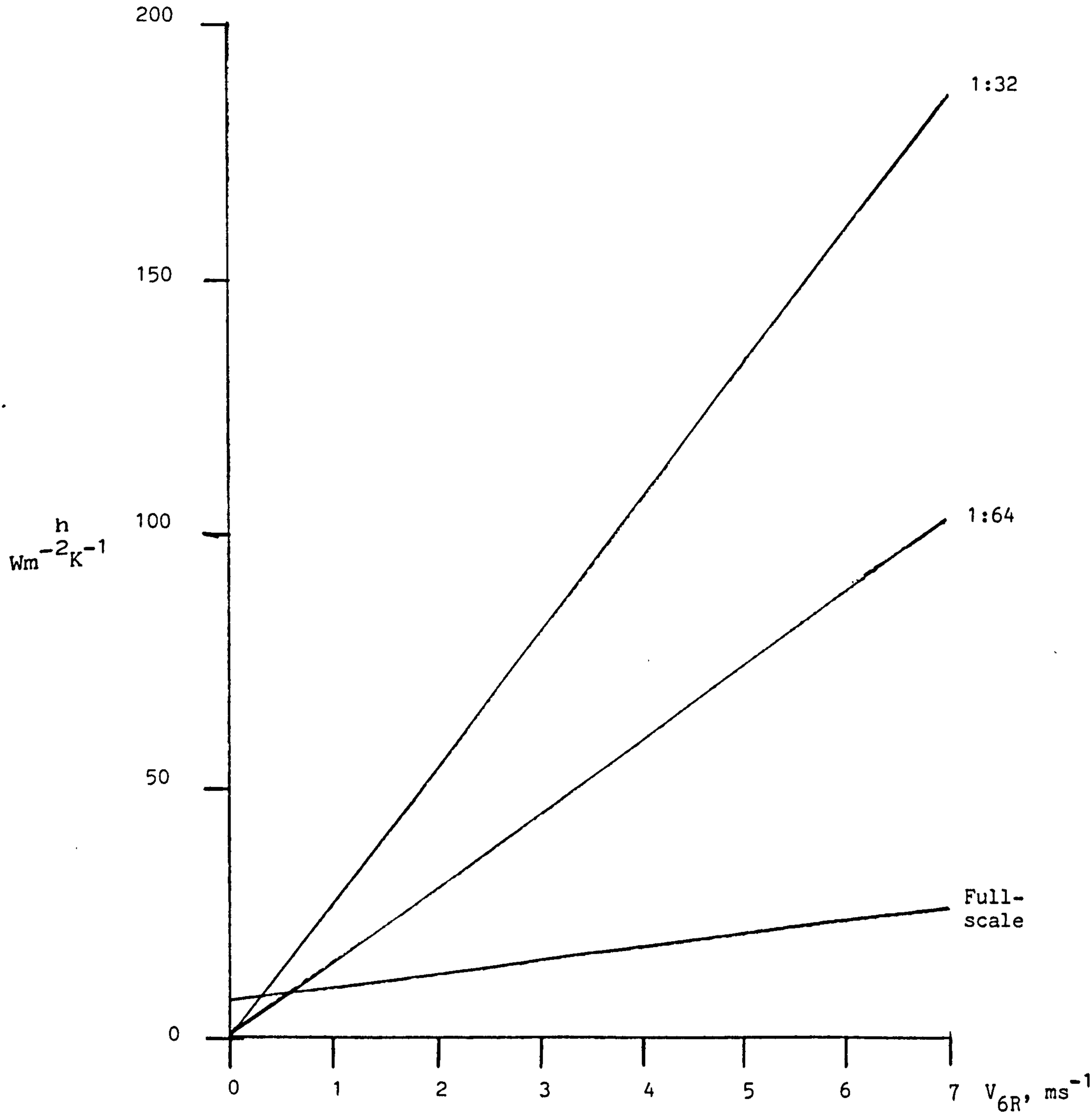


Figure 7.14 Comparison of linear extrapolations of two model series results with actual full-scale data

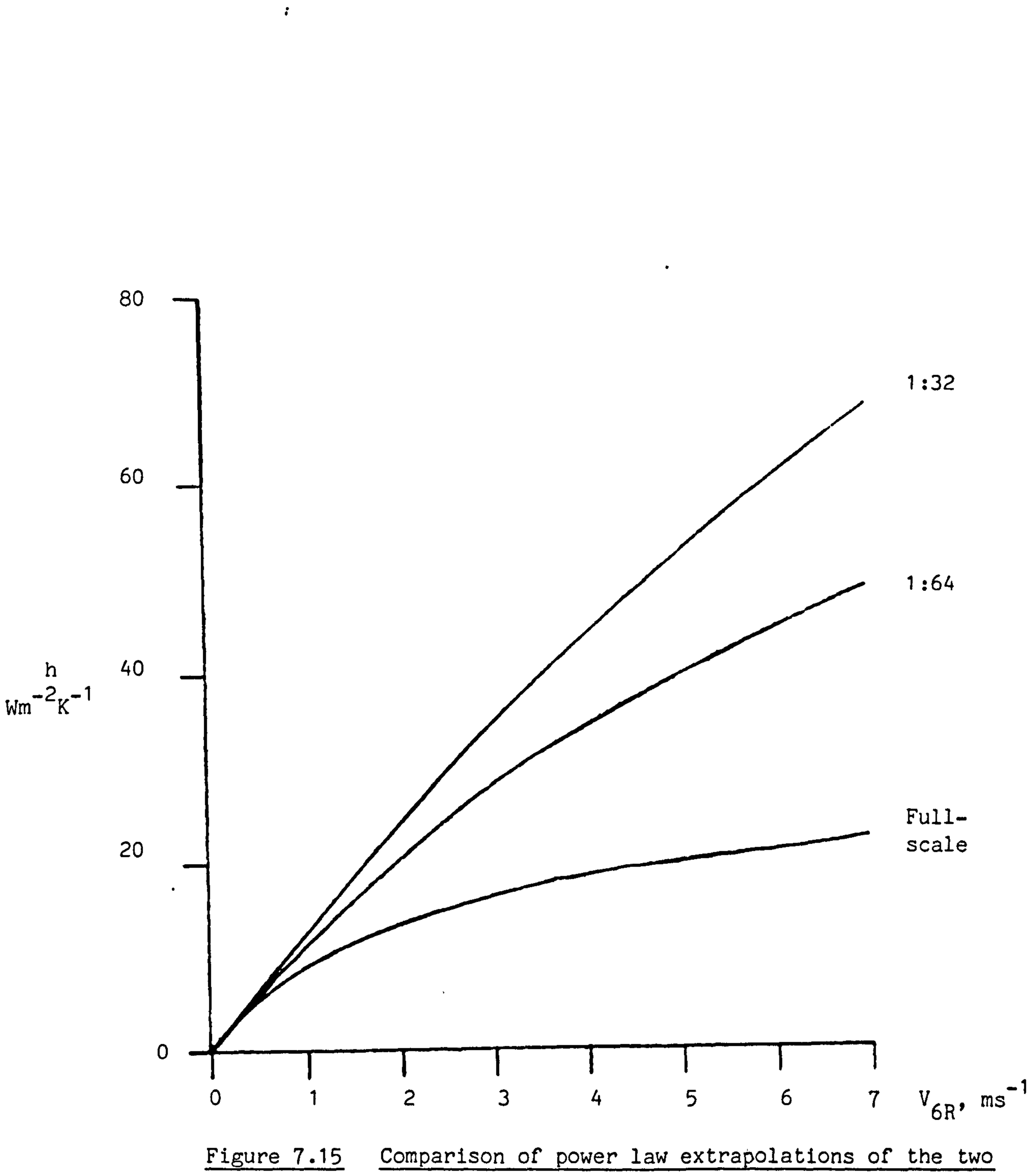


Figure 7.15 Comparison of power law extrapolations of the two model series results with actual full-scale data

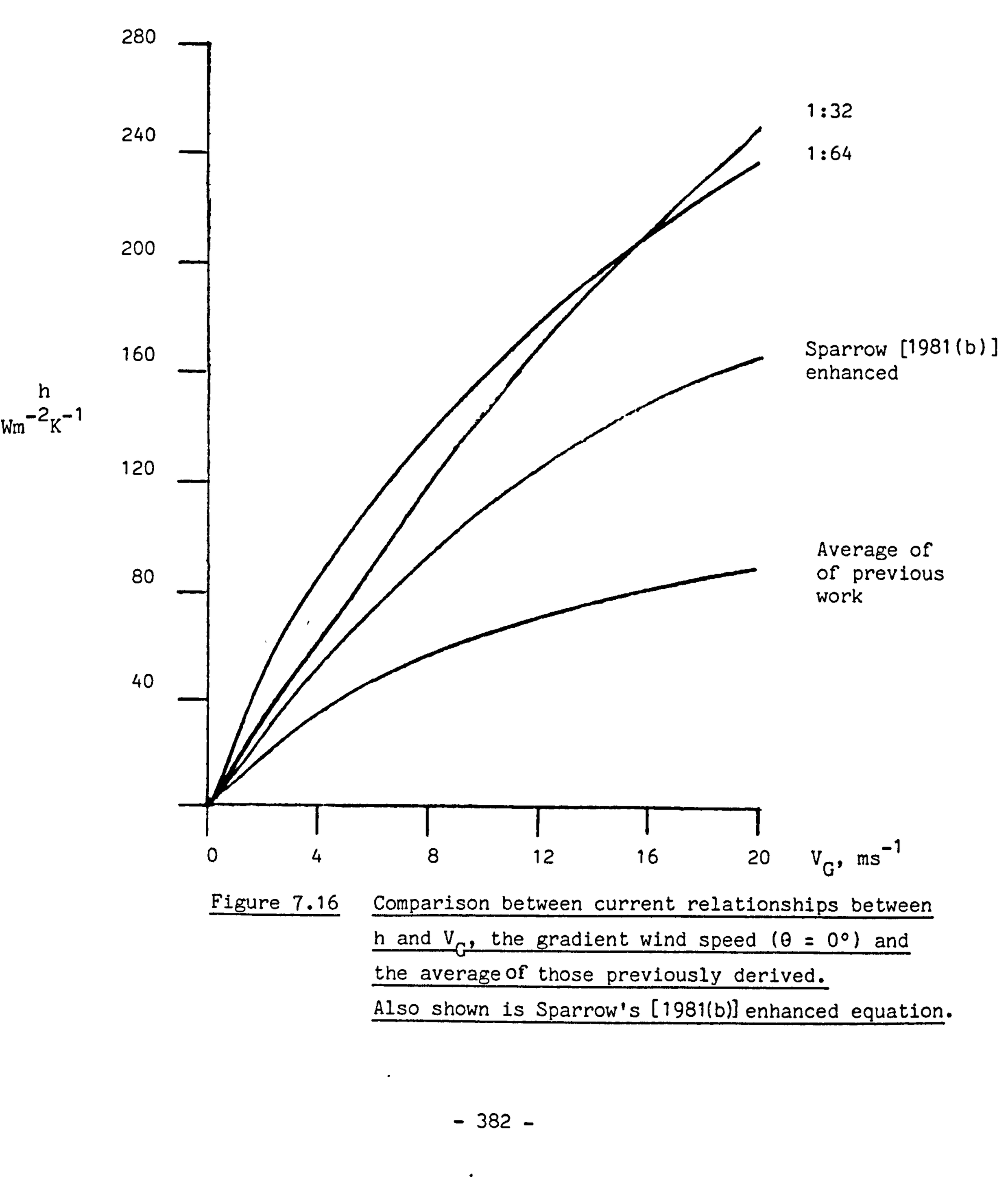


Figure 7.16 Comparison between current relationships between h and $V_G$, the gradient wind speed ($\theta$ = 0°) and the average of those previously derived. Also shown is Sparrow's [1981(b)] enhanced equation.

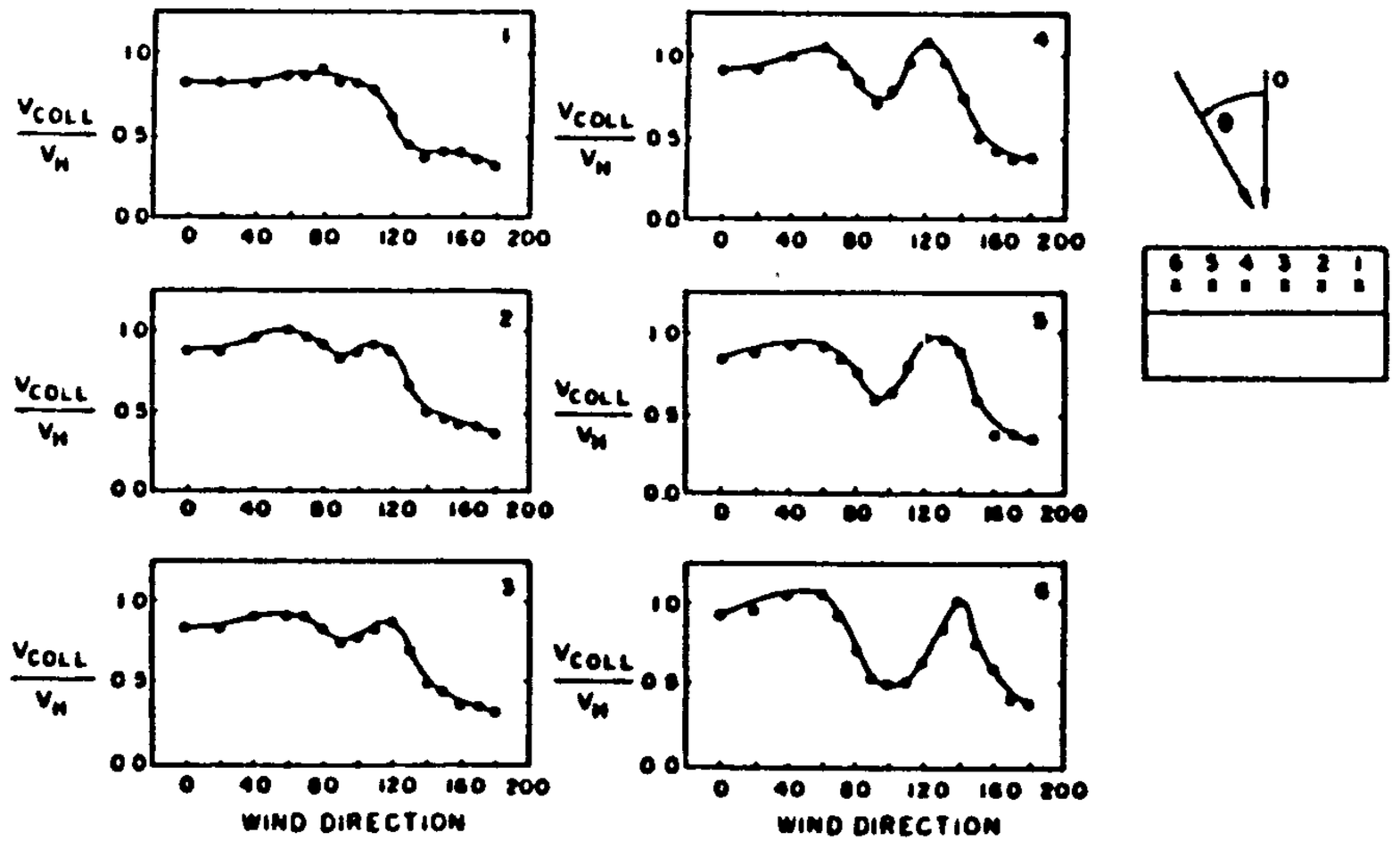


Figure 7.17 Wind speeds over a semi-detatched house roof - 22.5° roof pitch, After Lee and Evans [1984]

# CHAPTER EIGHT

# CONCLUSION

## 8.1 General Remarks

It has been shown that in order to determine the efficiency of a flat-plate solar collector it is necessary to be able to predict the convection loss from its upper surface. Previous methods employed to evaluate the heat lost in this manner have relied upon the direct application of small scale wind tunnel results to full-scale systems.

There are two main problem areas associated with this type of application.

(i) Wind tunnel models tend to be much smaller than real full-scale collector panels (often orders of magnitudes smaller). It has been shown, e.g. Parmelee and Huebscher [1947] that the size of a surface has a significant effect on the convection heat tranfer from it.

(ii) The derived convection coefficient of a surface is most often correlated against wind speed. In wind tunnel experiments wind speeds have been made at a variety of locations, e.g. centre of the tunnel, top of the boundary layer or at the same height as the test surface. How any of these wind speeds relate to the wind environment around full-scale building is not well understood.

The experiments conducted here afforded the opportunity to study the relationship between the convection coefficient, from a surface with the same size and geometry as a full-scale collector panel, and a wind speed measured, at a stated position, in the natural environment, $V_{6R}$. Whilst the location of the wind speed measurement is unique to this series of experiments it must be noted that, as yet, there is no standard design wind speed to be used as an input to convection relationships. Previous full-scale convection coefficients have been correlated against wind speeds measured at various positions, e.g. at some distance from the test surface, $V_S$, some distance above the test building roof, $V_R$, or the meteorological wind speed measured at a nearby weather station, $V_{10}$.

The most accessible wind speed statistic in the UK is the meteorological 10m wind speed $V_{10}$. This would seem to be the ideal design wind speed for convection relationships. Attempts were made in this series to correlate the convection coefficient against $V_{10}$; however, due to the restriction of site availability it was not possible to make measurements of $V_{10}$ concurrently with the convection experiments. This could be a limiting factor on the relationships between h and $V_{10}$ which are presented in Table 5.7.

Wind tunnel studies were also performed to assess the potential of using this type of experiment to predict full-scale heat losses. The results were discouraging, for whilst the wind tunnel results showed compatibility with other similar wind tunnel experiments, especially Sparrow [1981 (b)], they failed to come into line with the outdoor results when extrapolated to full-scale values.

The reason for this failure is not totally understood. It will, however, be recalled from Section 6.4.5 that the wind tunnel scaling laws were relaxed in order to be able to build models of workable size. Lee [1982] and Lee and Evans [1984] state that this relaxation is permissible when studying flow conditions around a building. This relaxation may not be valid for studies involving the measurement of the convection coefficient of a surface.

This scale dependence discrepancy is given further credence by the fact that the results from the two model series (1:32 and 1:64) are significantly different. One method by which this problem could be minimised would be to perform model experiments in a wind tunnel, with a scaling factor compatible with the scale required to produce models of a size sufficiently large so as to be able to assess accurately the convection coefficient.

A further possible factor, which may go some way to explain the failure of the model results to accurately predict full-scale values of the convection coefficient, is the levels of free-stream turbulence present in the wind tunnel.

These were comparable with the levels found in the natural environment i.e. 15-40%. (See Section 6.3.2). McCormak et al [1984] concluded that large levels of free-stream turbulence enhanced the convective heat transfer from a rectangular body by as much at 60%. (See Section 3.5.1). If this is the case, it is not surprising that the combination of a small heated surface placed in a wind flow with large levels of turbulence gives rise to high values of the convective heat transfer coefficient.

## 8.2 The Development of Algorithms for Calculating the Convection Coefficient, h, from the Upper Surface of a Roof Mounted Flat-Plate Solar Collector

As stated in Section 1.6, the primary objective of the study undertaken here was to derive a satisfactory method by which design values of h could be calculated. These design values could then be used as inputs into computational algorithms or empirical relationships, such as equation 1.6. This would then enable the total top loss coefficient, $U_t$, of the collector and hence its efficiency, $\eta$, to be evaluated.

Any method developed to evaluate design values of h should satisfy the following criteria.

(i) It should be presented in an easily understandable form and should be simple to use.

(ii) Any inputs which are required to evaluate the design values should be readily available or easily assessed.

(iii) The calculated design values of h should lie within the range of experimental data from which the method was developed.

(iv) The limitations, if any, of the method used should be noted.

### 8.2.1 A discussion of the factors affecting the development of design algorithms for h

In the series of full-scale experiments described in Chapter Four, the convection coefficient, h, was correlated for each defined wind incidence sector against the wind speed, as measured at a height of 1.5m above the ridge line of the test

building, $V_{6R}$. Therefore, if the wind speed at this height was known, then the results of this series of experiments (see Table 5.1) could be applied with some confidence to collectors and buildings of a similar geometry.

The use of this wind speed, i.e. $V_{6R}$ as an input for design algorithms to evaluate h fails to satisfy criteria (ii), as stated above, in that it is not readily available or easily assessed at any particular location. Also, the presentation of the eight equations given in Table 5.1 would render an over complicated method for evaluating h.

As mentioned in Section 5.4.1, the most readily available wind speed statistic in the UK is the standardised meteorological 10m wind speed, $V_{10}$. This wind speed could also be evaluated at a given location by using a simple mast arrangement as shown in Figure 4.13. Therefore, the use of this wind speed, i.e. $V_{10}$, is recommended as a design input for algorithms for calculating h.

It was shown in Section 5.3.2 that minimum values of h tended to occur when there was a leeward wind and maximum values of h generally occurred when the wind was blowing parallel to the ridge line of the test building. Average values of h were found to occur when the wind was incident directly normal to the collector surface. It would, therefore, be a justifiable simplification to derive design algorithms from the 0°, 180° and 90° wind sectors, these representing average, minimum and maximum exposure levels respectively. The 90° wind sector was chosen as opposed to the -90° wind sector as it will not be influenced by local flow conditions created by the small adjacent garage.

The major problem created by the choice of $V_{10}$ as a design input is that, in the full-scale experiments, concurrent measurements of h and $V_{10}$ were not made. This, as stated in Section 5.4.1, was due to restraints of site usage. It was, however, possible to derive a relationship between $V_{10}$ and the continually measured wind speed, $V_R$. (See Section 5.4.1).

$$V_{6R} = 0.48\ V_{10} + 1.17 \qquad ms^{-1} \qquad (8.1)$$

$$(1.4 < V_{6R} < 7.0)$$

$$(1.3 < V_{10} < 12.0)$$

By direct substitution of the above equation into those presented in Table 5.1 it is possible to derive relationships between h and $V_{10}$ for each wind sector (see Table 5.7). From Table 5.7 it can be seen that the developed equations cannot be applied with any confidence below $V_{10} = 1.3\ ms^{-1}$. However, a representative value of the natural convection coefficient, i.e. that which occurs under absolutely still wind conditions, has already been derived from the relationships between h and $V_{6R}$ (see Section 5.2.5). It can be assumed that at $V_{6R} = 0\ ms^{-1}$, $V_{10} = V_{6R}$. (Equation 8.1 seems to repudiate this assumption - however, see Section 5.4.1 for a discussion on this point.) Therefore, the derived value for the natural convection coefficient can be applied at $V_{10} = 0\ ms^{-1}$.

### 8.2.2 Design algorithms for h

The following algorithms are suggested for the calculation of the convective heat transfer coefficient from the upper surface of a flat-plate solar collector due to the wind, h. In all cases $V_{10}$ is the 10m meteorological wind speed.

(i) Natural convection

This value is independent of wind direction

$$V_{10} = 0 \text{ ms}^{-1}, \quad h = 8.1 \qquad \text{Wm}^{-2}\text{K}^{-1}$$

(ii) Leeward flow, 180° to the normal of the plate surface (minimum exposure)

$$h = 0.6\, V_{10} + 9.9 \qquad \text{Wm}^{-2}\text{K}^{-1} \quad (8.2)$$

$$(1.3 < V_{10} < 7.8 \text{ ms}^{-1})$$

(iii) Parallel flow, 90° to the normal of the plate surface (maximum exposure)

$$h = 1.6\, V_{10} + 10.3 \qquad \text{Wm}^{-2}\text{K}^{-1} \quad (8.3)$$

$$(1.3 < V_{10} < 10.3 \text{ ms}^{-1})$$

(iv) Windward flow, 0° to the normal of the plate surface (average exposure)

$$h = 1.1\, V_{10} + 10.8 \qquad \text{Wm}^{-2}\text{K}^{-1} \quad (8.4)$$

$$(1.3 < V_{10} < 10.8 \text{ ms}^{-1})$$

These algorithms are also illustrated in Figure 8.1.

### 8.2.3 Limitations and applicability of design algorithms

The algorithms presented in Section 8.2.2 are only strictly valid for the experimental conditions from which they were derived. However, they may be applied to other situations if the following points are taken into account.

(I) Collector size and geometry

Wind tunnel tests, e.g. Parmelee and Huebscher [1947] have shown that relationships between the convection coefficient and wind speed are dependent upon the size of the heated plate under test. Therefore, the algorithms are only valid for collector

plates of a similar magnitude, i.e. 1 x 2m. The geometry of the collector, especially its height above the roof surface, may also have an effect on the heat transfer from its upper surface (i.e. Sparrow [1981 (b)]. The presented algorithms may not be valid for collectors which do not stand proud of the roof surface.

This point is given further credence by the fact that the wind tunnel studies performed here show more agreement with the work performed on elevated, but isolated small flat-plates (Sparrow [1981 (b)] than with work performed on small flat-plates placed flush with the roof surface of a model building (Kind [1983]).

(II) Building size and geometry

Wind flow patterns around a building are often affected by the building's size and geometry (Penwarden and Wise [1975]). Hence the wind speed, as measured at a given location close to a building, may also be affected by the size and geometry of the building (Lee and Evans [1984]). The algorithms presented in Section 8.2.2 were derived from relationships based on a wind speed which was measured at a position in close proximity to the test site building, i.e. $V_{6R}$.

Therefore, the presented algorithms are only directly applicable to buildings which show an appreciable similarity, in terms of size and geometry, to the Norton test site building.

It will be recalled, from Section 4.1, that the Norton test building replicates the geometry of the standard semi-detached house, used by the Building Research Establishment for their wind pressure experiments on domestic dwellings. Whilst the Norton test building is somewhat smaller than the standard house (x 0.7 for linear dimensions) it is thought that this is not too great a limiting factor as regards applying the derived algorithms to standard housing stock.

(III) Surrounding terrain

The terrain surrounding the Norton test site building was relatively flat and uniform in all directions. However, major sheltering effects due to nearby buildings have been noted, in model work, by Kelnhofer et al [1976]. Therefore, the algorithms presented in Section 8.2.2 are only strictly valid for sites with surrounding terrain similar to the Norton site. If, however, there are no large nearby buildings and the surrounding terrain is fairly uniform, the presented algorithms may be expected to represent a reasonable approximation to the true relationship between h and $V_{10}$ for any given location.

## 8.3 Recommendations for Further Areas of Research

### 8.3.1 Full-scale

The Norton site measurements yielded useful fundamental results in an area in which there was a lack of full-scale data. Experiments of this type are required to assess the validity of laboratory or computer derived equation for h. There are several areas into which full-scale experimental programs could be expanded.

(I) Collector position

It is not possible for designers of solar collector systems to control the direction of the wind and panels must be placed, for greatest utilisation of solar radiation, generally, on a South facing roof pitch. Therefore, the only possible means of reducing h would be to examine the variation of convection coefficient from a panel placed at various positions on a roof pitch, under a variety of wind conditions. This may yield an optimum position for a collector panel on a particular roof slope. Wind tunnel studies (Lee and Evans [1984]) have already shown that the wind speed over a roof pitch is dependent upon the position of measurement (see Section 7.3.3).

(II) Wind speed measurements

It has been seen throughout this thesis that the convection coefficient of flat surfaces has been correlated against a variety of wind speeds, i.e. wind speeds measured at various locations. It has already been suggested that the difference between several convection experiments may be due to this variety of locations. It is thought that one area of research which could prove beneficial would be to assess how wind speeds measured simultaneously at different locations on or adjacent to low rise dwellings are related.

(III) Natural convection

Whilst pure natural convection rarely occurs in the natural environment it can be seen from Table 5.1 that the non-wind speed dependent value of the regression line represents

a substantial fraction of the total heat lost at higher wind speeds. It would, therefore, be of interest to examine the natural convection coefficient from a large flat-plate placed in laboratory and natural environments.

### 8.3.2 Model studies

Wind tunnel model studies of convective behaviour are important because they offer a more easily controllable environment to the experimenter. However, care must be exercised when extrapolating wind tunnel data to full-scale values. This study has shown that scale effects are apparent in wind tunnel work.

One further area of research is, a closer examination of scale effect on heat transfer studies, performed in wind tunnels on three dimensional bluff bodies. As stated in Section 8.1 the level of free-stream turbulence present may play an important role in the amount of heat lost from the plate surface by convection. It is, therefore, suggested that the effect of various levels of free-stream turbulence, on the convection coefficient from a three-dimensional bluff body, be examined.

## 8.4 Concluding Remarks

The full-scale measurements at the Norton site have shown that the convection coefficient, h, from the upper surface of a flat-plate solar collector is chiefly dependent upon wind speed and to some extent upon the direction of the prevailing wind. Linear relationships were found to express adequately the dependence of h upon wind speed.

It was found that even at very low wind speeds the heat loss from the plate was still substantial. This fact renders any equation used for predicting h, which does not contain a non wind speed dependent term, inapplicable at low wind speeds (e.g. Sparrow [1971]).

Wind tunnel model experiments were also performed. These showed some agreement with experiments previously performed in this area, and also some qualitative agreement with the full-scale convective scale work with regards to the effect of wind direction upon h. However, they were found to be inadequate as a means of predicting full-scale convective behaviour.

Finally a method of deriving design values of h has been presented (see Section 8.2). It is suggested that this design method offers a readily understandable and accessible method for evaluating the convective heat transfer coefficient from the upper surface of a flat-plate solar collector under a variety of environmental conditions.

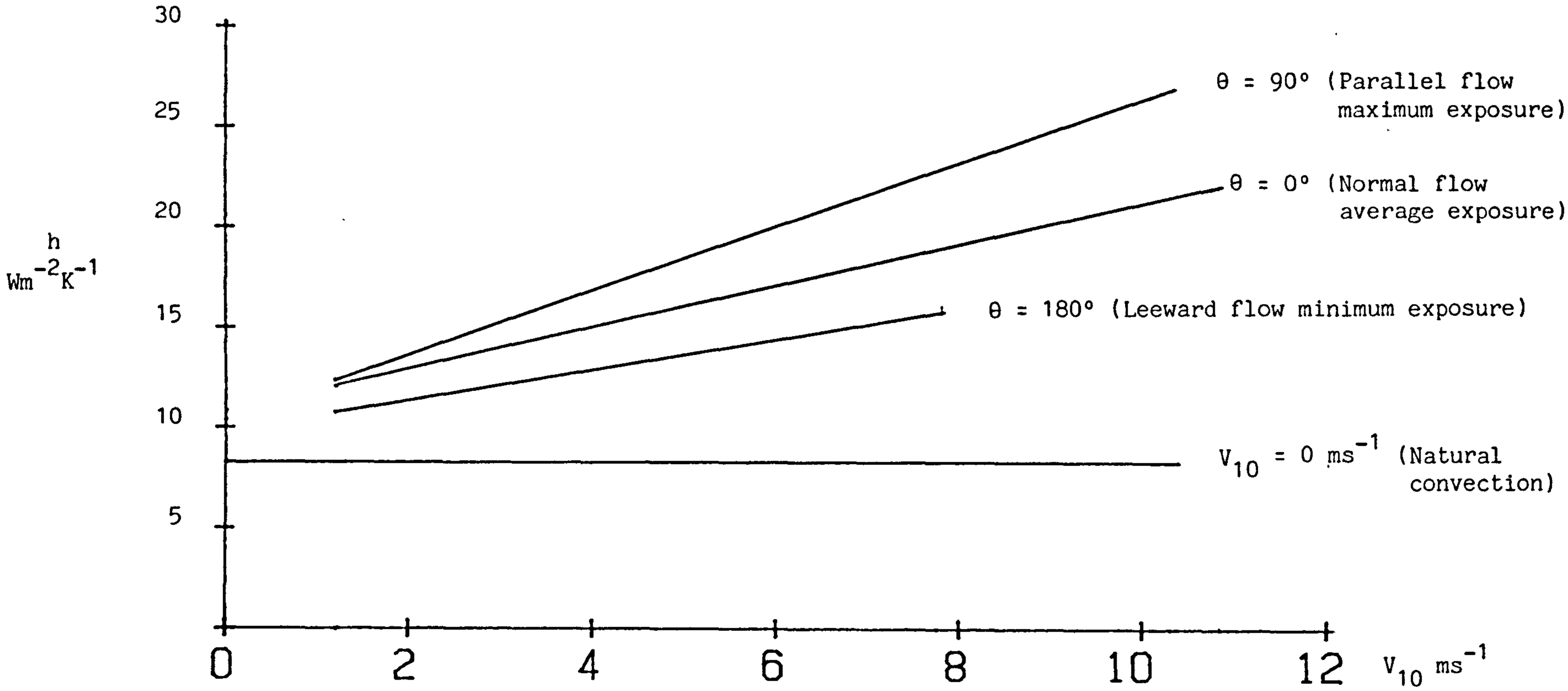


Figure 8.1 Algorithms of h against $V_{10}$ for three exposure levels and still conditions (See Section 8.2.2)

# APPENDIX A

## FULL SCALE ANALYSIS

## COMPUTER PROGRAM

```
10 REM NORTON SITE ANALYSIS PROGRAMME
20 REM P.S.CHARLESWORTH  1984
30 REM ANNOTATED VERSION
40 OPTION BASE 0
50 CLEAR
60 !  DIM PREDOMINACE COUNTER Z(I) AND DIRECTION S
ECTORS C(I)
70 DIM Z(7)
80 DIM C(7)
90 !  SET DIRECTION SECTORS
100 FOR I=0 TO 4
110 LET C(I)=45*I
120 NEXT I
130 FOR I=5 TO 7
140 LET C(I)=-(1*(360-45*I))
150 NEXT I
160 DIM S$[80]
170 !  PREPARE BUFFER FOR DATA INPUT
180 ASSIGN£ 1 TO "Data"
190 !  PREPARE PRINTER FOR OUTPUT
200 PRINTER IS 706,80
210 DISP "ENTER HEADING FOR PRINTOUT"
220 INPUT S$
230 PRINT S$
240 PRINT
250 DISP "FIRST  SCAN NUMBER,LAST SCAN NUMBER PLEA
SE"
260 INPUT N1,N9
270 !  DEFINE NBR HOURS OF DATA
280 LET N7=(N9-N1)/12
290 LET N7=INT(N7)
300 DISP "PLATE POWER ?"
310 INPUT W
320 DISP "START HOUR GMT"
330 INPUT G1
340 FOR V=1 TO N7
350 !  K1 IS TIME GMT
360 LET K1=V+G1-1
370 IF K1=24 THEN K1=0
380 IF K1>24 THEN K1=K1-24
390 !  SET VARIABLES TO ZERO
400 FOR I=0 TO 7
410 LET Z(I)=0
420 NEXT I
430 V1=0 @ V2=0 @ V3=0 @ V4=0 @ V5=0 @ V6=0 @ V7=0
 @ V8=0 @ V9=0 @ V0=0
440 Y1=0 @ Y2=0 @ Y3=0 @ Y4=0 @ Y5=0 @ Y6=0 @ Y7=0
 @ Y8=0 @ Y9=0
450 !  LOOP FOR HOURLY AVERAGES
```

```
460 FOR I=N1+12*(V-1) TO N1+12*V-1
470 LET Z1=2*I-1
480 LET Z2=2*I
490 !  READ DATA TO BUFFER
500 READ£ 1,Z1 ; A,A1,A2,A3,A$,S,D,B,C,N,E,F,G,H,P
,R,Y,O,Q,T1,T2,T3,T4,T5,T6,T7,T8,T9,L1,L2
510 READ£ 1,Z2 ; A,A1,A2,A3,A$,L3,L4,L5,U1,U2,U3,U
4,U5
520 ! MEAN PLATE TEMPERATURE
530 LET M1=(T1+T2+T3+T4+T5+T6+T7+T8+T9)/9
540 ! MEAN TEMP. INSULATION TOP
550 LET M2=(U1+U2+U3+U4+U5)/5
560 ! MEAN TEMP. INSULATION BOTTOM
570 LET M3=(L1+L2+L3+L4+L5)/5
580 ! PLATE TO AIR TEMP DIFF.
590 LET M4=M1-O
600 ! CONDUC LOSS W M SQ
610 LET Q1=.74*(M2-M3)
620 ! RADIATION LOSS  W M SQ
630 LET Q2=.00000005102l*(M1+273.15)^4
640 ! L+S RAD WATT M SQ IN
650 LET Q3=.0000000569*(O+273.15)^4+41.8*1000*R
660 ! SHORT WAVE W M SQ ABSOR
670 LET Q4=.97*(91.56*1000*Y+6.349)
680 IF Q4<30 THEN Q4=0
690 ! LONG WAVE AB W M SQ
700 LET Q5=(Q3-Q4/.97)*.9
710 ! CONV W M SQ
720 LET Q6=W/(.89*1.81)+Q4+Q5-Q1-Q2
730 ! HEAT TRANS COEFFIC
740 LET H1=Q6/(M1-O)
750 LET H2=(Q2-Q5)/M4
760 ! WIND SPEED
770 LET S1=S*4.83
780 ! DIRECTION
790 IF D>O THEN D1=45*D ELSE D1=360+45*D
800 LET D1=D1+25
810 ! PUT DIRECTION IN SECTOR
820 IF D1>360 THEN D1=D1-360
830 IF D1<=22.5 OR D1>337.5 THEN Z(O)=Z(O)+1
840 IF D1<=67.5 AND D1>22.5 THEN Z(1)=Z(1)+1
850 IF D1<=112.5 AND D1>67.5 THEN Z(2)=Z(2)+1
860 IF D1<=157.5 AND D1>112.5 THEN Z(3)=Z(3)+1
870 IF D1<=202.5 AND D1>157.5 THEN Z(4)=Z(4)+1
880 IF D1<=247.5 AND D1>202.5 THEN Z(5)=Z(5)+1
890 IF D1<=292.5 AND D1>247.5 THEN Z(6)=Z(6)+1
900 IF D1<=337.5 AND D1>292.5 THEN Z(7)=Z(7)+1
910 ! SUM INDIVIDUAL VALUES
920 LET M4=M1-O
930 LET VO=VO+S1
940 LET V1=V1+D1
950 LET V2=V2+H1
960 LET V9=V9+Q4
```

```
970 LET Y1=Y1+Q1
980 LET Y2=Y2+Q5
990 LET Y3=Y3+M4
1000 LET Y4=Y4+O
1010 LET Y9=Y9+H2
1020 NEXT I
1030 !  LOCATE PROMINANT DIRECTION
1040 LET V3=Z(0)
1050 LET V4=C(0)
1060 FOR I=0 TO 7
1070 IF Z(I)>V3 THEN V4=C(I)
1080 IF Z(I)>V3 THEN V3=Z(I)
1090 NEXT I
1100 ! FIND MEAN HOURLY VALUES
1110 LET S1=V0/12
1120 LET H1=V2/12
1130 LET H2=Y9/12
1140 LET Q4=V9/12/.97
1150 IF Q4<30.9 THEN Q4=0
1160 LET Q1=Y1/12
1170 LET Q5=Y2/12/.9
1180 LET M4=Y3/12
1190 LET O=Y4/12
1200 LET M5=273.15+(M4+2*O)/2
1210 ! PRINT HOURLY AVERAGES
1220 PRINT @ PRINT @ PRINT @ PRINT @ PRINT
1230 PRINT "**********************************
**********************************"
1240 PRINT
1250 PRINT USING 1400 ; "TIME ","WIND ","FREDOM-",
" INC. "," AIR   "," LONG  "," SHORT "
1260 PRINT USING 1400 ; "HOUR ","SPEED","INANCE ",
" ANG. "," TEMP. "," WAVE  ","  WAVE "
1270 PRINT USING 1400 ; "(GMT)","(M/S)","   %   ",
"(DEG.)","(DEG.C)","(W/M^2)","(W/M^2)"
1280 PRINT USING 1410 ; K1,S1,V3/12*100,V4,O,Q5,Q4

1290 PRINT
1300 PRINT USING 1420 ; "HEAT TRANSFER COEFFICIENT
S ","PLATE-AIR ","CONDUCTION"
1310 PRINT USING 1420 ; "      (W / M^2 / DEG.C)
  ","TEMP.DIFF."," LOSSSES  "
1320 PRINT USING 1430 ; "CONVECTIVE","RADIATIVE","
 (DEG.C) ","WATTS "
1330 PRINT USING 1440 ; H1,H2,M4,Q1
1340 PRINT
1350 PRINT
1360 PRINT "**********************************
**********************************"
1370 NEXT V
1380 ! GOTO NEXT HOUR
```

```
1385 !  CLEAR BUFFER
1390 ASSIGN£ 1 TO *
1395 !  FORMAT OUTPUT
1400 IMAGE 7X,5A,4X,5A,3X,7A,3X,6A,4X,7A,4X,7A,4X,
7A
1410 IMAGE 8X,DD,6X,DD.D,7X,DD,5X,DDDD,7X,DD.D,8X,
DDD,8X,DDD
1420 IMAGE 7X,27A, 5X,10A,10X,10A
1430 IMAGE 8X,10A,4X,9A,8X, 9A,13X,6A
1440 IMAGE 10X,DD.D,10X,DD.D,13X,DD.D,16X,DD.D
1450 END
1460 ! END OF PROGRAMME
```

# REFERENCES

Agarwal, V.K. and Larson, D.C. [1981]
Calculation of the top loss coefficient of a flat-plate collector.
Solar Energy, Vol. 27, pp. 69-71.

Agarwal, V.K. and Larson, D.C. [1983]
Erratum to Agarwal and Larson [1981]
Solar Energy, Vol. 30, No. 1, p. 86.

Angstrom, A. [1915]
A study on radiation of the atmosphere.
Smithsonian Miscellaneous Collection, Vol. 64, pp. 57-69.

Bedingfield, C.H. Jnr. and Drew, T.B. [1950]
Analogy between heat transfer and mass transfer - a psychrometric study.
Industrial and Engineering Chemistry, Vol. 42, pp. 1164-1173.

Berman, S. [1965]
Estimating the longitudinal wind spectrum near the ground.
Q.J.R. Met Soc. Vol. 91, pp. 302-317.

Blasius, H. [1908]
Grenzschichen in flussigkeiten mit kleiner reiburg.
Zeitschr Math U Phys., Vol. 56, No. 1.

Bradshaw, P. [1971]
An introduction to turbulence and its measurement.
Pergamon Press, Oxford, England.

British Standards Institute - Code of Practice [1972]
CP 3, Chapter 5, Part 2.

Brownlee, K.A. [1953]
Industrial experimentation,
Chemical Publishing Co., INC., New York, USA.

Burns, A.P. [1976]
An experimental study of heat transfer from a bluff body to a turbulent free-stream as applied to building heat loss.
Ph.D. Thesis, University of Glasgow.

Cermak, J.E. [1971]
Laboratory simulation of the atmospheric boundary layer.
A.I.A.A. Journal, Vol. 9, No. 9, pp. 1743-1754.

Chapman, A.J. [1974]
Heat Transfer, 3rd Edition,
MacMillan, New York.

Chatfield, C. [1970]
Statistics for technology,
Penguin Books Ltd., England.

Colburn, A.P. [1933]
A method of correlating forced convective heat transfer data with fluid friction.
Trans. A.I.Ch.Eng. Vol. 29, pp. 174-210.

Cole, R.J. [1976]
The longwave radiative environment around buildings.
Building and Environment, Vol. 11, pp. 3-13.

Cook, N.J. [1978]
On simulating the atmospheric boundary layer in wind tunnels.
Building Research Establishment - Current Paper BRE/CP - 71/78.

Cooper, P.I. [1981]
The effect of inclination on the heat loss from flat plate solar collectors.
Solar Energy, Vol. 5, pp. 413-420.

Coste, G., Renaud, M. and Charuel, R. [1981]
Expressions de correlation du coefficient de transfert thermique local sur une plaquette dons un ecoulment d'incidence variable (Correlation equations for the local heat transfer coefficient to a plate in a variable incidence flow)
Chemical Engineering Journal, Vol. 22, pp. 203-212.

Counihan, J. [1973]
Simulation of an adiabatic urban boundary layer in a wind tunnel.
Atmospheric Environment, Vol. 7, pp. 673-689.

Counihan, J. [1975]
Adiabatic atmospheric boundary layers: A review and analysis of data from the period 1880-1972.
Atmospheric Environment, Vol. 9, pp. 871-905.

Cunningham, M.J. [1981]
Measurement errors and instrument inaccuracies.
J. Phys.E.Sci. Instrumentation, Vol. 14, pp. 901-908.

Department of Energy (Energy Paper No. 39) [1979]
Energy Technologies for the UK.
HMSO Publication, London, England.

Deris, N. [1961]
Optimum angle of inclination - new chart for solar collector pin-points.
Air Conditioning, Heating and Ventilating, August, pp. 57-60.

Dhawan, S. [1952]
Direct measurement of skin friction.
NACA Tech. Note 2567.

Dickinson, W.C. and Cheremisinoff, P.N. [1980]
Solar Energy Technology Handbook, Part A, Engineering Fundamentals.
Dekker, New York.

Digest of UK Energy Statistics [1984]
Publication of the Government Statistical Service.
HMSO, London, England.

Dixon, A.E. and Leslie, J.D. [1979]
Solar Energy Conversion.
Pergamon Press, Oxford, UK.

Drake, E.M. [1949]
Investigation of the variation of point unit heat transfer coefficient for laminar flow over an inclined flat plate.
Applied Mechanics, March Issue, pp. 1-8.

Duffie, J.A. and Beckman, W.A. [1980]
Solar Energy Thermal Processes.
J. Wiley and Sons Inc., New York, 1980.

Eaton, K. and Mayne, J.A. [1974]
The measurement of wind pressures on two-storey houses at Aylesbury.
BRE Current Paper CP 70/74.

Edwards, A. and Furber, B.N. [1956]
The influence of free-stream turbulence on heat transfer by convection from an isolated region of a plane surface in parallel air flow.
Proc. Inst. Mech. Eng. Vol. 170, pp. 941-948.

Evans, R.A. and Lee, B.E. [1980]
Some observations on the problem of defining mean wind speeds representative of flow over urban and suburban terrain.
Department of Building Science, University of Sheffield - Internal Report No. BS 52.

Evans, R.A. and Lee, B.E. [1983]
The evaluation of wind speeds over roof mounted solar collectors.
Department of Building Science, University of Sheffield - Internal Report No. BS 73.

Fage, A. and Faulkner, U.M. [1931]
Relation between heat transfer and surface friction for laminar flow.
Aeronautical Research Committee Reports and Memoranda, No. 1408.

Flay, R.G.J., Stevenson, D.C. and Lindley, D. [1982]
Wind structures in a rural atmospheric boundary layer near the ground.
J. Wind Engineering and Industrial Aerodynamics, Vol. 10, pp. 63-78.

Fujii, T. and Imura, H. [1972]
Natural convection heat transfer from a plate with arbitory inclination.
Int. J. Heat Mass Transfer, Vol. 15, pp. 755-767.

Fussey, D.E. and Warneford, I.P. [1976]
An analysis of laminar free convection from upward facing flat plates.
Letters in Heat and Mass Transfer, Vol. 3, pp. 443-448.

Gerhart, K. [1967]
Modellversuche uber die verteilung des konvektiven warmeuberganges an gebaudegassaden.
(Model experiments on the local variation of convection heat transfer processes at building facades.)
Kaltetechnik - Klimatisierung, 19 Jahrgang, Heft 5.1967, pp. 122-128.

Gill, G.C. [1973]
The Helicoid Anemometer.
Atmosphere, Vol. 11, No. 4, pp. 145-155.

Gosset, W.S. [1908]
The probable error of a mean.
Biometrika, Vol. 6, pp. 1-25.

Green, A.A. [1979]
The influence of environmental parameters on flat plate collector performance.
UK-ISES Conf. Proc. C18 "Meteorology for solar energy applications", London.

Green, A.A., Kenna, J.P. and Rawcliffe, R.W. [1981]
The influence of wind speed on flat plate solar collector performance.
Solar Energy Unit, University College, Cardiff, UK.
(Publication)

Hewlett-Packard - Operator's Handbook [1981]
3054 DL Data Logger
Operators Handbook
Hewlett-Packard, Loveland, Colorado, USA.

Holman, J.P. [1981]
Heat Transfer - 5th Edition
McGraw-Hill, New York.

Hottel, H.C. and Woertz, B.B. [1942]
Performance of flat-plate solar-heat collectors.
Trans. Am. Soc. Mech. Engrs. Vol. 64, 91.

Hottel, H.C. and Whillier, A. [1958]
Evaluation of flat-plate collector performance.
Trans. Conf. on the use of Solar Energy, Vol. 2, Part I, p. 74
University of Arizona Press, 1958.

Houghten, F.C. and McDermott, P. [1931]
Wind velocity gradients near a surface and their effect of film conductance.
Trans. ASHVE, Vol. 37, pp. 301-322.

Iqbal, M. and Khatry, A.K. [1977]
Wind induced heat transfer coefficients from glasshouses.
Trans. ASAE, pp. 157-160.

Ito, N., Sato, A., Oka, T. and Kimura, K. [1967]
Convective heat transfer from the external wall surfaces of buildings in natural wind.
Trans. Architectural Inst., Japan. Paper No. 3038, p. 522.

Ito, N., Kimura, K. and Oka, J. [1972]
A field experiment study on the convective heat transfer coefficient on the exterior surface of a building.
Trans. ASHRAE, Vol. 78, pp. 184-191.

Jakob, M. and Kerzios, S.P. [1950]
Defrosting and ice prevention.
Final report 1950, Illionois Inst. of Tech.
Contract No. W33-038ac-16808.
Illinois, USA.

Jenson, M. [1958]
The model-law for phenomena in natural wind.
Ingenioren - International Edition Vol. 2, No. 4, pp. 121-128.

Johnson, H.A. and Rubensin, M.W. [1949]
Aerodynamic heating and convective heat transfer - a summary of literature survey.
Trans. ASME, Vol. 71, pp. 447-456.

Jurges, W. [1924]
Der wormeubergang on einer ebenen Wand
(Heat transfer at a plane wall)
Beih 2, Gesundh-Ing, Series I, Vol. 19.

Kelnhofer, W.J. and Thomas, C.J. [1976]
External convection heat transfer coefficients on a building model.
ASME Paper No. 76-WA/FE-30
ASME Annual winter meeting (1976).

Kestin, J., Maeder, P.F. and Wang, H.E. [1961]
Influence of turbulence on the transfer of heat from plates with and without a pressure gradient.
Int. J. Heat Mass Transfer, Vol. 3, pp. 133-154.

Kind, R.J., Gladstone, D.H. and Moizer, A.D. [1983]
Convective heat losses from flat plate solar collectors in turbulent winds.
J. Solar Energy Engineering, Vol. 105, pp. 80-85.

King, L.V. [1914]
On the convection of heat from small cylinders in a stream of fluid.
Phil. Trans. Royal Society, A214/373.

Klein, S.A. [1975]
Calculation of flat plate collector loss coefficient.
Solar Energy, Vol. 17, pp. 79-80.

Kreith, F. [1976]
Principles of heat transfer, 3rd Edition.
Harper and Row, London.

Lacy, R.E. [1977]
Climate and building in Britain.
HMSO London.

Lee, B.E. [1977]
The simulation of atmospheric boundary layers in the Sheffield University 1.2 x 1.2m boundary layer wind tunnel
Department of Building Science, University of Sheffield - Internal Report No. BS 38.

Lee, B.E. [1982]
Force and Pressure Measurements in Wind Tunnels - A prepared critique.
Proc. Int. Workshop on Wind Tunnel Modelling for Civil Engineering Applications.
US Nat. Bureau of Standards, Washington, USA.

Lee, B.E. and Evans, R.A. [1984]
The measurement of wind flow patterns over building roofs.
Building and Environment, Vol. 19, No. 4, pp. 235-241.

Loudon, A.G. [1965]
In discussion on Lumb [1964]
Quart. J. Roy. Met. Soc. Vol. 90, (386), pp. 439-495.

Lumb, F.E. [1964]
The influence of cloud on hourly total amounts of total solar radiation at the seas surface.
Quart. J. Roy. Met. Soc. Vol. 90, (383), pp. 43-56.

McAdams, W.H. [1954]
Heat transmission, 3rd Edition.
McGraw-Hill, New York.

McCormick, D.C., Test, F.L. and Lessmann, R.C. [1984]
The effect of free-stream turbulence on heat transfer from a rectangular prism.
J. Heat Transfer, Vol. 106, pp. 268-275.

Meinel, A.B. and Meinel, M.P. [1976]
Applied Solar Energy.
Prentice-Hall, New York.

Nicol, K. [1977]
The energy balance of an exterior window surface, Inuvick, N.W.T., Canada.
Building and Environment, Vol. 12, pp. 215-219.

Nicholls, P. [1924]
Measuring heat transmission in building structures and a heat transmission meter.
Trans. ASHVE, Vol. 30, pp. 65-104.

Norris, D.J. [1974]
Calibration of Pyranometers in inclined and inverted positions.
Solar Energy, Vol. 16, p. 53.

Oka, T., Sato, A., Ito, N. and Kimura, K. [1967]
Construction and characteristics of an apparatus for measurement of exterior heat transfer rate.
Trans. Architectural Inst. Japan. Paper No. 3037, p. 521.

Oka, T. and Kon, N. [1974]
Heat transfer in the separated and reattached flow on a blunt flat plate.
J. Heat Transfer, Nov. Issue, pp. 459-462.

Oka, T. and Itasaka, M. [1976]
A separated and reattached flow on a blunt flat plate.
J. Fluids Engineering, March Issue, pp. 79-86.

Oka, T. and Kon, N. [1979]
heat transfer in the separated and reattached flow over blunt flat plates - effect of nose shape.
Int. J. Heat Mass Transfer, Vol. 22, pp. 197-206.

Oliphant, M.V. [1980]
Measurement of wind speed distributions across a solar collector.
Solar Energy, Vol. 24, p. 403.

Ower, E. and Pankhurst, R.C. [1977]
The measurement of air flow.
Pergamon Press, Oxford, England.

Parmelee, G.W. and Heubscher, R.G. [1946]
Forced convection heat transfer coefficients along a flat surface.
Heating Piping and Air Conditioning - ASHVE Journal, May Issue, pp. 112-116.

Parmelee, G.W. and Huebscher, R.G. [1947]
Forced convection heat transfer from flat surfaces - smooth surfaces.
Trans. ASHVE, Vol. 53, pp. 245-284.

Penwarden, A.D. and Wise, A.F.E [1975]
Wind environment around buildings.
BRE Report, C1/SfB 9 (E7). Department of the Environment - HMSO, London, England.

Pohlhausen, E. [1921]
Der warmeaustaugh zurischen festen korpern und flussig - keiten mit kleiner keibung un kleiner warmeleitung.
Zeitscher fur Angew. Math. und Mech., Vol. 1, p. 115.

Ramsey, J.W. and Charmchi, M. [1980]
Variances in solar collector performance predictions due to different methods of evaluating wind heat transfer coefficients.
J. Heat Transfer, Vol. 102, pp. 766-768.

Reynolds, O. [1874]
On the extent and action of the heating surface for steam boilers.
Proc. Manchester Lit. Phil. Soc., Vol. 14, pp. 7-12.

Reynolds, W.C., Kays, W.M. and Kline, S.J. [1958(a)]
Heat transfer in turbulent incompressible boundary layer.
I, Constant wall temperature.
NASA Memorandum 12-1-58W, Washington, USA.

Reynolds, W.C., Kays, W.M. and Kline, S.J. [1958(b)]
Heat transfer in turbulent incompressible boundary layer.
II, Step wall-temperature distribution
NASA Memorandum 12-2-58W, Washington, USA.

Reynolds, W.C., Kays, W.M. and Kline, S.J. [1958(c)]
Heat transfer in turbulent incompressible boundary layer.
III, Arbitary wall temperature and heat flux.
NASA Memorandum 12-3-58W, Washington, USA.

Rowley, F.B., Algren, A.B. and Blackshaw, J.L. [1930(a)]
Effects of air velocities on surface coefficients.
Transactions ASHVE, Vol. 36, pp. 123-136.

Rowley, F.B., Algren, A.B. and Blackshaw, J.L. [1930(b)]
Surface conductances as affected by air velocity temperature and character of surface.
Transactions ASHVE, Vol. 36, pp. 429-446.

Rowley, F.B. and Eckley, W.A. [1932]
Surface coefficients as affected by direction of wind.
Trans. ASHVE Vol. 38, pp. 33-45.

Sam, R.G., Lessmann, R.C. and Test, F.L. [1979]
An experimental study of flow over a rectangular body.
J. Fluids Engineering, Dec. Issue, pp. 443-448.

Sharples, S. [1981]
Forced convective heat transfer from building facades.
Department of Building Science, University of Sheffield.
Ph.D. Thesis.

Sharples, S. [1984]
Full-scale measurements of convective energy losses from exterior building surfaces.
Building and Environment, Vol. 19, No. 1, pp. 31-39.

Smith, F.B. [1970]
The profile of shearing stress in the boundary layer of the atmosphere.
Unpublished note. Met. Office.

Sogin, H.H. and Providence, R.I. [1958]
Sublimation from discs to air streams flowing normal to their surfaces.
Trans. ASME. Jan. issue, pp. 61-69.

Sparrow, E.M. and Tien, K.K. [1971]
Forced convection heat transfer at an inclined and yawed square plate - Application to solar collectors.
J. Heat Transfer, Vol. 99, pp. 507-512.

Sparrow, E.M., Ramsey, J.W. and Mass, E.A. [1979]
Effect of finite width on heat transfer and fluid flow about an inclined rectangular plate.
Journal of Heat Transfer, Vol. 101, pp. 199-204.

Sparrow, E.M. and Lau, S.C. [1981(a)]
Effect of adiabatic co-planar extension surfaces on wind related solar collector heat transfer coefficients.
J. Heat Transfer, Vol. 103, pp. 268-271.

Sparrow, E.M., Somie, F. and Lau, S.C. [1981(b)]
Heat transfer from a plate elevated above a host surface and washed by a separated flow induced by an elevation step.
J. Heat Transfer, Vol. 103, pp. 441-447.

Sparrow, E.M., Nelson, J.S. and Tao, W.Q. [1982]
Effect of leeward orientation, adiabatic framing surfaces, and eaves on solar collector related heat transfer coefficients.
Solar Energy, Vol. 29, No. 1, pp. 33-41.

Streed, E.R. and Waksman, D. [1981]
Uncertainty in determining the thermal performance of liquid heating flat-plate solar collectors.
J. Solar Energy Engineering, Vol. 103, pp. 126-134.

Sturrock, N.S. [1971]
Localised boundary layer heat transfer form external building surfaces.
University of Liverpool, Ph.D. Thesis.

Sugawara, S., Sato, T. Komatsu, H. and Osaka, H. [1958]
The effect of free-stream turbulence on heat transfer from a flat plate.
N.A.C.A. Tech. Memo. No. 1441.

Surridge, A.D. [1982]
On the measurement of atmospheric winds.
Boundary Layer Meteorology, Vol. 24, pp. 421-428.

Swinbank, W.C. [1963]
Longwave radiation from clear skies.
Quart. J. Roy. Met Soc., Vol. 89, pp. 339-348.

Szokolay, S.V. [1975]
Solar energy and building.
The Architectural Press, London, 1975.

Test, F.L. and Lessmann, R.C. [1980]
An experimental study of heat transfer during forced convection over a rectangular body.
J. Heat Transfer, Vol. 102, pp. 146-151

Test, F.L., Lessman, R.C. and Johary, A. [1981]
Heat transfer during wind flow over rectangular bodies in the natural environment.
J. Heat Transfer, Vol. 103, pp. 262-267.

Von Karman, T. [1939]
The analogy between fluid friction and heat transfer.
Trans. ASME, Vol. 61, pp. 705-710.

Wang, X.A. [1982]
An experimental study of mixed forced and free convection heat transfer from a flat plate to air.
J. Heat Transfer, Vol. 104, pp. 139-144.

Watmuff, J.H., Charters, W.W.S. and Proctor, D. [1977]
Solar and wind induced external coefficients for solar collectors.
Comples - International Review D'Helio Technique, Vol. 2, p. 56.

Wozniak, S.J. [1979]
Solar heating systems for the UK: design, installation and economic aspects.
Department of the Environment, HMSO, 1979.